EVALUATION OF DISPLACEMENT AMPLICATION FACTOR FOR SEISMIC DESIGN PROVISIONS

by

Chia-Ming Uang and Ahmed Maarouf

Department of Civil Engineering
Northeastern University, Boston

Data Utilization Report CSMIP/96-02

California Strong Motion Instrumentation Program

September 1996

CALIFORNIA DEPARTMENT OF CONSERVATION
DIVISION OF MINES AND GEOLOGY
OFFICE OF STRONG MOTION STUDIES

OSMS 96-10

DIVISION OF MINES AND GEOLOGY
JAMES F. DAVIS
STATE GEOLOGIST

DISCLAIMER

The content of this report was developed under Contract No. 1090-526 from the Strong Motion Instrumentation Program in the Division of Mines and Geology of the California Department of Conservation. This report has not been edited to the standards of a formal publication. Any opinions, findings, conclusions or recommendations contained in this report are those of the authors, and should not be interpreted as representing the official policies, either expressed or implied, of the State of California.

EVALUATION OF DISPLACEMENT AMPLICATION FACTOR FOR SEISMIC DESIGN PROVISIONS

by

Chia-Ming Uang* and Ahmed Maarouf

Department of Civil Engineering
Northeastern University, Boston

Data Utilization Report CSMIP/96-02

California Strong Motion Instrumentation Program

September 1996

* Now at Department of Applied Mechanics and Engineering Sceiences, University of California, San Diego.

This study was conducted at the Northeastern University in Boston, Massachusetts and was supported by the Department of Conservation under Contract No. 1090-526.

California Department of Conservation
Division of Mines and Geology
Office of Strong Motion Studies
801 K Street, MS 13-35
Sacramento, California 95814-3531

PREFACE

The California Strong Motion Instrumentation Program (CSMIP) in the Division of Mines and Geology of the California Department of Conservation promotes and facilitates the improvement of seismic codes through the Data Interpretation Project. The objective of the this project is to increase the understanding of earthquake strong ground shaking and its effects on structures through interpretation and analysis studies of CSMIP and other applicable strong motion data. The ultimate goal is to accelerate the process by which lessons learned from earthquake data are incorporated into seismic code provisions and seismic design practices.

The specific objectives of the CSMIP Data Interpretation Project are to:

1. Understand the spatial variation and magnitude dependence of earthquake strong ground motion.

2. Understand the effects of earthquake motions on the response of geologic formations, buildings and lifeline structures.

3. Expedite the incorporation of knowledge of earthquake shaking into revision of seismic codes and practices.

4. Increase awareness within the seismological and earthquake engineering community about the effective usage of strong motion data.

5. Improve instrumentation methods and data processing techniques to maximize the usefulness of SMIP data. Develop data representations to increase the usefulness and the applicability to design engineers.

This report is the fifteen in a series of CSMIP data utilization reports designed to transfer recent research findings on strong-motion data to practicing seismic design professionals and earth scientists. CSMIP extends its appreciation to the members of the Strong Motion Instrumentation Advisory Committee and its subcommittees for their recommendations regarding the Data Interpretation Research Project.

Anthony F. Shakal
CSMIP Program Manager

Moh J. Huang
CSMIP Data Interpretation
Project Manager

ABSTRACT

Displacement amplification factor (*DAF*) for seismic design of multistory buildings has been investigated. Expressed in terms of the seismic force reduction factor (*FRF*), which is better known as the R_w factor in Uniform Building Code (UBC) and R factor in NEHRP Recommended Provisions, it was observed that the *DAF*/*FRF* ratios used in UBC and NEHRP are much smaller than those used in the Mexican Code and Eurocode.

Four buildings (two steel and two reinforced concrete structures) which have been instrumented by the California Division of Mines and Geology were studied to investigate if the *DAF* used in UBC or NEHRP significantly underestimates maximum (inelastic) deformations. Building response recorded during the 1989 Loma Prieta earthquake was used to calibrate mathematical models of these buildings. Dynamic analyses were performed to investigate the relationship between the *DAF* and *FRF*; an assemble of California historical earthquake records was used as input ground motions. The effects of structural overstrength, types of collapse mechanism, stiffness degradation, damping, fundamental period, and earthquake characteristics (impulse versus "standard" type earthquakes, strong motion duration, earthquake predominant period) on the *DAF* were investigated. The reliability of using a *DAF* as derived from either single-degree-of-freedom (SDOF) systems or shear building models (i.e., "stick" models) for practical design was also studied.

The results have indicated that neither SDOF systems nor shear building models provides reliable prediction of *DAF* for multistory buildings. It was found that the *DAF*/*FRF* ratio is practically independent of the structure's fundamental period as long as it is longer than 0.3 of the earthquake predominant period. The *DAF*/*FRF* ratio for estimating roof drift does not appear to be affected by the type of failure mechanism and stiffness degradation. Nevertheless, this is not true for estimating story drift; the *DAF*/*FRF* ratio can be significantly higher than 1.0 for stiffness degrading systems with a soft story. Although the *DAF* required to estimate roof drift is slightly less than *FRF*, the *DAF* for estimating story drift can be significantly higher than *FRF*. For simplicity, it is recommended that a *DAF* which is equal to *FRF* be used for design purposes.

ACKNOWLEDGMENTS

The contents of this report were developed under Contract No. 1090-526 from the California Department of Conservation, Division of Mines and Geology, Strong Motion Instrumentation Program. However, these contents do not necessarily represent the policy of that agency nor do endorsement by the State Government. Much appreciation is given to the staff of the SMIP, especially Drs. M. J. Huang and A. F. Shakal, for providing processed data and design drawings.

Table of Contents

Chapter 1

Introduction

1.1. Problem Statement

Modern seismic design provisions assume that buildings will undergo inelastic deformations during severe earthquakes. Therefore, these provisions allow the designer to reduce the elastic seismic force demand by a force reduction factor (*FRF*). Since reduced seismic forces are used in design, the computed displacements from an elastic analysis have to be amplified in order to estimate the actual deformations that develop in severe earthquakes. Seismic provisions usually use a displacement amplification factor (*DAF*) for this purpose.

Recognizing that *DAF* and *FRF* are interrelated, seismic codes usually assign *DAF* in terms of *FRF*. The Uniform Building Code (ICBO 1991), which uses R_w as the force reduction factor, assigns $3R_w/8$ as the displacement amplification factor. This factor, which is also used as an amplification factor to estimate the forces that may develop in nonductile structural components during severe earthquakes, is a direct carryover of the $3.0/K$ factor which was used as the *DAF* in previous UBC editions. The Commentary of the SEAOC Recommended Lateral Force Requirements (SEAOC 1990), which forms the basis for UBC seismic design provisions, states that this factor is "probably on the low side and that the maximum deformations can be as high as R_w times the design level deformations." It appears that this factor is based more on tradition than on hard facts.

A review of the National Building Code of Canada (*NBCC* 1990), the Mexico Code (*Complementary* 1988), and the Eurocode (*Structures* 1988) indicated that the ratios between *DAF* and *FRF* vary considerably from one code to another. Both the Mexico Code and Eurocode use a *DAF* which is no smaller than *FRF*. The contradiction among these seismic design codes and the lack of sufficient theoretical basis for the *DAF* of multistory building systems prompted the need for evaluating the appropriate *DAF* that should be used in seismic design of building structures.

1.2. Objectives and Scope

The first objective of this research is to evaluate the appropriate displacement amplification factor for seismic design of multistory building frames; displacement amplification factors for estimating both the maximum story drift and roof drift will be established. The second objective is to compare the displacement amplification factor of multistory buildings with those developed previously for single-degree-of-freedom systems and multi-degree-of-freedom "shear" buildings (i.e., "stick" models.) The third objective is to investigate the characteristics of structures and earthquake ground motions that most affect the displacement amplification factor.

Since it is essential that the response of realistic buildings be studied for evaluating code requirements, four buildings (two steel and two reinforced concrete buildings) which have been instrumented by the Strong Motion Instrumentation Program (SMIP) of the California Division of Mines and Geology (CDMG) were selected for extensive studies. Dynamic analyses of these buildings with fundamental periods ranging from 0.3 to 2.2 seconds were performed in order to investigate the relationship between *DAF* and *FRF*. Building responses recorded during the 1989 Loma Prieta earthquake were used to calibrate the mathematical models, and eight historical earthquake records were used in the dynamic analysis.

Chapter 2

Problems of Displacement Amplification Factor in Seismic Codes

2.1. Current Code Approach for Estimating Maximum Displacements

It is well known that modern seismic provisions take advantage of the structure's energy dissipation capacity. Because of this dissipation capacity, the prescribed seismic force level for design purposes is obtained by reducing the elastic seismic force demand by a force reduction factor, *FRF*. [UBC uses R_w and NEHRP (BSSC 1991) uses R as the *FRF*.] Designers perform elastic analysis and the displacements at this reduced design seismic force level can be computed. To estimate the maximum (inelastic) deformations that may develop in severe earthquakes, seismic codes usually specify a displacement amplification factor (*DAF*) to amplify the computed elastic deformations. (UBC uses $3R_w/8$ and NERHP uses C_d factors as the *DAF*.) The specification of a reliable *DAF* in seismic codes is essential for (i) estimating maximum story drifts, (ii) checking deformation capacity of critical structural members (e.g., shear links in eccentrically braced frames), (iii) estimating minimum building separation to avoid pounding, (iv) check P-delta effects (BSSC 1991), and (v) detailing connections for nonstructural components.

Consider the typical lateral force versus deformation relationship of a structural system in Fig. 2.1. The elastic force demand, expressed in terms of the ratio between base shear and total building weight, for a severe earthquake is expressed as C_e (base shear ratio). Idealizing the actual structural response curve by a linearly elastic-perfectly plastic curve in Fig. 2.1, the structure's system ductility factor can be defined as

$$\mu_s = \frac{\Delta_{\max}}{\Delta_y} \tag{2.1}$$

where the deformation is expressed in terms of story drift, Δ.

The ratio between the elastic force demand (C_e) and the structure's yield strength level (C_y) is defined as the ductility reduction factor, R_μ:

$$R_\mu = \frac{C_e}{C_y} \tag{2.2}$$

The reserve strength that exists between the structure's ultimate strength (C_y) and the design base shear ratio (C_w) for working stress design is defined as the structural overstrength factor (Ω_w):

$$\Omega_w = \frac{C_y}{C_w} \tag{2.3}$$

Based on these definitions, the force reduction factor (*FRF*) for working stress design can be derived from Fig. 2.1 as follows (Uang 1991a):

$$FRF = \frac{C_e}{C_w} = \frac{C_e}{C_y}\frac{C_y}{C_w} = R_\mu\,\Omega_w \tag{2.4}$$

The displacement amplification factor (*DAF*) can also be derived from Fig. 2.1 as follows:

$$DAF = \frac{\Delta_{\max}}{\Delta_w} = \frac{\Delta_{\max}}{\Delta_y}\frac{\Delta_y}{\Delta_w} = \mu_s \frac{\Delta_y}{\Delta_w} \tag{2.5}$$

Since Δ_y/Δ_w is equal to C_y/C_w by proportions (see Fig. 2.1), it follows that

$$DAF = \mu_s \frac{C_y}{C_w} = \mu_s\,\Omega_w \tag{2.6}$$

From Eqs. 2.4 and 2.6, the ratio between *DAF* and *FRF* is

$$\frac{DAF}{FRF} = \frac{\mu_s \Omega_w}{R_\mu \Omega_w} = \frac{\mu_s}{R_\mu} \tag{2.7}$$

Since the structural overstrength factor, Ω_w, cancels out in Eq. 2.7, the *DAF*/*FRF* ratio is only a function of the ductility factor.

It should be noted that the above derivations are also valid for the strength design method, the only difference being that the structural overstrength factor (Ω_w) has to be reduced by a seismic load factor (= 1.4 ~ 1.5.) Since the structural overstrength factor cancels out in the ratio *DAF*/*FRF*, the relationship in Eq. 2.7 is still valid for seismic provisions (e.g., NEHRP) which specify seismic forces for strength design.

2.2. Comparison of DAF in Seismic Design Provisions

Since different seismic design provisions use different *FRF* factors and the *DAF* and *FRF* are interrelated, a comparison of *DAF* among seismic codes should be based on the *DAF*/*FRF* ratio, not the *DAF* alone. A survey of seismic design codes that include the 1991 Uniform Building Code (ICBO 1991) of the U.S.A., the 1990 National Building Code (*NBCC* 1990) of Canada, the 1987 Mexico Code (*Complementary* 1988), and the 1988 Eurocode (*Structures* 1988) shows that the *DAF*/*FRF* ratios vary considerably from one code to another. Table 2.1 lists the *DAF*/*FRF* ratios used in these codes. On one extreme, both the Mexico Code and Eurocode use a *DAF* which is no smaller than *FRF*. At the other extreme, UBC uses a *DAF* which is only three-eights that of the *FRF*.

Although each of the four codes compared above uses a fixed ratio between *DAF* and *FRF*, the NEHRP Recommended Seismic Provisions (1991) uses a ratio which varies from one lateral-load-resisting system to another†. Table 2.2 shows that the *DAF*/*FRF* ratio (= C_d/R according to the NEHRP notations) varies from 0.5 to 1.0 for structural steel systems and from 0.69 to 1.0 for reinforced concrete systems. Since the values assigned to the *FRF* and *DAF* of each framing system are based on engineering judgement and general consensus, it is difficult to justify the variations of the *DAF*/*FRF* ratios among different systems.

2.3. DAF for Single-Degree-of-Freedom Systems

The relationship between elastic and inelastic responses of a single-degree-of-freedom (SDOF) system has been studied extensively by many researchers. In a simple format, Newmark and Hall (1973) indicated that for elasto-plastic systems in the "acceleration" region of response spectra (natural period approximately in the range of 0.1 to 0.5 seconds), the ductility reduction factor R_μ (= C_e/C_y) as derived on the basis of energy conservation (see Fig. 2.2a) is

$$R_\mu = \sqrt{2\mu_s - 1} \tag{2.8}$$

† In addition to using a C_d factor, the 1991 NEHRP Seismic Provisions (Chapter 10) also uses (2/5)*FRF* (i.e., 2*R*/5 in NEHRP) as the *DAF* for estimating maximum deformations and checking deformation capacities of steel connections and shear links (Popov 1991). The (2/5)*FRF* in NEHRP is compatible with, although a little bit more conservative than, the *DAF* of (3/8)*FRF* in UBC.

By substituting the above equation into Eq 2.7, it follows that

$$\frac{DAF}{FRF} = \frac{\mu_s}{\sqrt{2\mu_s - 1}} \geq 1.0 \tag{2.9}$$

In the "velocity" and "displacement" regions (natural period ≥ 0.5 seconds), the equal displacement rule applies (see Fig. 2.2b), and

$$R_\mu = \mu_s \tag{2.10}$$

Substituting Eq. 2.10 into Eq. 2.7 gives

$$\frac{DAF}{FRF} = \frac{\mu_s}{\mu_s} = 1.0 \tag{2.11}$$

Eqs. 2.9 and 2.11 indicate that the *DAF* for SDOF systems should be equal to or greater than *FRF*, depending on the natural period of the structure. This simple rule is in agreement with the *DAF* adopted in the Mexico Code and Eurocode. This rule also agrees with the relationship between the *DAF* and *FRF* for "inverted pendulum structures" in NEHRP (see Table 2.2). If a multistory frame were to behave like an SDOF system, then the UBC's *DAF* will be too low and nonconservative.

2.4. Definition of DAF for Multi-Degree-of-Freedom Systems

The problem associated with the *DAF* of multi-degree-of-freedom (MDOF) systems is much more complicated than that of SDOF systems. Unlike the SDOF system, in MDOF systems there is no simple definition for *DAF*. The reason is simple; in a multistory building, the displacement amplification in each story is usually not the same. Nevertheless, one can define a *DAF* for the purpose of estimating maximum roof drift and two types of *DAF* for estimating maximum story drift.

(1) DAF for Estimating Roof Drift

To avoid pounding of adjacent buildings during earthquakes, which appeared to be a problem during the 1985 Mexico City earthquake Bertero (Bertero 1986) and the 1989 Loma Prieta earthquake (Kasai and Maison 1990), the maximum roof drift has to be estimated properly. The

DAF for estimating maximum roof drift can be calculated as

$$DAF = \frac{\Delta^r_{\max}}{\Delta^r_w} \tag{2.12}$$

where $\Delta^r_{\max}$ and Δ^r_w are the roof drifts resulting from severe earthquake excitations and the UBC design seismic forces, respectively. The *DAF* for roof drift is generally less than that of the story drift, as the former is an "average" drift along the height of the building.

(2) Maximum DAF for Estimating Story Drift

For a multistory building with N stories, the DAF_i of the i-th story is defined as

$$DAF_i = \frac{\Delta^i_{\max}}{\Delta^i_w} \tag{2.13}$$

where $\Delta^i_{\max}$ is the maximum inelastic story drift of the i-th story, and Δ^i_w is the corresponding elastic story drift at the UBC design seismic force level. Then, the maximum *DAF* (which will be called as the *DAF* later for simplicity) is computed as

$$DAF = \max(DAF_i) \quad \text{for} \quad i = 1, N \tag{2.14}$$

It should be noted that the story with a maximum elastic drift is not necessarily the one with a maximum inelastic drift.

Using the *DAF* as defined in Eq. 2.14 leads to an upper bound estimate of the story drift envelope. To demonstrate this, Table 2.3 shows the elastic and inelastic story drifts measured in two different levels of shaking table tests of a 0.3-scale model of a 6-story concentrically braced steel structure (Uang and Bertero 1986). The peak ground acceleration (*PGA*) during the "Elastic" and "Inelastic" tests were 0.063 g and 0.65 g, respectively. *Assuming* that the elastic design story drifts (Δ_w) and inelastic story drifts ($\Delta_{\max}$) can be represented by these two test results, the *DAF* as calculated from Eq. 2.14 is equal to 17.2 (in the fifth story, which experienced severe brace buckling). If a *DAF* equal to 17.2 is used to amplify Δ_w for all the stories, Fig. 2.3 shows that it will overestimate the actual inelastic story drifts in all but the fifth story, where the maximum displacement amplification took place.

(3) Critical DAF for Estimating Story Drift

The critical *DAF*, or simply DAF_{cr}, is computed as follows:

(a) Compute the critical story drift ratio (DR_w) from elastic design story drifts produced by UBC prescribed design seismic forces.

(b) Compute the critical story drift ratio ($DR_{\max}$) from inelastic story drifts produced by severe design earthquakes.

(c) Define the critical *DAF* as:

$$DAF_{cr} = \frac{DR_{\max}}{DR_w} \tag{2.15}$$

The significance of DAF_{cr} lies in the fact that it estimates the maximum inelastic story drift ratio once the maximum elastic story drift ratio at the design seismic force level is known. The disadvantage of this definition is that the location of the story where this maximum inelastic drift ratio occurs is not readily known. Referring to the 0.3-scale steel test model again, Table 2.3 shows that the maximum elastic story drift ratio which occurred in the fourth story is equal to 0.15%, while the maximum inelastic story drift ratio which took place in the fifth story is equal to 1.89%; therefore, the DAF_{cr} is equal to 12.6. Fig. 2.3 shows that the DAF_{cr} will estimate the maximum story drift ratio correctly, but in a different story. If the maximum elastic and inelastic story drifts happen to occur in the same story, then the *DAF* and DAF_{cr} will be identical. As design engineers are usually concerned about the maximum story drift ratio regardless of the story in which it will occur, it appears that the DAF_{cr}, rather than the more conservative *DAF* as defined in Eq. 2.14, is more appropriate for design purposes.

2.5. Estimating DAF from Building Responses

2.5.1. Selection of Buildings

Four buildings located in California and instrumented by the California Strong Motion Instrumentation Program (CSMIP) were selected for this study. These buildings (see Table 2.4) include two steel buildings designated as CSMIP 57357 and CSMIP 58496, as well as two

reinforced concrete buildings designated as CSMIP 57355 and CSMIP 58490. Building CSMIP 57357 is a 13-story steel special moment-resisting space frame with a fundamental period of 2.2 seconds. Building CSMIP 57496 is a 2-story (in addition to a basement) eccentrically braced steel frame with a fundamental period of 0.3 seconds. Building CSMIP 57355 is a 10-story ductile reinforced concrete moment frame with a fundamental period of 1.0 second. CSMIP 58490 is a 6-story reinforced concrete building with a perimeter moment-resisting frame and has a fundamental period of 0.8 seconds.

2.5.2. Method of Analysis

For each building, the steps listed below were followed to calculate the *DAF* for both roof and story drifts.

(1) The building response recorded during the Loma Prieta earthquake was used to identify the building's natural periods and to calculate the relative displacements of the instrumented floors.

(2) A 2-D mathematical model for the building was established from the design drawings. Reasonable assumptions were made to model structural damping, member stiffness, and mass distribution.

(3) The natural periods of the building model were calculated by the DRAIN-2DX computer program (Prakash and Powell 1992). The fundamental period was then compared to that identified from the measured building response. A good correlation ensures that the stiffness and mass distributions of the building have been properly modeled.

(4) Using the base acceleration recorded during the Loma Prieta earthquake as input ground motion, the DRAIN-2DX computer program was used to perform dynamic time history analysis. The computed response was then correlated with that measured during the Loma Prieta earthquake. The correlation was used to calibrate modeling assumptions such as structural stiffness, member strength, and damping. If necessary, the mathematical model was revised until an acceptable correlation between measured and computed responses was achieved.

(5) Nonlinear dynamic analyses of the mathematical model were performed; eight historical earthquake records that simulate ground motions implied by the UBC design response spectra were used as input motions. In the analysis, each earthquake record was scaled to different intensities using the method described later in Section 2.5.4. Maximum roof and story drifts (Δ_{max} in Fig. 2.1) were obtained from the dynamic analysis. The corresponding elastic roof and story drifts (Δ_e) were also calculated from linear dynamic analyses.

(6) Referring to Fig. 2.1, the ratio between Δ_{max} and Δ_e is the same as the ratio between *DAF* and *FRF* because

$$\frac{\Delta_{max}}{\Delta_e} = \frac{DAF\ (\Delta_w)}{FRF\ (\Delta_w)} = \frac{DAF}{FRF} \tag{2.16}$$

It follows that evaluating the *DAF*/*FRF* ratio can be achieved by evaluating the Δ_{max}/Δ_e ratio. According to the *DAF* definitions described in Section 2.4, the *DAF*/*FRF* ratios for roof and story drifts were calculated for each earthquake record. The results from all earthquake ground motion records were then averaged.

2.5.3. Selection of Earthquakes

Eight California earthquake acceleration records (see Table 2.5) were chosen to simulate the UBC design response spectra. The selection included records with large as well as small peak ground accelerations (*PGA*). In addition to "standard" earthquake records like the 1940 El Centro and 1952 Taft records, impulse-type earthquakes like the Pacoima Dam, Parkfield, and IVC were also included. The selected records (see Fig. 2.4) have different predominant periods, frequency contents, and response spectral shapes. Fig 2.5 shows that the mean response spectra of the eight earthquakes as normalized by either the *PGA* or the effective peak acceleration (*EPA*) are similar to the UBC elastic design response spectrum for rock sites (soil type S_1).

2.5.4. Scaling Earthquake Records

As was mentioned earlier, the earthquake records that were used as input ground motions for dynamic analyses were scaled to different intensities. The idea of using a series of earthquake scaling factors is to investigate the relationship between earthquake intensity and *DAF*. As

several earthquake records were used, these records have to be normalized to the same level of intensity before the response results can be averaged. It is well understood that there is no agreement on the parameters used in earthquake record normalizations. Instead of using a very simple approach like using the *PGA* as a normalizing parameter or using one of the many complicated normalizing expressions, the following procedure was used (see Fig. 2.6).

1. For each earthquake record, calculate the average pseudo-acceleration (*PSA*) around the fundamental period of the structure.
2. The earthquake scale factor is calculated as:

$$\text{Scale Factor} = \frac{PSA}{gC_w} \tag{2.17}$$

where C_w is the UBC design base shear ratio.

The objective of this method is to achieve, for a given scale factor, a similar level of elastic force demand for all earthquake records. Since the response of low- to medium-rise buildings is dominated by the first mode, it should be noted that the PSA/g at the fundmental period of the structure is generally a fairly good approximation of the maximum elastic base shear ratio, C_e. To demonstrate this, consider building CSMIP 57355 with C_w = 0.058 (see Section 5.2.2). By setting the scale factor in Eq. 2.17 equal to one (i.e., the target *PSA* is 0.058 g), results from elastic dynamic analyses for an assemble of eight earthquake records give an average base shear ratio of 0.055, which is about 95% of the target PSA/g (see Table 2.6). Therefore, when presenting the average results of each building in the following chapters, the scale factor in Eq. 2.17 will be replaced by C_e/C_w.

Chapter 3

San Jose 13-story Government Office Building

3.1. Building Description

3.1.1. General Layout

This is a steel office building which consists of 13 stories and a penthouse, all above grade (see Fig. 3.1). It is located in the City of San Jose, California, at a distance of 21 miles from the epicenter of the Loma Prieta earthquake. The building, which is designated as CSMIP57357, was designed in 1972 and constructed in 1975-76. Other than two extra bays along the south and west sides of the building which were provided to accommodate the elevators and stairs, the building is generally regular in plan (see Fig. 3.2).

3.1.2. Structural System

Typical floor system of the building consists of 3.5-in. light-weight concrete slab on metal deck supported by a complete steel space frame. The lateral-force-resisting system of the structure consists of steel moment-resisting space frame. With few exceptions, Grade 50 steel is used for the frame members. The building foundation is a 173 by 167 square ft., 4-ft. thick reinforced concrete mat founded on alluvial soil.

3.2. Review of the UBC Seismic Design

3.2.1. Building Reactive Weight

It is assumed that the reactive weight of the building includes all the dead load of the bare structure, as well as an additional 15 pounds per square foot for partitions, ceiling, or anything else that might be tied down to the floors. The reactive weights for a typical floor and the roof were estimated to be 1,900 and 1,800 kips, respectively. The reactive weights of the mechanical

floor (12th floor) and the penthouse were estimated to be 2,100 and 400 kips, respectively. The total reactive weight of the building, W, was estimated to be 25,200 kips.

3.2.2. UBC Design Base Shear

The original design base shear, V, according to the 1970 UBC is equal to 1,154 kips; the design base shear ratio is 4.6% (Uang and Maarouf 1991). According to the 1991 UBC, the minimum design base shear is calculated by the following formula:

$$V = \frac{ZIC}{R_w} W \tag{3.1}$$

where Z (= 0.4) is the seismic zone factor. Because the building height exceeds the 160 ft. limitation for ordinary moment-resisting space frames, this building has to be designed as a special moment-resisting space frame, i.e., R_w is equal to 12. The factor C is calculated by the following formula:

$$C = \frac{1.25S}{T^{2/3}} \tag{3.2}$$

where the period T of the building in both directions is calculated as

$$T = 0.035(h_n)^{3/4} = 1.8 \text{ seconds} \tag{3.3}$$

The soil factor S is taken as 1.5, which corresponds to soil type S_3 (alluvial soil). Therefore the minimum design base shear V is equal 1,075 kips (or the base shear ratio is equal to 4.3%).

One can notice that the 1991 and 1970 UBC design base shears for this building are nearly identical. This could lead to the expectation that the original member design will also satisfy the 1991 UBC.

3.3. Mathematical Model of the Building

3.3.1. Modeling Method and Assumptions

Based on the design drawings, a two-dimensional mathematical model for one of the interior frames in the E-W direction was established. It was assumed that floors are rigid in their own plane; floor mass was assumed to be lumped at each floor level. Since no shear connectors between girders and slabs were used in the building design, composite action was not considered. The column bases were assumed to be fixed to the foundation. The columns and girders were framed together through welded connections. A 50% rigid-end zone was used to account for the panel zone flexibility of the rigid connections (Tsai and Popov 1990); member strain hardening was not considered. Rayleigh damping which is proportional to the mass and initial stiffness matrices was used. A 5% of critical damping was assigned to the first two modes (Chai 1991).

3.3.2. Mass Associated with the 2-D Frame Model

Since floor slabs were considered rigid in their own plane, the mass associated with the 2-D frame had to be estimated from the lateral stiffness of the frame in relation to the overall lateral stiffness of the building. A 3-D mathematical model of the building structure was used for that purpose (Uang and Maarouf 1991); the ETABS computer program (Maison and Neuss 1983) was used for structural analysis. The model was laterally loaded with the UBC seismic forces at the center of mass of each floor. A comparison of story shears resisted by the 2-D frame and the total story shears indicated that the lateral stiffness of this frame amounts to approximately 11% of the building overall lateral stiffness. Therefore, it is concluded that the effective mass associated with the selected frame is about 11% of the total building mass. A similar observation was reported by Maison and Ventura (1991).

3.3.3. Measured versus Predicted Natural Periods

Transfer function for the average horizontal accelerations between the roof and base (see Fig. 3. 3) was used to identify natural periods from the records in the 1989 Loma Prieta earthquake. (Uang and Maarouf 1991). The measured fundamental period was 2.2 seconds (or 0.46

Hz). The natural periods of vibration of the 2-D model were calculated by using the DRAIN-2DX computer program (Prakash and Powell 1992); the fundamental period is 2.2 seconds, which correlates very well with the measured one.

3.3.4. Correlation of Measured and Predicted Time History Responses

The objective of this correlation is to ensure that the mathematical model is a reasonable representation of the dynamic characteristics and strength distribution of the actual structure.

The building responses in the E-W direction were measured during the 1989 Loma Prieta earthquake by ten sensors located at the base level, 2nd, 7th, 12th floors, and the roof (see Fig. 3.4). The responses of each of these floors were recorded by two sensors located at the south and north ends of the building. Assuming the floor slabs to act as rigid diaphragms in their own plane, the relative displacement and acceleration responses of the selected frame at any instrumented floor can be calculated from the floor geometry. For example, the frame roof displacement time history, D_{roof}, can be calculated as

$$D_{roof} = 0.33D_4 + 0.67D_5 \tag{3.4}$$

where D_4 and D_5 are the roof displacement records at sensor locations 4 and 5, respectively (see Fig. 3.5). Relative displacement of the instrumented floors was calculated by subtracting the base displacement from the absolute floor displacement.

The acceleration record at the base level was used as input motion for nonlinear dynamic analyses by using the computer program DRAIN-2DX. Both dead and live loads tributary to the 2-D frame were first applied to the structure. The live load was assumed to be 50% of the design live load; the UBC live load reduction was also considered.

The computed response showed that some members were very close to reaching the yield moment. Fig. 3.6 shows that the computed and measured relative displacement responses correlated very well for the first 20 seconds during which the peak response occurred. After that time the magnitude of computed displacements is smaller than the measured ones. This discrepancy might result form the beating phenomenon which has been observed in the recorded building response (Papageorgiou and Lin 1989). Because the beating phenomenon results from the

coupling of torsional and translational modes, it cannot be reproduced in the 2-D analysis.

3.3.5. Structural Overstrength and Failure Mechanism

To investigate the frame's actual lateral strength and the associated failure mechanism, the model was loaded monotonically by two types of lateral load patterns. Prior to applying lateral loads, dead and reduced live loads were applied to the frame to simulate the gravity load effects.

The first pattern was the UBC lateral load pattern. The analysis shows that the frame has a very high structural overstrength; this is expected as the original design was governed by drift limits (Uang and Maarouf 1991). Fig. 3.7 shows that the failure occurred at a base shear ratio of $6.8C_w$, where C_w (= 0.043) is the UBC design base shear ratio. The first plastic hinge occurred at a base shear ratio of $4.5C_w$. Fig. 3.8 indicates that the frame exhibits a partial collapse mechanism (from the base to the seventh floor) with basically a weak-beam, strong-column performance.

The actual failure mechanism and the associated structural overstrength (or ultimate strength) is a function of the lateral load pattern, which is not exactly known during severe earthquakes. Hence, a "uniform" lateral load pattern in which the lateral force at each floor is proportional to its mass was used to investigate the trend of the failure mechanism and overstrength. Fig. 3.7 shows that the failure mechanism associated with this load pattern is formed between the base and fourth floor. The first plastic hinge occurred at a base shear ratio equal to $5.2C_w$ and the structure was rendered unstable when the base shear ratio reaches $8.2C_w$, which is higher than that produced by the triangular load pattern. The idealized elastic-perfectly plastic load versus deformation relationship is assumed to have a yield base shear ratio (C_y) of approximately $6C_w$; that is, the overstrength factor (Ω_w) is as high as 6. This high overstrength is expected to limit the ductility demand at the level of severe design earthquake, which is assumed to produce an elastic base shear ratio of $12C_w$, i.e., 2 times C_y. The required ductility reduction factor, R_μ, as calculated from Eq. 2.2 is consequently as low as 2.0.

3.4. Estimating DAF for Roof and Story Drifts

3.4.1. Earthquake Scale Factors

The 2-D frame has a fundamental period of 2.2 seconds. The average *PSA* in the period range of 2.0 to 2.4 seconds was calculated for each of the eight earthquake records. As previously indicated, the earthquake scale factor is defined as the ratio between the average *PSA* of each earthquake, expressed in terms of g, and the UBC design base shear ratio.

Since this structure has a very high structural overstrength, the earthquake acceleration records had to be scaled significantly high to produce sufficient plastic deformation and ductility demand which are compatible with those expected in UBC. For example, the 1940 El Centro (ELC) record had to be scaled by a factor of 5.2 to produce a ductility reduction factor, R_μ, of about 4.2; this scale factor corresponds to a *PGA* of 1.8 g. For earthquakes like the Parkfield record (PAR) with low response spectral ordinates in long period range, the *PGA* at $PSA/C_w = 25$ (or $R_\mu = 4.2$) is equal to 3.5 g.

3.4.2. DAF for Roof Drift

To calculate the *DAF* for estimating maximum roof drift, eight scaled earthquake records were used as input ground motions in the nonlinear dynamic analysis. Figs. 3.9 through 3.16 show a summary of the computed responses of the frame for the eight earthquakes; one data point in each plot was calculated from one nonlinear dynamic analysis. In each of these figures, the extent of global deformation, expressed in terms of the roof drift ratio, is demonstrated in Fig. (a). Fig. (b) shows the variation of the *DAF/FRF* ratio, which is calculated from Eq. 2.12, as a function of the earthquake scale factor. The earthquake scale factor is represented by PSA/C_w as well as R_μ. In these figures, it is assumed that the overstrength factor Ω_w calculated from the static collapse analysis is a reasonable estimate of the actual overstrength that can be developed during earthquake excitations.

The figures show that, other than the Parkfield (PAR) earthquake record, the *DAF/FRF* ratio is less than one as the earthquake intensity is increased. Impulse-type earthquakes like the PAC, PAR, and IVC records are similar to "standard" earthquakes as far as the *DAF* is

concerned. Earthquakes like the IVC with a relatively long predominant period is not much different from earthquakes like the LPSC record with a short predominant period.

Fig. 3.17 shows the mean results for eight earthquakes. It shows that the mean roof drift ratio at $C_e/C_w = 12$, which is the intensity of the UBC severe design earthquake in regions of high seismicity, is on the order of 1.3%. At this level of excitation, the average DAF/FRF ratio is about 0.87. As the earthquake intensity increases, the DAF/FRF ratio decreases slightly; this ratio stabilizes around 0.8 when the ductility reduction factor, R_μ, exceeds 3. For similar frames which do not have significant structural overstrength an R_μ value of 3 or higher may be required in severe earthquakes. For these frames, the appropriate DAF for estimating maximum roof drift should not be less than $0.8FRF$.

To investigate the uncertainty associated with the analysis results, the coefficients of variation (COV) for roof drift ratio and DAF/FRF ratio were calculated (see Figs. 3.18a and b). The COV for both roof drift ratio and DAF/FRF ratio is less than 0.2. This is a reasonable level of variation considering the uncertainties involved in earthquake engineering in general.

3.4.3. DAF for Story Drift

Figs. 3.9 through 3.16 also show the DAF_{cr}/FRF (in figure c) as well as DAF/FRF (in figure d) ratios for story drifts. The figures indicate that the DAF_{cr}/FRF and DAF/FRF ratios are generally not equal. Obviously, this indicates that the maximum elastic and inelastic story drift ratios do not necessarily occur in the same story. Therefore, the DAF_{cr} is expected to be smaller than the DAF as discussed in Chapter II. A comparison of results of eight earthquakes indicates that impulse-type earthquakes like PAC, PAR, and IVC records are likely to be associated with similar DAF and DAF_{cr} for moderate ductility reduction. It implies that for this type of earthquakes the story with the maximum elastic story drift ratio is more likely to be the one with the maximum inelastic story drift ratio. Comparing results from LPSC, which has a short predominant period, and IVC, which has a relatively long predominant period, demonstrates that the effect of earthquake predominant period is insignificant on the DAF; the difference observed in case of DAF_{cr} is attributed to the impulse-type characteristics of the IVC record.

The figures show that for six of the eight earthquakes, the maximum *DAF* is larger than 1.0 when R_μ exceeds 3. The *DAF* tends to increase with the earthquake scale factor. This tendency is clearly shown from the average results in Figs. 3.17c and d. It also suggests that the average DAF_{cr}/FRF ratio is practically equal to 1.0. The average *DAF* from eight earthquakes at $C_e/C_w = 12$ is equal to $1.1FRF$. Within the practical range of ductility demand ($R_\mu = 3 \sim 4$), the average *DAF* is about $1.2FRF$. The COV associated with these results is on the order of 0.25 (see Figs. 3.18c and d). The results suggest that neither DAF_{cr} nor *DAF* should be taken less than *FRF*. The UBC approach of using a *DAF*/*FRF* ratio equal to 0.375 is too low for this type of long period structure.

3.5. Correlation with SDOF System

The objective of this correlation is to investigate whether the preceding results for an MDOF system can be predicted by an SDOF system having the same natural period and damping ratio. The analysis was performed by using the NONSPEC computer program (Mahin and Lin 1983); the same set of earthquake ground motions was used as input motions.

The average *DAF*/*FRF* ratio of the SDOF system together with the *DAF*/*FRF* ratio of the MDOF system are shown in Fig. 3.19. It indicates that the *DAF* derived from the SDOF system is very similar to the *DAF* for estimating maximum roof drift of the MDOF system. For estimating story drift in the MDOF system, however, the *DAF* as derived from the SDOF system is too low (i.e., unconservative).

3.6. Conclusions

Based on the results presented above, the following conclusions can be drawn for the 13-story building CSMIP 57357.

(1) The *DAF* for estimating roof drift should not be less than $0.8FRF$.

(2) For estimating story drifts, DAF_{cr} and *DAF* should not be less than *FRF* and $1.2FRF$, respectively.

(3) The earthquake predominant period has an insignificant effect on the *DAF* of this long period structure.

(4) Impulse type earthquakes were found to be similar to "standard" earthquakes as far as the *DAF* is concerned.

(5) The SDOF model gave a reasonable estimate of *DAF* for roof drift; but it significantly underestimated the *DAF* for story drifts.

Chapter 4

Berkeley 2-Story Hospital Building

4.1. Building Description

4.1.1. General Layout

This is a steel building which consists of two stories and a basement (see Fig. 4.1). It is located in Berkeley, California, at a distance of 78 miles from the epicenter of the Loma Prieta earthquake. The building, which is designated as CSMIP 58496, was designed in 1984. The building is rectangular in plan with minor irregularity in the south-west corner (see Fig. 4.2). The basement of the building is surrounded by reinforced concrete shear walls. Except for the north end wall which is 12-in. thick with minor openings, the basement shear walls are 18-in. thick. The basement is not exactly underneath the super-structure; it is slightly shifted towards the south. The roof of the building has a mechanical room and a plaza with heavy landscape, concrete curb walls, planted as well as paved areas. The building facade consists of precast concrete panels.

4.1.2. Structural System

Typical floor system of the building consists of metal deck with 2.5-in. reinforced stone concrete fill supported by steel frames. The lateral-force-resisting system of the structure consists primarily of two eccentrically braced frames (EBF) in the N-S and E-W directions, respectively (see Fig 4.3). Each of these frames has three braced bays extending from the first floor above the ground level to the roof. Lateral forces in the EBF are transmitted to the basement shear walls through the first floor slab and horizontal steel trusses. Moment-resisting steel frames parallel to the EBF also resist lateral loads. A36 steel is used for beams and columns, and ASTM A500 Grade B structural tubing is used for braces. The building foundation is a 3-ft. thick reinforced concrete mat founded on alluvial soil.

4.2. Review of the UBC Seismic Design

4.2.1. Building Reactive Weight

It is assumed that the reactive weight of the building includes all the dead load of the structure, as well as an additional 20 pounds per square foot for partitions, ceiling, or anything else that might be tied down to the floors. The reactive weight of the first floor is estimated to be 1,600 kips. For the roof, which includes an elevator room, mechanical room, and heavy landscape, the reactive weight is 2,550 kips. The reactive weight, W, of the building above ground level was estimated to be 4,150 kips.

4.2.2. 1982 UBC Design Base Shear

According to the 1982 UBC, the minimum design base shear, V, was calculated from the following formula:

$$V = ZKICSW \tag{4.1}$$

where Z (= 1.0) is the zone factor, K (= 1.0) is the building system coefficient, and I (=1.5) is the importance factor. The factor C was calculated from the following formula:

$$C = \frac{1}{15\ T^{1/2}} \leq 0.12 \tag{4.2}$$

The fundamental period, T, of the building in Eq. 4.2 was calculated as

$$T = \frac{0.05 h_n}{D^{1/2}} \quad \text{or} \quad 0.1N \tag{4.3}$$

where h_n is the building height in feet, D is the dimension of the building in feet in a direction parallel to the applied lateral seismic forces, and N is the number of stories. The period computed from Eq. 4.3 is equal to 0.11 or 0.20 seconds. Using the latter value, the C factor is equal to 0.12. The soil factor S (= 1.17) was calculated from the following formula:

$$S = 1.0 + \frac{T}{T_s} - 0.5\left(\frac{T}{T_s}\right)^2 \tag{4.4}$$

where T_s (= 1.1 sec.), as indicated in the design drawing, is the estimated characteristic site

period. The design base shear V is equal to 872 kips (or the design base shear ratio is equal to 21%).

4.2.3. 1991 UBC Design Base Shear

As the lateral-force-resisting system consists of steel EBF with special moment-resisting frame, the building can be classified by UBC as a dual system with R_w equal to 12. The period T of the building in both directions is calculated as

$$T = 0.02(h_n)^{3/4} = 0.22 \text{ seconds} \tag{4.5}$$

According to Eqs. 3.1 and 3.2, given that the seismic zone factor Z is equal to 0.4, the importance factor I is equal to 1.25 (hospital building), and the soil factor S is taken as 1.5 (alluvial soil), the minimum design base shear V is equal 477 kips (or the base shear ratio is equal to 11.5%).

One can notice that the original design base shear is almost twice that of the 1991 UBC. It indicates that the original building design was very conservative.

4.3. Mathematical Model of the Building

4.3.1. Modeling Method and Assumptions

The frames in the E-W direction were chosen for 2-D dynamic analysis. The 2-D mathematical model included two EBF and one moment-resisting frame (see Fig. 4.3). Fig 4.3 shows that the frame bracing does not continue to the building foundation. Instead, the horizontal shear force from the two stories above ground level is transmitted through the first floor slab and horizontal steel trusses to the shear walls surrounding the building basement. Since the in-plane stiffness of the basement reinforced concrete shear walls is much larger than the lateral stiffness of the super-structure, it is possible to simplify the mathematical model by assuming the shear walls to act as rigid lateral supports for the super-structure.

It was assumed that floors are rigid in their own plane; floor mass was lumped at the floor levels. Since no shear connectors between girders and slabs were used in the original building design, composite action was not considered. Column bases were assumed to be fixed to the

foundation. The columns and girders were rigidly framed together by welded connections. A 50% rigid-end zone was used to model the panel zone flexibility of the rigid connections. Member strain hardening was not considered, although test results indicate that strain hardening can be significant in shear links (Kasai and Popov 1986). For dynamic analyses, the Rayleigh damping which is proportional to the mass and initial stiffness matrices was used. A 5% of critical damping was assigned to the first and second modes.

4.3.2. Measured versus Predicted Natural Periods

The building response in the E-W direction was measured during the 1989 Loma Prieta earthquake by seven sensors. Two sensors are positioned on each floor to measure the response of the two EBF (see Fig. 4.2). The basement response in this direction was recorded by a single sensor (sensor 12) located between the two EBF; the *PGA* is 0.12 *g*. Fig. 4.4 shows the measured acceleration records in the E-W direction.

As the basement shear walls are relatively rigid, the responses of the first floor and base were very similar. Therefore, transfer function of the average horizontal accelerations between the roof and the first floor (see Fig. 4.5) was used to identify the natural periods. The identified fundamental period was 0.3 seconds (2.9 Hz). The natural periods of the mathematical model were calculated from the computer program DRAIN-2DX. The building mass, which is not easy to estimate accurately due to the nature of roof landscape, was calibrated so that the fundamental period of the model is identical to the measured one (0.3 sec.) It should be noted that the mass "adjustment" was minimal and was within 5% difference of the initial mass estimate from design drawings.

4.3.3. Correlation of Measured and Predicted Responses

The relative displacements of the second floor and the roof were calculated by subtracting the first floor displacement from the absolute displacement records. Fig. 4.6a shows that relative displacement response contained low frequency noises; noise below 0.5 Hz was filtered numerically (see Fig. 4.6b) for this correlation study.

The first floor acceleration record was used as input motion for nonlinear dynamic analyses. Both dead and live loads which were tributary to the members were first applied to the model. The live load was assumed to be 50% of the design live load.

Member yielding was not observed in the computed response. Fig. 4.7 shows that reasonable correlation of floor responses could be achieved.

4.3.4. Structural Overstrength and Failure Mechanism

Two types of lateral load patterns were applied to the structure. Prior to applying lateral loads, dead and reduced live loads were applied to the structure to simulate the gravity load effect.

Fig. 4.8 shows that collapse occurred at base shear ratios equal to 6.8 C_w and 7.0 C_w for the UBC and "uniform" lateral load patterns, respectively, where C_w (= 0.115) is the 1991 UBC design base shear ratio. The first plastic hinge occurred at a base shear ratio equal to 4.2 C_w and 4.3 C_w for the UBC and uniform load patterns, respectively. The failure mode for both load patterns is a global mechanism above the first floor level. The idealized elastic-perfectly plastic load versus deformation relationship is assumed to have a yield base shear ratio (C_y) of 6.3C_w; that is, the overstrength factor (Ω_w) is 6.3. This high overstrength is expected to reduce the ductility demand for severe design earthquakes, which is assumed to produce an elastic base shear ratio of 12C_w. The ductility reduction factor, R_μ, as calculated from Eq. 2.2 is therefore as low as 1.9.

4.4. Estimating DAF for Roof and Story Drifts

4.4.1. Earthquake Scale Factors

The building model has a fundamental period of 0.3 seconds. For such a stiff structure, the average *PSA* for a period range of 0.1 to 0.5 seconds (in log scale) was calculated for each of the eight earthquake records. As previously defined, the earthquake scale factor is defined as the ratio between the average *PSA* and the UBC design base shear ratio. It is worth noting that the scale factor for this structure is proportional to the effective peak acceleration (EPA), since the latter is also calculated in the same period range as (ATC 1978):

$$EPA = \frac{\text{average of } PSA}{2.5} \tag{4.6}$$

Since this structure was conservatively designed, it has a very high overstrength factor; therefore the earthquake acceleration records had to be scaled significantly high to produce sufficient plastic deformation and ductility demand compatible with those implicitly assumed in seismic provisions. For example, the ELC record had to be scaled by a factor of 3.6 to produce a ductility reduction factor (R_μ) of 3.4; this scale factor corresponds to an *EPA* of 1.0 *g* (or a *PGA* of 1.26 *g*).

4.4.2. DAF for Roof Drift

To calculate the *DAF* for estimating maximum roof drift, eight scaled earthquake records were used as input ground motions in the nonlinear dynamic analysis. Figs. 4.9 through 4.16 show a summary of the computed response of the building. The figures show that the *DAF*/*FRF* ratio tends to be less than one at low earthquake intensities. At high earthquake intensities, the *DAF*/*FRF* ratio tends to increase (except for the LPSC record). At a scale factor PSA/C_w of 20, five out of the eight figures show that the *DAF* is larger than *FRF*. The three impulse-type earthquakes (PAC, PAR, and IVC) require a *DAF* which is greater than *FRF* at higher earthquake intensities.

Earthquakes like the IVC record with a relatively long predominant period (T_g) are very different from earthquakes like the LPSC record with a short predominant period. The IVC record, which has the longest predominant period among the eight records, requires the largest *DAF*/*FRF* ratio at higher earthquake intensities. This is different from what was observed in building CSMIP 57357, which has a 2.2 sec. fundamental period. It appears that the *DAF*/*FRF* ratio for MDOF systems is a function of the ratio between the building fundamental period and the earthquake predominant period, not the fundamental period of the building alone.

Fig. 4.17 shows the mean results for eight earthquakes. The figure shows that the mean roof drift ratio at $C_e/C_w = 12$, which is the UBC severe design earthquake level, is on the order of 0.5%. At the same level of excitation, the average *DAF* is about $0.82FRF$. The *DAF*/*FRF* ratio tends to increase slightly at higher earthquake intensities. If this building were not conservatively

designed, the overstrength may not be that high and the ductility demand may require that an R_μ equal to 3 or higher be developed. Then the appropriate *DAF* for estimating roof drift will be equal to *FRF*. It should be noted that the *DAF* for this type of short period structure is relatively higher than that of the long period structure CSMIP 57357; the *DAF* of building CSMIP 57357 was only $0.8FRF$ at the same level of earthquake excitation.

To investigate the uncertainty associated with the results, the coefficients of variation (COV) for roof drift ratio and *DAF/FRF* ratio were calculated (see Fig. 4.18). The COV for both roof drift ratio and *DAF/FRF* ratio is less than 0.3. This is slightly larger than the COV of the 13-story building CSMIP 57357. Considering the sensitivity of structural response in the short period range, this level of variation is expected.

4.4.3. DAF for Story Drift

Figs. 4.9 through 4.16 also show the DAF_{cr}/FRF (in figure c) as well as *DAF/FRF* (in figure d) ratios for estimating maximum story drifts. The figures indicate that the DAF_{cr}/FRF and *DAF/FRF* ratios are identical; it implies that the maximum elastic and inelastic story drifts occur in the same story. Except for the 1989 Loma Prieta records (LPSC and LPC) — both of them have very short predominant periods — the *DAF* exceeds the *FRF*. The *DAF* for story drift estimations is generally higher than that required for roof drift estimations, although this building has only two stories. Impulse-type earthquakes like PAC, PAR, and IVC records are not much different from "standard" earthquakes as far as the *DAF* is concerned. As in the case of *DAF* for estimating roof drift, earthquakes with a relatively long predominant period like the IVC record is very different from earthquakes with a short predominant period like the LPSC record. The IVC record, which has the longest predominant period among the eight records, resulted in the largest *DAF/FRF* ratio at higher earthquake intensities.

The mean results for the eight earthquakes in Fig. 4.17 show that the *DAF* is practically equal to the *FRF*, although the *DAF* tends to increase slightly with earthquake intensities. The COV associated with these results is on the order of 0.3 (see Fig. 4.18).

Since the *DAF* for building CSMIP 57357 is calculated as the maximum of thirteen stories, and the damage is more likely to concentrate in a particular story as the number of stories is

increased, it appears from the results of buildings CSMIP 57357 and 58496 that the *DAF* for estimating story drifts could be larger for taller buildings. Nevertheless, this is not true for the *DAF* of roof drift.

4.5. Correlation with SDOF System

The same set of earthquake records was used to perform nonlinear dynamic analysis of an SDOF oscillator having a 0.3-second natural period and 5% critical damping. The average *DAF/FRF* ratio for the SDOF system is plotted together with those of the MDOF system of CSMIP 58496 (see Fig. 4.19). Although the trends of the *DAF/FRF* ratios are similar, the figure shows that the SDOF model tends to overestimate the *DAF* for the MDOF model. Fig. 4.19 also shows the *DAF/FRF* ratio as derived from the Newmark-Hall's equal energy concept (see Eq. 2.9). Apparently the equal energy concept for the SDOF system is too conservative to estimate the *DAF* for this short period building.

4.6. Conclusions

Based on the results presented above, the following conclusions can be drawn for the 2-story building CSMIP 58496.

(1) The *DAF* for both roof and story drifts should not be taken less than *FRF*.

(2) The ratio between the fundamental period of the structure and earthquake predominant period has a significant effect on the *DAF*.

(3) Impulse type earthquakes were found to be similar to "standard" earthquakes as far as the *DAF* is concerned.

(4) The *DAF* as derived from the SDOF system overestimates the *DAF* of this stiff building. The Newmark-Hall's equal energy concept also significantly overestimates the *DAF* for this building.

Chapter 5

San Jose 10-Story Commercial Building

5.1. Building Description

5.1.1. General Layout

This 10-story Commercial Building is designated as CSMIP 57355 (see Fig. 5.1). It is located in the City of San Jose, California, at a distance of 20 miles from the epicenter of the Loma Prieta earthquake. This building was designed in 1964 and constructed in 1967. The building is regular in plan and elevation (see Fig. 5.2).

5.1.2. Structural System

The vertical-load-carrying system consists of reinforced concrete one-way slabs supported by concrete pan joists and reinforced concrete frames. In the transverse (E-W) direction, the lateral-force-resisting system of the structure consists of two exterior reinforced concrete shear walls and six interior reinforced concrete frames. In the longitudinal (N-S) direction, the lateral-force-resisting system is composed of two exterior and two interior reinforced concrete frames. The building is founded on alluvial soil with a base dimension of 190 ft by 96 ft. The foundations of the structure is a 5-foot mat at one story level below grade. The materials used for construction of the building are light-weight concrete for the slabs and 5,000 psi normal-weight concrete for the walls and frames. The steel reinforcement varies from Grade 40 in the upper stories to Grade 60 in the lower stories.

5.2. Review of the UBC Seismic Design

5.2.1. Building Reactive Weight

The reactive weight of the building includes all the dead load of the slabs, walls, as well as additional 15 pounds per square foot for partitions, ceiling, or anything else that might be tied down to the floors. The reactive weights for the typical floors and roof were estimated to be 2,500 and 2,200 kips, respectively. The reactive weight of the building, W, was estimated to be 24,500 kips.

5.2.2. UBC Design Base Shear

The original design base shear, V, according to the 1964 UBC is equal to 2,146 kips; the design base shear ratio is 8.7% (Uang and Maarouf 1991). The building can be classified by the 1991 UBC as a reinforced concrete moment-resisting frame with R_w equal to 12. The period T of the building in both directions is calculated as

$$T = 0.03(h_n)^{3/4} = 1.1 \text{ seconds} \tag{5.1}$$

According to Eqs. 3.1 and 3.2, given that the seismic zone factor Z is equal to 0.4, the importance factor I is equal to 1.0 , and the soil factor S is 1.5 (alluvial soil), the minimum design base shear V is equal to 1,428 kips (or the base shear ratio is equal to 5.8%). As the base shear of the original design is about 50% larger than the 1991 UBC design base shear, the building is expected to satisfy the latest UBC.

5.3. Mathematical Model of the Building

5.3.1. Modeling Method and Assumptions

A 2-D interior frame in the N-S direction was selected for extensive study. Based on the design drawings, a 2-D mathematical model was established (see Fig. 5.3). Floor mass was lumped at the floor levels. Since it was assumed that floors are rigid in their own plane, the horizontal degrees of freedom of all the joints on each floor were slaved to a single horizontal degree of freedom.

Moment-curvature diagrams for the beams and moment-axial force interaction diagrams for the columns were constructed using the computer program UNCOLA (Kaba and Mahin 1983). Fig. 5.4a shows the idealized stress-strain relationship of concrete. Steel reinforcement was assumed to have an elastic-perfectly plastic stress-strain relationship. The moment-curvature diagrams of the beams were idealized by bilinear relationships (see Fig. 5.4b), which were used to model the beam strength in the DRAIN-2DX computer program (Prakash and Powell 1992). The reinforced concrete columns were assumed to reach the ultimate moment capacity at a concrete strain of 0.003. Fig. 5.4c shows a typical moment-axial force interaction diagram for a column in the first story. The column bases were assumed to be fixed at the foundation. The contribution of shear walls, which are located at the east and west sides of the building, to the lateral strength and stiffness of exterior columns were considered in the analysis; the ACI recommendations for the effective width of T-beam sections were used for this purpose.

For dynamic analyses the Rayleigh damping which is proportional to the mass and initial stiffness matrices was used. A 5% of critical damping is assigned to the first two modes. To examine the effect of stiffness degradation of reinforced concrete structures, the Takeda model (Riddell and Newmark 1979) was used to model the reinforced concrete elements. Since the extent of stiffness degradation is dependent on the earthquake intensity, number of yielding reversals, member confinement, etc., the beam-column element without stiffness degradation was also used to model the upper bound stiffness of the structure.

5.3.2. Mass Associated with the 2-D Frame Model

Since floor slabs were considered rigid in their own plane, the mass associated with the 2-D frame had to be estimated from the lateral stiffness of the frame in relation to the overall lateral stiffness of the building. A 3-D mathematical model of the building structure was used for this purpose (Uang and Maarouf 1991). The model was laterally loaded with the UBC seismic lateral load profile at the center of mass of each floor. A comparison of story shear forces developed in the 2-D frame and total story shears indicated that the lateral stiffness of this frame amounts to approximately 19% of the building overall lateral stiffness. Therefore, it is concluded that the effective mass associated with the selected 2-D frame is 19% of the total building mass.

5.3.3. Measured versus Computed Natural Periods

Transfer function for the average horizontal accelerations between the roof and base (see Fig. 5. 5) was used to identify natural periods from the records in the 1989 Loma Prieta earthquake (Uang and Maarouf 1991). The "average" fundamental period in the N-S direction was 1.0 second.

The DRAIN-2DX computer program was used to calculate the natural periods of the model. It is understood that lateral stiffness of reinforced concrete structures deteriorates with concrete cracking that develops during earthquake excitations and consequently the fundamental period lengthens. The amount of stiffness loss and period lengthening is dependent on the magnitude of deformations that take place during earthquakes. Accordingly, the lateral stiffness (or fundamental period) of a typical reinforced concrete structure is not unique throughout the earthquake excitation and the building life time in general. Period lengthening on the order of 50% has been reported for concrete structures during severe earthquakes (Hart et al. 1975, Freeman et al. 1980). For example, the fundamental period of this building was identified as 0.82 seconds from the initial portion of the response recorded during the 1984 Morgan Hill earthquake (Papageorgiou and Lin 1989). Therefore, the fundamental period has lengthened by 17% after the 1989 Loma Prieta earthquake.

Using the gross stiffness of the uncracked concrete members, the fundamental period of the mathematical model was found to be 0.83 seconds, which is in a good agreement with the period measured during the 1984 Morgan Hill earthquake. To match the period (= 1.0 second) measured during the 1989 Loma Prieta earthquake, the stiffness of the mathematical model had to be decreased by 25%. This magnitude of stiffness loss is reasonable, given the moderate intensity of excitation during this earthquake.

5.3.4. Correlation of Measured and Predicted Responses

The building response in the N-S direction was measured during the 1989 Loma Prieta earthquake by three sensors located on the roof, fifth floor, and basement (see Fig. 5.2). Fig. 5.6 shows the recorded accelerations of these floors. Relative displacements of the instrumented floors were calculated by subtracting the base displacement from their absolute displacement

records. Because a low frequency noise was observed in the relative displacement time histories, frequency contents up to 0.6 Hz. have been filtered numerically.

The acceleration record at the basement level was used as input motion for nonlinear dynamic analyses. In the analysis, both dead and live loads were first applied to the frame. The live load was assumed to be 50% of the design live load; the UBC live load reduction was also considered.

The analytical response indicated that the structure remained elastic. A few beams exceeded their yield moments (defined by tension reinforcement yielding), but none has reached the ultimate moment capacity. Given the complex nature of response of reinforced concrete structures, Fig. 5.7 shows that computed displacements correlate reasonably well with the measured responses.

5.3.5. Structural Overstrength and Failure Mechanism

The building model was loaded by two types of lateral load patterns up to failure. Prior to applying lateral loads, dead and reduced live loads were applied to the frame to simulate the gravity load effect.

The first one was the UBC "triangular" load pattern. Fig. 5.8 shows that the failure occurred at a base shear ratio of $4.1C_w$, where C_w (= 0.058) is the UBC design base shear ratio. The first plastic hinge occurred at a base shear ratio of $2.1C_w$. The failure mechanism shown in the same figure indicates that the frame exhibits a partial collapse mechanism which runs from the base to the seventh floor.

For the "uniform" lateral load pattern wherein the seismic force at each floor is proportional to its reactive weight, Fig. 5.8 shows that the failure mechanism also runs from the base to the seventh floor. The first plastic hinge occurred at a base shear ratio of $2.2C_w$ and the structure became unstable at $4.7C_w$. The idealized elastic-perfectly plastic load-deformation relationship is assumed to have a yield base shear ratio (C_y) of approximately $3.9C_w$; that is, the overstrength factor (Ω_w) is equal to 3.9. At the level of the UBC severe design earthquake, which corresponds to an elastic base shear ratio of $12C_w$, the ductility reduction factor (R_μ) as calculated from Eq. 2.2 is consequently equal to 3.1 (= 12/3.9).

5.4. Estimating DAF for Roof and Story Drifts

5.4.1. Stiffness Assumptions for UBC Design

As mentioned earlier, the lateral stiffness of reinforced concrete structures deteriorates during earthquake excitations. The reduction of lateral stiffness depends on the severity of ground shaking. Therefore, the mathematical model which correlated reasonably well with the recorded building response during the Loma Prieta earthquake may be inappropriate to simulate the condition of lateral stiffness during severe earthquakes. Since the objective of this study is to develop a *DAF* to estimate maximum drifts which may develop in severe design earthquakes, the assumptions used in the calculation of elastic design drifts should be examined first.

The stiffness assumptions affect the nature periods of the mathematical model, which in turn affect the design base shear and consequently the elastic design drifts. To simplify the problem of whether to use uncracked stiffness (stiffness calculated from the gross moment of inertia of member cross-sections) or some kind of reduced (cracked) stiffness, the UBC and ACI ("Building" 1989) allow the designer to use any set of "reasonable" assumptions as long as these assumptions are consistent throughout the analysis. It should be noted that although the design base shear may be lower if reduced stiffness is used, the corresponding story drifts are always larger than those computed from uncracked stiffness. This can be demonstrated as follows.

Assume that the generalized lateral stiffness, K_g, of the structure based on the gross moment of inertia is reduced to K_r by a factor r as follows:

$$K_r = r\, K_g \tag{5.2}$$

The ratio between the roof drift Δ_r based on K_r and the roof drift Δ_g based on K_g can be calculated from Fig. 5.9 as follows:

$$\frac{\Delta_r}{\Delta_g} = \frac{\dfrac{C_r}{K_r}}{\dfrac{C_g}{K_g}} = \frac{K_g C_r}{K_r C_g} \tag{5.3}$$

where C_g and C_r are the design base shear ratios corresponding to the gross and reduced

stiffnesses, respectively. Substituting Eq. 5.2 into Eq. 5.3 gives

$$\frac{\Delta_r}{\Delta_g} = \frac{C_r}{r\,C_g} \tag{5.4}$$

Since the UBC design base shear ratio is inversely proportional to $T^{2/3}$ — which is true as long as the period of the structure is not too short — it follows that

$$\frac{C_r}{C_g} = \left(\frac{T_g}{T_r}\right)^{2/3} = \left(\frac{K_r}{K_g}\right)^{2/3} \tag{5.5}$$

where T_g and T_r are the fundamental periods based on gross and cracked sections, respectively. Substituting Eqs. 5.5 and 5.2 into Eq. 5.4 gives

$$\frac{\Delta_r}{\Delta_g} = \frac{1}{r}\left(\frac{K_r}{K_g}\right)^{2/3} = \frac{1}{r^{1/3}} \tag{5.6}$$

Since the r factor is no larger than one, it can be concluded from the above equation that the reduced stiffness assumption will always produce a conservative (i.e., larger) estimate of elastic design drifts. Furthermore, Freeman et al. (1980) suggested that half of the uncracked stiffness be used as the reduced stiffness for severe earthquakes. Therefore, the calculation of elastic and inelastic drifts in this study will be based on a mathematical model with 50% of the uncracked stiffness. The corresponding fundamental period of this model is equal to 1.2 seconds.

5.4.2. Earthquake Scale Factors

The average *PSA* for a period range from 1.0 to 1.4 seconds was calculated for each of the eight earthquake records. The earthquake records were scaled such that the ductility demand, expressed in terms of R_μ, on the order of 4 could be developed. To develop an R_μ equal to 4.5 for example, the LPSC record had to be scaled by a factor of 18; on the other hand, the scale factor for the PAC record was only 0.94.

5.4.3. DAF for Roof Drift

Figs. 5.10 to 5.17 show a summary of the computed responses of the frame for the eight earthquakes; the results for both the models with and without stiffness degradation are presented. The figures show that, except for the LPC earthquake record, the *DAF* tends to be less than *FRF*. The effect of stiffness degradation on roof drift is minimal. The three impulse-type earthquakes (PAC, PAR, and IVC) show very similar response curves as the others, although they tend to produce a smaller *DAF*. Earthquakes like the IVC record with a relatively long predominant period is not much different from earthquakes with a short predominant period. This is similar to that observed in building CSMIP 57357, which has a 2.2-second fundamental period.

Fig. 5.18 shows the mean results for eight earthquakes. The figure shows that the mean roof drift ratio at $C_e/C_w = 12$ (or $R_\mu = 3.1$), which is the UBC severe design earthquake level, is on the order of 0.75%. At the same level of excitation, the average *DAF* is about $0.82FRF$. The *DAF/FRF* ratio stabilizes at 0.82 as the earthquake intensity is increased. The figure shows that stiffness degradation does not produce a larger roof drift in an average sense. Fig. 5.19 shows that the COV for the *DAF/FRF* ratio is less than 0.26.

5.4.4. DAF for Story Drift

Figs. 5.10 to 5.17 also show the DAF_{cr}/FRF (in figure c) as well as *DAF/FRF* (in figure d) ratios for estimating maximum story drifts. The figures indicate that the DAF_{cr}/FRF and *DAF/FRF* ratios are not the same, which indicates that maximum elastic and inelastic story drift ratios do not occur in the same story. Except for the three impulse-type earthquakes (PAC, PAR, and IVC), the *DAF/FRF* ratio increases with the earthquake intensity. As in the case of estimating roof drift, these impulse-type earthquakes produce the smallest *DAF/FRF* ratio at higher earthquake intensities. The *DAF* for story drift is generally higher than that for roof drift. Earthquakes like the IVC record with a relatively long predominant period produce a *DAF* not much different from other earthquakes. The stiffness degrading model produces a *DAF* which is only about 10% higher than the model without stiffness degradation.

The mean results for the eight earthquakes in Fig. 5.18 show that the DAF_{cr} is practically equal to *FRF*. The *DAF*, however, is larger than the *FRF*. At C_e/C_w equal to 12 (or $R_\mu = 3.1$),

the *DAF/FRF* ratio is equal to 1.2 (or 1.3 for stiffness degrading model). The COV associated with these results is less than 0.25 (see Fig. 5.19).

5.5. Correlation with SDOF System

To correlate the preceding results with an SDOF system, the same set of earthquakes was used to perform nonlinear dynamic analysis of an oscillator having a natural period of 1.2 seconds and 5% critical damping; stiffness degradation was not considered for the SDOF oscillator. The average *DAF/FRF* ratio for the SDOF system is plotted together with those of the MDOF system in Fig. 5.20. The figure shows that the results for the SDOF system are consistent with the equal displacement concept as proposed by Newmark and Hall (1973). Nevertheless, the results as predicted from the SDOF system underestimate the *DAF* for story drift and overestimate the *DAF* for roof drift of the MDOF system.

5.6. Conclusions

Based on the results presented above, the following conclusions can be drawn for the 10-story building CSMIP 57355.

(1) The *DAF* for roof drift is equal to $0.82FRF$ and for story drift is equal to $1.2FRF$.

(2) The effect of stiffness degradation increases the *DAF* for story drift by only 10%; its effect on the *DAF* for roof drift is minimal.

(3) Impulse-type earthquakes do not produce a higher *DAF*; instead, the *DAF* tends to decrease at higher earthquake intensities.

(4) The *DAF* as derived from the SDOF system is consistent with the Newmark-Hall's equal displacement concept. But it underestimates the *DAF* for story drift and overestimates the *DAF* for roof drift estimations of this 10-story reinforced concrete building.

Chapter 6

San Bruno 6-story Office Building

6.1. Building Description

6.1.1. General Layout

This 6-story Office Building is designated as CSMIP 58490 (see Fig. 6.1). It is located in the City of San Bruno, California, at a distance of about 50 miles from the epicenter of the 1989 Loma Prieta earthquake. CSMIP 58490 was designed in 1977 (according to the 1973 UBC) and constructed in 1978. The building has a rectangular plan and no irregularity is observed in the elevation or plan of the structure (see Fig. 6.2).

6.1.2. Structural System

The vertical-load-carrying system consists of reinforced concrete one-way slabs supported by precast post-tensioned reinforced concrete beams. The beams are supported by reinforced concrete columns. In the transverse (E-W) direction, the lateral-force-resisting system of the structure consists of two exterior and one interior moment-resisting reinforced concrete frames; the interior frame is slightly offset to the south end. In the longitudinal (N-S) direction, the lateral-force-resisting system is composed of two exterior moment-resisting reinforced concrete frames. The building is founded on stiff soil with a base dimension of 200 ft by 90 ft. The foundations of the structure consists of reinforced concrete spread footings. The materials used for the construction of the building are: 4,000 psi light-weight concrete for the slabs, 5,000 psi normal-weight concrete for beams and columns, and Grade 60 steel reinforcement. The dimensions and steel reinforcement of columns and beams are constant along the building height.

6.2. Review of the UBC Seismic Design

6.2.1. Building Reactive Weight

The reactive weight of the building includes all the dead load of the slabs, walls, as well as additional 20 pounds per square foot for partitions, ceiling, or anything else that might be tied down to the floors. The reactive weights for the typical floors and roof are 2,200 and 1,860 kips, respectively. The reactive weight of the building, W, was estimated to be 12,860 kips.

6.2.2. 1973 UBC Design Base Shear

According to the 1973 UBC, the minimum design base shear V was calculated by the following formula:

$$V = ZKCSW \tag{6.1}$$

where Z (= 1.0) is the zone factor, K (= 0.67 for ductile moment frame) is the building system coefficient, and S is the soil factor (= 1.0 for stiff soil). The factor C was calculated by the following formula:

$$C = \frac{0.05}{T^{1/3}} \tag{6.2}$$

The fundamental period T of the building was calculated as

$$T = \frac{0.05 h_n}{D^{1/2}} \text{ or } 0.1N \tag{6.3}$$

The period computed from Eq. 6.3 in the N-S direction, which is the direction of dynamic analysis in this study, is equal to 0.27 or 0.60 seconds. Using the more realistic value for T (= 0.6 seconds), the design base shear is equal to 508 kips and the design base shear ratio is equal to 3.95%.

6.2.3. 1991 UBC Design Base Shear

The building can be classified by UBC as a reinforced concrete moment-resisting frame with R_w equal to 12. The period T of the building as calculated from Eq. 5.1 is equal to 0.8 seconds in both directions. According to Eqs. 3.1 and 3.2, given that the seismic zone factor Z is

equal to 0.4, the importance factor I is equal to 1.0, and the soil factor S is taken as 1.0 (stiff soil), the minimum design base shear V is equal to 628 kips (or the base shear ratio is equal to 4.88%). Therefore the 1991 design base shear is 24% larger than that of the 1973 UBC.

6.3. Mathematical Model of the Building

6.3.1. Modeling Method and Assumptions

For the purpose of this study, one of the two exterior frames in the N-S direction was modeled. Based on the design drawings of the building, a 2-D mathematical model was established (see Fig. 6. 3). Floor mass was assumed to be lumped at the floor levels. Since it was assumed that floors are rigid in their own plane, the horizontal degrees of freedom at each floor were slaved to a single horizontal degree of freedom.

Moment-curvature diagrams for the beams and moment-axial force interaction diagrams for the columns were constructed by using the computer program UNCOLA (Kaba and Mahin 1983). The same concrete and steel stress-strain relationships for building CSMIP 57355 (see Fig. 5.4) were used. The ACI recommendations for the effective width of T-beam sections were used in the analysis. The column bases were assumed to be fixed to the foundation.

For dynamic analyses Rayleigh damping which is proportional to the mass and initial stiffness matrices was used. A 5% of critical damping is assigned to the first two modes. To examine the effect of stiffness degradation, both beam-column elements with degrading and non-degrading stiffnesses were used. Since lateral forces in the N-S direction are resisted by two identical moment frames, one half of the total building mass was assigned to the mathematical model.

6.3.2. Measured versus Predicted Natural Periods

Transfer function for the average horizontal accelerations between the roof and base (see Fig. 6. 4) was used to identify natural periods from the records in the 1989 Loma Prieta earthquake. The identified fundamental period in the N-S direction has a value of 0.8 seconds (or 1.2 Hz).

The computer program DRAIN-2DX was used to calculate the natural periods of the mathematical model. Using the uncracked stiffness, the fundamental period of the mathematical model was found to be 0.76 seconds. To match the period (0.8 seconds) measured during the Loma Prieta earthquake, the stiffness of the members had to be decreased by 18%. This magnitude of stiffness loss is reasonable, given the moderate intensity of excitation during this earthquake.

6.3.3. Correlation of Measured and Predicted Responses

The building response in the N-S direction was measured during the 1989 Loma Prieta earthquake by four sensors located on the roof, fifth, second, and ground floors (see Fig. 6.2). Fig. 6.5 shows the recorded accelerations of these four floors. Relative displacements of the instrumented floors were calculated by subtracting the ground floor displacement from their absolute displacement records.

The acceleration record at the ground level was used as input motion for the nonlinear dynamic analysis. Both dead and live loads were first applied to the frame in the analysis. The live load was assumed to be 50% of the design live load.

Fig. 6.6 shows that the computed displacements correlate reasonably well with the measured ones in the first 30 seconds. The analytically predicted response indicated that some of the first story members might have yielded during the Loma Prieta earthquake.

6.3.4. Structural Overstrength and Failure Mechanism

The building model was loaded by two types of lateral load patterns up to failure. Prior to applying lateral loads, dead and reduced live loads were applied to the frame to simulate the gravity load effect.

The first one was the UBC "triangular" load pattern. Fig. 6.7 shows that the failure occurred at a base shear ratio of $2.58C_w$, where C_w (= 0.0488) is the UBC design base shear ratio. The first plastic hinge occurred at a base shear ratio of $1.56C_w$. Since the column and beam strengths are approximately constant along the height of the building, the failure mechanism shown in Fig. 6.7 consists of a soft first story.

For the "uniform" lateral load pattern, Fig. 6.7 shows that the failure mechanism is also concentrated in the first story. The first plastic hinge occurred at a base shear ratio equal to $1.6C_w$ and the structure became unstable at a base shear ratio of $2.66C_w$, which is slightly larger than the collapse base shear ratio produced by the triangular load pattern. The idealized elastic-perfectly plastic load versus deformation relationship is assumed to have a yield base shear ratio (C_y) of $2.6C_w$; that is, the overstrength factor (Ω_w) is 2.6 — the lowest among the four buildings studied in this project.

At the UBC severe design earthquake level, which corresponds to an elastic base shear ratio of $12C_w$, the ductility reduction factor, R_μ, as calculated from Eq. 2.2 is equal to 4.6 (= 12/2.6). The ductility demand of this building is higher than the other three buildings.

6.4. Estimating DAF for Roof and Story Drifts

6.4.1. Cracked Stiffness of the Mathematical Model

To consider the stiffness deterioration and period elongation expected from severe earthquake excitations, the calculations of elastic and inelastic drifts were based on a mathematical model with 50% of the uncracked stiffness. The fundamental period of this model is therefore equal to 1.1 seconds.

6.4.2. Earthquake Scale Factors

The average *PSA* for a period range from 0.9 to 1.3 seconds was calculated for each of the eight earthquake records. Since the structural overstrength of this building is relatively low, the earthquake scale factors are not as high as those of the other three buildings. The earthquake records were scaled such that the ductility demand, expressed in terms of R_μ, on the order of 4 could be developed. To develop an R_μ equal to 4.6 for example, the LPSC record had to be scaled by a factor of 12. On the other hand, the scale factor for the PAC record was only 0.53.

6.4.3. DAF for Roof Drift

Figs. 6.8 to 6.15 show a summary of the computed responses of the frame for the eight earthquakes; the results for both the models with and without stiffness degradation are presented. The figures show that the *DAF/FRF* ratio is generally less than one at low earthquake intensities and then tends to increase with earthquake intensities. This ratio exceeds 1.5 for the OLY earthquake record.

The effect of stiffness degradation is significant in many cases. The three impulse-type earthquakes (PAC, PAR, and IVC) show similar response curves; at high earthquake intensities, the *DAF* for the stiffness degrading model is larger than that without stiffness degradation. This is not the case for the other five "standard" earthquakes.

Earthquakes like the IVC record with a relatively long predominant period are not much different from earthquakes like the PAC and PAR records with a short predominant period. This is similar to those observed in buildings CSMIP 57357 and CSMIP 57355, which have fundamental periods of 2.2 and 1.2 seconds, respectively.

Fig. 6.16 shows the mean results for eight earthquakes. The figure shows that the mean roof drift ratio at $C_e/C_w = 12$ (or $R_\mu = 4.6$), which corresponds to the UBC severe design earthquake level, is on the order of 0.9%. At the same level of excitation, the average *DAF/FRF* ratios are about 0.8 and 0.85 for the stiffness degrading and non-degrading models, respectively. In other words, the *DAF* for estimating maximum roof drift is insensitive to stiffness degradation. Fig. 6.17 shows that the COV for the *DAF/FRF* ratio of roof drift is less than 0.25 and is relatively higher for the model without stiffness degradation.

6.4.4. DAF for Story Drift

Figs. 6.8 to 6.15 also show the DAF_{cr}/FRF (in figure c) as well as *DAF/FRF* (in figure d) ratios for story drifts. The figures indicate that the DAF_{cr}/FRF and *DAF/FRF* ratios are equal, indicating that the maximum elastic and inelastic story drifts occur in the same story. This is expected from the static collapse analysis since the building has a soft first story failure mechanism. Because plastic deformations are concentrated in the first story, the *DAF/FRF* ratio is generally high.

Stiffness degradation has a significant effect on the *DAF* of this building. The degradation of lateral stiffness in the first soft story leads to larger deformations with repeated yielding reversals. The three impulse-type earthquakes (PAC, PAR, and IVC) are not different from "standard" earthquakes as all of them produce significant yielding in the first story.

The mean results from the eight earthquakes in Fig. 6.16 show that the DAF_{cr} and *DAF* are larger than *FRF*. At C_e/C_w equal to 12 (or $R_\mu = 4.6$), the *DAF* is equal to $1.7FRF$ and $1.3FRF$ for models with and without stiffness degradation, respectively. The COV associated with these results is on the order of 0.4; a COV of this magnitude implies that the *DAF* of such a high value might not be conservative for structures with a soft first story.

6.5. Correlation with SDOF System

To correlate the preceding results of an MDOF system to the response of an SDOF system, nonlinear dynamic analysis of an oscillator having a natural period of 1.1 seconds and 5% critical damping was conducted. Stiffness degradation was not considered in the analysis. The average *DAF/FRF* ratio for the SDOF system is plotted together with the *DAF/FRF* ratios of the MDOF system (see Fig. 6.18). The figure shows that the *DAF* as derived from the SDOF system is very similar to the *DAF* for estimating roof drift. This is very similar to that observed in building CSMIP 57357. Nevertheless, the *DAF* for the SDOF system significantly underestimates the *DAF* for story drift estimations of the MDOF system.

6.6. Conclusions

Based on the results presented above, the following conclusions can be drawn for the 10-story building CSMIP 58490.

(1) Nonlinear static analyses indicate that this 6-story building has a soft first story.

(2) The *DAF* for roof drift estimations is about $0.8FRF$; the effect of stiffness degradation on *DAF* is minimal.

(3) Because the damage is concentrated in the soft first story, the *DAF* for story drift estimations is as high as $1.7FRF$ if stiffness degradation is considered. Otherwise the *DAF* is about $1.3FRF$.

(4) Impulse-type earthquakes do not seem to increase the *DAF* value. The effect of the earthquake predominant period on the *DAF* is also insignificant for this 6-story frame.

(5) The *DAF* as derived from the SDOF system is very similar to that for estimating maximum roof drift of the MDOF system; but it significantly underestimates the *DAF* required to estimate maximum story drift of this 6-story frame.

Chapter 7

Factors Affecting the Displacement Amplification Factor

7.1. Introduction

It has been shown in the previous chapters that the ratio between *DAF* and *FRF* is generally much larger than that used in the UBC. The study has also shown that the *DAF* for roof and story drifts is not constant and is affected by several factors. Based on the results of four buildings, the effects of structural overstrength, types of collapse mechanism, stiffness degradation, damping, fundamental period, and earthquake characteristics (impulse versus "standard" type earthquakes, strong motion duration, earthquake predominant period) on the *DAF* are investigated in this chapter. The reliability of using a *DAF* as derived from single-degree-of-freedom (SDOF) systems or shear building models (i.e., "stick" models) for practical design will also be studied.

7.2. Effect of Structural Overstrength

From Eq. 2.4, the structural overstrength factor, Ω_w, and the structural ductility reduction factor, R_μ, are related by the following for a given *FRF*:

$$R_\mu = \frac{FRF}{\Omega_w} \tag{7.1}$$

As the *FRF* (or R_w in UBC) is constant for a given building system (= 12 for the four CSMIP buildings considered in this study), the above relationship shows that the ductility demand (R_μ) is inversely proportional to the structural overstrength (Ω_w).

A structure which has a very large overstrength ($\Omega_w \geq FRF$) will remain elastic at the UBC severe design earthquake level; thus, the *DAF*/*FRF* ratio will be equal to one. For a structure with a low structural overstrength (Ω_w), the ductility demand (R_μ) is higher. The *DAF*/*FRF* ratio deviates from one once the structure undergoes inelastic deformation.

Figs. 3.17, 4.17, 5.18, and 6.16 show that as the ductility demand (R_μ) is increased (or the structural overstrength, Ω_w, is low), the mean DAF_{cr}/*FRF* and *DAF*/*FRF* ratios for story drift

increase (with insignificant deviation from this rule in Fig. 5.18c). In other words, a larger *DAF* should be used for structures with low structural overstrength. Unfortunately, the current seismic design practice in the United States does not require designers to quantify structural overstrength, although some other codes like the Japanese Code (IAEE 1988) and the Eurocode (ECCS 1988) do require so (Uang 1991b).

These figures also show that the mean *DAF/FRF* ratio for roof drift gets smaller than one as R_μ increases (or Ω_w decreases). The ratio reaches a certain lower bound — a level which is still much higher than the three-eights adopted by the UBC — and it tends to increase with R_μ. The figures show that the structural overstrength at which the trend is reversed gets smaller as the fundamental period of the structure gets shorter (see Table 2.4 for fundamental periods).

7.3. Effect of Types of Collapse Mechanisms

The collapse mechanism of a structure under monotonically increasing static lateral loading is generally not unique; it varies with the profile of the lateral load. Nevertheless, a collapse mechanism based on the UBC lateral load profile (or even a "uniform" load pattern which is proportional to the mass distribution) can give an indication of the potential mechanisms that develop during severe earthquakes. While a global mechanism means that plastic deformations, or damage in general, are uniformly distributed, systems with a soft story mechanism suffer from damage concentration during intense earthquake excitations.

Buildings CSMIP 57355 and 58490 are ductile reinforced concrete moment frames with approximately the same fundamental period. The main difference between these two buildings is the collapse mechanism. While the 10-story building CSMIP 57355 has a partial collapse mechanism which extends from the base to the seventh floor, the 6-story CSMIP 58490 has a soft first story. At the same ductility demand (R_μ) level, a comparison of the mean *DAF/FRF* ratios in Figs. 5.18 and 6.16 shows that the *DAF* for a system with a soft story is larger than that with a partial mechanism. At an R_μ equal to 4, the *DAF/FRF* ratios for roof drift (with stiffness degradation) are about the same for both buildings. For estimating story drift, the DAF_{cr}/FRF ratio of CSMIP 57355 is equal to 1.1 while for CSMIP 58490 it is 1.6. The *DAF/FRF* ratio for story drift of CSMIP 57355 is equal to 1.3 but for CSMIP 58490 it is 1.6. This comparison shows that

the displacement amplification factor for systems with a soft story mechanism may be 45% higher than those without a soft story mechanism.

7.4. Effect of Shear Building Modeling Assumptions

Because of its simplicity, "shear" building model (or "stick" model) has been popularly used by researchers to study the seismic performance of multistory structures. This type of modeling is characterized by "lumping" the stiffness and strength of the structure in each story; only one degree of freedom is assigned at each floor level. In shear buildings it is difficult to avoid damage concentration after yielding because plastic deformations tend to accumulate in a small part of the structure. Hence, the *DAF* is expected to be high. The objective of this section is to compare the *DAF* derived from previous chapters with those derived from the shear building models.

Hwang and Jaw (1989) used shear building model to perform nonlinear dynamic analysis in their statistical study of the response modification factor for reinforced concrete buildings. The research which included nonlinear analysis of twelve structural models using ninety synthetic earthquake records resulted in the following relationship:

$$\ln\left(\frac{C_e}{C_y}\right) = \left(e^{-0.1857(T/T_g)} - e^{-2.1673(T/T_g)} - 0.0276\xi\right) \ln \mu_s \tag{7.2}$$

where ξ is the damping ratio, μ_s is the system ductility factor as determined from the maximum story drift ductility factor, and T_g is the predominant period of the ground motion. In another statistical analysis of the displacement amplification factor for reinforced concrete structures, Hwang et al. (1989) reported that

$$\ln\left(\frac{\Delta_{max}}{\Delta_e}\right) = 0.414 \ln \mu_s \tag{7.3}$$

Since Δ_{max}/Δ_e is equal to DAF/FRF (see Eq. 2.16), the above equation can be rewritten as

$$\ln\left(\frac{DAF}{FRF}\right) = 0.414 \ln \mu_s \tag{7.4}$$

Eliminating μ_s from Eqs. 7.2 and 7.4 gives the following:

$$\ln\left(\frac{C_e}{C_y}\right) = 2.415\left(e^{-0.1857(T/T_g)} - e^{-2.1673(T/T_g)} - 0.0276\xi\right)\ln\left(\frac{DAF}{FRF}\right) \qquad (7.5)$$

Replacing C_e/C_y by R_μ (see Eq. 2.2) gives

$$\ln R_\mu = 2.415\left(e^{-0.1857(T/T_g)} - e^{-2.1673(T/T_g)} - 0.0276\xi\right)\ln\left(\frac{DAF}{FRF}\right) \qquad (7.6)$$

For a shear building model with a 5% damping ratio and a T/T_g ratio equal to 2.0, which is the mean ratio for building CSMIP 58490 based on the set of earthquake records used, the *DAF/FRF* ratio from Eq. 7.6 is

$$\frac{DAF}{FRF} = R_\mu^{0.614} \qquad (7.7)$$

This ratio is compared with the mean *DAF/FRF* ratio for story drift of CSMIP 58490 (with stiffness degradation) in Fig. 7.1. It is observed that both results show a similar trend, i.e., the *DAF/FRF* ratio increases with the ductility demand, which is expressed in terms of R_μ. Nevertheless, the shear building model significantly overestimates the *DAF/FRF* ratio. Therefore, special care should be taken when interpreting the results derived from the shear building model.

7.5. Effect of Stiffness Degradation

Stiffness degradation is generally observed in the response of reinforced concrete structures. The Takeda model (Riddell and Newmark 1979) which simulates stiffness degradation was used in this study to model beams and columns of two reinforced concrete buildings (CSMIP 57355 and CSMIP 58490).

A comparison of the *DAF/FRF* ratios in Fig. 5.18 of the 10-story CSMIP 57355 shows that the effect of stiffness degradation is insignificant for systems without a soft story mechanism. The *DAF/FRF* ratio for roof drift is practically not affected. The DAF_{cr}/FRF and *DAF/FRF* ratios for story drift are slightly increased.

For the 6-story CSMIP 58490, which has a soft first story, Fig. 6.16 also shows that the effect of stiffness degradation on the *DAF/FRF* ratio of roof drift is minimal. Nevertheless, stiffness degradation has a dramatic effect on the DAF_{cr}/FRF or *DAF/FRF* ratio of story drift; the *DAF* is increased considerably as can be seen from Fig. 7.2.

The conclusion drawn from this limited comparison is that stiffness degradation has a negligible influence on the *DAF* in general, unless a soft story is developed. For building CSMIP 58490, stiffness degradation increases the *DAF* by as much as 40% at the UBC severe design earthquake level.

7.6. Effect of Damping

Damping in building structures is known to increase with response amplitude. Newmark and Hall (1982) recommended that for reinforced concrete structures the damping ratio at the working stress level may be taken as 3% to 5% of critical damping; this ratio can be increased to 7% to 10% if the structure were to reach yielding. Because an increase of damping may result in smaller response amplitudes, higher damping ratios associated with yielding may help to reduce the *DAF*.

The 10-story building CSMIP 57357 was selected to investigate the effect of increased damping on *DAF*. The elastic response was computed from the 5% damping model, while the inelastic response was computed from the 10% damping model. The same set of earthquakes was used in the analysis; stiffness degradation was not considered.

Figs. 7.3 and 7.4 show the responses from ELC and TAF earthquake records. Both figures indicate that increasing the damping ratio from 5% to 10% for nonlinear analysis lowers the *DAF*/*FRF* ratio in general and this favorable effect should not be neglected. The mean results for the eight earthquakes (see Fig. 7.5) show that increasing damping lowers the *DAF* of roof and story drifts by 13%.

7.7. Effect of Fundamental Period

Elastic and inelastic responses of a building structure depend to a great extent on its fundamental period. To investigate the dependence of *DAF* on the structure's fundamental period, results of buildings CSMIP 58496 (T = 0.3 sec.), 57355 (T = 1.2 sec.) and 57357 (T = 2.2 sec.) are compared. These buildings represent short, intermediate, and long period structures, respectively. They also have similar collapse mechanisms. Building CSMIP 58490 is excluded from the comparison because it has a distinct soft story mechanism. In this comparison, models

without stiffness degradation were considered. To eliminate the effect of structural overstrength variations among these buildings, the comparison is based on the constant ductility reduction factor, R_μ.

Fig. 7.6 shows the variation of *DAF/FRF* ratios with fundamental period. It is observed that, for the set of earthquake records used in this study, the *DAF/FRF* ratios are insensitive to the period of the structure. For the stiff CSMIP 58496 building (T = 0.3 sec.), the higher *DAF/FRF* ratio which was expected from the Newmark and Hall's equal energy concept for SDOF systems was not observed. It should be noted that according to a statistical study of the shear building model conducted by Hwang et al. (1989), the *DAF/FRF* ratio was also found to be independent of the fundamental period of the structure (see Eq. 7.4). Their findings are consistent with the results of this study.

7.8. Effect of Earthquake Characteristics

7.8.1. Duration of Earthquake Strong Motion

To study the effect of earthquake duration on the displacement amplification factor, three artificial earthquake records with different durations but with similar elastic response spectra were used as input ground motions for the dynamic analysis of building CSMIP 57357. These artificial earthquakes were generated by the computer program SIMQKE (Gasparini and Vanmarcke 1976). The elastic response spectra of these earthquakes are similar to the response spectrum derived from the UBC equation for design base shear (soil type S_3). Durations of strong motion are 20, 25, and 30 seconds, respectively (see Fig. 7.7). The *PGA* of the three earthquake records (before scaling) was set to 0.4 g.

The *DAF/FRF* ratios for estimating roof and story drifts are presented in Fig. 7.8. A comparison of these *DAF/FRF* ratios shows that the *DAF* for roof drift is unaffected by the strong motion duration. For story drift estimations, a longer duration tends to increase slightly the *DAF*.

7.8.2. Impulse Type Earthquake Ground Motions

It has been shown that impulse type earthquake ground motions, which are characterized by long-duration acceleration pulses, are particularly damaging to certain types of structures (Mahin and Bertero 1981, Anderson and Bertero 1987). The eight earthquake records used in this study included three impulse-type records (PAC, PAR, and IVC). It was observed, however, that there is no consistent trend in *DAF* that makes these earthquakes different from other "standard" earthquakes. For the 13-story building CSMIP 57357, these earthquakes have insignificant effect on the *DAF*. For buildings CSMIP 58496 and 58490, although the *DAF* of roof drift is larger at higher earthquake intensities, the *DAF* for story drift is similar to that derived from "standard" earthquake records. For building CSMIP 57355 the *DAF* of roof drift as well as story drift is even smaller for impulse-type earthquakes.

7.8.3. Structural Fundamental Period versus Earthquake Predominant Period

The earthquake predominant period (T_g) is calculated from the pseudo-velocity (*PSV*) response spectrum. By idealizing the *PSV* spectrum (10% damping) as a bi-linear curve, T_g is defined as the period at which the two straight lines intersect. This period is approximately equal to the period at the intersection of constant-velocity and constant-acceleration regions of the earthquake response spectrum. Soft site earthquake records usually have a large T_g while rock site records are associated with a small T_g. Fig. 7.9 shows the *PSV* spectra and T_g of the eight earthquake records.

It has been shown that the earthquake input energy to a structure is associated with pseudo-velocity (Housner 1956). As a structure yields, its fundamental period increases. While structures with a fundamental period shorter than T_g attracts more input energy after yielding, structures whose fundamental period is longer than T_g will not attract more input energy after it yields (Akiyama 1985). Therefore, structures with a fundamental period shorter than T_g are expected to have a *DAF* which is larger than those with a period which is longer than T_g.

Shimazaki and Sozen (1984) indicated that the T/T_g ratio is a key parameter to correlate the *DAF* of SDOF systems. It was observed in their study that for stiffness degrading SDOF systems with 2% damping the Δ_{max} is larger than or equal to Δ_e (i.e., $DAF/FRF \geq 1$) if the summation of

T/T_g and C_y/C_e (= $1/R_\mu$ according to Eq. 2.2) satisfies the following relationship:

$$\frac{T}{T_g} + \frac{1}{R_\mu} \leq 1 \tag{7.8}$$

To investigate how the T/T_g ratio affects the *DAF* for multistory buildings, two more records with long predominant periods were included in order to widen the range of T/T_g for this study. They are the SCT record of the 1985 Mexico City earthquake and the Point Bonita (BON) record of the 1989 Loma Prieta earthquake. Fig. 7.10 shows the acceleration time histories, pseudo-acceleration, and pseudo-velocity response spectra of these two records. The predominant periods of SCT and BON records are 2.0 and 1.5 seconds, respectively. To obtain the smallest T/T_g ratio, these two records were used as input ground motions to the two-story model (CSMIP 58496) with a fundamental period of 0.3 seconds. Figs. 7.11 and 7.12 indicate that the roof drift ratio and the *DAF/FRF* ratios are very high. The SCT record was also used as input motion for building CSMIP 57357, which has a fundamental period slightly longer than the T_g of SCT record. Fig. 7.13 shows that the difference of *DAF* between CSMIP 57357 (with $T/T_g = 1.1$) and CSMIP 58496 (with $T/T_g = 0.15$) is dramatic.

Fig. 7.14 compares the *DAF/FRF* ratio of roof drift for building CSMIP 58496; the T/T_g ratio ranges from 0.15 to 0.68. The figure clearly indicates that for small T/T_g ratios, the *DAF* can significantly exceed *FRF*. Fig. 7.15 shows the change of *DAF/FRF* ratio with T/T_g for the four buildings. To investigate the effect of earthquake intensity relative to structural strength, several curves corresponding to different levels of ductility demand (R_μ) were presented. The figure indicates that for T/T_g greater than 0.3, the effect of T/T_g ratio on the *DAF/FRF* ratio is minimal. In other words, the *DAF* can be taken as constant as long as the fundamental period of the structure is no less than $0.3T_g$. Taking the UBC design response spectra as an example, Fig. 7.16 shows that the T_g used by UBC is equal to 0.4 and 0.9 seconds for stiff soils and soft clays, respectively. Therefore, the *DAF* will be significantly higher than *FRF* only when the fundamental period of the structure is less than 0.12 and 0.36 seconds for stiff soils and soft clays, respectively.

If T/T_g is less than 0.3, the *DAF/FRF* ratio increases dramatically with the increase of the ductility demand. It should be noted that for the *DAF/FRF* ratio to be larger than one, Eq. 7.8 as proposed by Shimazaki and Sozen for SDOF systems requires that the T/T_g ratio should be less than 1/2, 2/3, and 3/4 for R_μ equal to 2, 3, and 4, respectively. Nevertheless, this relationship was not observed in Fig. 7.15 for multistory frames. For *DAF/FRF* ratio to be significantly larger than one, Fig. 7.15 shows that the T/T_g ratio should be even smaller (= 0. 3).

To conclude, the *DAF/FRF* ratio can be significantly larger than 1.0 only when the T/T_g ratio is smaller than a threshold value. Based on the results of this study, this threshold value is about 0.3, a value which is significantly smaller than that proposed by Shimazaki and Sozen (1984) for SDOF systems. Based on the UBC response spectra, the T_g for soil type 3 is equal to 0.9 seconds. Under such circumstances, a *DAF* which is much higher than *FRF* is needed only for structures whose fundamental period is equal to or less than 0.27 seconds.

Chapter 8

Summary, Conclusions and Recommendations

8.1. Summary

A review of the Uniform Building Code (UBC) of the U.S.A., the National Building Code of Canada, the Mexico Code, and the Eurocode indicates that the ratios between displacement amplification factor (*DAF*) and force reduction factor (*FRF*) vary considerably from one code to another. The UBC, which uses R_w as the *FRF*, assigns $3R_w/8$ as the *DAF*. Both the Mexico Code and Eurocode use a *DAF* which is no smaller than *FRF*.

Four buildings (two steel and two reinforced concrete buildings) located in California were selected for extensive analysis. These buildings, which have been instrumented by the California Division of Mines and Geology (CDMG), are designated as CSMIP 57357, 58496, 57355, and 58490. For each building, dynamic response was computed by the computer program DRAIN-2DX. Dynamic analyses of these buildings, which have fundamental periods ranging from 0.3 to 2.2 seconds, were performed to investigate the relationship between *DAF* and *FRF*. As input motions, eight historical earthquake records whose average normalized response spectrum resembles the UBC elastic design spectrum were used in the analysis. By scaling each earthquake record to different intensities, roof and story drifts from inelastic dynamic analyses were compared to those that would develop if the structure were to respond elastically. Results from analyses of the four buildings are summarized as follows.

CSMIP 57357 (San Jose 13-story Government Office Building)

The lateral-force-resisting system of this building is a steel moment-resisting space frame (R_w = 12); the fundamental period is 2.2 seconds. A design review based on the 1991 UBC indicated that story drift limit controlled the design. A 2-D interior frame in the E-W direction was modeled for the analysis. To calibrate the properties of the 2-D model, a correlation study based on the recorded response from the 1989 Loma Prieta earthquake was first conducted. Nonlinear

static analyses were also conducted to determine the lateral strength of the building. The analysis indicated that the lateral strength of the building significantly exceeds the UBC seismic design strength. The failure mechanism is initiated at the base and continues to the seventh floor. The results from dynamic analyses indicated that the *DAF* for estimating roof drift should not be less than $0.8FRF$. For estimating story drifts, *DAF* and DAF_{cr} (as defined in Eqs. 2.14 and 2.15) should not be taken less than 1.2 and 1.0 of the *FRF*, respectively. It was also shown that the earthquake predominant period has an insignificant effect on the *DAF* of this long period structure. Impulse type earthquakes were found to be similar to "standard" earthquakes as far as the *DAF* is concerned. *DAF* tend to be equal. Three artificial earthquake records were also used to study the effect of strong motion duration on *DAF*; it was found that the *DAF* increases only slightly with the earthquake strong motion duration.

CSMIP 58496 (Berkeley 2-story Hospital Building)

The lateral-force-resisting system of this hospital building consists of two eccentrically braced and one moment-resisting steel frames in the E-W direction; the fundamental period is 0.3 seconds. The lateral strength of the building is 6.3 times that of the UBC prescribed design base shear.

The analysis results indicated that the *DAF* for estimating both roof and story drifts should not be taken less than *FRF*. The analysis also showed that the ratio between the fundamental period of the structure and the earthquake predominant period may have a significant effect on the *DAF*. The *DAF* required for impulse-type earthquakes was similar to that of "standard" earthquakes.

CSMIP 57355 (San Jose 10-story Commercial Building)

The lateral-force-resisting system of this building consists of four reinforced concrete ductile moment-resisting frames in the N-S direction; the fundamental period is 1.0 second. The ultimate base shear of this building is about four times the UBC prescribed design base shear. The building has a partial failure mechanism (from the base to the seventh floor). Takeda model was used to simulate the stiffness degradation of structure members.

At an earthquake intensity similar to the UBC severe design earthquake, the results indicated that the *DAF* for roof drift is 0.82 *FRF*. For story drift, the DAF_{cr} and *DAF* are equal to *FRF* and $1.2FRF$, respectively.

The effect of earthquake predominant period on the *DAF* is insignificant. Impulse-type earthquakes were found to produce a smaller *DAF* than that of "standard" earthquakes. Stiffness degradation tends to increase slightly the *DAF*. Assuming that the damping ratios are increased from 5% to 10% to account for large amplitude vibrations in severe earthquakes, the *DAF* which is required to amplify the elastic deformations of a 5% damping model can be reduced. It was found that the favorable effect of increased damping can lower the *DAF* by 13%.

CSMIP 58490 (San Bruno 6-story Office Building)

The lateral-force-resisting system of this building consists of a perimeter moment-resisting frame; the fundamental period is about 0.8 seconds in the N-S direction. Lateral displacements computed from the 2-D mathematical model correlated well with those measured during the Loma Prieta earthquake; results from dynamic analysis indicated that yielding might have occurred in a number of beams. The structural overstrength of this building is relatively low, which is expected for perimeter frame systems. The ultimate base shear of the building is 2.6 times the UBC prescribed design base shear. The failure mechanism consists of a soft first story; this is associated with the fact that the same cross sections and same amount of reinforcements were used for both beams and columns along the height of the building.

At an earthquake intensity similar to the UBC severe design earthquake, results from models with and without stiffness degradation show that the *DAF* for roof drift are about $0.8FRF$ and $0.85FRF$, respectively. The *DAF* for story drift is equal to $1.7FRF$ and 1.3 *FRF* for models with and without stiffness degradation, respectively. These relatively high ratios result from the damage concentration in the soft first story.

The effect of stiffness degradation significantly increases the *DAF* for story drift, but only slightly increases the *DAF* for roof drift. The *DAF* required for impulse-type earthquakes is similar to that required for "standard" earthquakes.

8.2. Conclusions

Based on the observed dynamic responses of four planar frames subjected to eight historical earthquake records, the following conclusions can be drawn.

1. The *DAF/FRF* ratio is equal to one by definition if a structure has a very large structural overstrength such that it will not yield under severe earthquakes. As the structural overstrength gets smaller, the ductility demand is increased and the *DAF/FRF* ratio deviates from unity.

2. The mean *DAF/FRF* ratio for roof drift gets smaller than one as the ductility demand, expressed in terms of the ductility reduction factor (R_μ), is increased. After the *DAF/FRF* ratio reaches a certain lower bound, which is still much higher than the three-eights as adopted by the UBC, this trend is reversed. Within the practical range of ductility demand ($R_\mu = 2 \sim 4$), the *DAF/FRF* ratio is approximately equal to 0.8.

3. The mean DAF_{cr}/FRF and *DAF/FRF* ratios for story drift are generally no smaller than one and they increase with ductility demand. Within the practical range of ductility demand, the DAF_{cr}/FRF ratio is approximately equal to one if the structure does not have a soft story. Otherwise, a DAF_{cr}/FRF ratio as high as 1.7 has been observed. The *DAF/FRF* ratio is generally higher than DAF_{cr}/FRF. As design engineers are primarily concerned about the maximum story drift ratio, regardless of the story in which it will occur, the DAF_{cr} rather than the more conservative *DAF* should be used for design purposes.

4. Types of failure mechanisms do not seem to affect the *DAF/FRF* ratio of roof drift, although this is not true for the *DAF/FRF* ratio of story drift; the effect is especially significant when a soft story exists. While the DAF_{cr}/FRF ratio is equal to 1.0 for the 10-story frame (CSMIP 57355), this ratio is increased to 1.3 for the 6-story perimeter frame (CSMIP 58490) which has a soft first story.

5. Stiffness degradation does not seem to affect the *DAF/FRF* ratio of roof drift either. This is also true for the *DAF/FRF* ratio of story drift, except when stiffness degradation is combined with a soft story formation. Because of stiffness degradation, the DAF_{cr}/FRF ratio for the 6-story perimeter frame (CSMIP 58490) is increased from 1.3 to 1.7.

6. An increase of damping ratio from 5% at the elastic level to 10% at the inelastic level to account for larger amplitude vibrations lowers the *DAF/FRF* ratio for roof and story drifts of building CSMIP 57355 by 13%.

7. The *DAF/FRF* ratio can be significantly larger than one only when the T/T_g ratio is smaller than a threshold value. Based on the results of this study, this threshold value is about 0.3, a value which is significantly smaller than that proposed by Shimazaki and Sozen (1984) for SDOF systems. For the set of California earthquake records used, this explains why the *DAF/FRF* ratios for a stiff structure (T = 0.3 sec.) and a flexible structure (T = 2.2 sec.) are similar. Based on the UBC design response spectra, the T_g for soil type 3 (soft soils) is equal to 0.9 seconds. Under such circumstances, a *DAF* which is much higher than *FRF* is needed only for structures whose fundamental period is equal to or less than 0.27 (= 0.9×0.3) seconds.

8. The correlation of the *DAF/FRF* ratios between SDOF and MDOF systems is not conclusive. For estimating roof drifts, it appears that the SDOF system tends to give an upper bound estimate of the *DAF/FRF* ratio. For estimating story drifts, however, the SDOF system tends to underestimate the *DAF/FRF* ratio, although the 2-story building (CSMIP 58496) is the exception.

9. The *DAF/FRF* ratio for a shear building model (i.e., "stick" model) is much higher than that of a moment frame even if the latter has a soft story mechanism. In other words, the shear building idealization will overestimate the *DAF* which is needed for multibay, multistory buildings.

10. The *DAF/FRF* ratio is not significantly affected by the impulse-type earthquake ground motions.

11. The *DAF/FRF* ratio is slightly increased with the earthquake strong motion duration.

8.3. Recommendations

Displacement amplification factors (*DAF*) as used in the Uniform Building Code and the NEHRP Recommended Provisions are too low. This study has shown that the *DAF* for estimating roof drift can be slightly less than the force reduction factor (*FRF*), and for estimating story drift it can be much larger than *FRF*. Before a rational *DAF* which includes all the important parameters is developed, it is suggested that a *DAF* which is equal to *FRF* be adopted in seismic provisions.

REFERENCES

1. Akiyama, H., *Earthquake Resistant Limit-State Design for Buildings,* Univ. of Tokyo Press, 1985.
2. Anderson, J. C. and Bertero, V. V., "Uncertainties in Establishing Design Earthquakes," *J. Struct. Engrg.*, vol. 113, no. 8, pp. 1709-1724, ASCE, 1987.
3. ATC,, "Tentative Provisions for the Development of Seismic Regulations for Buildings," *ATC-3-06*, Applied Technology Council, Palo Alto, Calif., 1978.
4. Bertero, V. V., "Observations of Structural Pounding," *Proc. Int. Conf.: The Mexico Earthquake*, ASCE, 1986.
5. BSSC,, *NEHRP Recommended Provisions for the Development of Seismic Regulations for New Buildings,* Bldg. Seismic Safety COuncil, Washington, D.C., 1991.
6. "Building Code Requirements for Reinforced Concrete," *ACI 318-89*, Amer. Concr. Inst., Detroit, Mich., 1989.
7. Chai, J. C., "Ibrahim Time Domain Identification of Modal Parameters for Civil-Engineered Structure," *Master Thesis*, Dept. Civil Engrg., Northeastern Univ., Boston, Mass., 1991.
8. ECCS,, *European Recommendations for Steel Structures in Seismic Zones,* ECCS Technical Committee, Brussels, Belgium, 1988.
9. Freeman, S. A., Czarnecki, R. M., and Honda, K. K., "Significance of Stiffness Assumptions on Lataral Force Criteria," *Special Publication SP-63*, pp. 437-457, ACI, 1980.
10. Gasparini, D. A. and Vanmarcke, E. H., "Simulated Earthquake Motions Compatible with Prescribed Response Spectra," R76-4, Dept. of Civil Engrg., MIT, Cambridge, MA, 1976.
11. Gofnez, R. and Garcia-Ranz, F., "Complementary Technical Norms for Earthquake Resistant Design, 1987 Edition," *Earthquake Spectra*, vol. 4, no. 3, pp. 441-459, Earthquake Engrg. Res. Inst., 1988.
12. Hart, G. C., DiJulio, R. M., and Lew, M., "Torsional Response of High-Rise Buildings," *J. Struct. Div.*, vol. 102, no. ST2, pp. 397-416, ASCE, 1975.
13. Housner, G. W., "Limit Design of Structures to Resist Earthquake," *Proc. 1st World Conf. Earthquake Engrg.*, pp. 5-1 to 5-13, Berkeley, Calif., 1956.
14. Hwang, H. H. M. and Jaw, J.-W., "Statistical Evaluation of Response Modification Factors for Reinforced Concrete Structures," NCEER-89-0002, Nat. Ctr. for Earthquake Engrg. Res., State University of New York, Buffalo, New York, 1989.
15. Hwang, H. H. M., Jaw, J.-W., and Chńg, A. L., "Statistical Evaluation of Deflection Amplification Factors for Reinforced Concrete Structures," NCEER-89-0028, Nat. Ctr. for Earthquake Engrg. Res., State University of New York, Buffalo, New York, 1989.

16. IAEE,, *Earthquake Resistant Regulations - A World List,* Int. Assoc. for Earthquake Engrg., Tsukuba, Japan, 1988.

17. ICBO,, *Uniform Building Code (UBC),* Int. Conf. of Bldg. Officials, Whittier, Calif., 1991.

18. Kaba, S. A. and Mahin, S. A., "Interactive Computer Analysis Methods for Predicting the Inelastic Cyclic Behavior of Structural Sections," *Report No. UCB/EERC-83/18*, Earthquake Engrg. Res. Ctr., Univ. of California, Berkeley, 1983.

19. Kasai, K. and Popov, E. P., "General Behavior of WF Steel Shear Link Beams," *J. Struct. Engrg.*, vol. 112, no. 2, pp. 362-382, ASCE, 1986.

20. Kasai, K. and Maison, B. F., "Structural Pounding Damage due to Loma Prieta Earthquake," *Proc. 59th Annual Convention*, pp. 141-164, SEAOC, 1990.

21. Mahin, S. and Bertero, V. V., "An Evaluation of Inelastic Seismic Design Spectra," *J. Struct. Div.*, vol. 107, no. ST9, pp. 1177-1195, ASCE, 1981.

22. Mahin, S. A. and Lin, J., "Construction of Inelastic Response Spectrum for Single Degree of Freedom System," *Report No. UCB/EERC-83/17*, Earthquake Engrg. Res. Ctr., Univ. of California, Berkeley, 1983.

23. Maison, B. F. and Ventura, C. E., "Dynamic Analysis of Thirteen-Story Building," *J. Struct. Engrg.*, vol. 117, no. 12, pp. 3783-3803, ASCE, 1991.

24. Maison, B. F. and Neuss, C. F., "SUPER-ETABS: An Enhanced Version of the ETABS Program," Technical Report to the National Science Foundation, J. G. Bouwkamp, Inc., Berkeley, Calif., 1983.

25. *National Building Code of Canada (NBCC),* Nat. Res. Council Canada, Ottawa, Ontario, 1990.

26. Newmark, N. M. and Hall, W. J., *Earthquake Spectra and Design,* Earthquake Engrg. Res. Inst., 1982.

27. Newmark, N. M. and Hall, W. J., "Procedures and Criteria for Earthquake Resistant Design," *Building Science Series No. 46*, pp. 209-236, Building Practices for Disaster Mitigation, Nat. Bureau of Standards, 1973.

28. Papageorgiou, A. S. and Lin, B. C., "Influence of Lateral Load Resisting System on the Earthquake Response of Structures - A System Identification Study," *Earthquake Engrg. Struct. Dyn.*, vol. 18, pp. 799-814, 1989.

29. Popov, E. P., "U.S. Seismic Steel Codes," *Engrg. J.*, pp. 119-128, Amer. Inst. of Steel Constr., Third Quarter, 1991.

30. Prakash, V. and Powell, G. H., "DRAIN-2DX," *User Guide*, Univ. of California, Berkeley, Calif., 1992.

31. Riddell, R. and Newmark, N. M., "Statistical Analysis of the Response of Nonlinear Systems Subjected to Earthquake," *Structural Research Series No. 468*, Univ. of Illinois, Urbana, Ill., 1979.

32. SEAOC,, *Recommended Lateral Force Requirements and Commentary,* Struct. Engrs. Assoc. of Calif., San Francisco, Calif., 1990.

33. Shimazaki, K. and Sozen, M. A., "Seismic Drift of Reinforced Concrete Structures," *Technical Research Report,* pp. 145-165, Hazama-Gumi, Ltd., 1984.

34. "Structures in Seismic Regions," *Eurocode No. 8*, Commission of the European Communities, Luxembourg, 1988.

35. Tsai, K.-C. and Popov, E. P., "Seismic Panel Zone Design Effect on Elastic Story Drift in Steel Frames," *J. Struct. Engrg.*, vol. 116, no. 12, pp. 3285-3301, ASCE, 1990.

36. Uang, C.-M. and Bertero, V. V., "Earthquake Simulation Tests and Associated Studies of a 0.3-Scale Model of a 6-Story Concentrically Braced Steel Structure," *Report No. UCB/EERC-86/10*, Earthquake Engrg. Res. Ctr., Univ. of California, Berkeley, Calif., 1986.

37. Uang, C.-M., "Establishing R (or R_w) and C_d Factors for Building Seismic Provisions," *J. Struct. Engrg.*, vol. 117, no. 1, pp. 19-28, ASCE, 1991a.

38. Uang, C.-M., "Structural Overstrength and Limit State Philosophy in Seismic Design Provisions," *Report No. CE-91-1*, Final Report submitted to the NSF, Dept. of Civil Engr., Northeastern Univ., Boston, Mass., 1991b.

39. Uang, C.-M. and Maarouf, A., "An Investigation of UBC Seismic Serviceability Requirements from Building Responses Recorded during the 1989 Loma Prieta Earthquake," Final Report, Calif. Dept. of Mines and Geology, Dept. of Civil Engr., Northeastern Univ., Boston, Mass., 1991.

APPENDIX — NOTATION

The following symbols are used in this report:

C_e elastic base shear ratio produced by an earthquake ground motion;

C_w UBC design base shear ratio;

C_y yield base shear ratio;

DAF displacement amplification factor;

FRF force reduction factor;

h story height;

I importance factor;

K structural system factor (1985 UBC);

K_g lateral stiffness of an R.C. structure based on gross moment of inertia;

K_r lateral stiffness of an R.C. structure based on reduced moment of inertia;

R_μ structural (or system) ductility reduction factor;

R_w system modification factor (1991 UBC);

S UBC site coefficient for soil;

T fundamental period of structure;

T_g earthquake predominant period;

W weight of reactive masses;

Z UBC seismic zone factor;

Δ story drift;

Δ_w UBC elastic design story drift produced by seismic forces $C_w W$;

Δ_{max} maximum (inelastic) story drift produced by an earthquake ground motion;

Ω_w structural overstrength factor ($= C_y/C_w$);

μ_s structural (or system) ductility factor.

Tables

Building Code	FRF	DAF	$\frac{DAF}{FRF}$
UBC (1991)	R_w	$3R_w/8$	0.375
NBCC (1990)	$R/0.6$	R	0.6
Mexico (1987)	Q^*	Q	1.0
Eurocode (1988)	q	q	1.0

* less than Q in short period range

Table 2.1 Comparison of DAF/FRF Ratios in Seismic Codes

Framing System	$FRF\ (=R)$	$DAF\ (=C_d)$	$\frac{DAF}{FRF}\left(=\frac{C_d}{R}\right)$
Moment Resisting Frame System			
SMRF	8	5.5	0.69
OMRF	4.5	4	0.89
Dual System			
EBF + SMRF	8	4	0.5
CBF + SMRF	6	5	0.83
Building Frame System			
EBF	8	4	0.5
CBF	5	4.5	0.9
Bearing Wall System			
CBF	4	3.5	0.88
Framed Walls with Shear Panels	6.5	4	0.62
Inverted Pendulum Structures			
SMRSF	2.5	2.5	1.0
OMRSF	1.25	1.25	1.0

(a) Structural Steel System

Framing System	$FRF\ (=R)$	$DAF\ (=C_d)$	$\frac{DAF}{FRF}\left(=\frac{C_d}{R}\right)$
Moment Resisting Frame System			
SMRF	8	5.5	0.69
IMRF	5	4.5	0.9
OMRF	3	2.5	0.83
Dual System			
R.C. Shear Wall + SMRF	8	6.5	0.81
Reinforced Masonry Shear Wall + SMRF	6.5	5.5	0.85
Building Frame System			
R.C. Shear Wall	5.5	5	0.91
Reinforced Masonry Shear Wall	4.5	4	0.89
Unreinforced Masonry Shear Wall	1.5	1.5	1.0
Bearing Wall System			
R.C. Shear Wall	4.5	4	0.89
Reinforced Masonry Shear Wall	3.5	3	0.86
Unreinforced Masonry Shear Wall	1.25	1.25	1.0
Inverted Pendulum Structures			
SMRF	2.5	2.5	1.0

(b) Reinforced Concrete System

SMRF = special moment-resisting frame; OMRF = ordinary moment-resisting frame;
EBF = eccentrically braced frame; CBF = concentrically braced frame.

Table 2.2 DAF/FRF ($=C_d/R$) Ratios Used in NEHRP Recommended Provisions (1991)

Story	Story Drift Ratio (%)		$\frac{\Delta_{max}}{\Delta_w}$
	Elastic Test ($PGA = 0.063\ g$)	Inelastic Test ($PGA = 0.65\ g$)	
6th	0.14	0.66	4.7
5th	0.11	**1.89**	**17.2**
4th	**0.15**	1.20	8.0
3rd	0.12	0.81	6.8
2nd	0.11	0.83	7.5
1st	0.11	0.87	7.9

Table 2.3 Story Drift Ratios from Experimental Tests of a 6-story Braced Frame
(Uang and Bertero 1986)

CSMIP Bldg. No.	Frame System	Reactive Weight (kips)	C_w ($R_w = 12$)	Direction of frame	Period (sec)		
					UBC	Measured	Model
57357	13-story steel (MRSF)	25,200	0.043	E-W	1.8	2.2	2.2
58496	2-story steel (EBF)	4,550	0.115	E-W	0.2	0.3	0.3
57355	10-story R.C. (MRSF)	24,500	0.058	N-S	1.1	1.0	1.2
58490	6-story R.C. (MRSF)	6,430	0.049	N-S	0.8	0.8	1.1

Table 2.4 Description of Buildings

Earthquake	Station	Abbreviation	Comp.	PGA (g)	EPA (g)
Imperial Valley (1940)	El Centro	ELC	S90E	0.35	0.28
Washington (1949)	Olympia	OLY	S86W	0.28	0.22
Kern County (1952)	Taft	TAF	S69E	0.18	0.15
Parkfield (1966)	Cholane	PAR	N85E	0.43	0.33
San Fernando (1971)	Pacoima Dam	PAC	S16E	1.17	0.80
Imperial Valley (1979)	I. V. C.	IVC	S40E	0.33	0.20
Loma Prieta (1989)	Corralitos	LPC	S00E	0.63	0.52
Loma Prieta (1989)	Santa Cruz	LPSC	S90E	0.41	0.33

Table 2.5 Earthquake Records

Earthquake Record	elastic base shear ratio (C) from normalized record	$\frac{C}{C_w}$
LPSC	0.077	1.32
LPC	0.048	0.82
ELC	0.054	0.93
TAF	0.051	0.88
OLY	0.042	0.72
PAR	0.062	1.06
PAC	0.052	0.89
IVC	0.055	0.95
Average	0.055	0.95

Table 2.6 Comparison of Base Shear Ratios of Normalized Earthquake Records (CSMIP 57355)

Figures

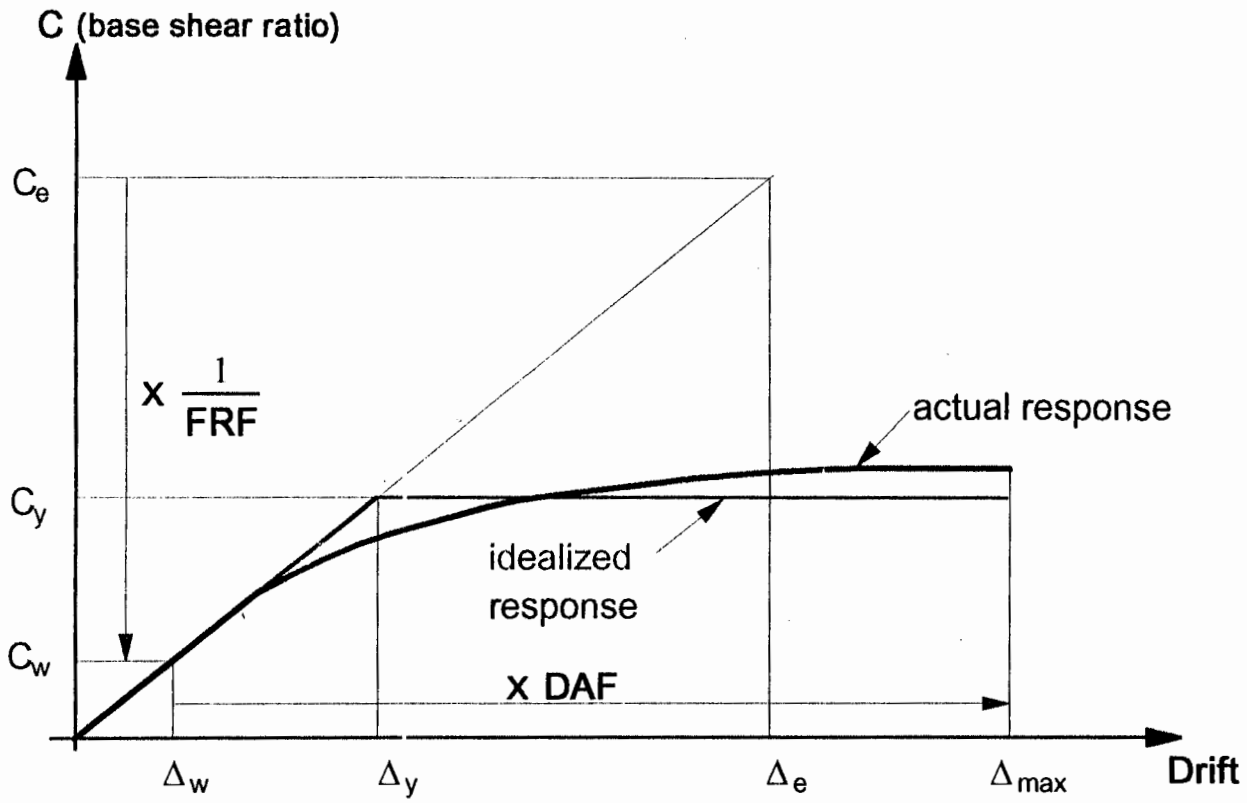

Fig. 2.1 General Structural Response

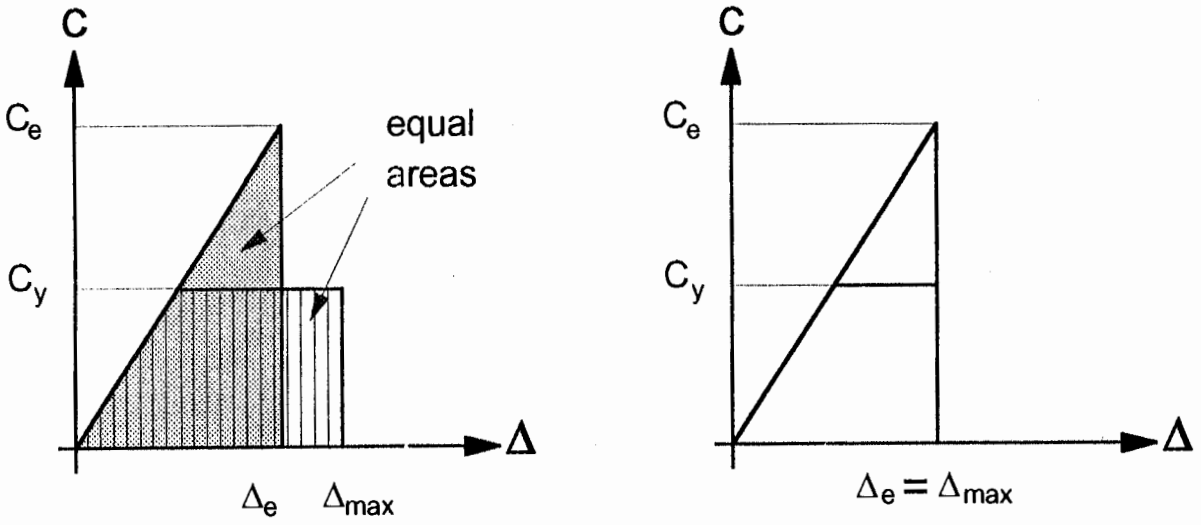

(a) Equal Energy Concept

(b) Equal Displacement Concept

Fig. 2.2 Newmark-Hall Rules for SDOF Systems

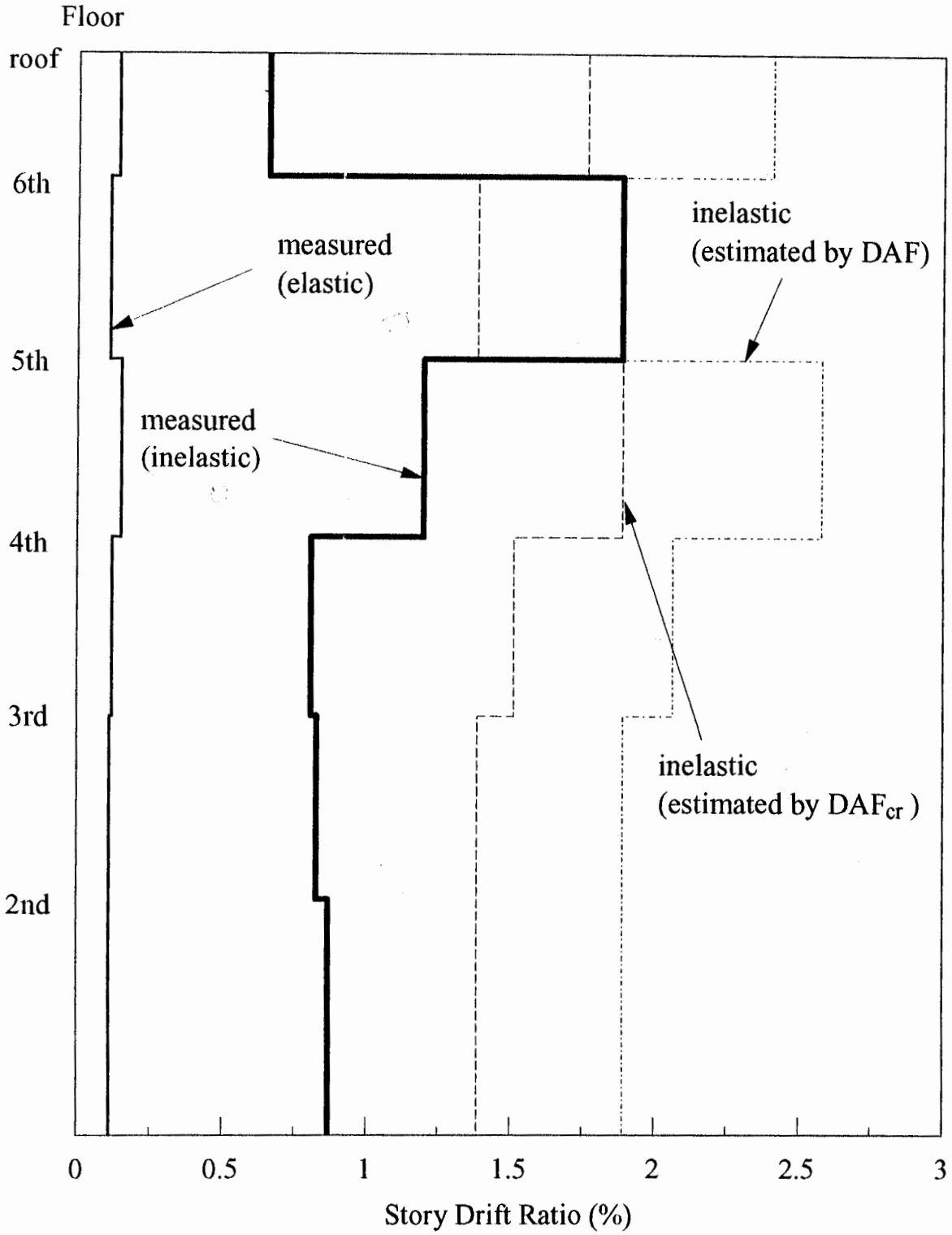

Fig. 2.3 Estimated versus Measured Story Drift Ratios

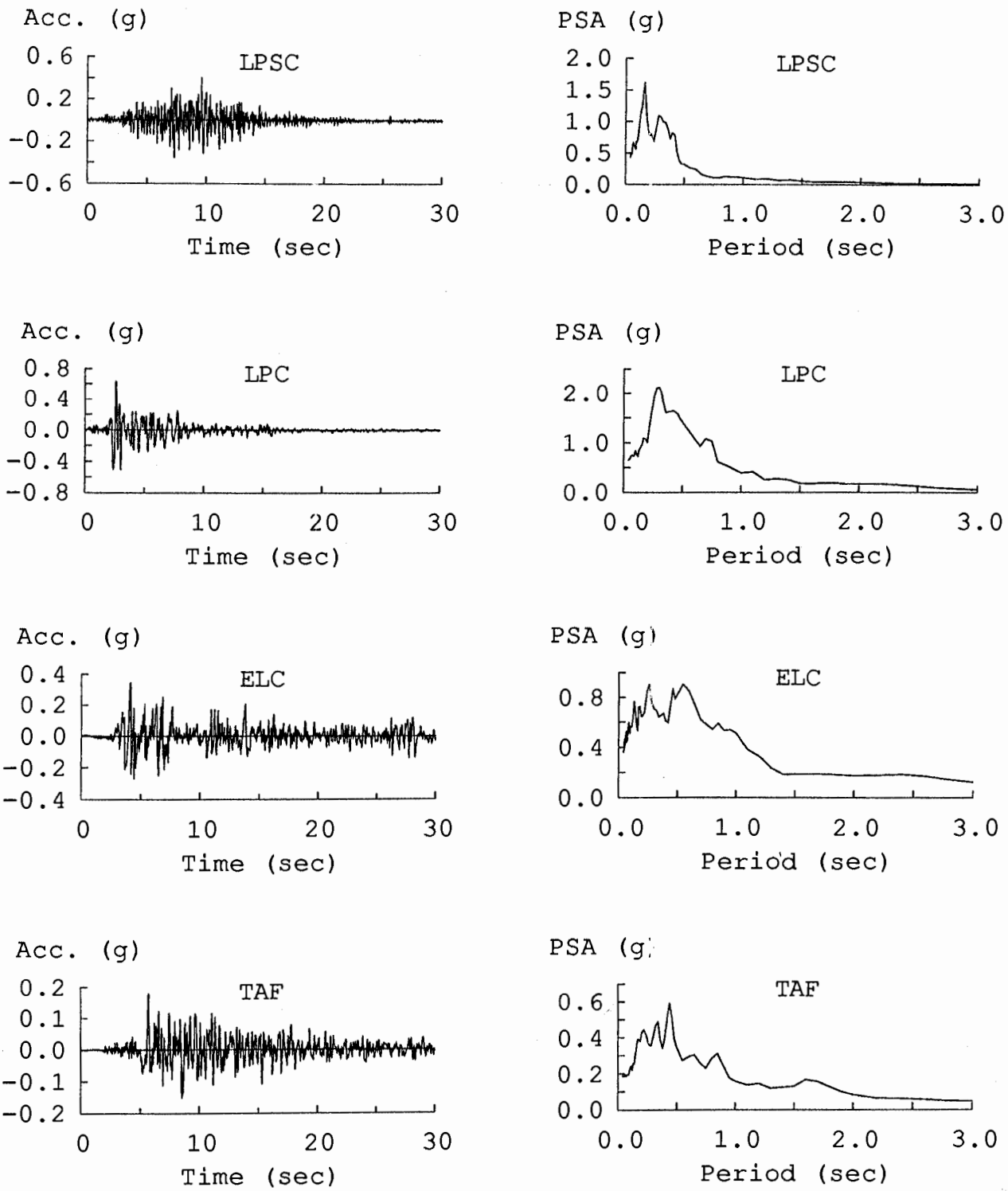

Fig. 2.4 Acceleration Time Histories and Response Spectra of Eight Historical Earthquakes

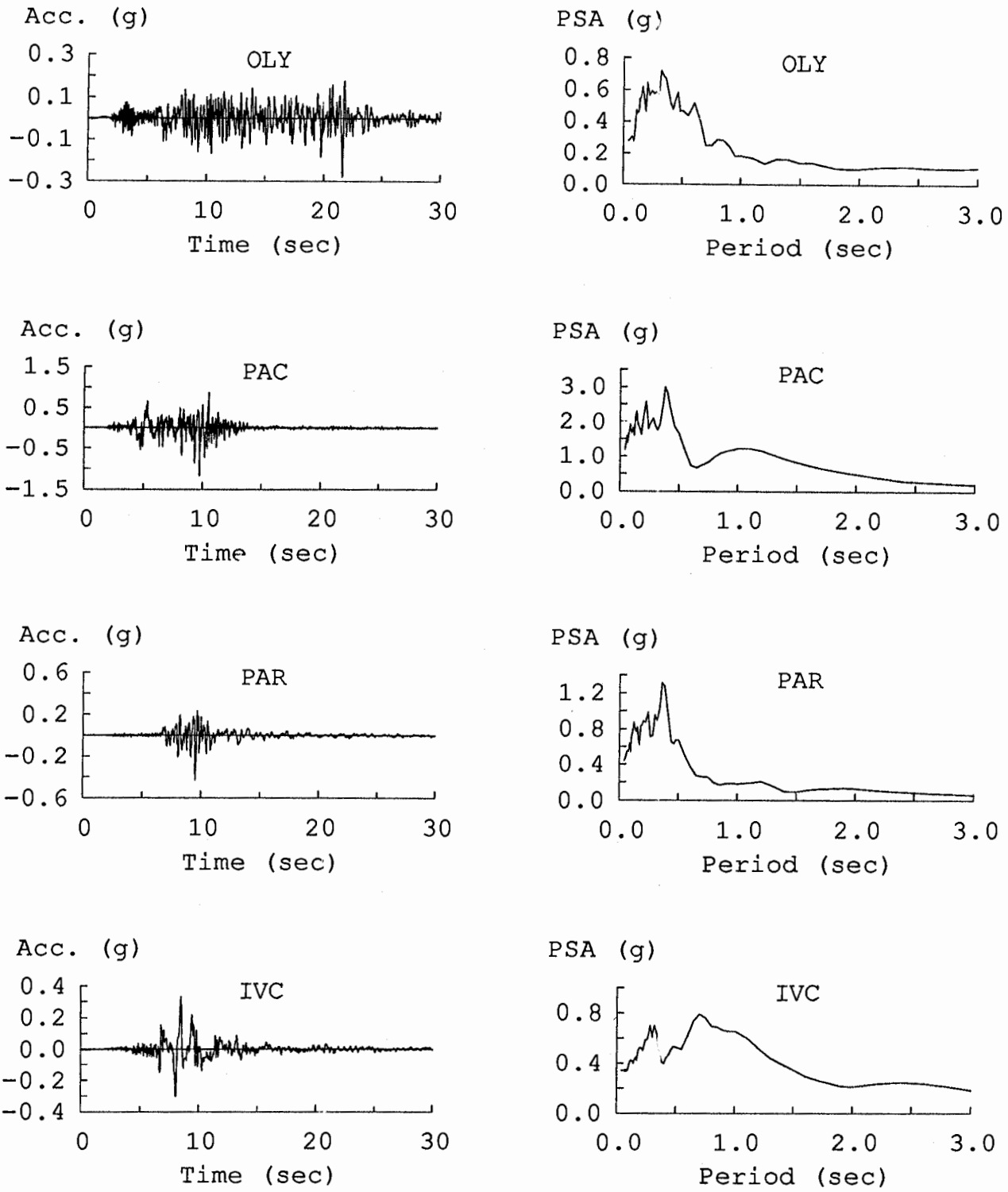

Fig. 2.4 (Continued)

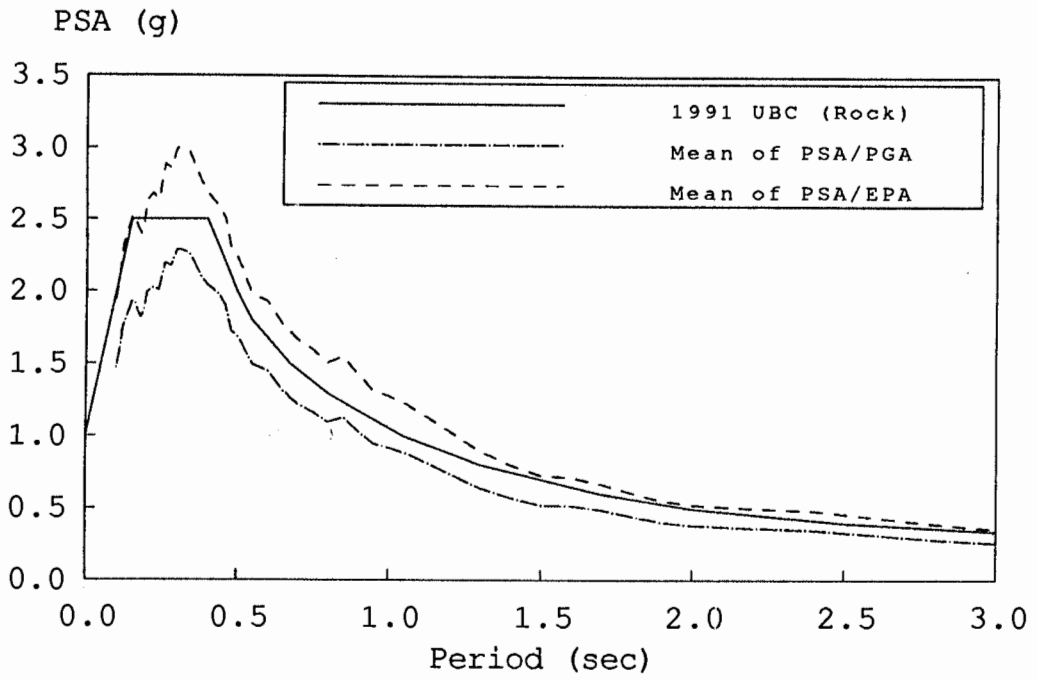

Fig. 2.5 Mean Response Spectra of Eight Historical Earthquakes

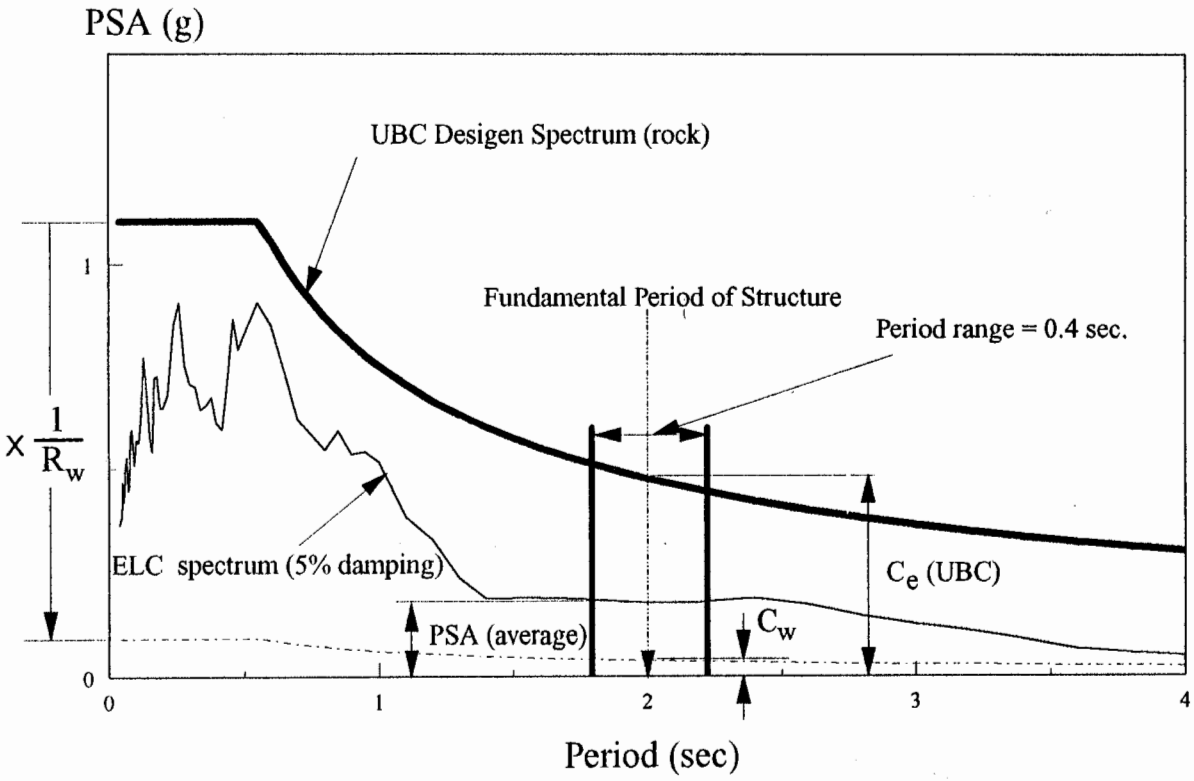

Fig. 2.6 Normalizing Earthquake Records using UBC Design Response Spectra

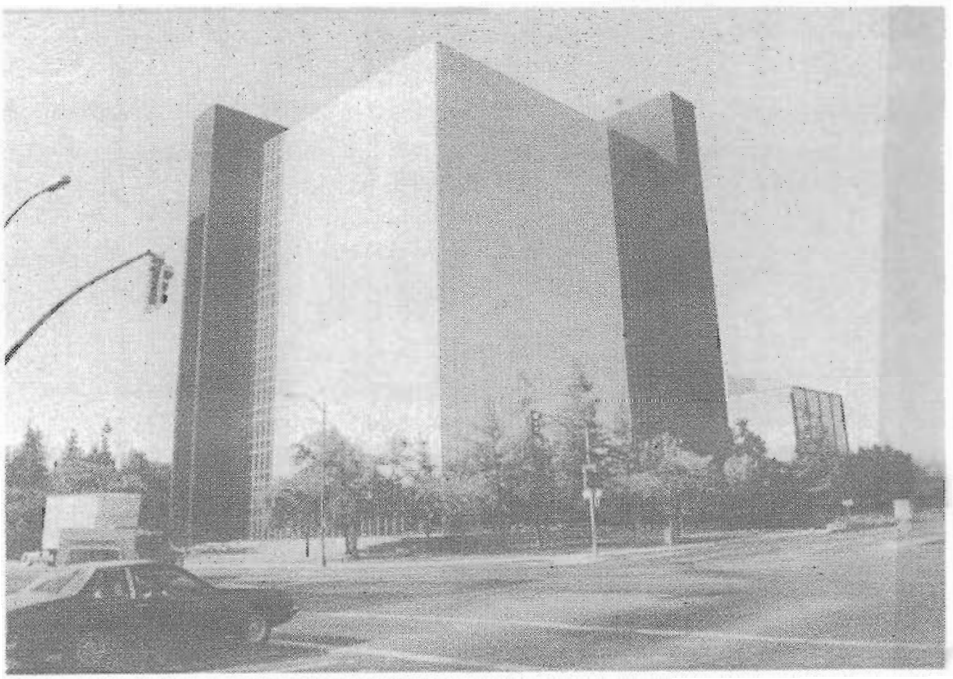

Fig. 3.1 San Jose 13-story Government Office Building (CSMIP 57357)

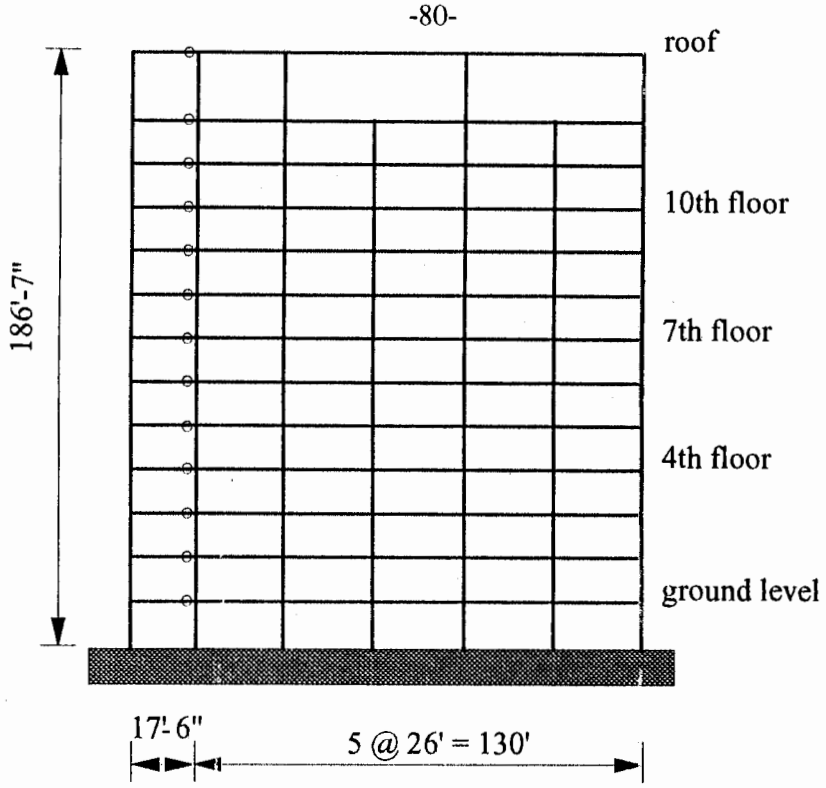

(a) SMRSF of Bldg. CSMIP 57357 (E-W)

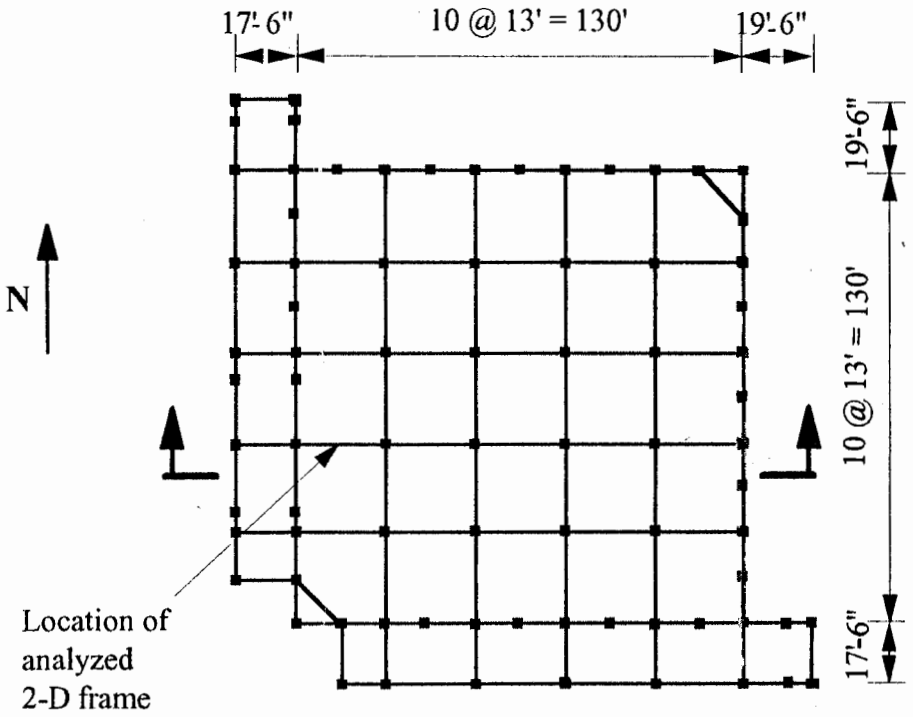

(b) Typical Floor Plan

Fig. 3.2 General Layout of Building CSMIP 57357

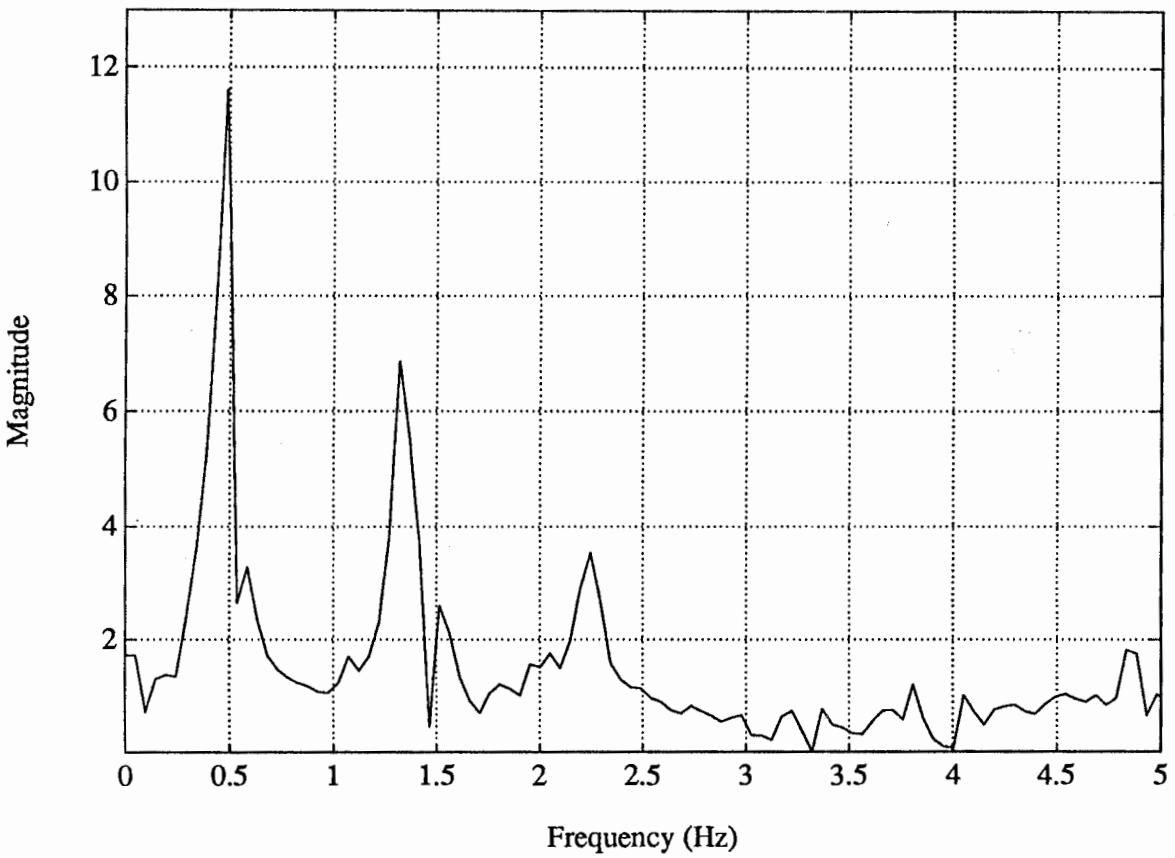

Fig. 3.3 Magnitude of Acceleration Transfer Functions between the Base and the Roof (CSMIP 57357)

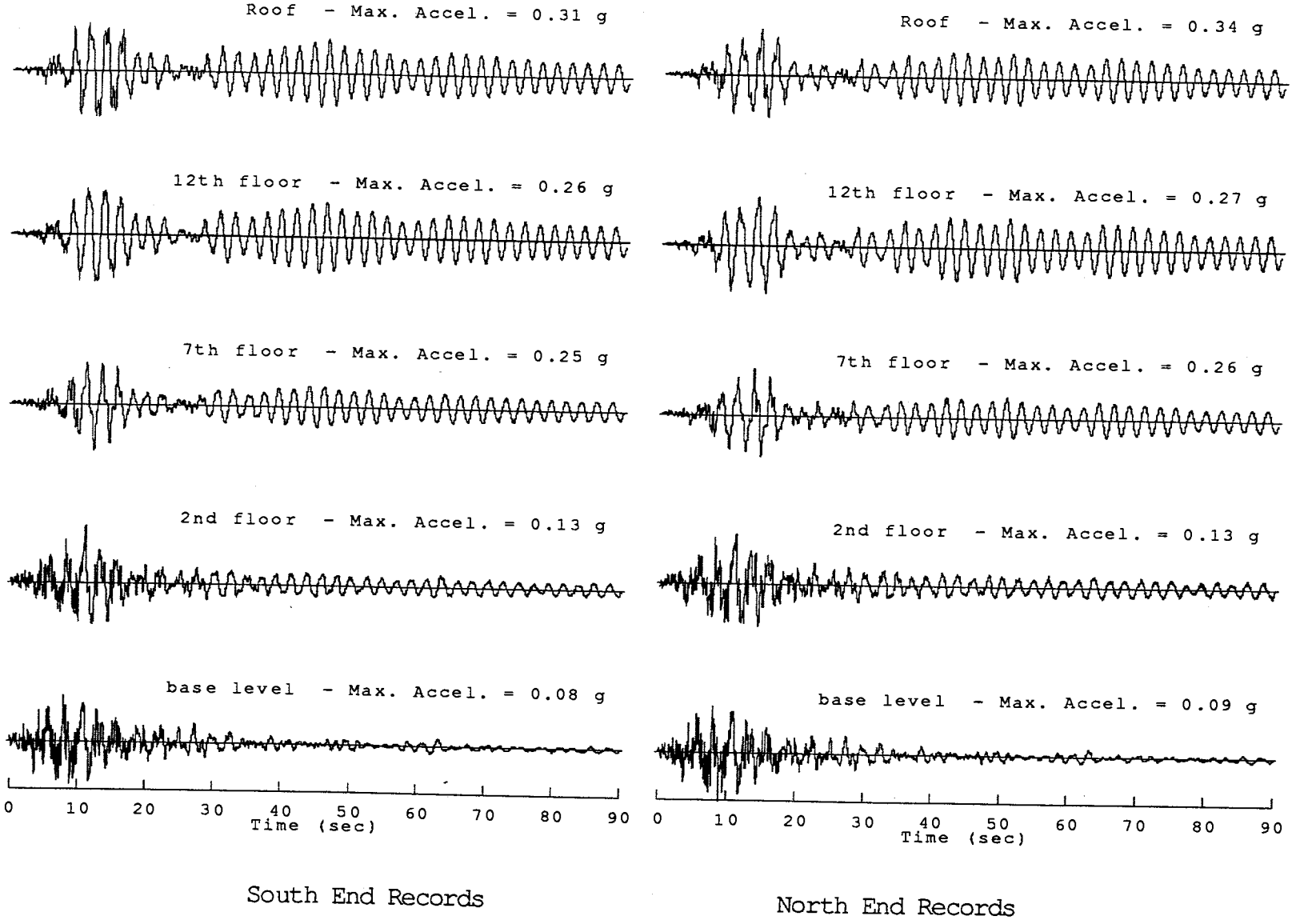

Fig. 3.4 Building CSMIP 57357 Acceleration Records

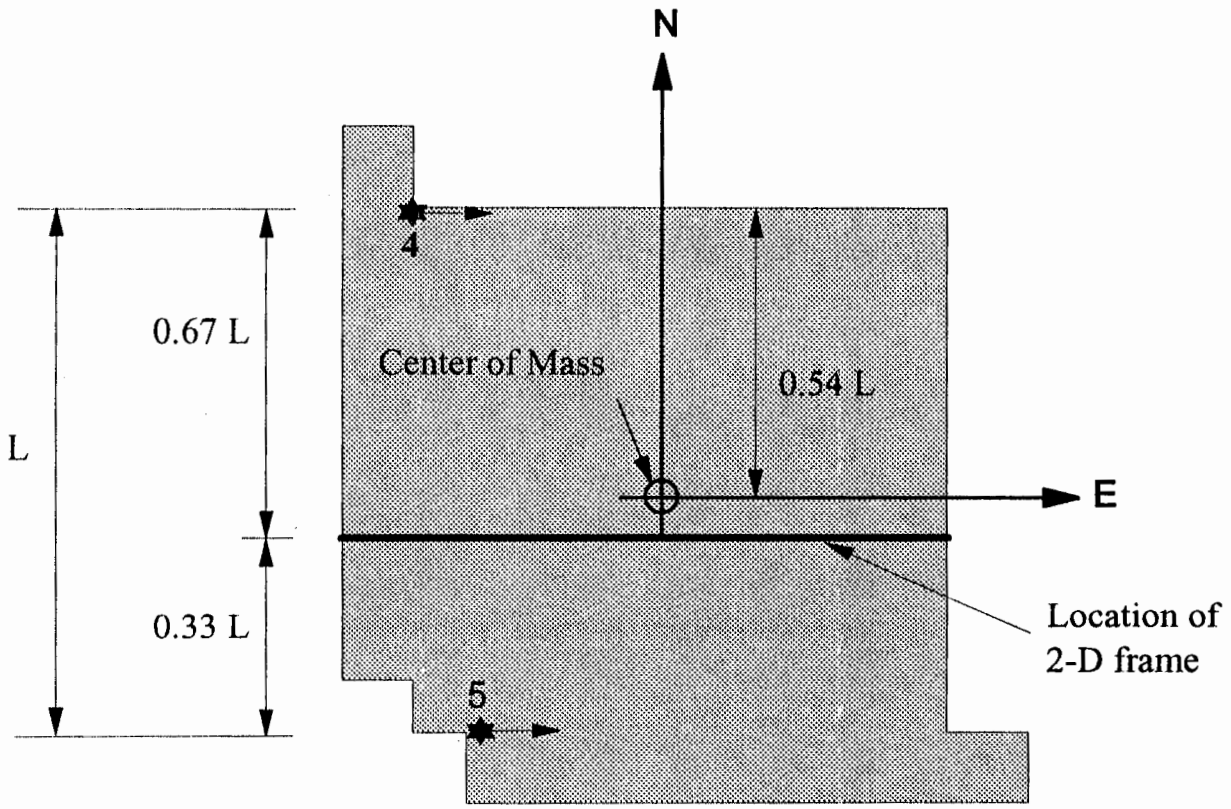

Fig. 3.5 Roof Geometry for Calculating E-W Displacement

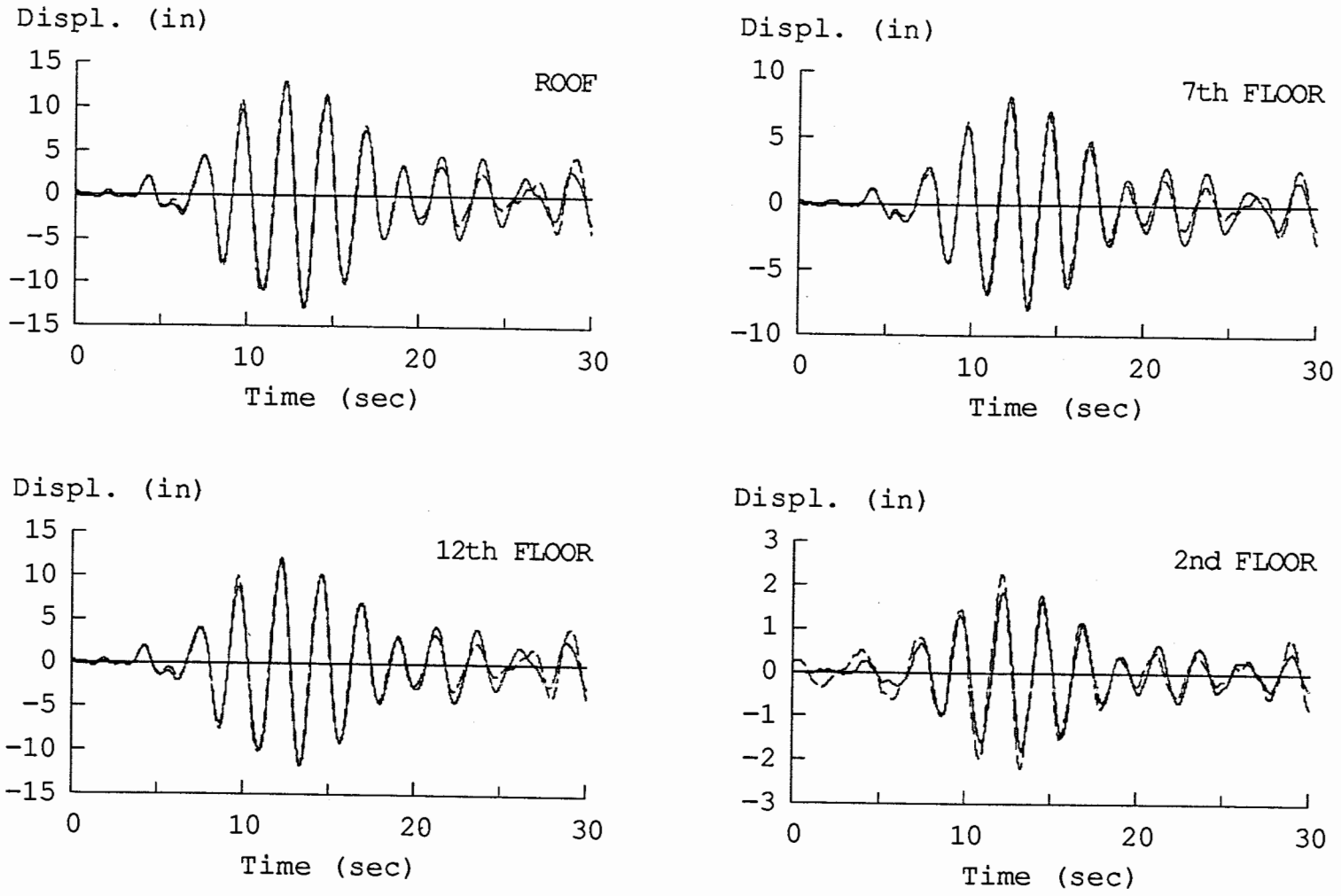

Fig. 3.6 Recorded (dashed) Versus Predicted Relative Displacement Time Histories (CSMIP 57357)

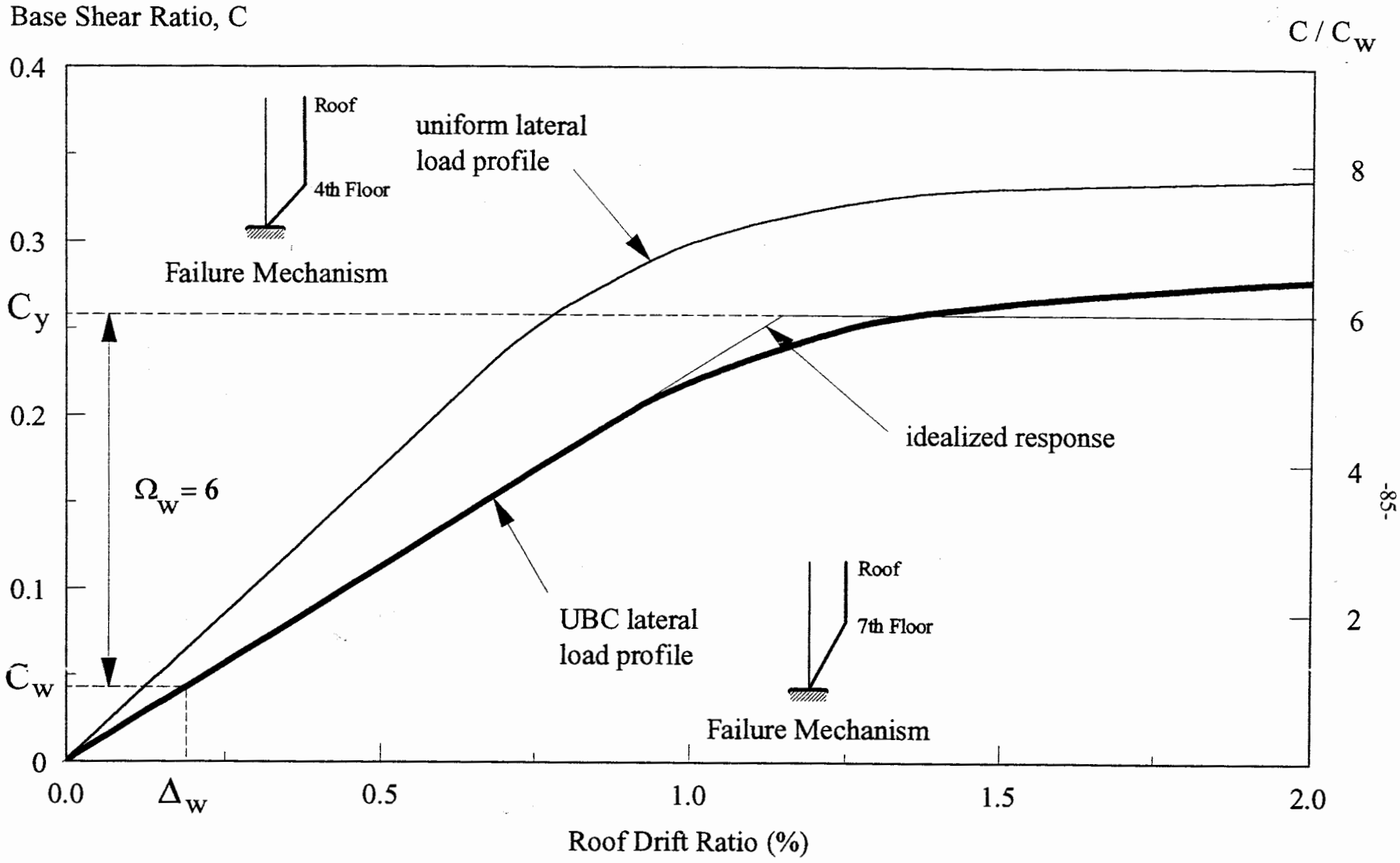

Fig. 3.7 Lateral Strength of CSMIP 57357 (E-W)

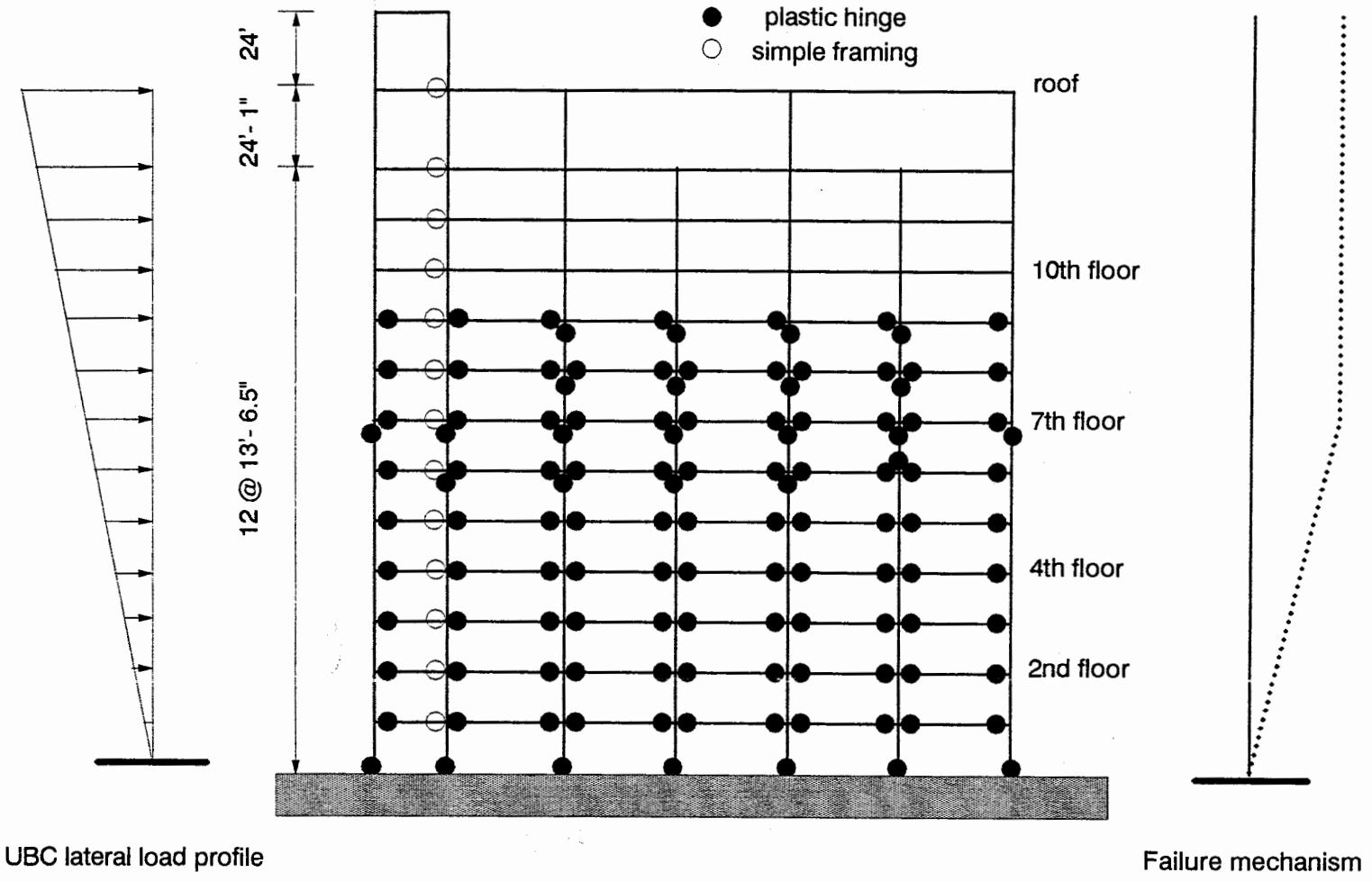

Fig. 3.8 Failure Mechanism of CSMIP 57357 Using UBC Lateral Load Profile

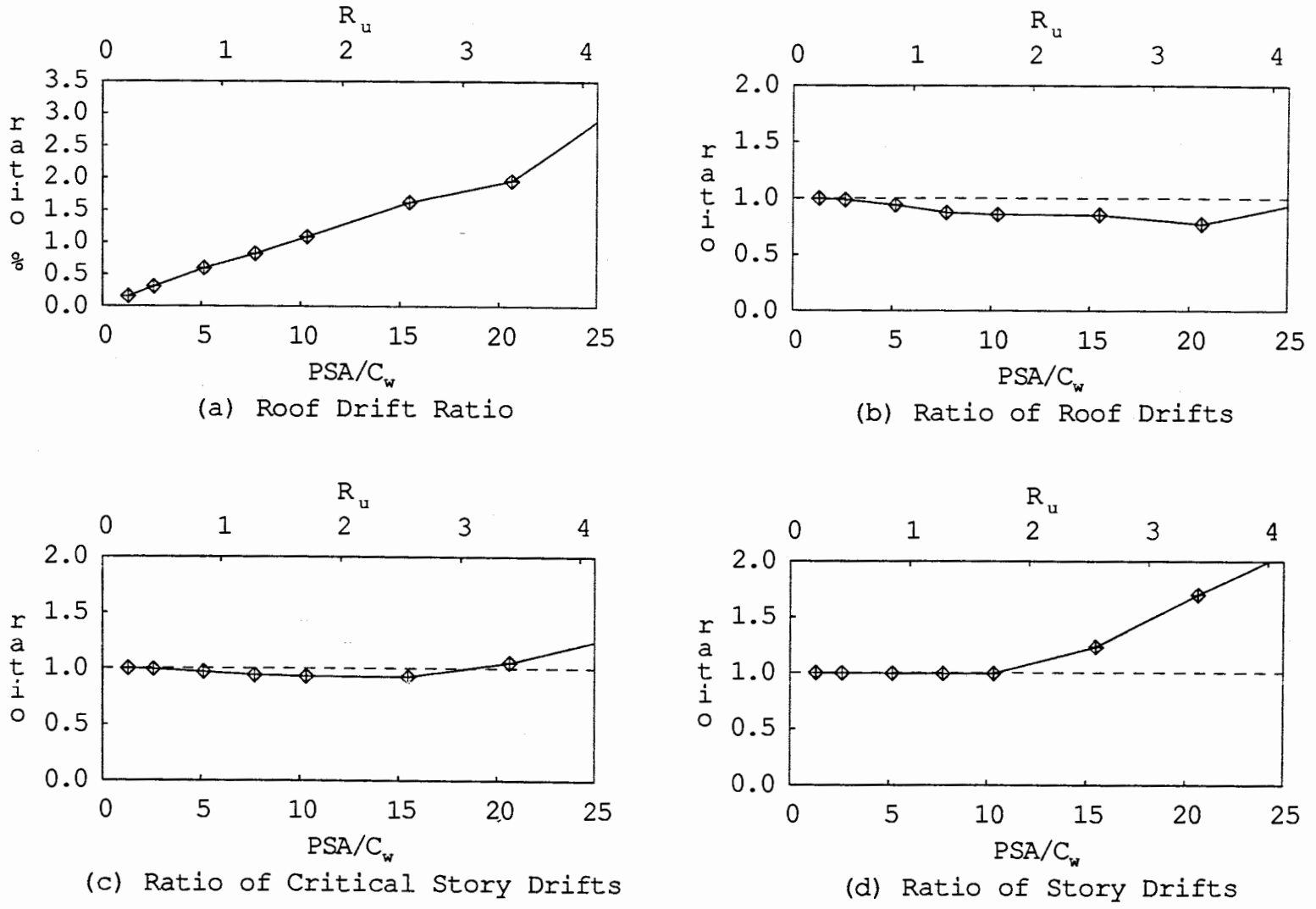

Fig. 3.9 Response Ratios of CSMIP 57357 to Scaled LPSC Earthquake Record

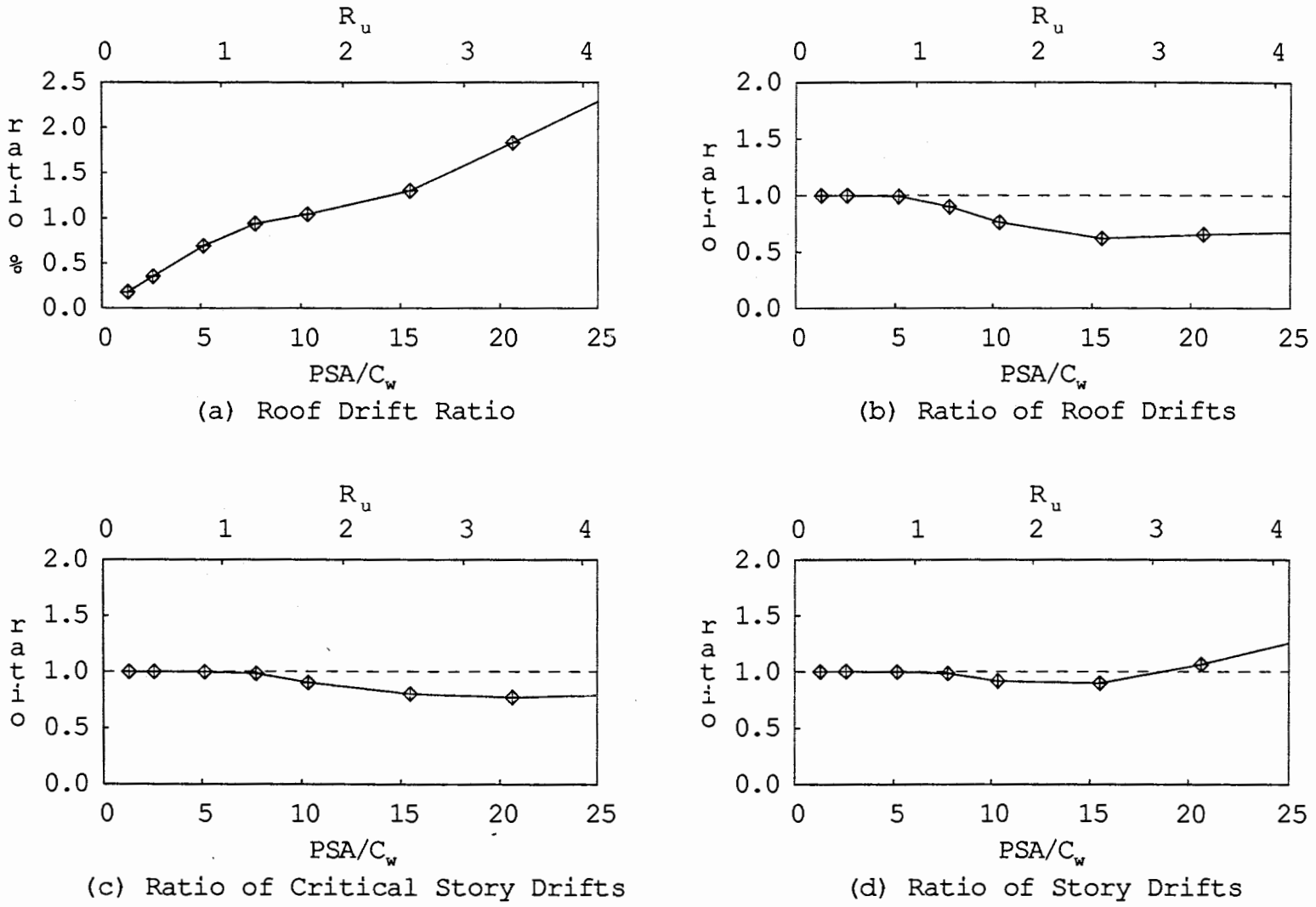

Fig. 3.10 Response Ratios of CSMIP 57357 to Scaled LPC Earthquake Record

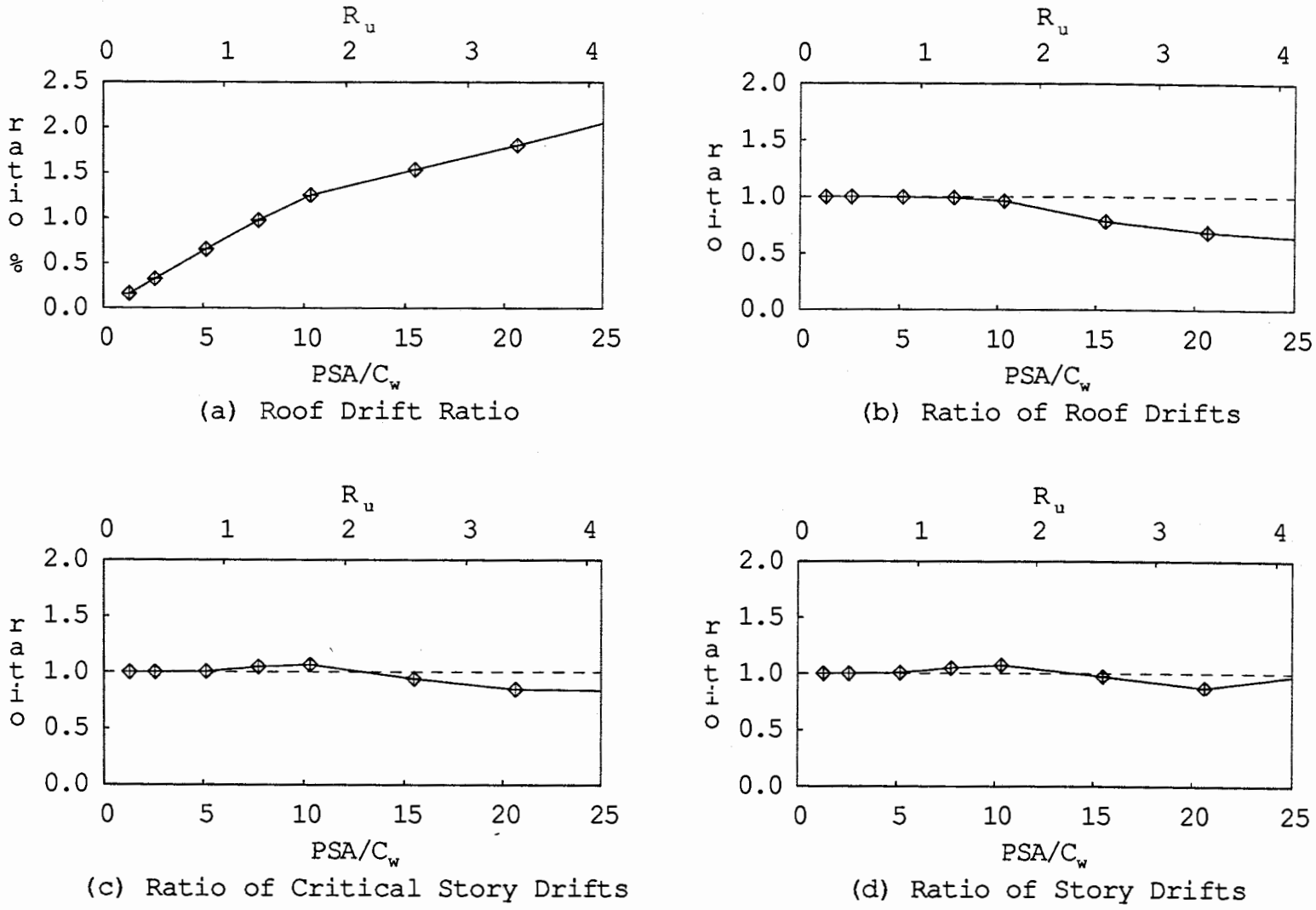

Fig. 3.11 Response Ratios of CSMIP 57357 to Scaled ELC Earthquake Record

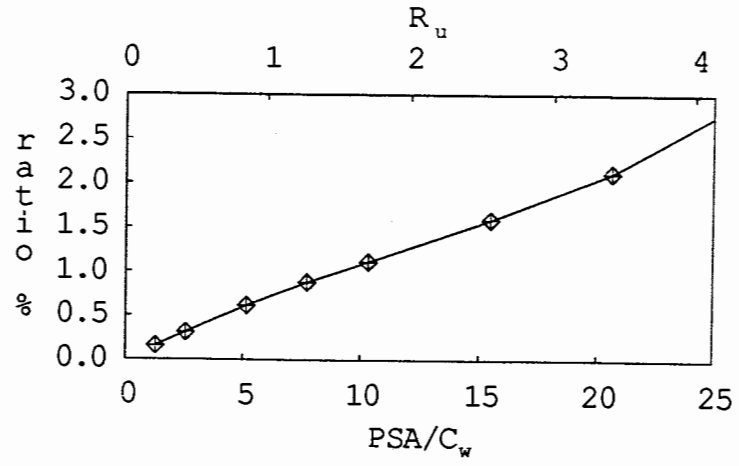

(a) Roof Drift Ratio

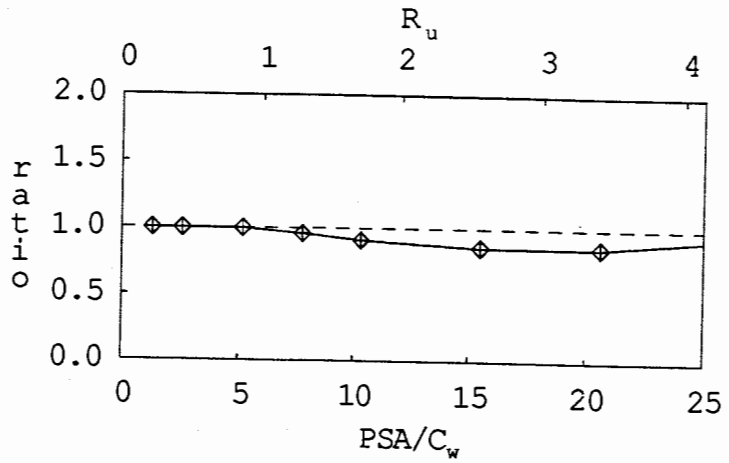

(b) Ratio of Roof Drifts

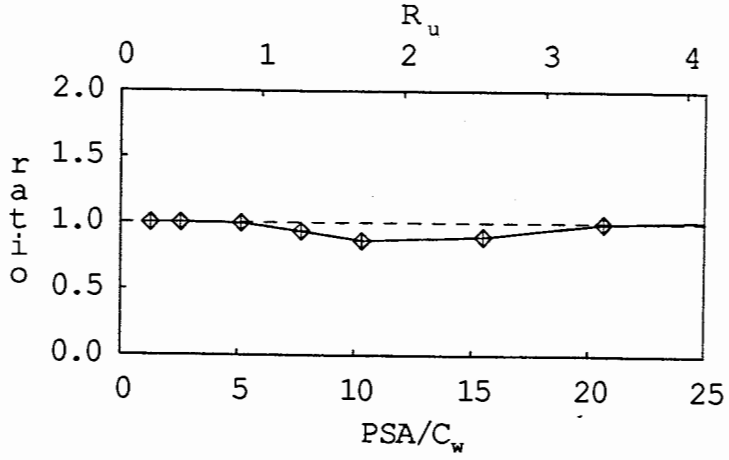

(c) Ratio of Critical Story Drifts

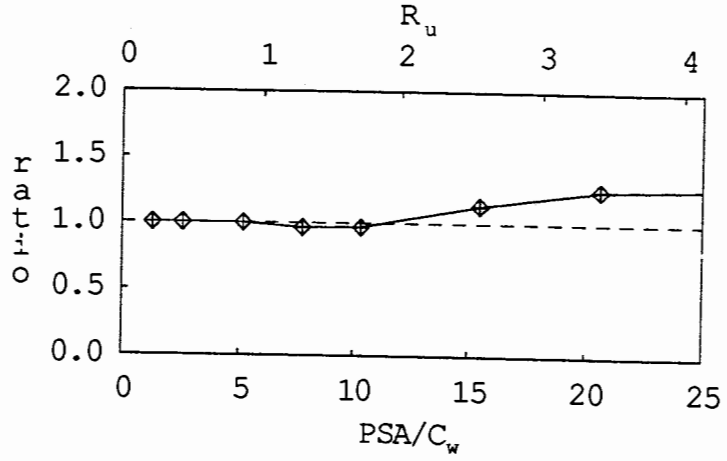

(d) Ratio of Story Drifts

Fig. 3.12 Response Ratios of CSMIP 57357 to Scaled TAF Earthquake Record

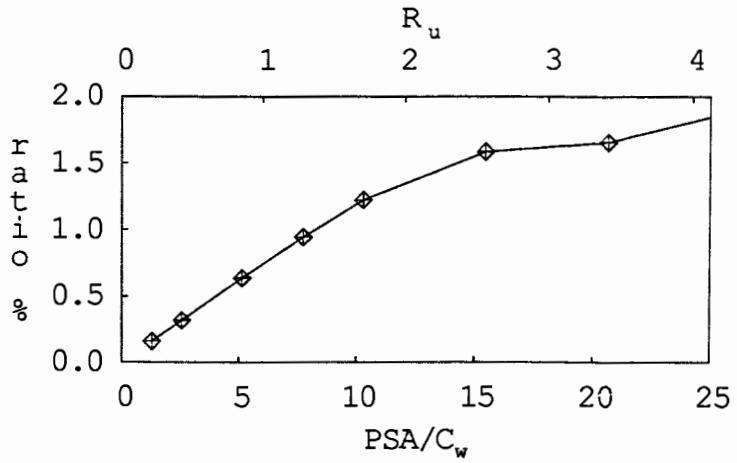

(a) Roof Drift Ratio

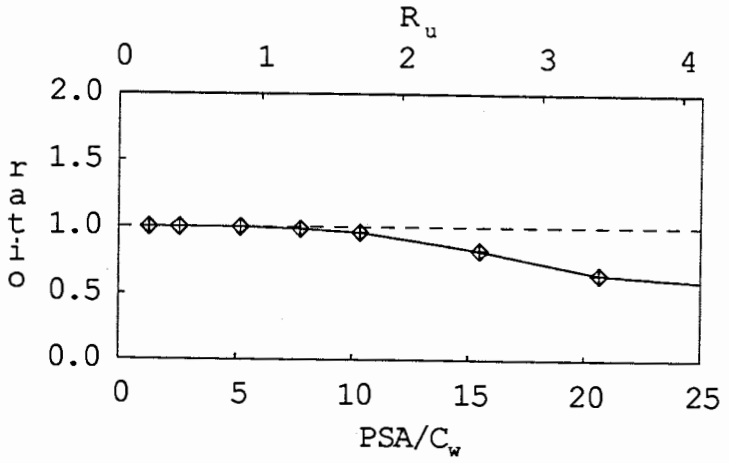

(b) Ratio of Roof Drifts

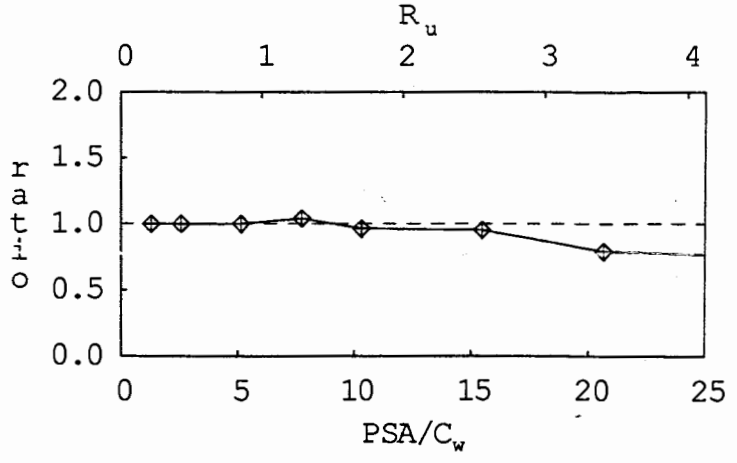

(c) Ratio of Critical Story Drifts

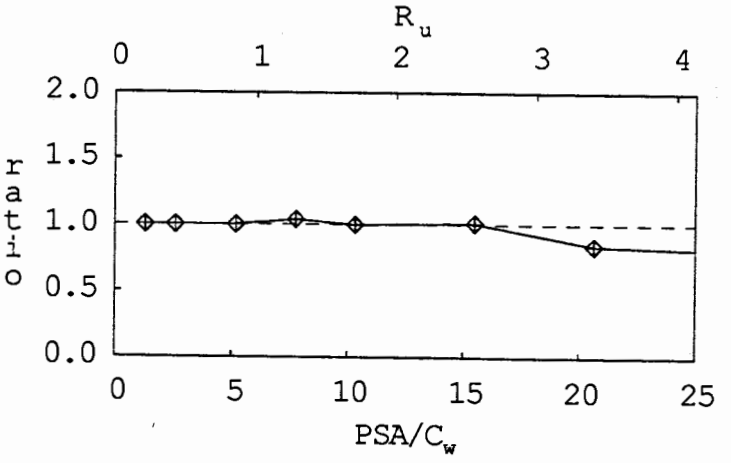

(d) Ratio of Story Drifts

Fig. 3.13 Response Ratios of CSMIP 57357 to Scaled OLY Earthquake Record

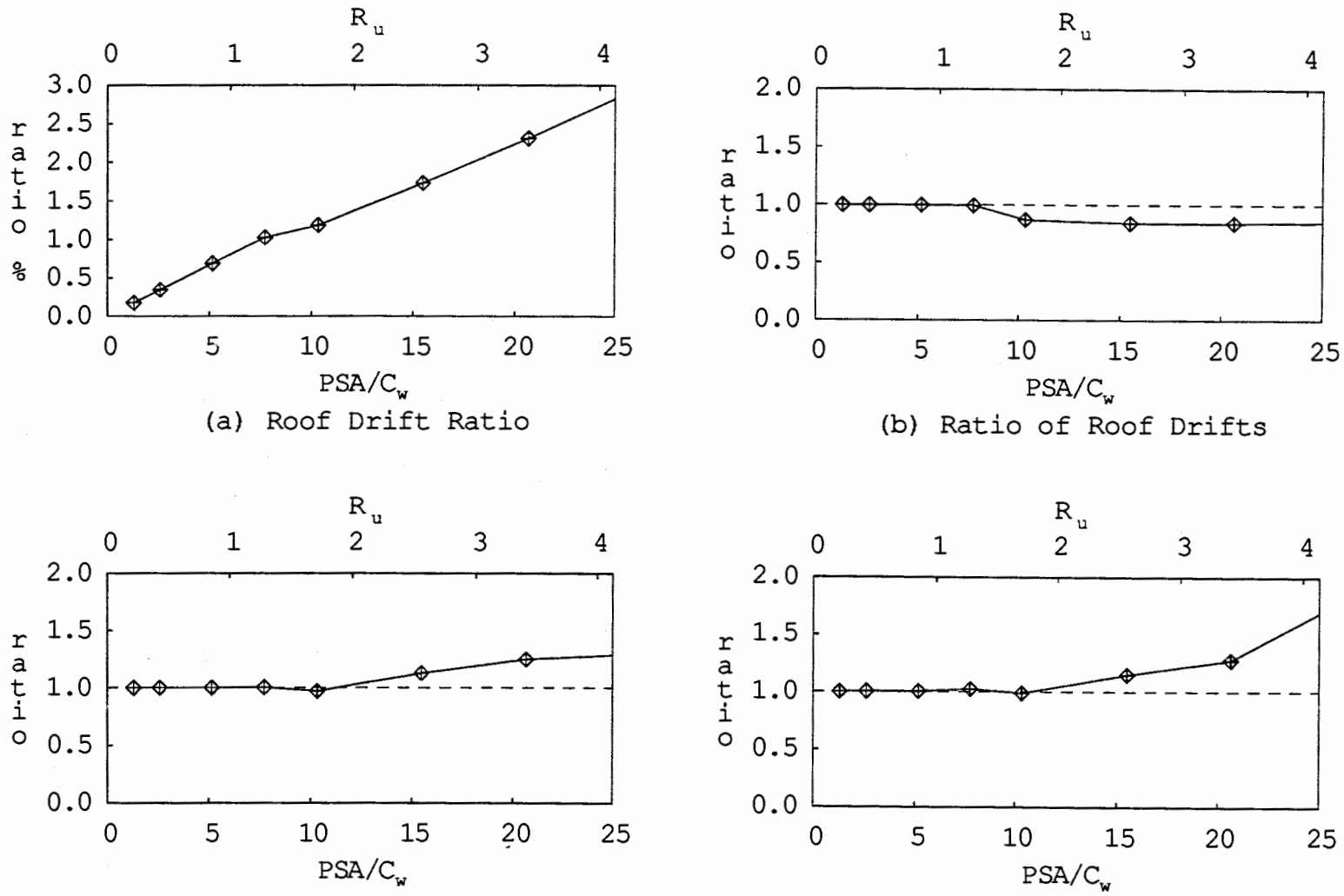

Fig. 3.14 Response Ratios of CSMIP 57357 to Scaled PAC Earthquake Record

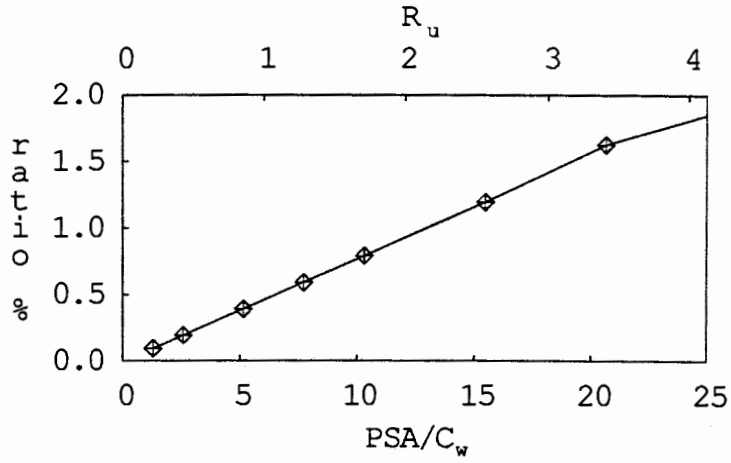

(a) Roof Drift Ratio

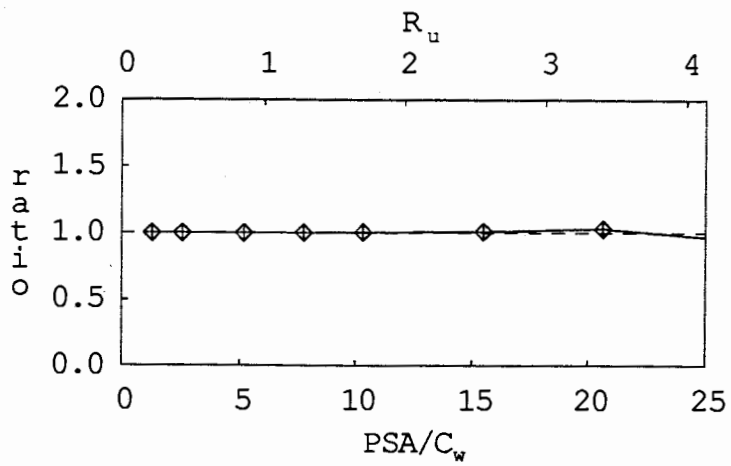

(b) Ratio of Roof Drifts

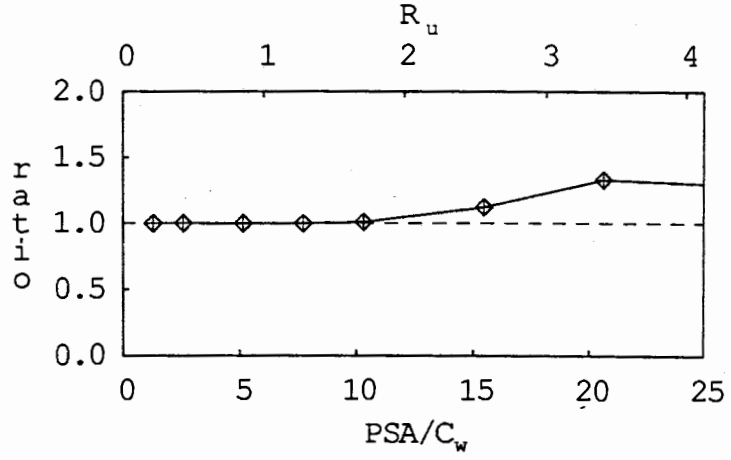

(c) Ratio of Critical Story Drifts

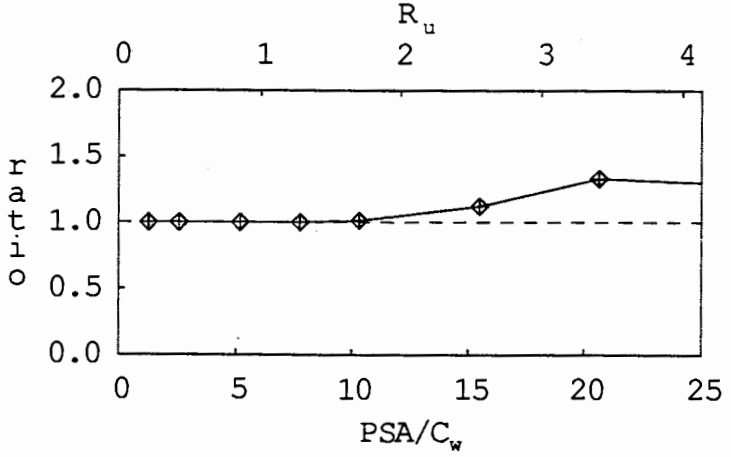

(d) Ratio of Story Drifts

Fig. 3.15 Response Ratios of CSMIP 57357 to Scaled PAR Earthquake Record

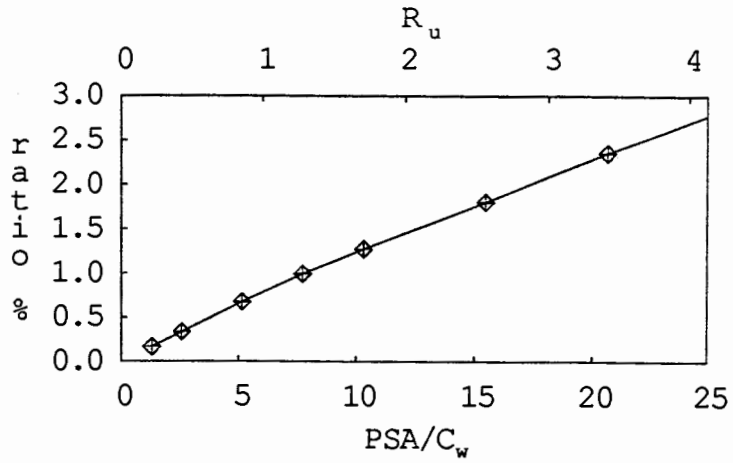

(a) Roof Drift Ratio

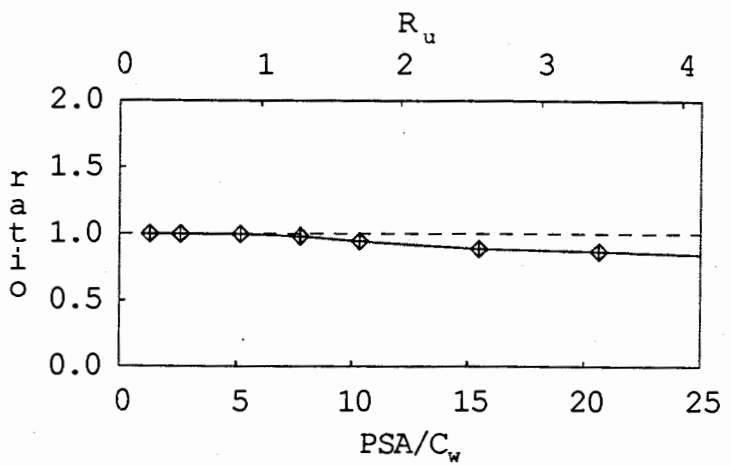

(b) Ratio of Roof Drifts

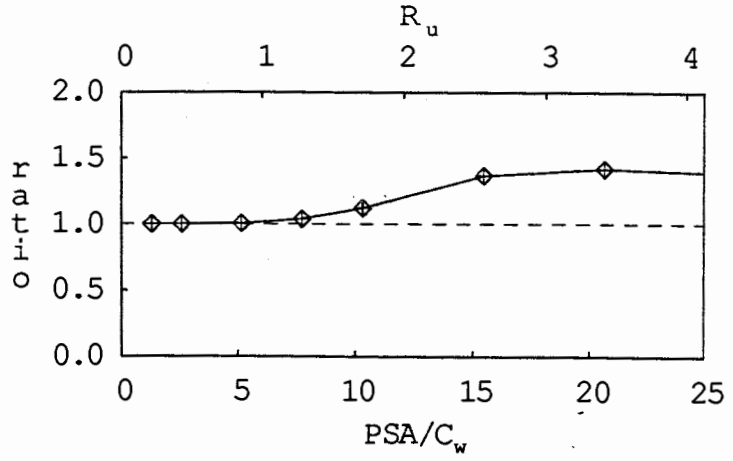

(c) Ratio of Critical Story Drifts

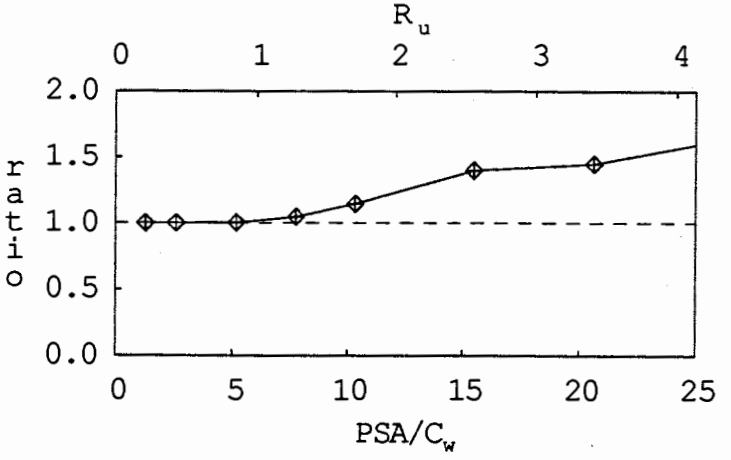

(d) Ratio of Story Drifts

Fig. 3.16 Response Ratios of CSMIP 57357 to Scaled IVC Earthquake Record

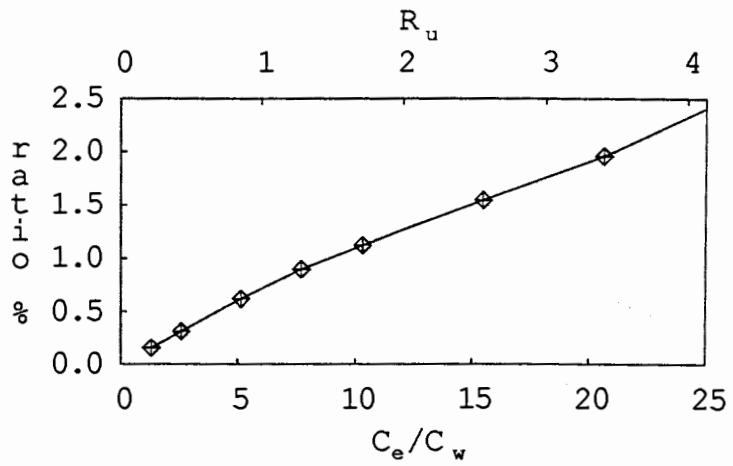

(a) Mean Roof Drift Ratio

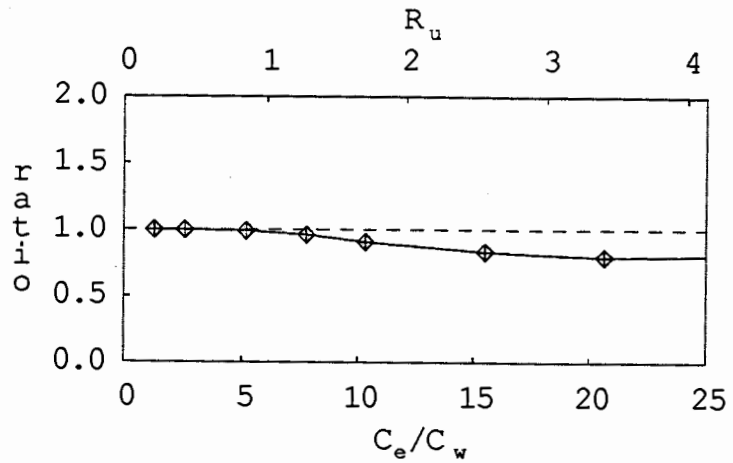

(b) Mean Ratio of Roof Drifts

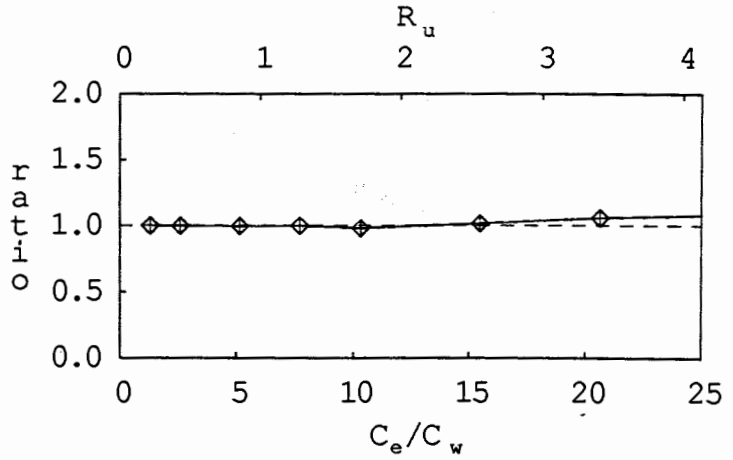

(c) Mean Ratio of Critical Story Drifts

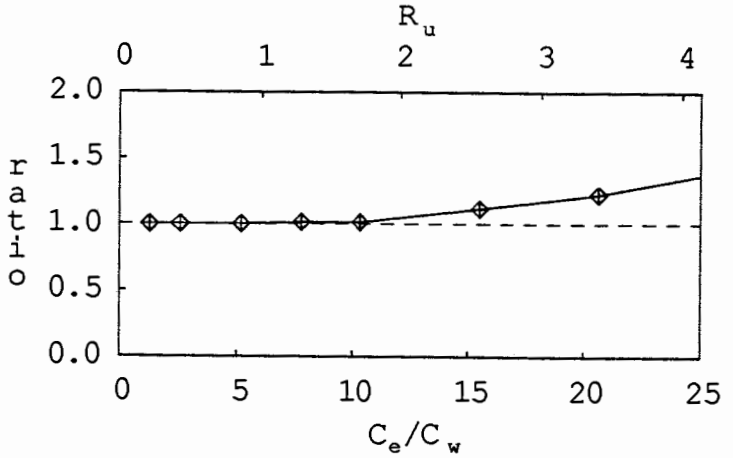

(d) Mean Ratio of Story Drifts

Fig 3.17 Mean Response Ratios of CSMIP 57357 to Eight Scaled Earthquake Records

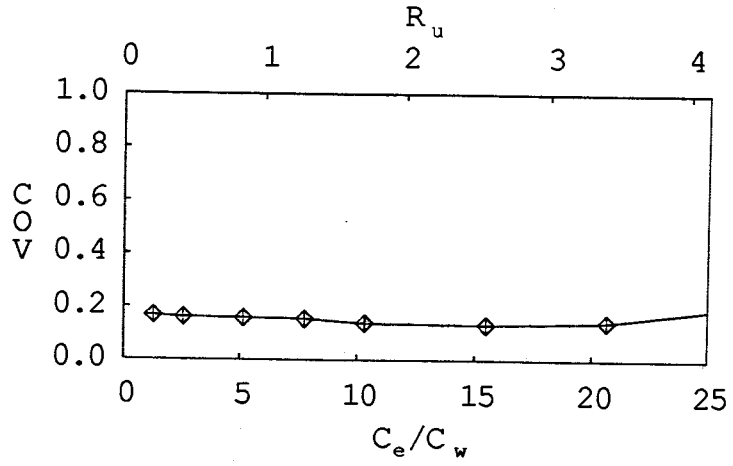

(a) COV for Roof Drift Ratio

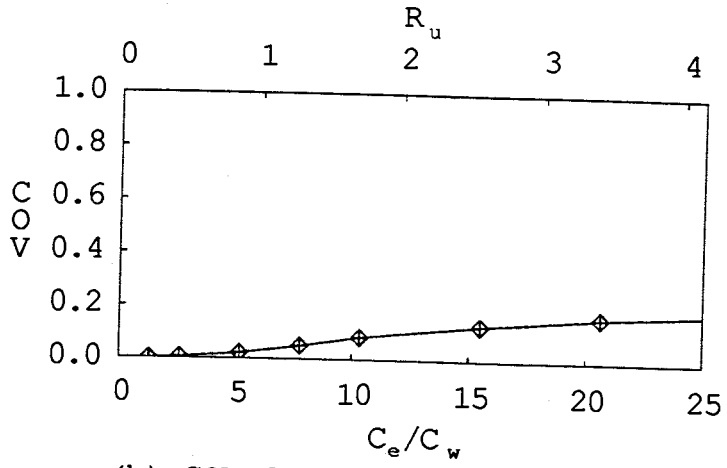

(b) COV for Ratio of Roof Drifts

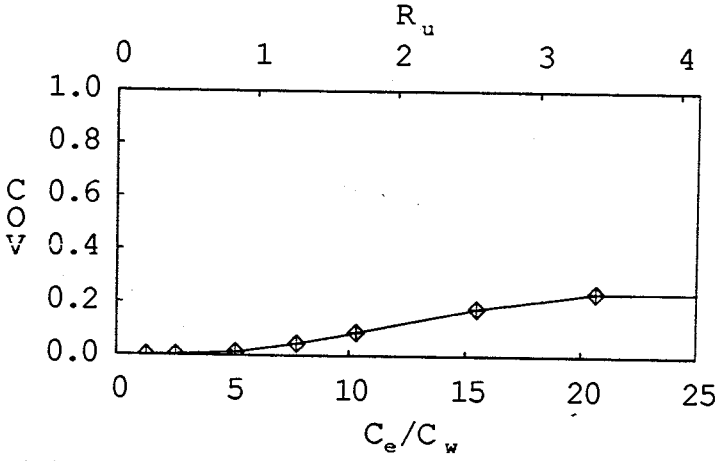

(c) COV for Ratio of Critical Story Drifts

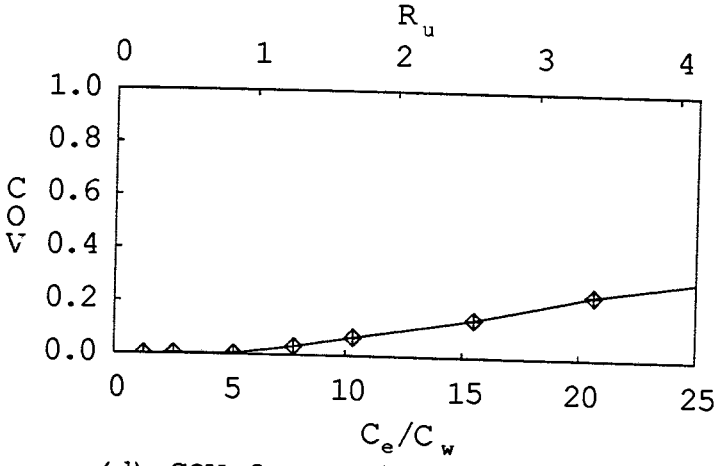

(d) COV for Ratio of Story Drifts

Fig. 3.18 COV for Response Ratios of CSMIP 57357 to Eight Scaled Earthquake Records

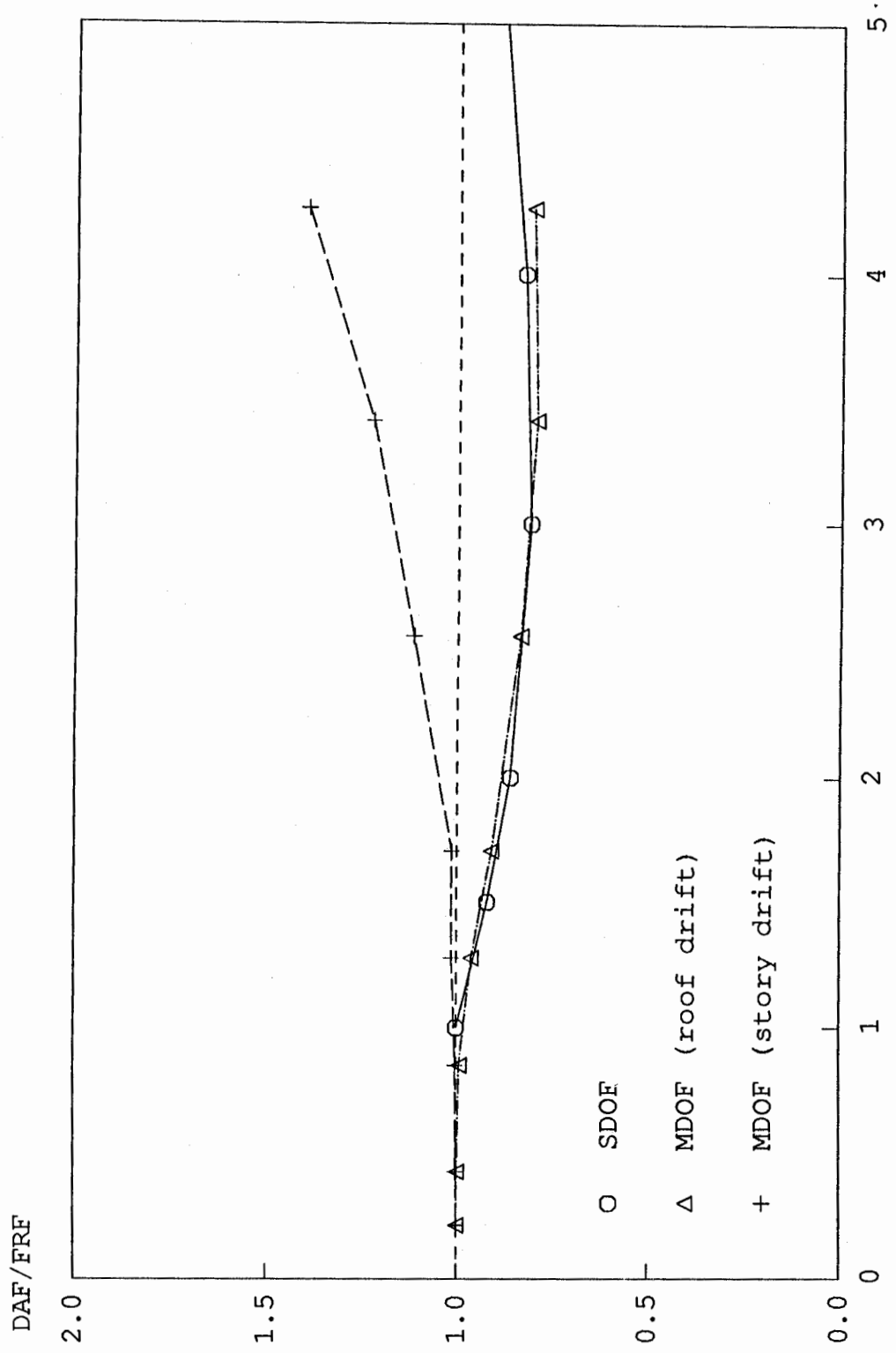

Fig. 3.19 Comparison of Mean Response Ratios between SDOF and MDOF systems (CSMIP 57357)

Fig. 4.1 **Berkeley 2-story Hospital Building (CSMIP 58496)**

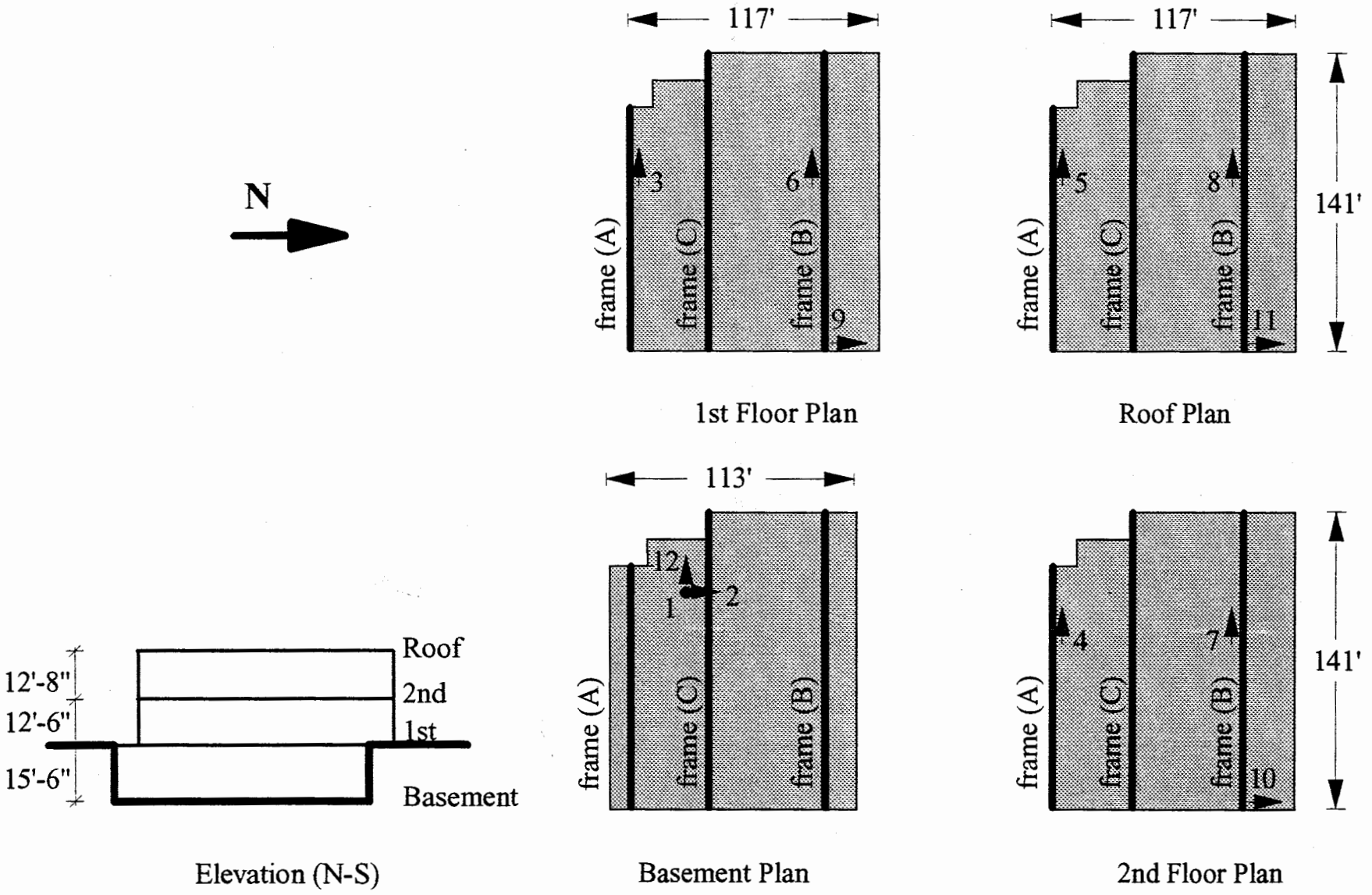

Fig. 4.2 Sensor Locations (CSMIP 58496)

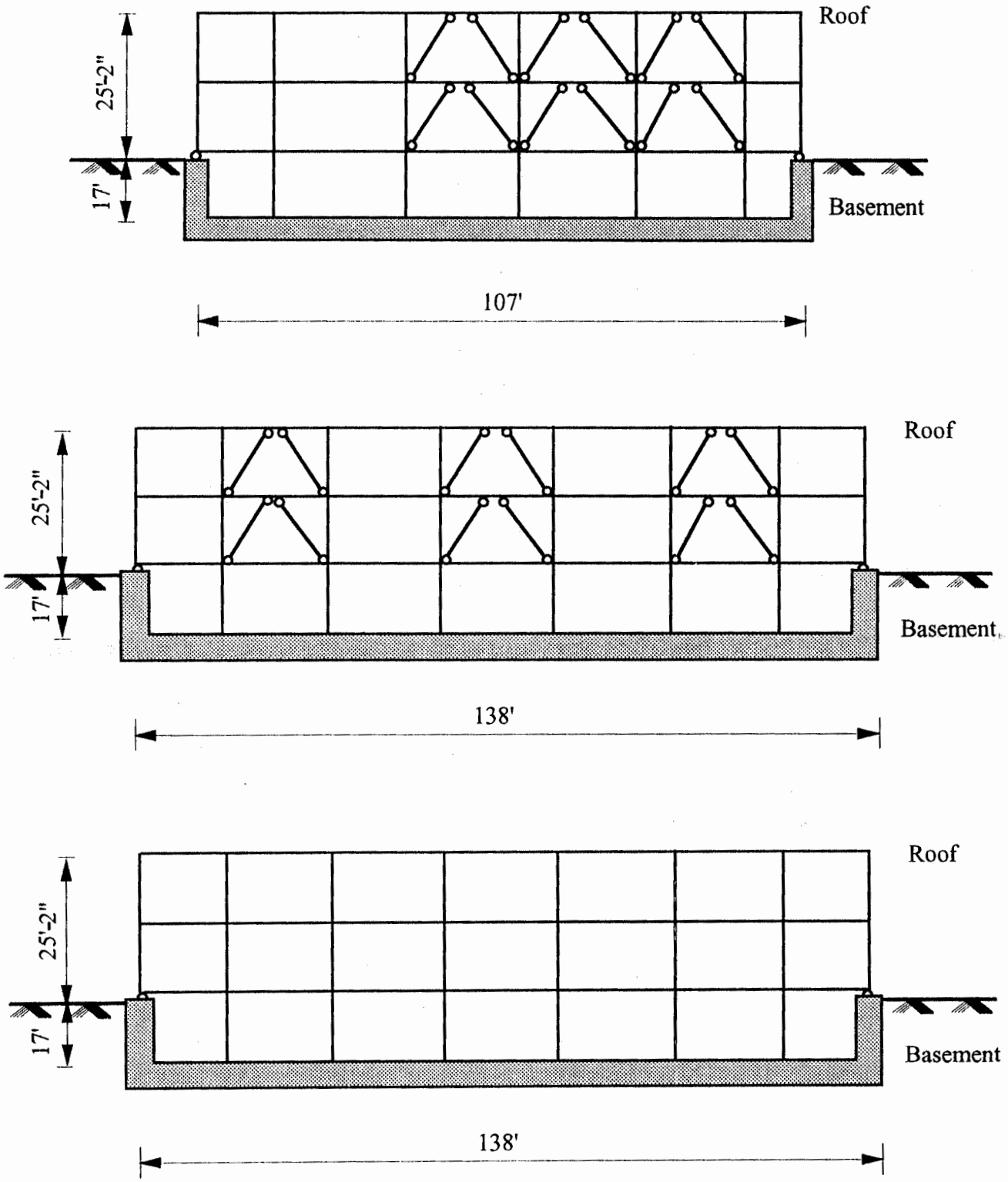

Fig. 4.3 Lateral-Force-Resisting System in the E-W Direction (CSMIP 58496)

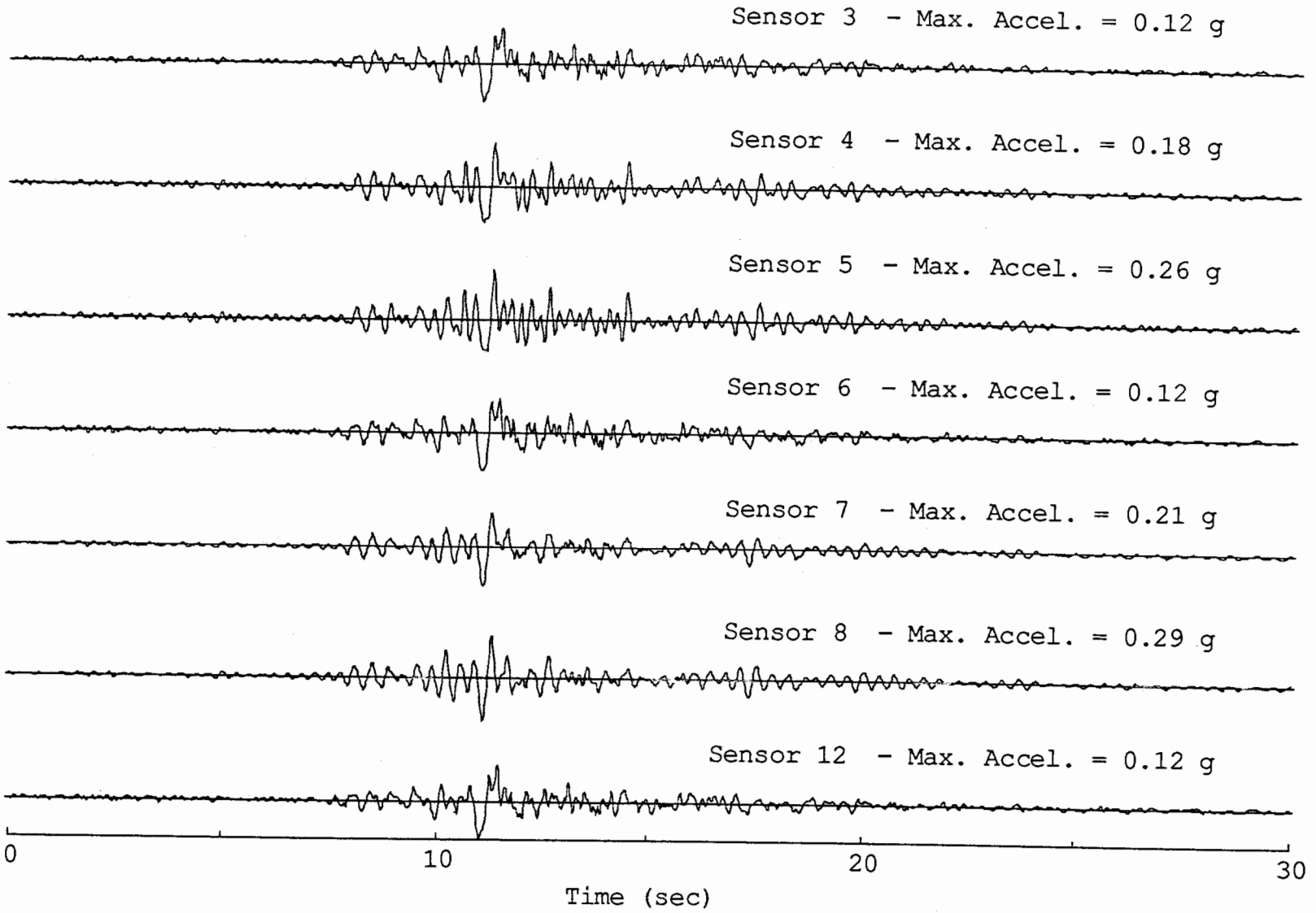

Fig. 4.4 Building CSMIP 58496 Acceleration Records in the E-W Direction

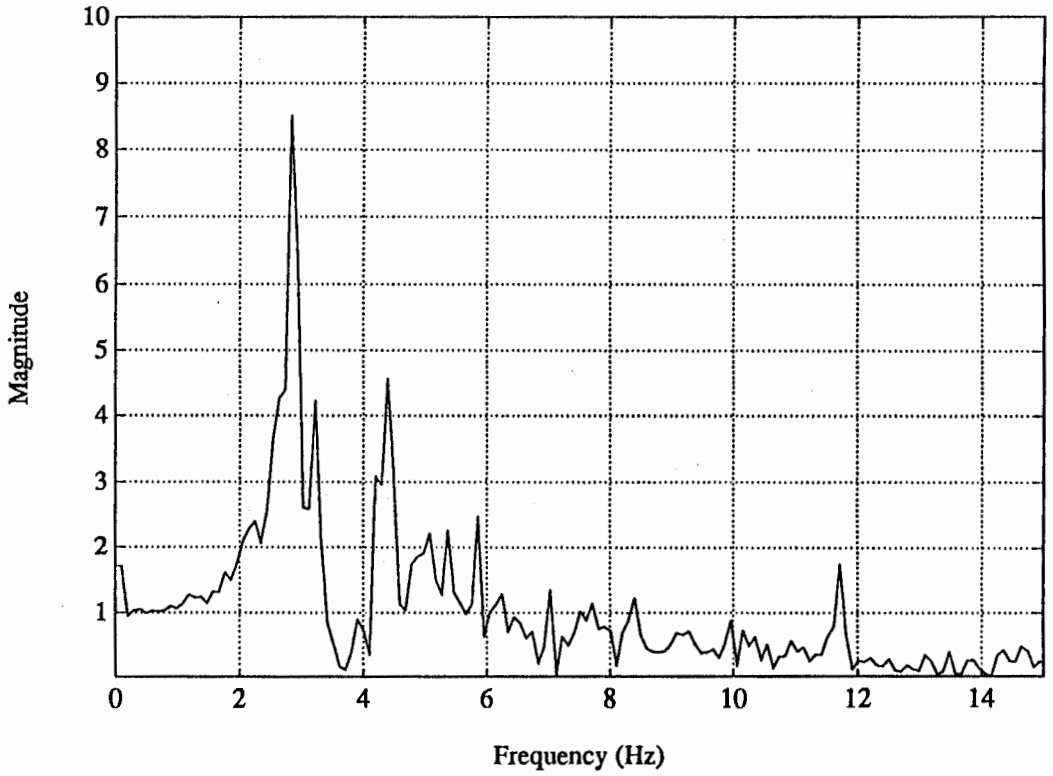

Fig. 4.5 Magnitude of Acceleration Transfer Functions between the Base and the Roof (CSMIP 58496)

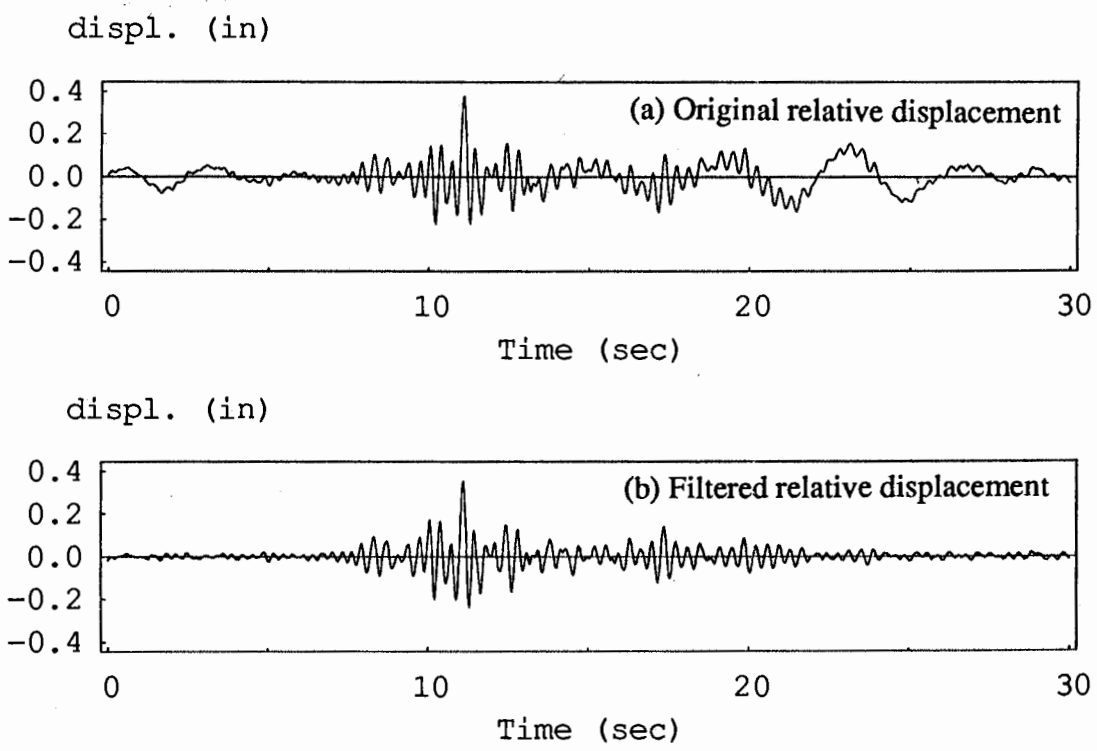

Fig. 4.6 Roof Relative Displacement Time History at Sensor 8 (CSMIP 58496, E-W)

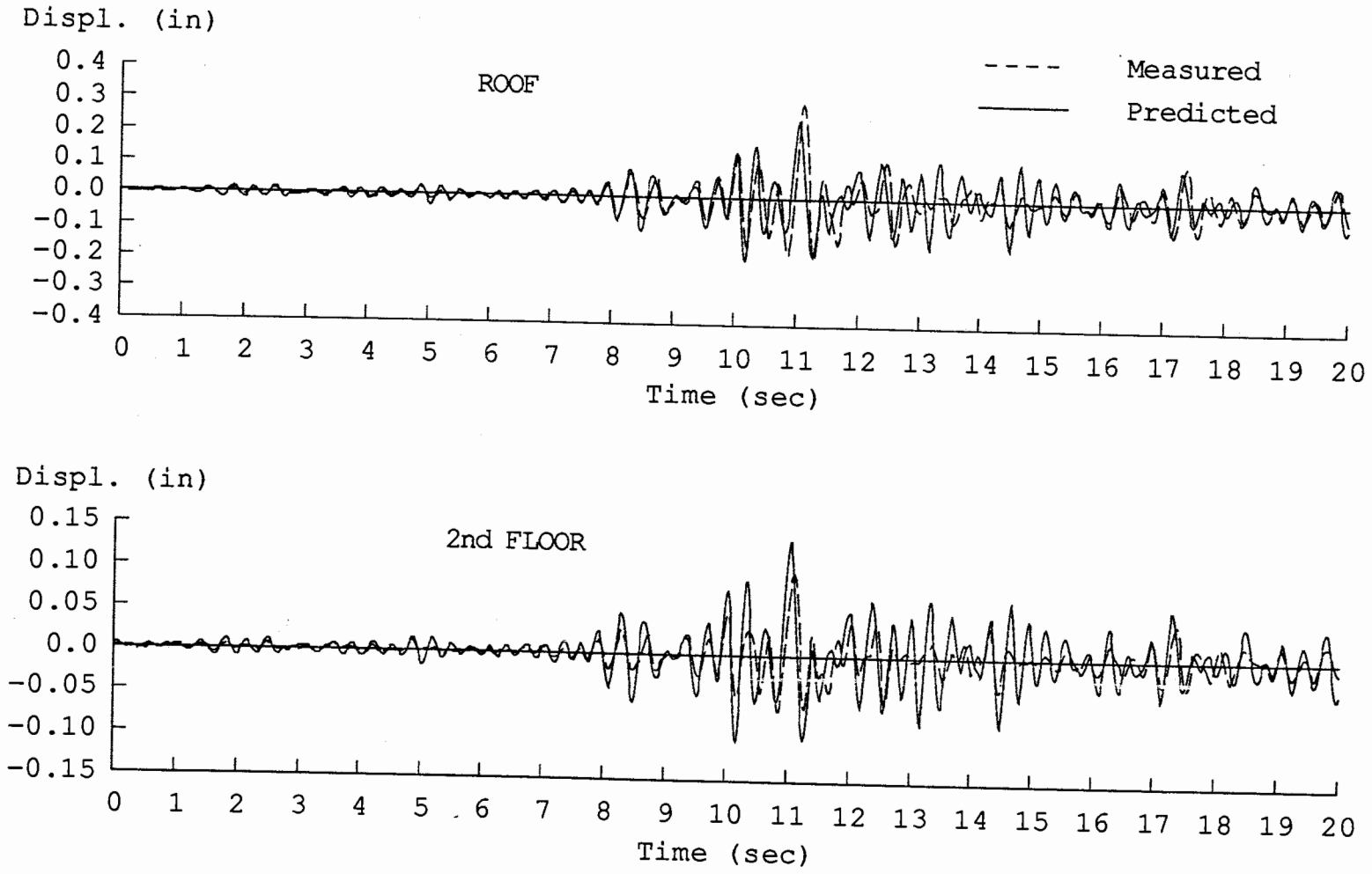

Fig. 4.7 Measured versus Predicted Relative Displacement Time Histories (CMSIP 58496, E-W)

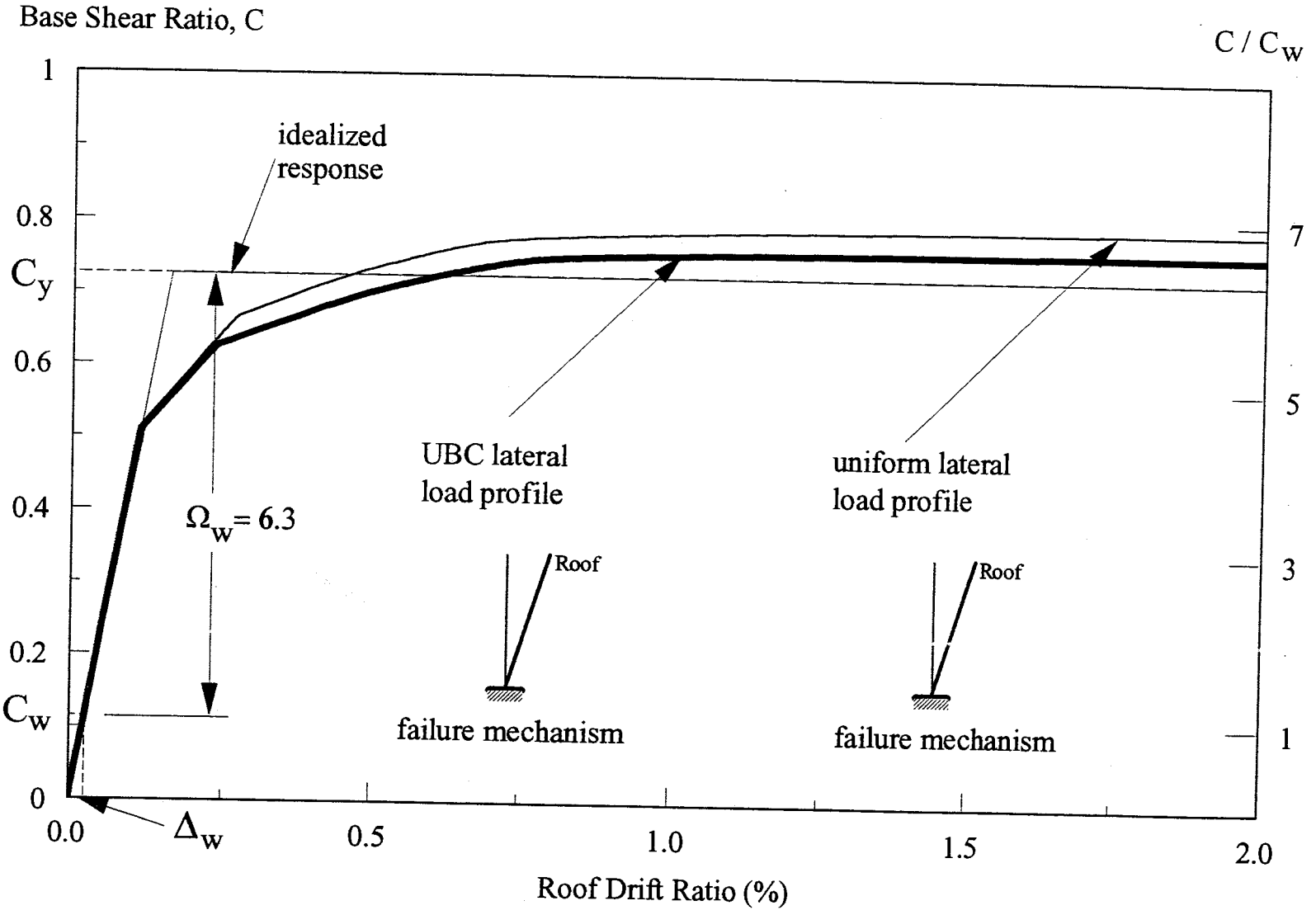

Fig . 4.8 Lateral Strength of CSMIP 58496 (E-W)

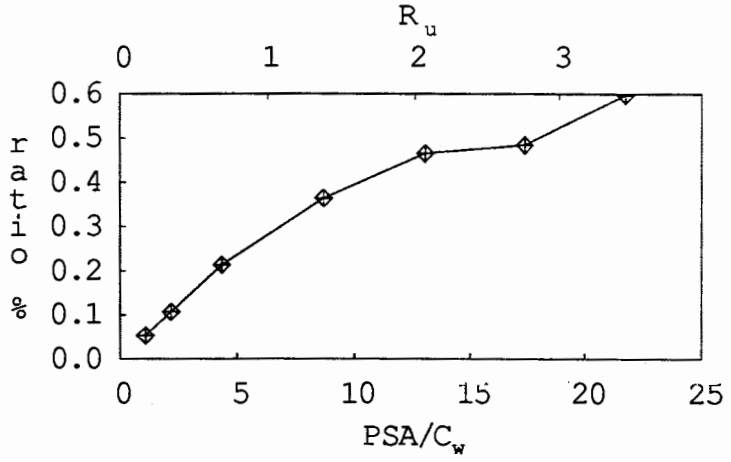

(a) Roof Drift Ratio

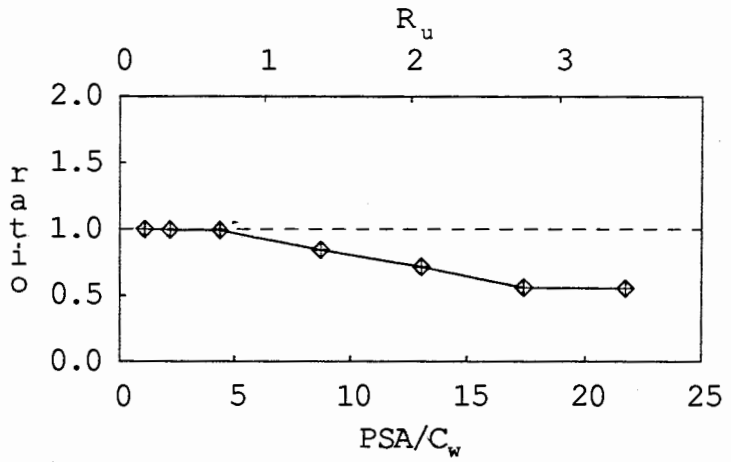

(b) Ratio of Roof Drifts

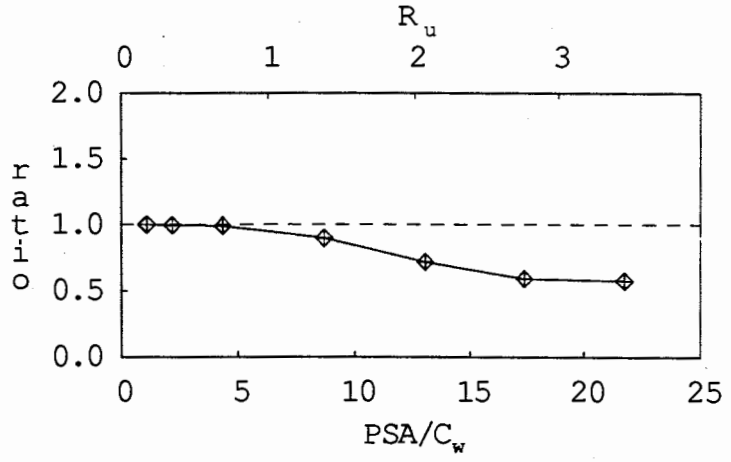

(c) Ratio of Critical Story Drifts

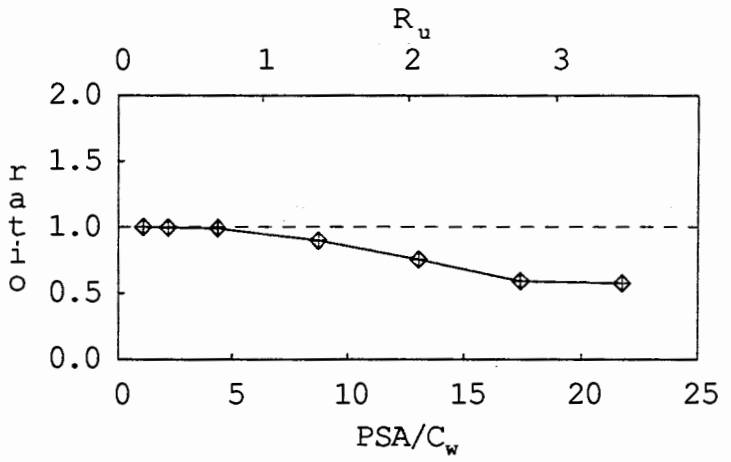

(d) Ratio of Story Drifts

Fig. 4.9 Response Ratios of CSMIP 58496 to Scaled LPSC Earthquake Record

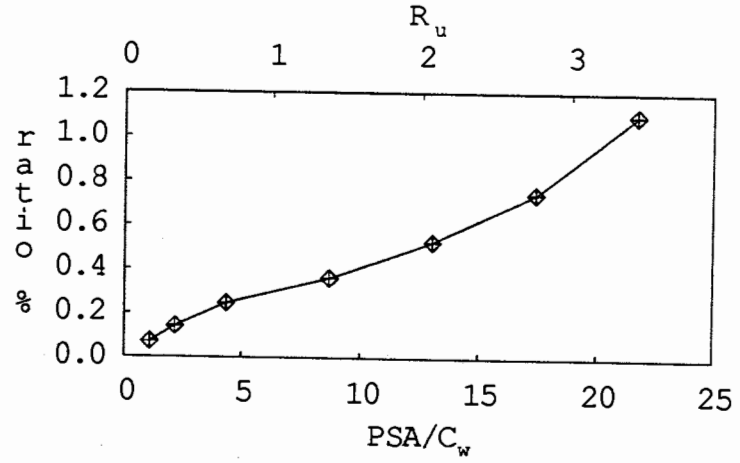

(a) Roof Drift Ratio

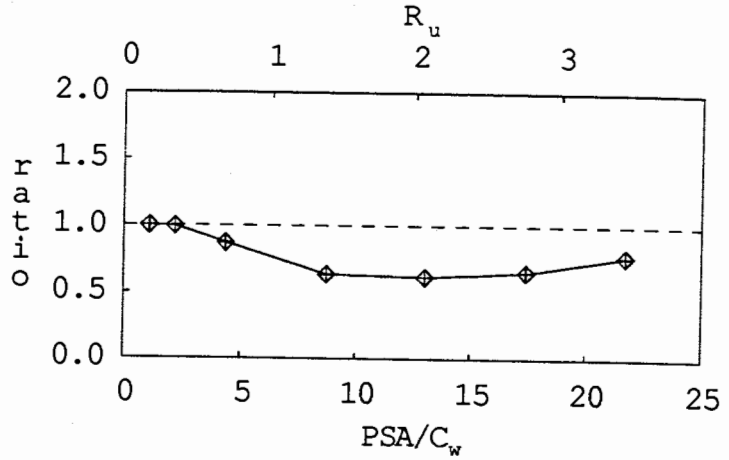

(b) Ratio of Roof Drifts

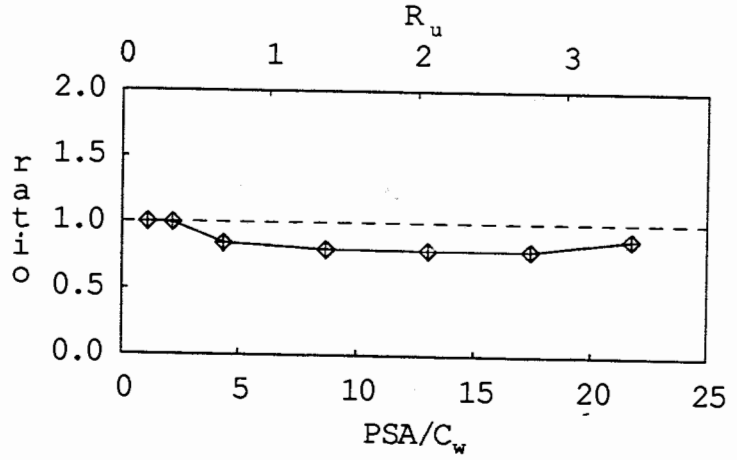

(c) Ratio of Critical Story Drifts

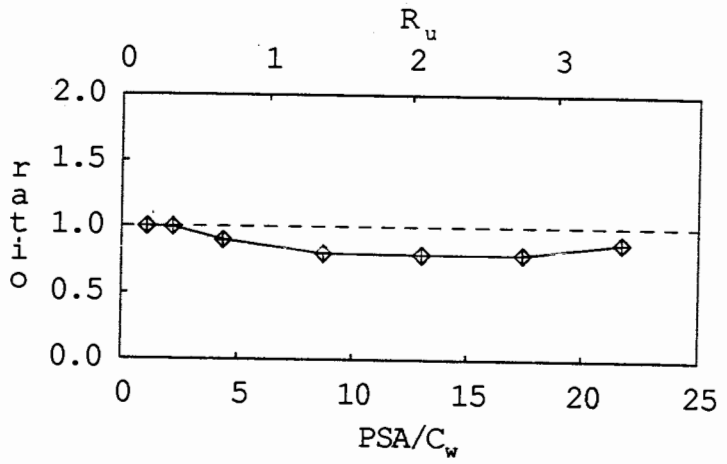

(d) Ratio of Story Drifts

Fig. 4.10 Response Ratios of CSMIP 58496 to Scaled LPC Earthquake Record

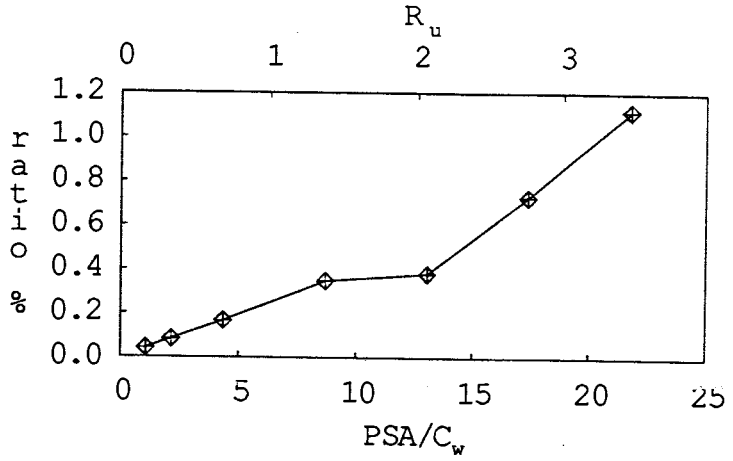

(a) Roof Drift Ratio

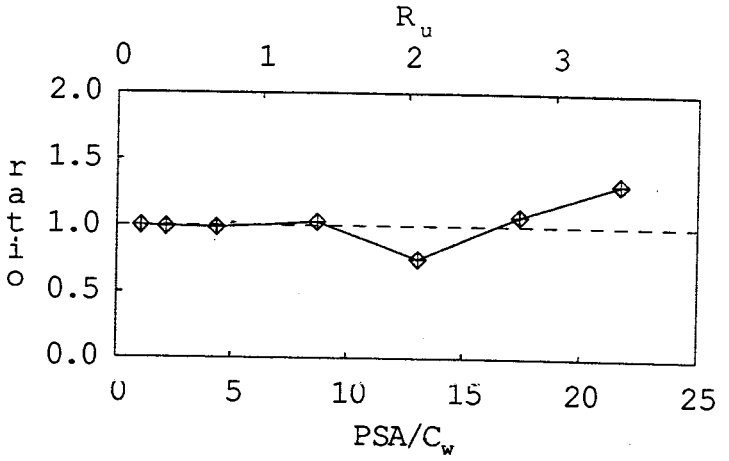

(b) Ratio of Roof Drifts

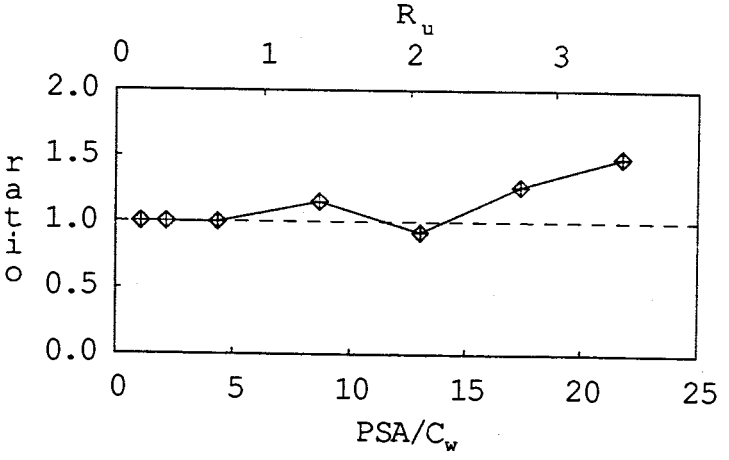

(c) Ratio of Critical Story Drifts

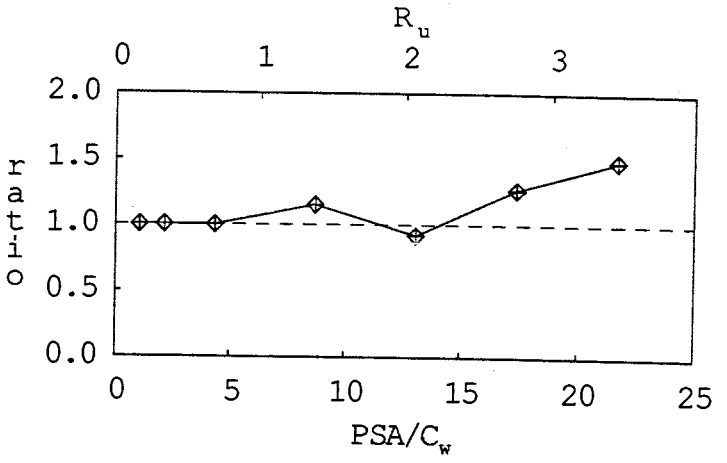

(d) Ratio of Story Drifts

Fig. 4.11 Response Ratios of CSMIP 58496 to Scaled ELC Earthquake Record

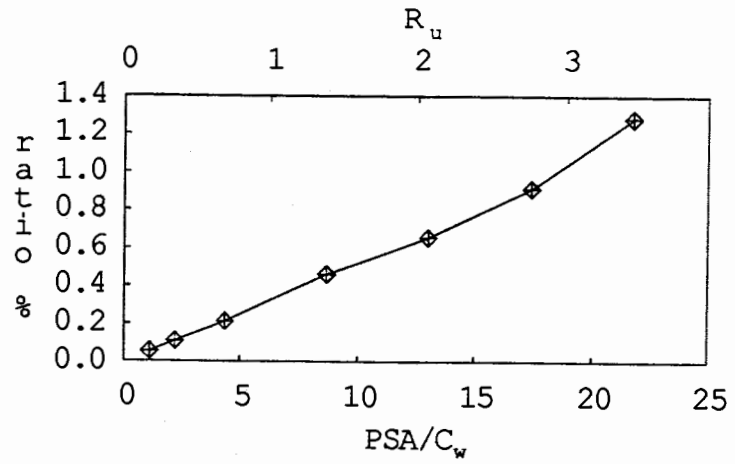

(a) Roof Drift Ratio

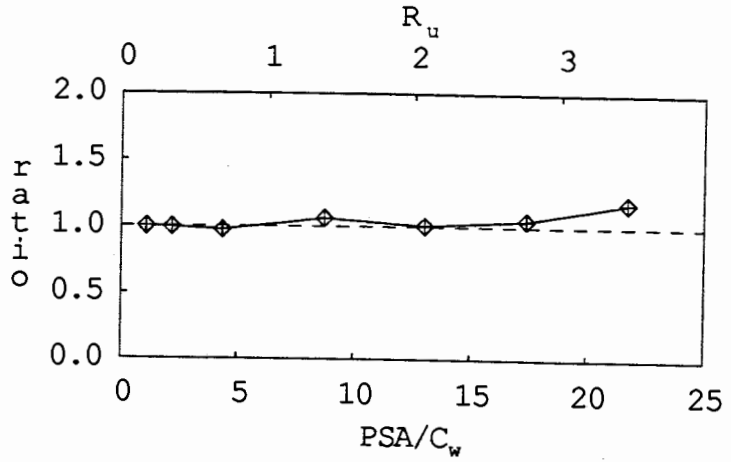

(b) Ratio of Roof Drifts

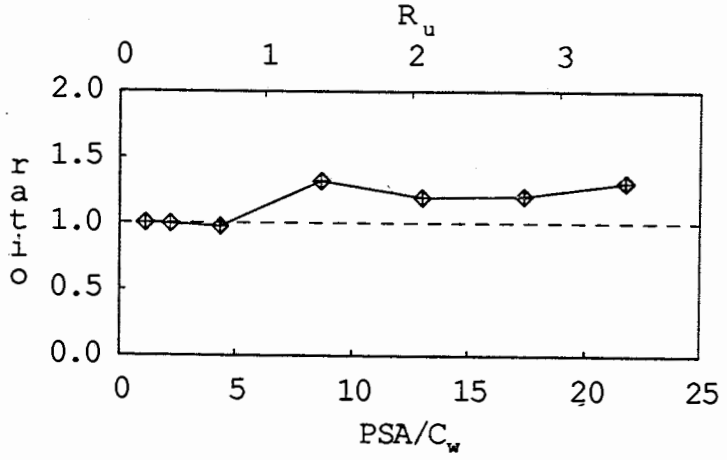

(c) Ratio of Critical Story Drifts

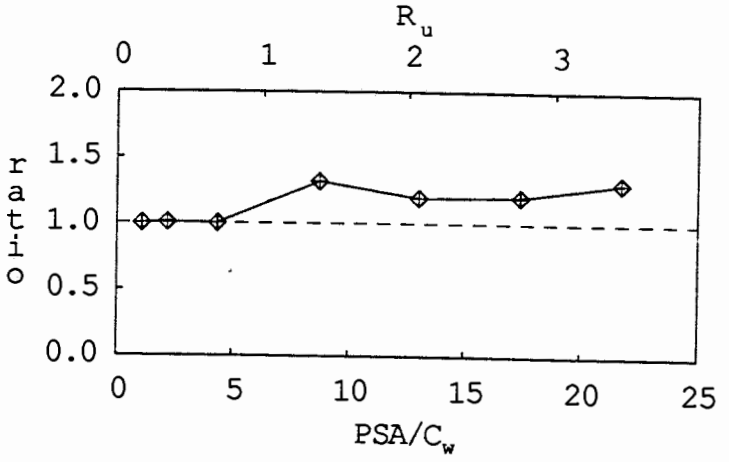

(d) Ratio of Story Drifts

Fig. 4.12 Response Ratios of CSMIP 58496 to Scaled TAF Earthquake Record

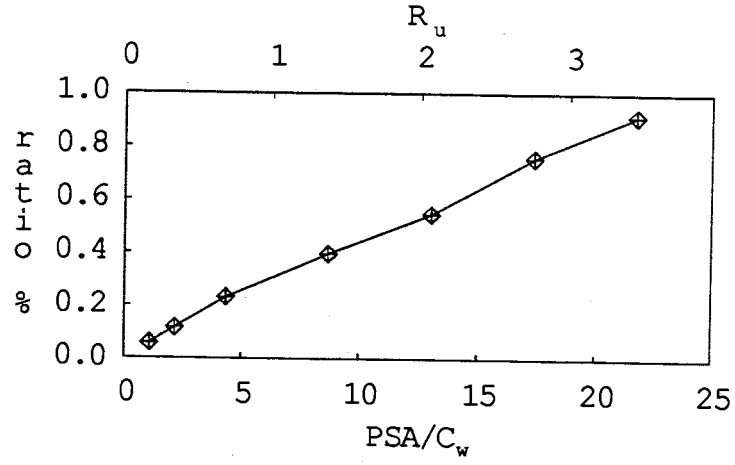

(a) Roof Drift Ratio

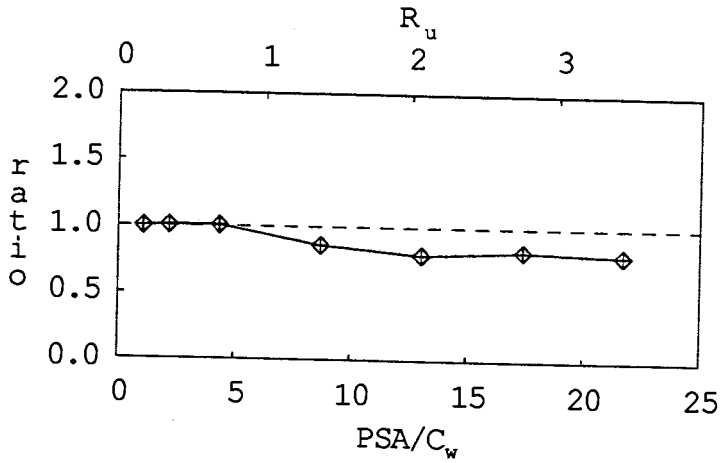

(b) Ratio of Roof Drifts

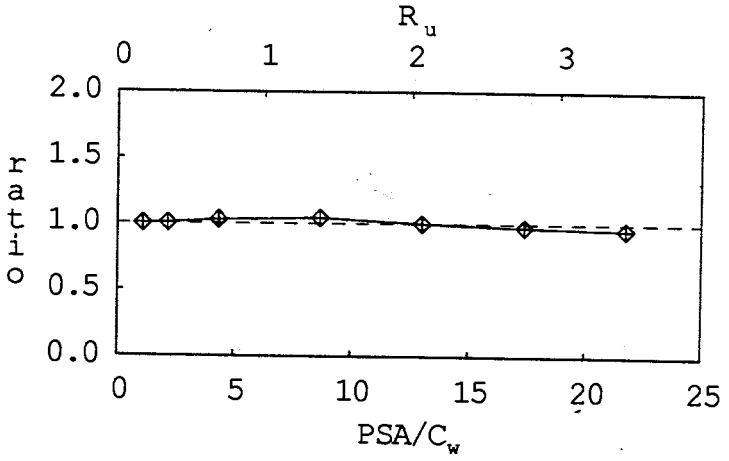

(c) Ratio of Critical Story Drifts

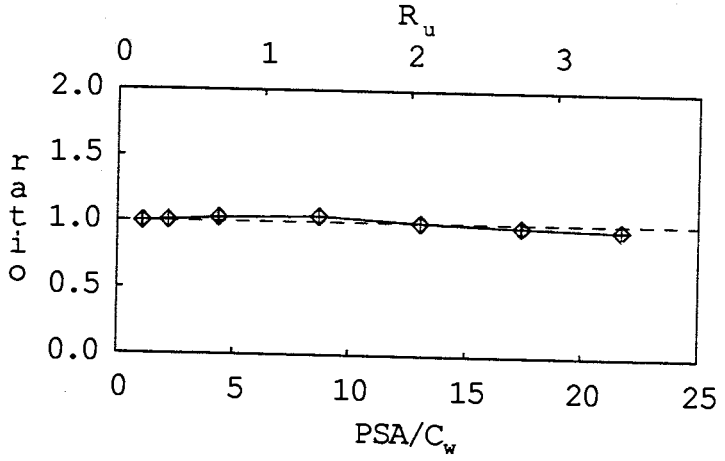

(d) Ratio of Story Drifts

Fig. 4.13 Response Ratios of CSMIP 58496 to Scaled OLY Earthquake Record

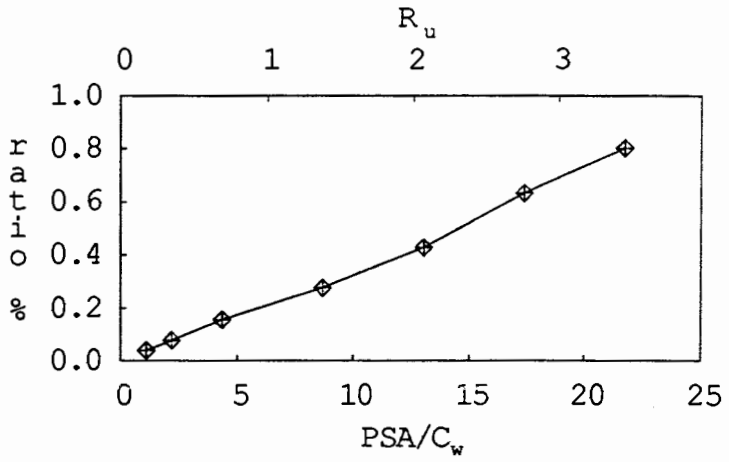

(a) Roof Drift Ratio

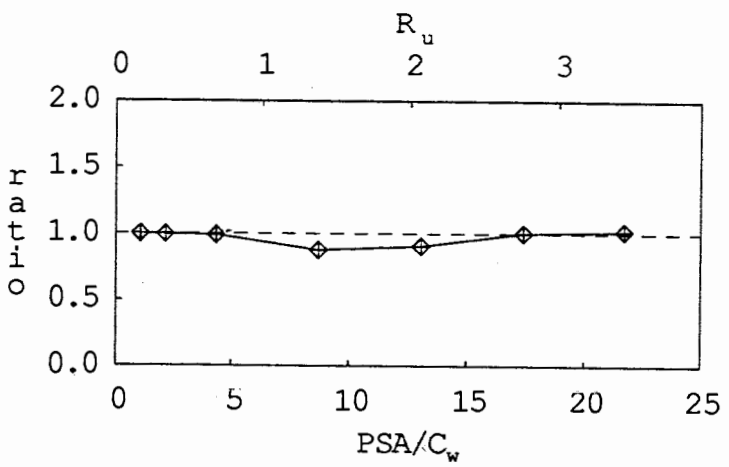

(b) Ratio of Roof Drifts

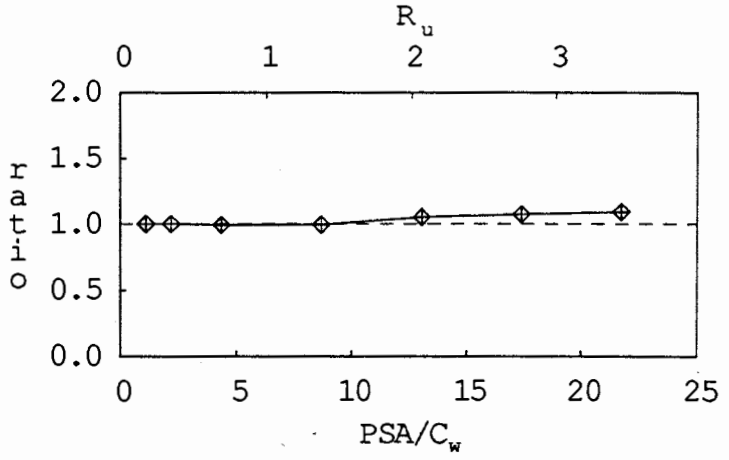

(c) Ratio of Critical Story Drifts

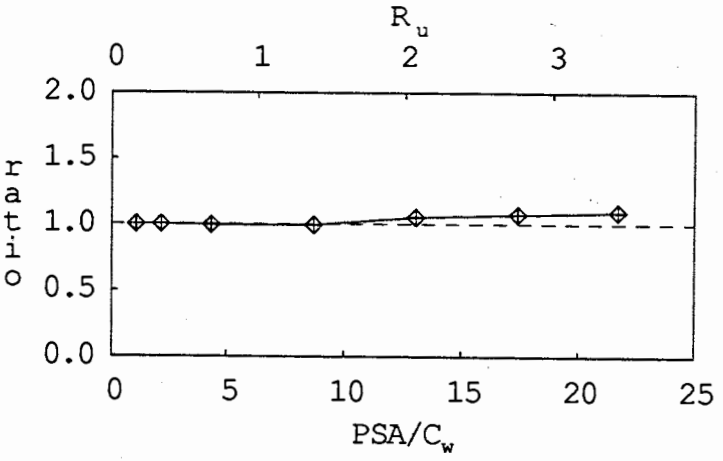

(d) Ratio of Story Drifts

Fig. 4.14 Response Ratios of CSMIP 58496 to Scaled PAC Earthquake Record

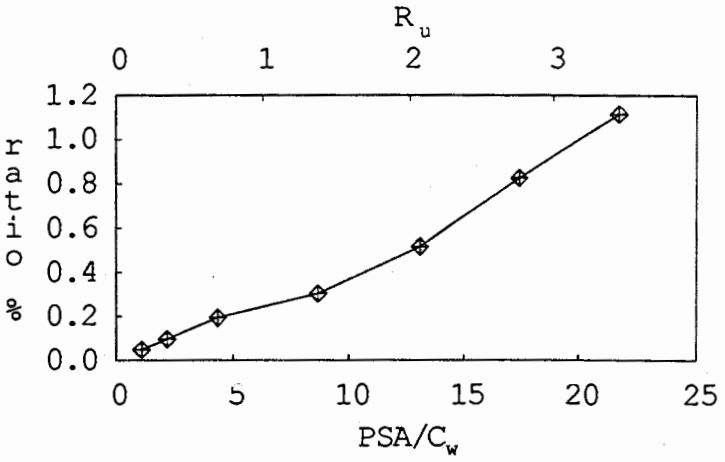

(a) Roof Drift Ratio

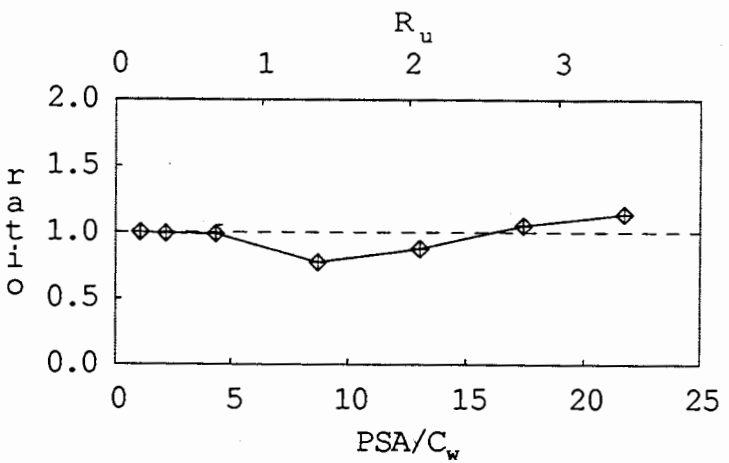

(b) Ratio of Roof Drifts

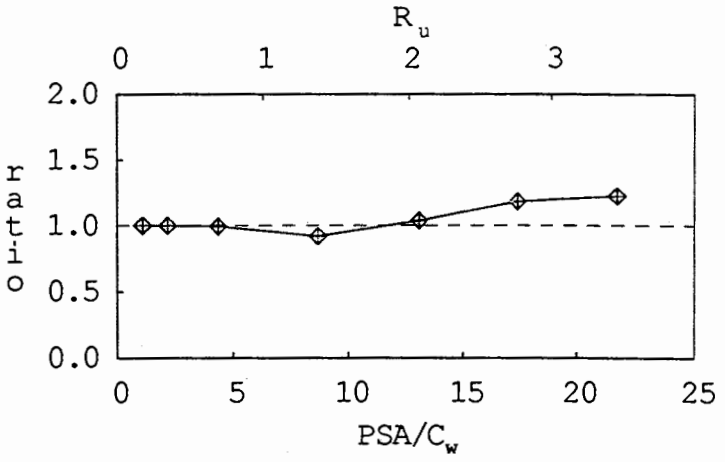

(c) Ratio of Critical Story Drifts

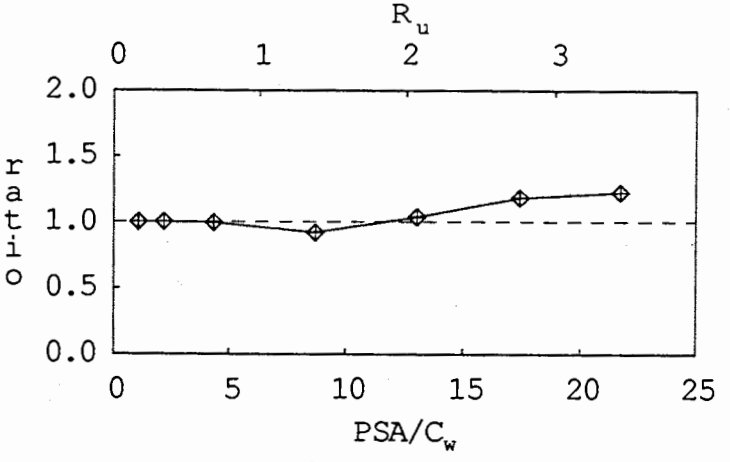

(d) Ratio of Story Drifts

Fig. 4.15 Response Ratios of CSMIP 58496 to Scaled PAR Earthquake Record

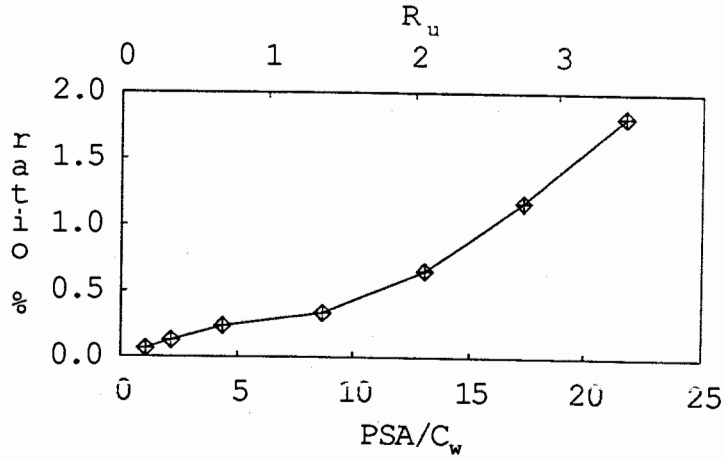

(a) Roof Drift Ratio

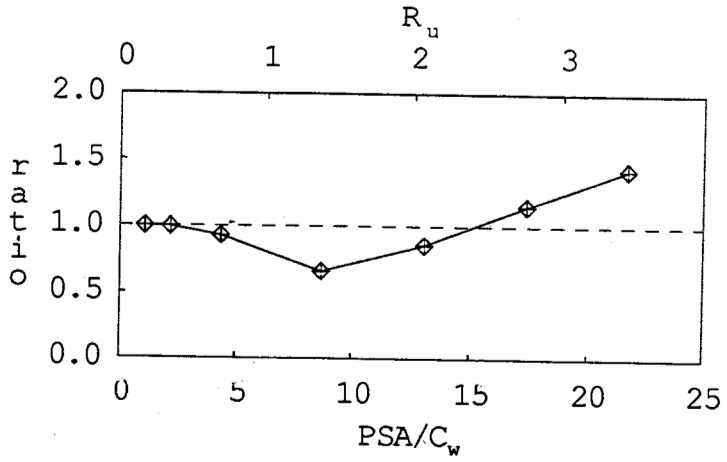

(b) Ratio of Roof Drifts

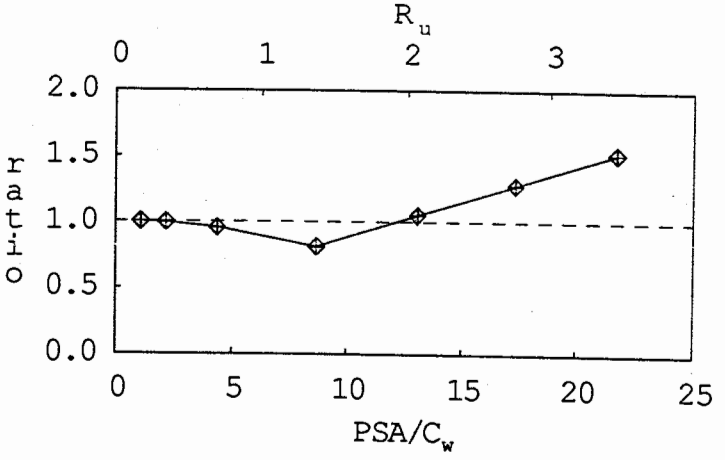

(c) Ratio of Critical Story Drifts

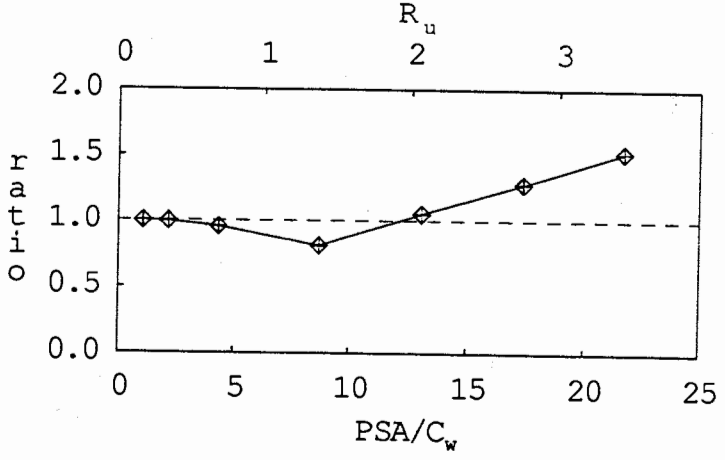

(d) Ratio of Story Drifts

Fig. 4.16 Response Ratios of CSMIP 58496 to Scaled IVC Earthquake Record

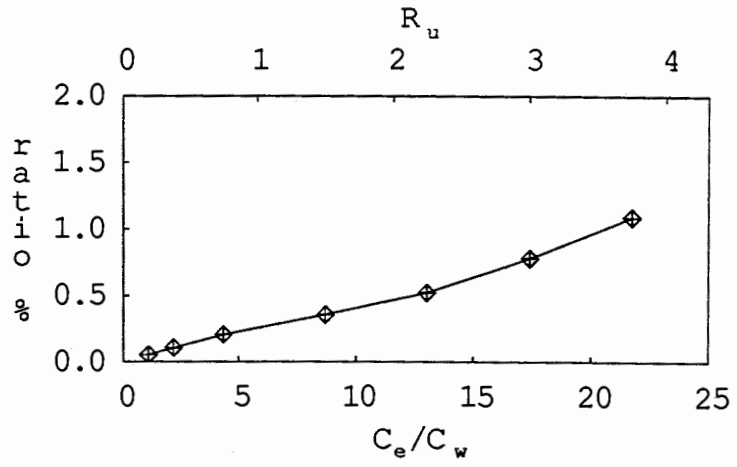

(a) Mean Roof Drift Ratio

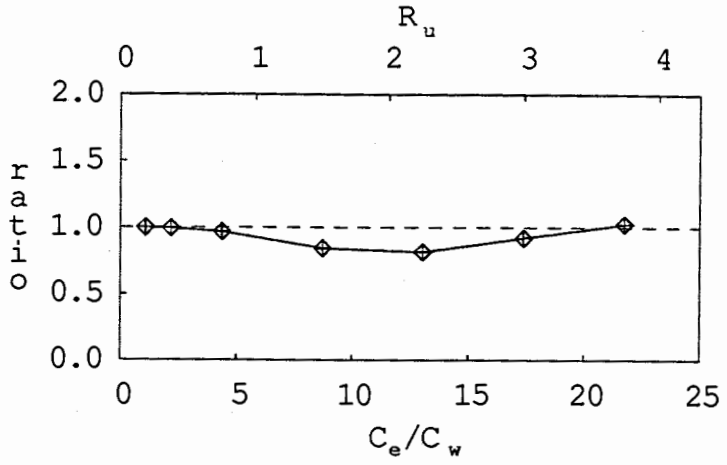

(b) Mean Ratio of Roof Drifts

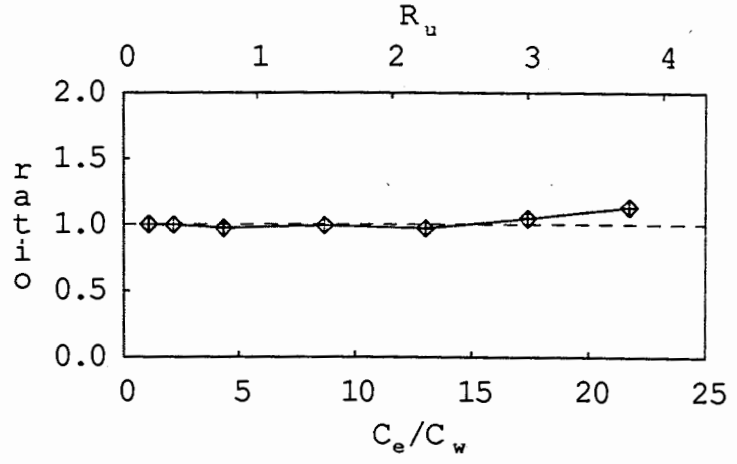

(c) Mean Ratio of Critical Story Drifts

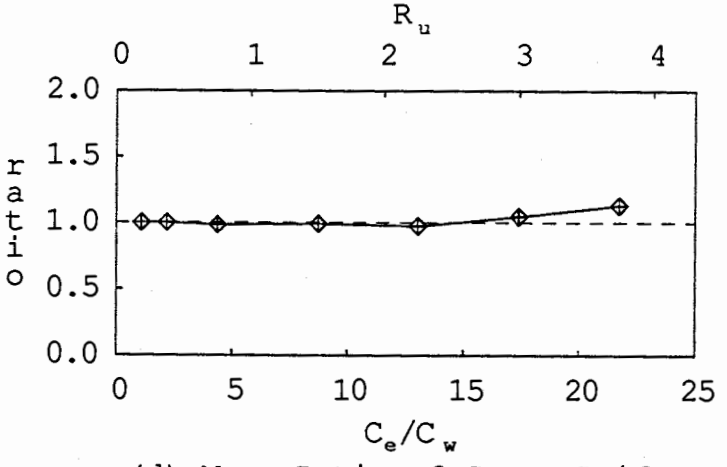

(d) Mean Ratio of Story Drifts

Fig. 4.17 Mean Response of CSMIP 58496 to Eight Scaled Earthquake Records

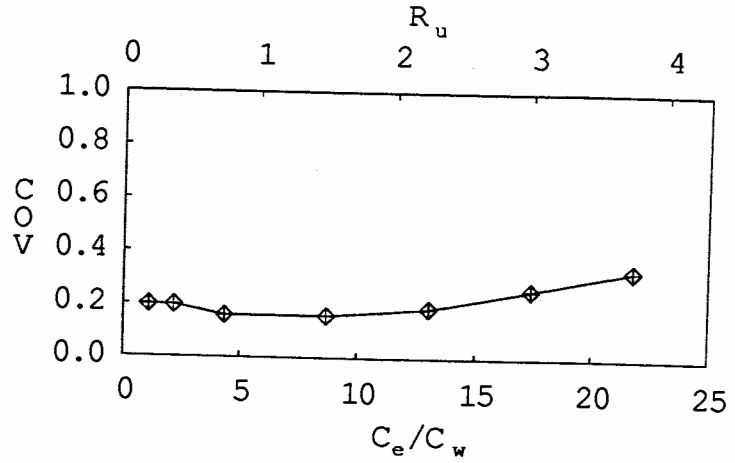

(a) COV for Roof Drift Ratio

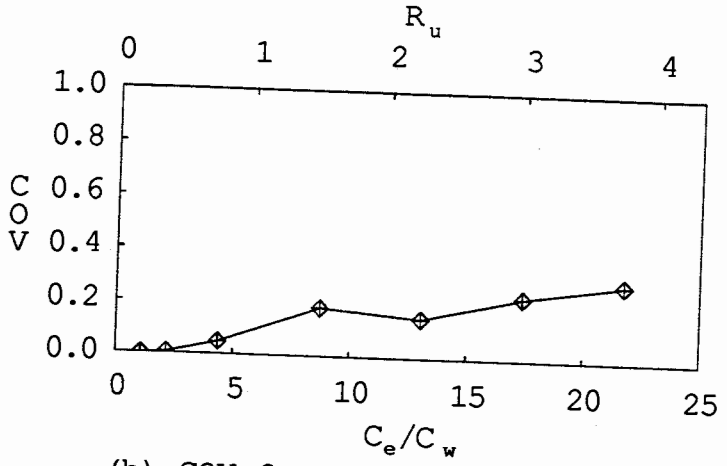

(b) COV for Ratio of Roof Drifts

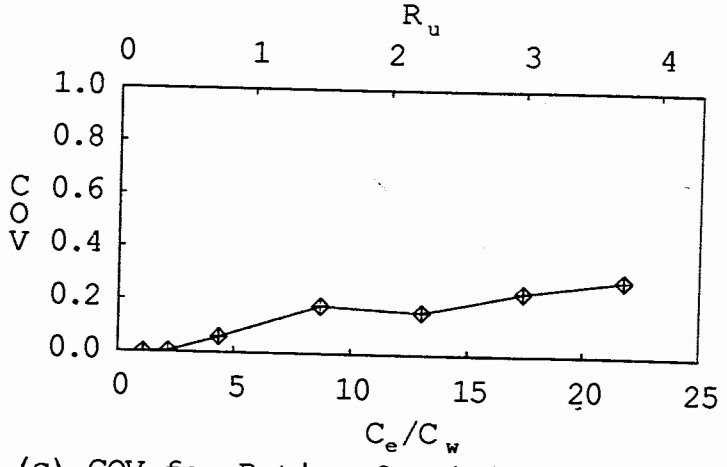

(c) COV for Ratio of Critical Story Drifts

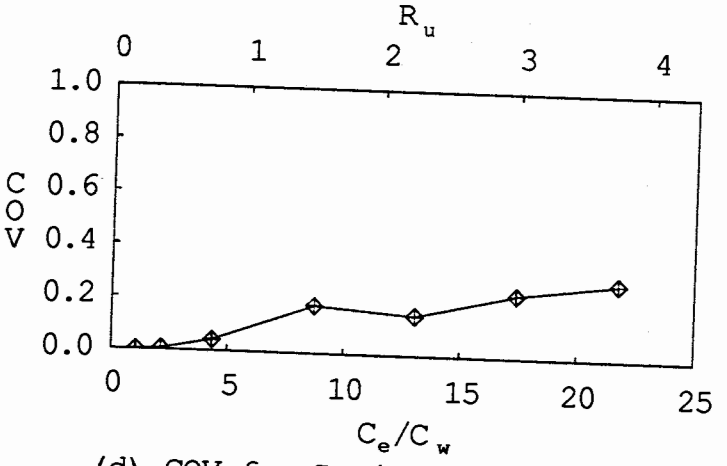

(d) COV for Ratio of Story Drifts

Fig. 4.18 COV for Response of CSMIP 58496 to Eight Scaled Earthquake Records

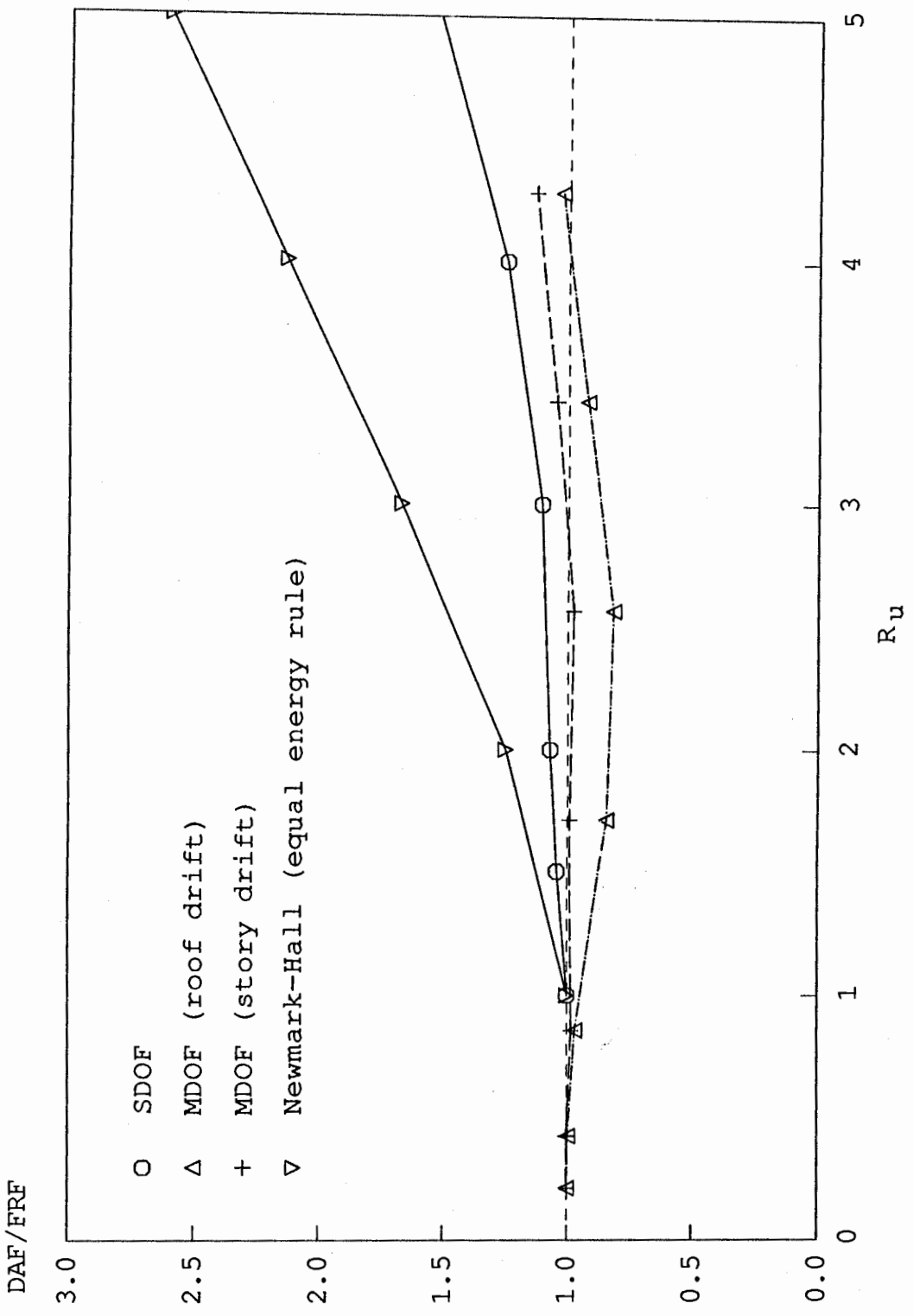

Fig. 4.19 Comparison of Mean Response Ratios between SDOF and MDOF systems (CSMIP 58496)

Fig. 5.1 **San Jose 10-story Commercial Building (CSMIP 57355)**

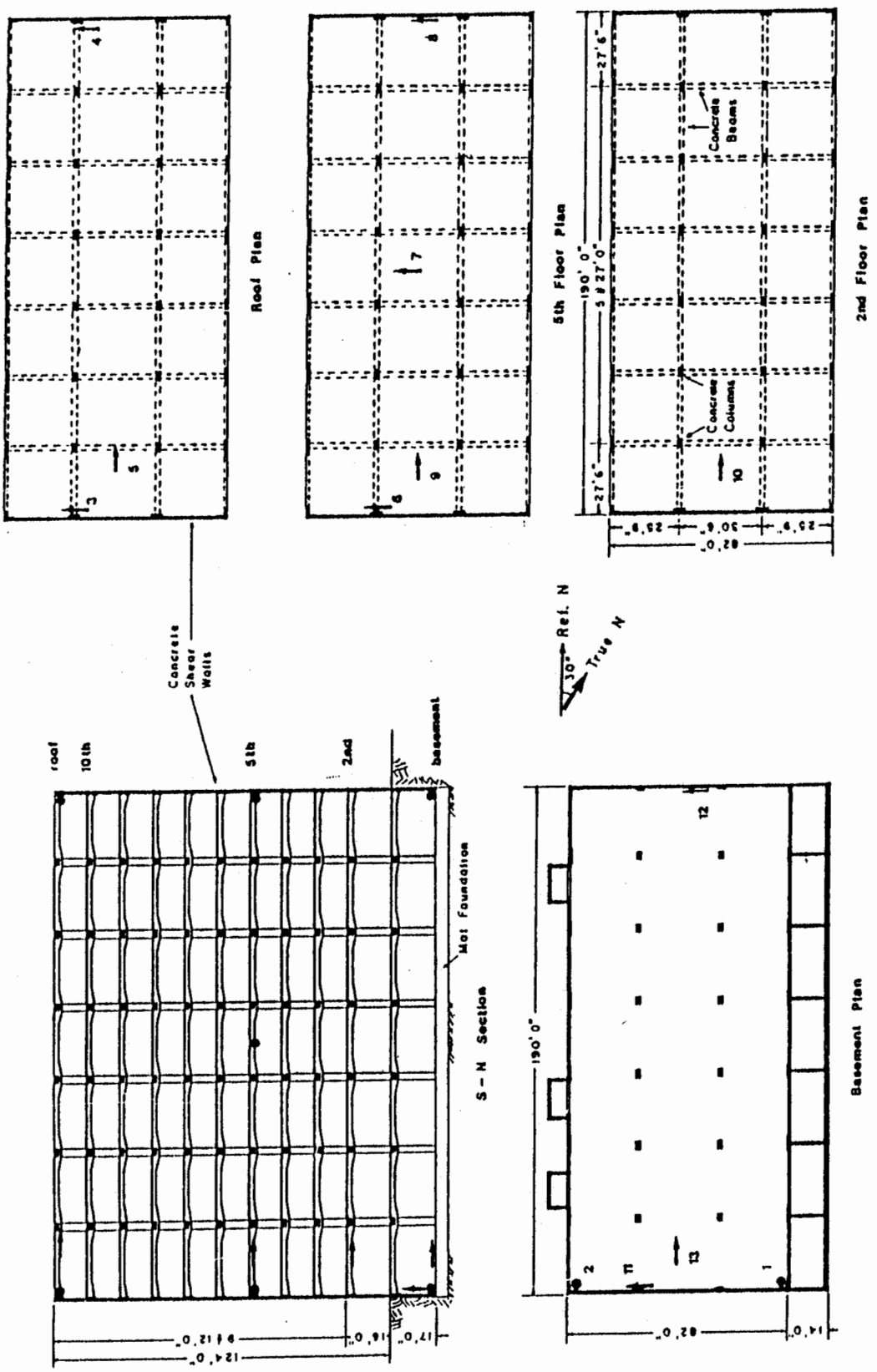

Fig. 5.2 General Layout of Building CSMIP 57355

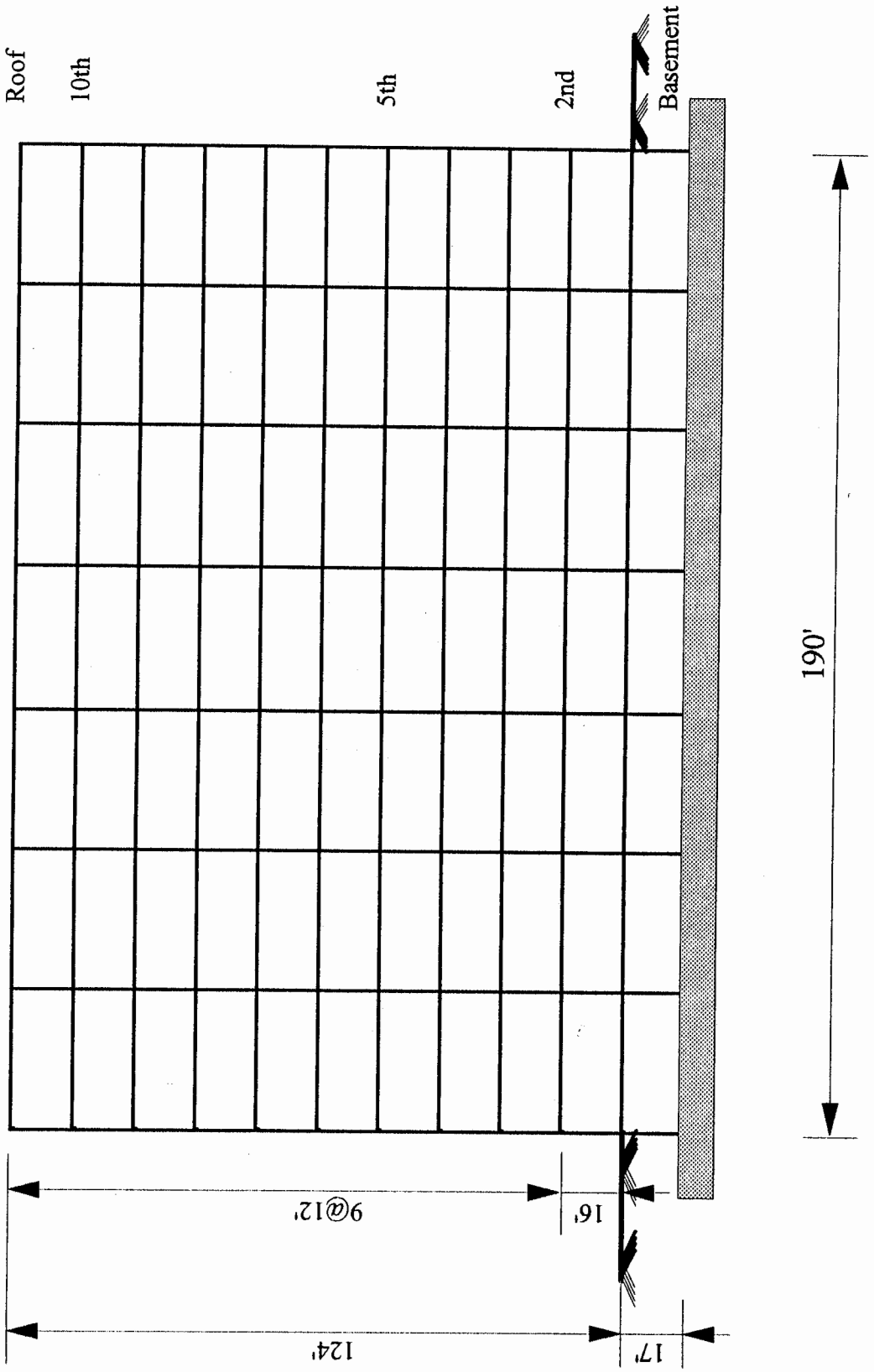

Fig. 5.3 SMRSF of Building CSMIP 57355 (N-S)

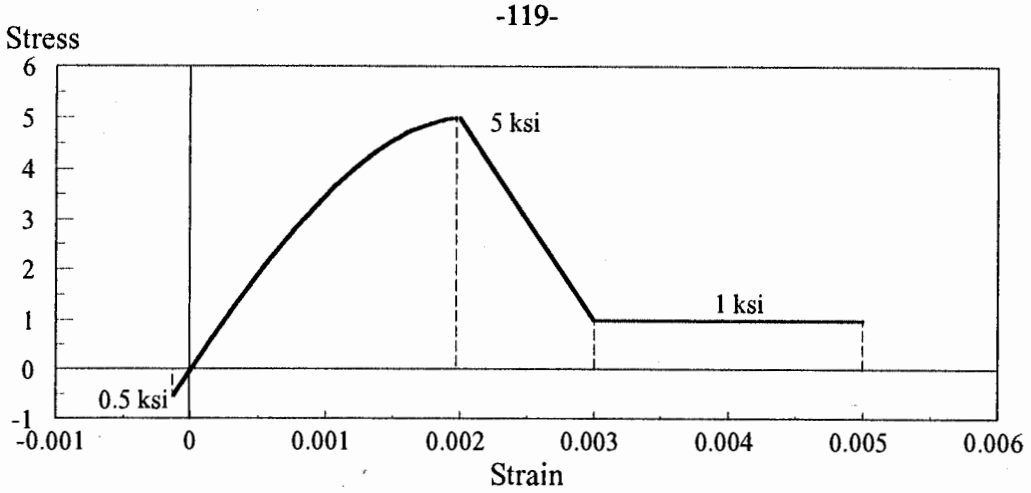

(a) Idealized Concrete Stress-Strain Relationship

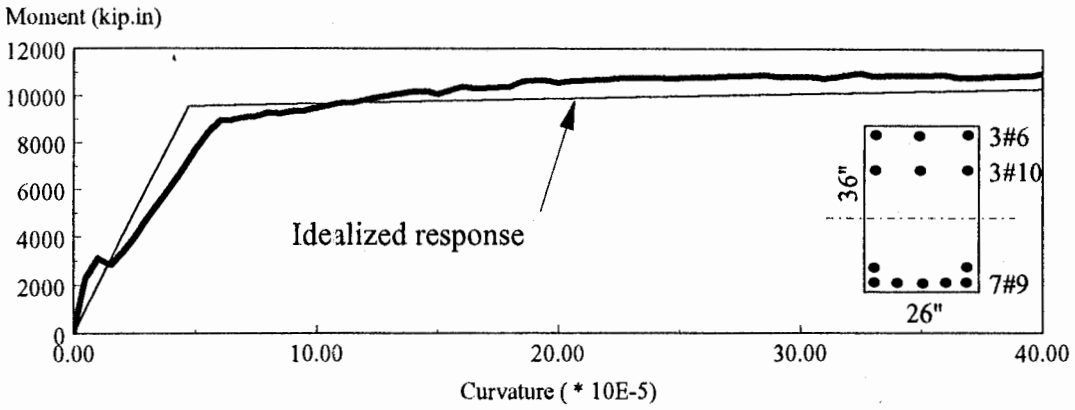

(b) Beam Moment-Curvature Diagram

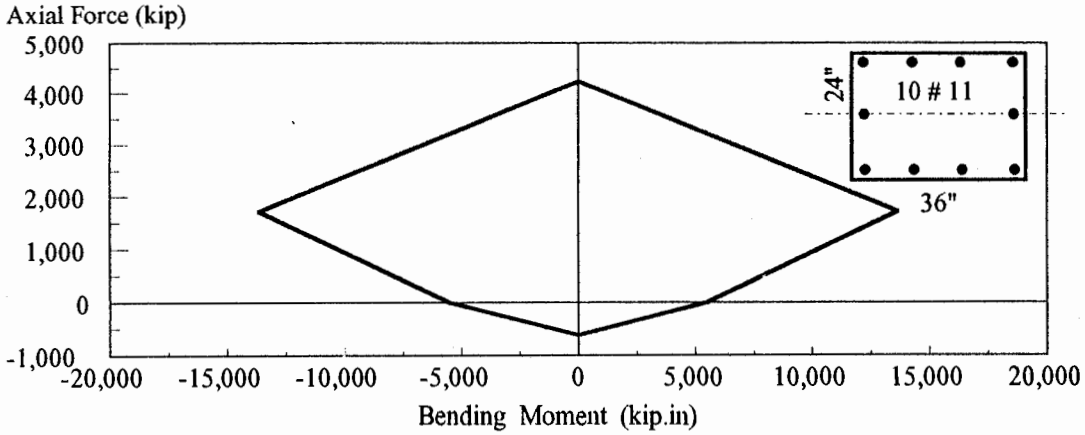

(c) Column Moment-Axial Force Interaction Diagram

Fig. 5.4 Modelling of Reinforced Concrete Members

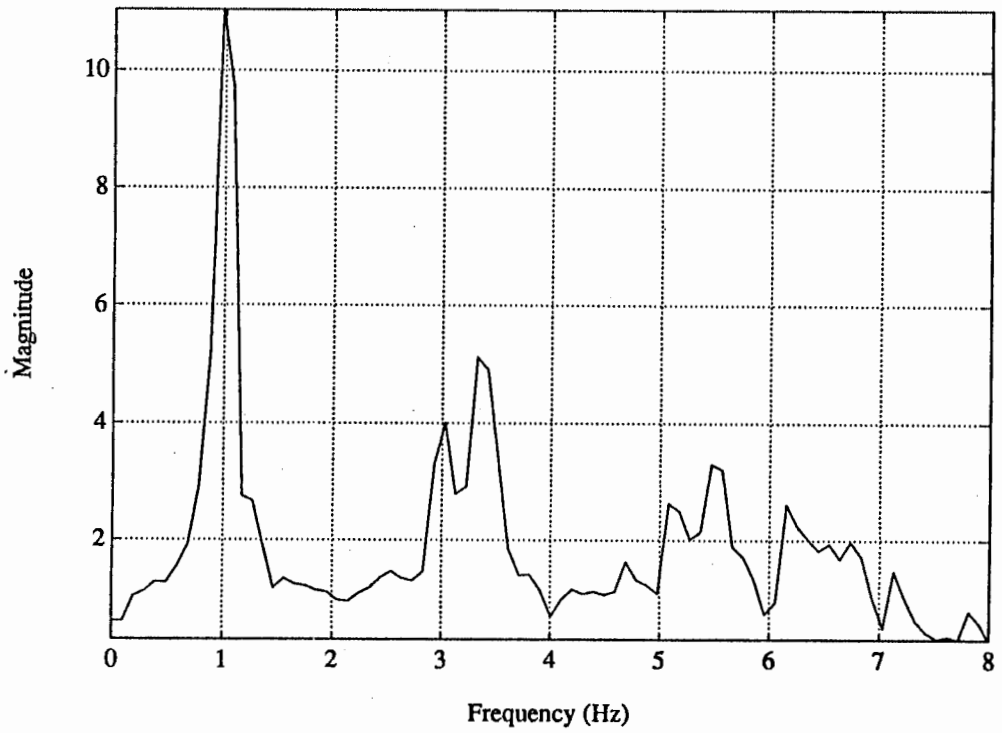

Fig. 5.5 Magnitude of Acceleration Transfer Functions between the Base and the Roof (CSMIP 57355)

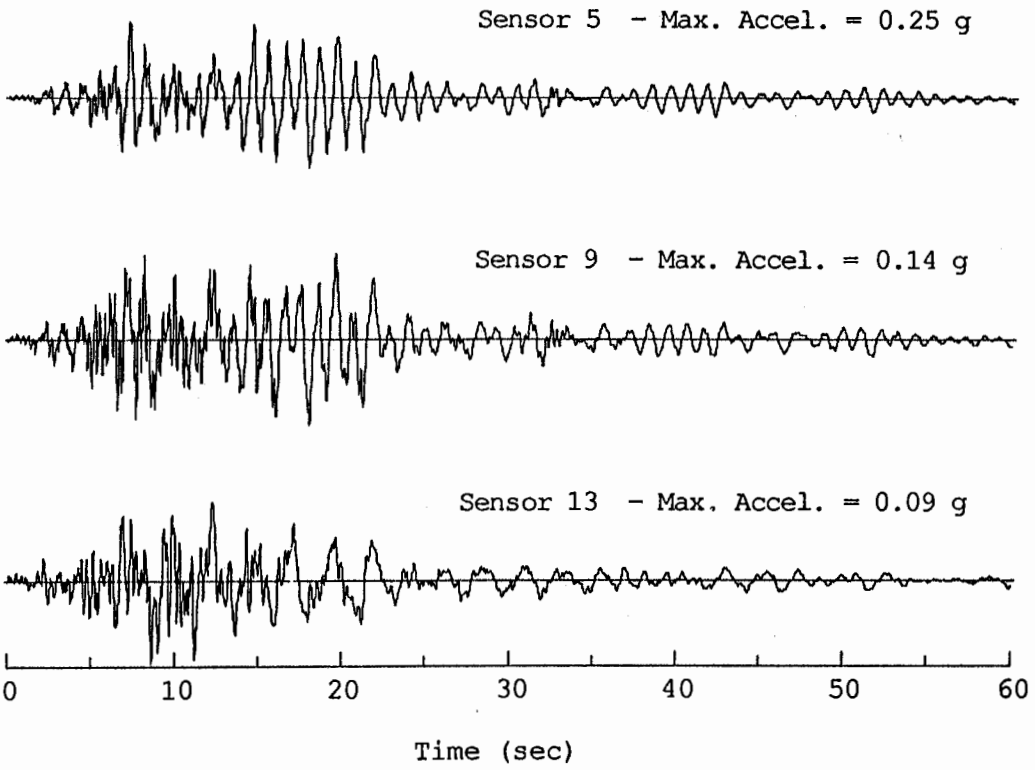

Fig. 5.6 Building CSMIP 57355 Acceleration Records (N-S)

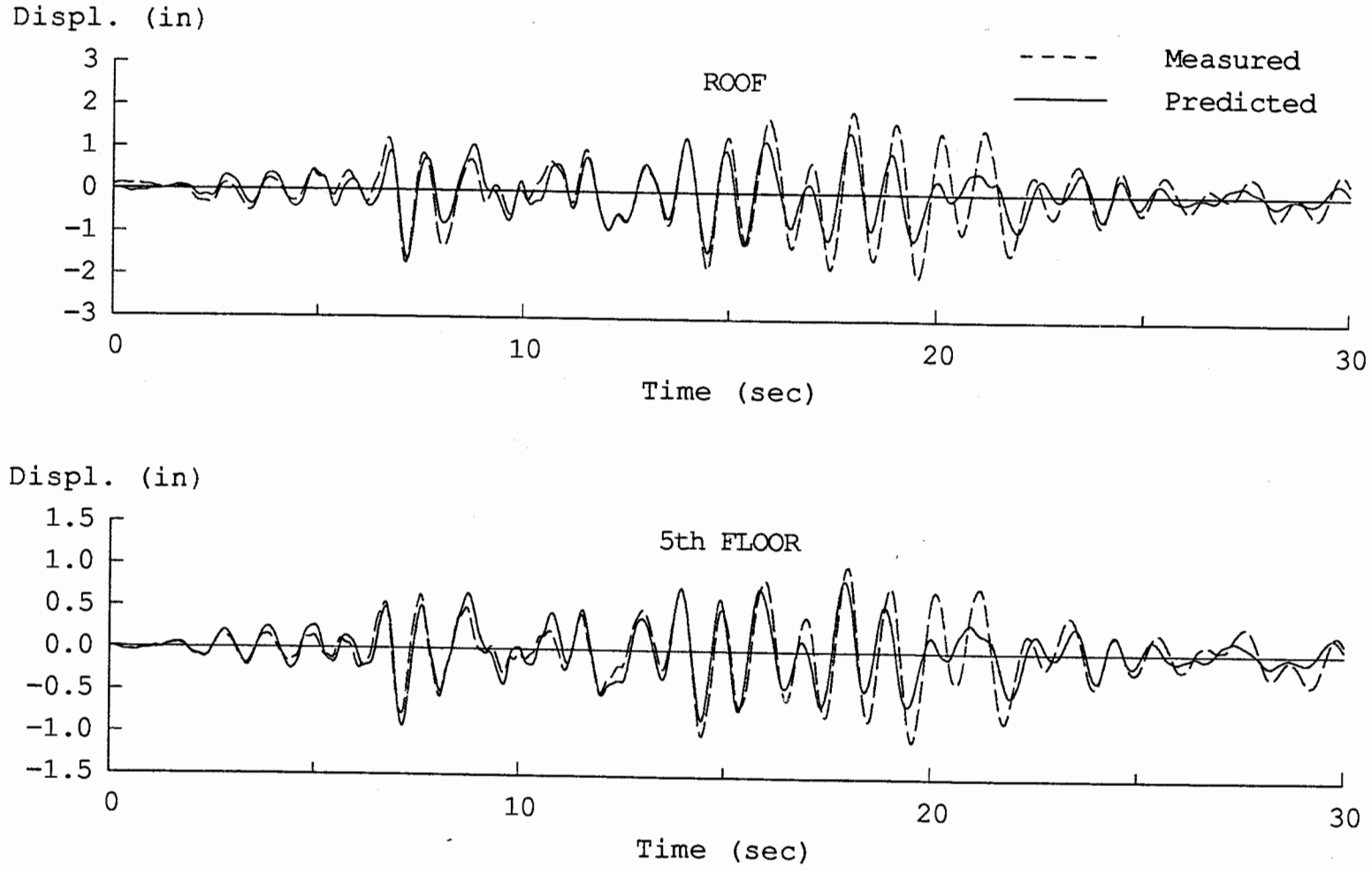

Fig. 5.7 Measured versus Predicted Relative Displacement Time Histories (CMSIP 57355, N-S)

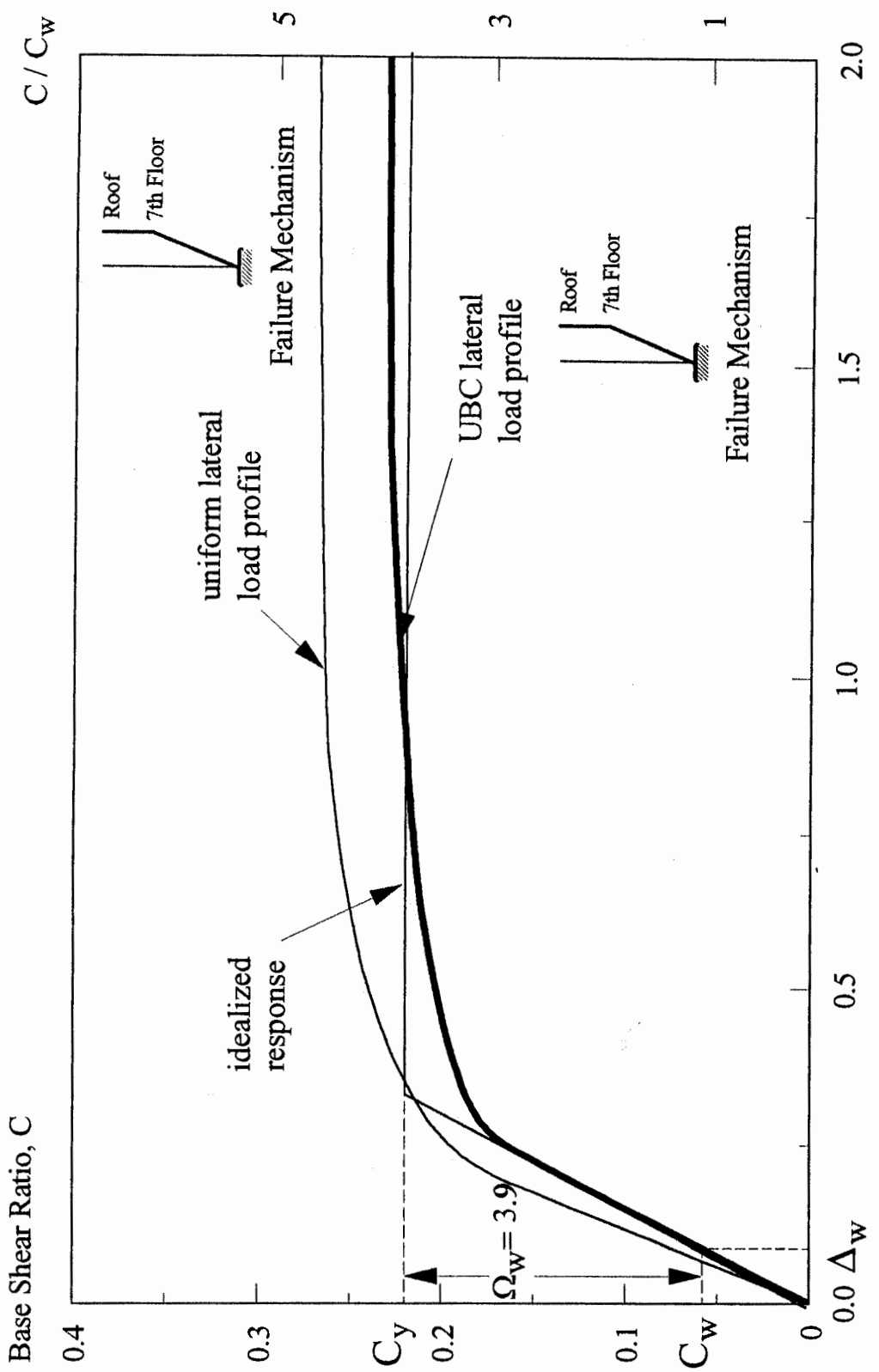

Fig. 5.8 Lateral Strength of CSMIP 57355 (N-S)

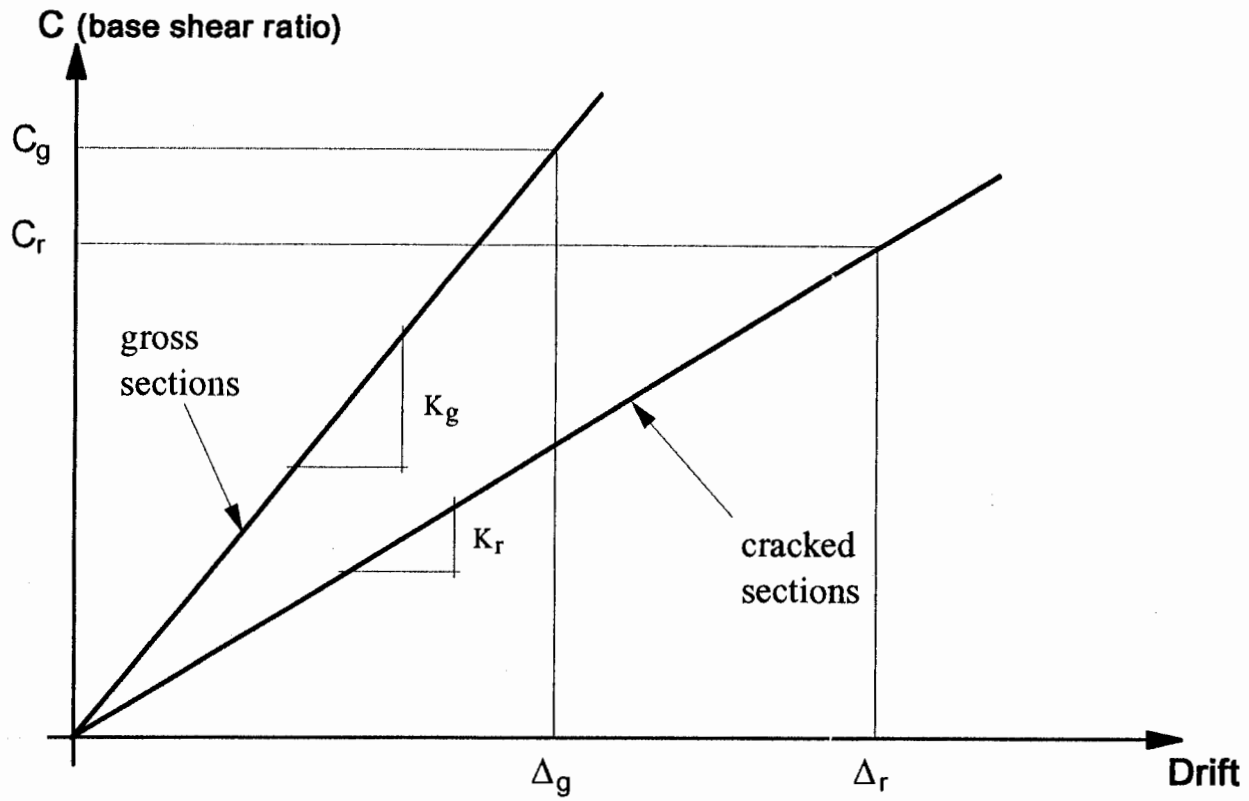

Fig. 5.9 Stiffness Reduction of Reinforced Concrete Buildings

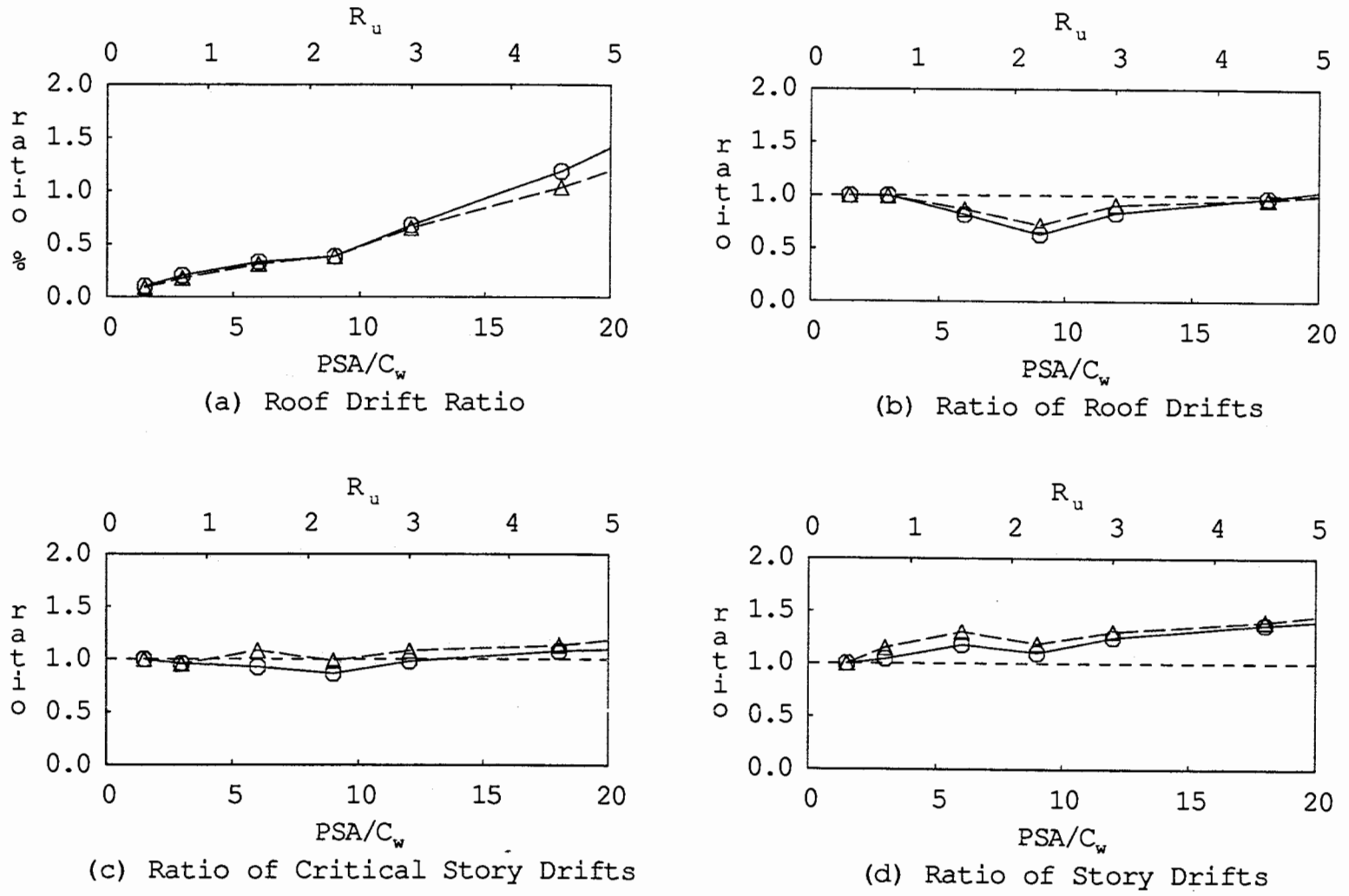

Fig. 5.10 Response Ratios of CSMIP 57355 to Scaled LPSC Earthquake Record

[No stiffness degradation (solid), stiffness degradation (dashed)]

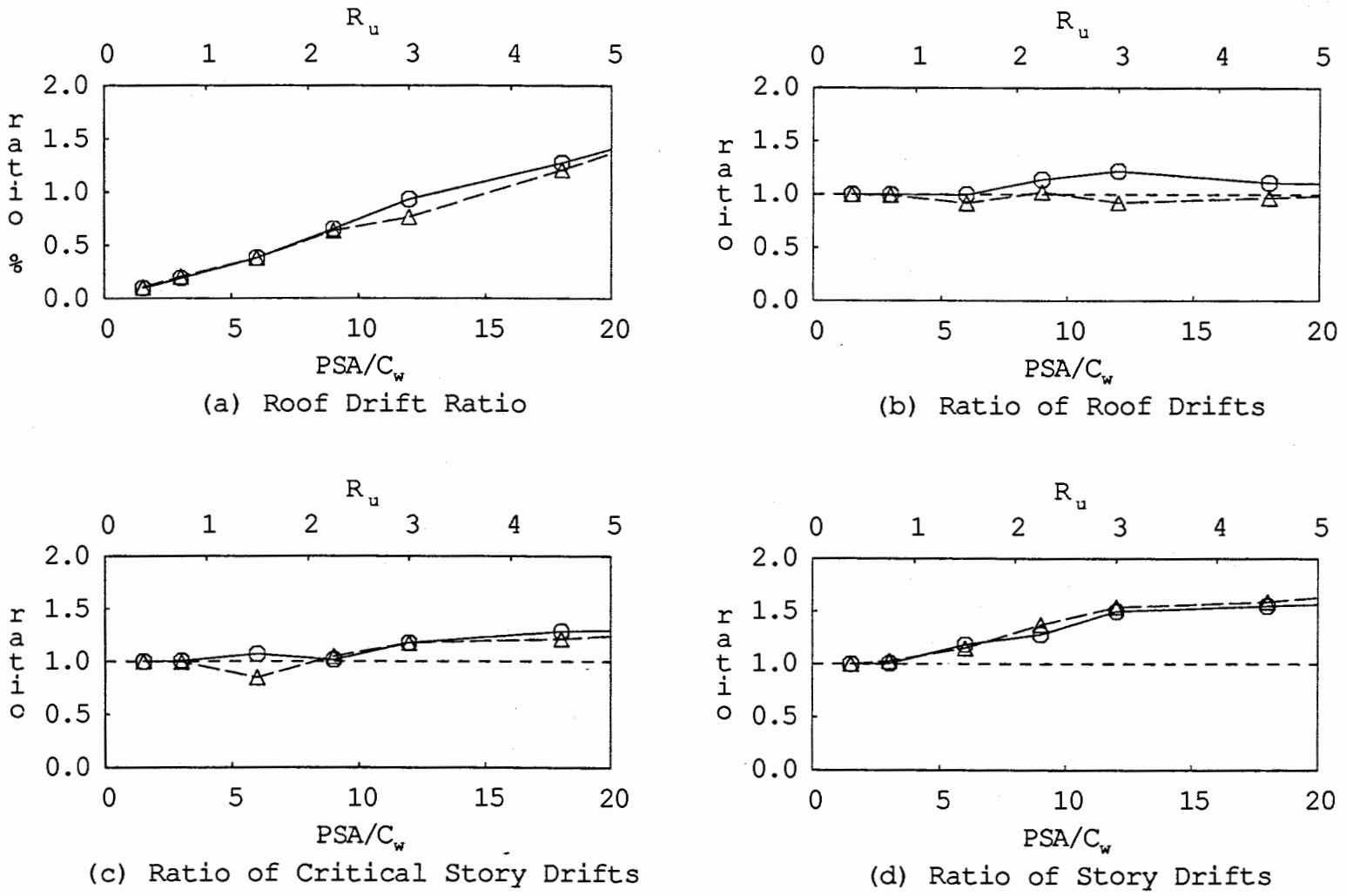

Fig. 5.11 Response Ratios of CSMIP 57355 to Scaled LPC Earthquake Record

[No stiffness degradation (solid), stiffness degradation (dashed)]

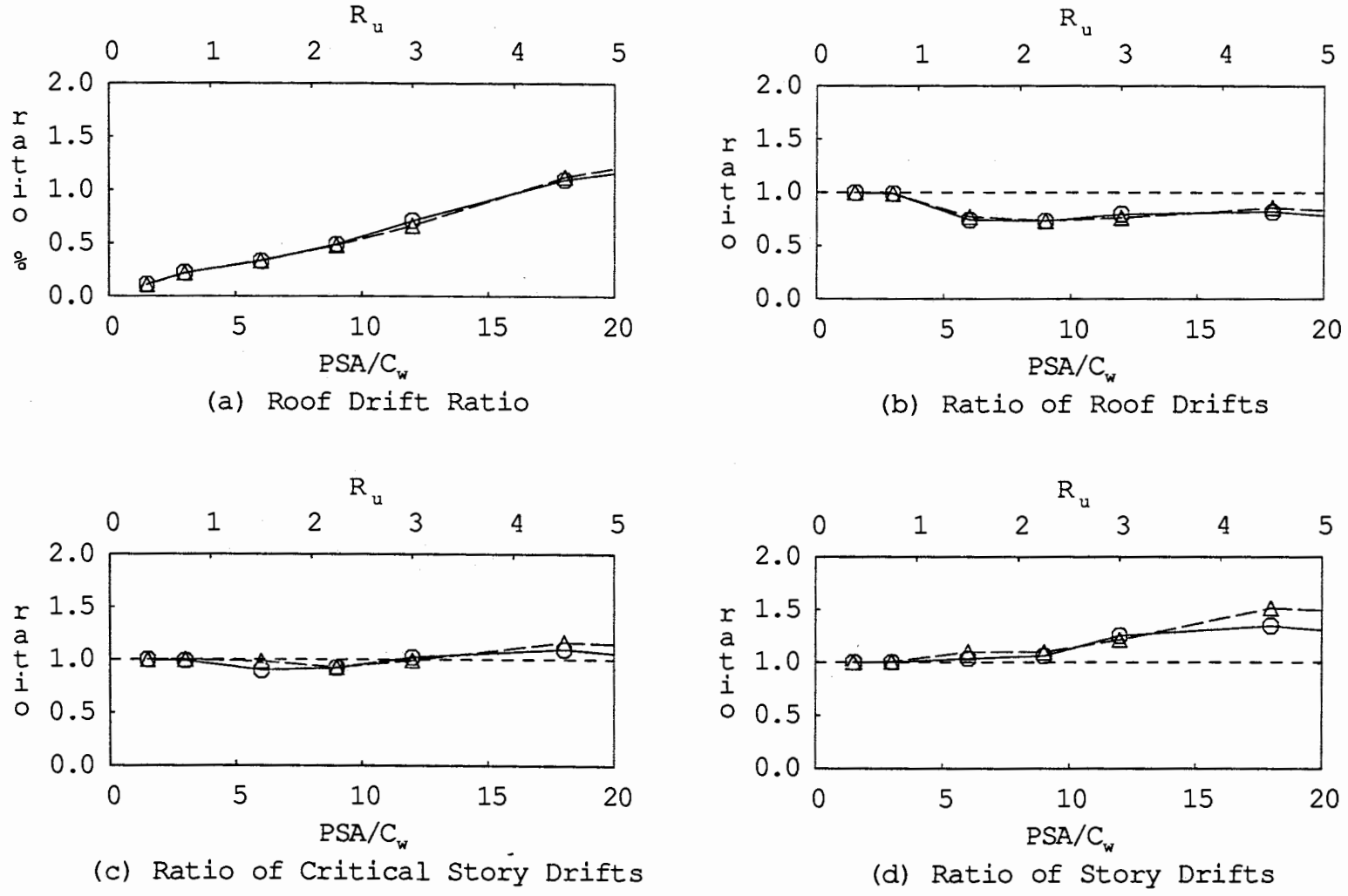

(a) Roof Drift Ratio

(b) Ratio of Roof Drifts

(c) Ratio of Critical Story Drifts

(d) Ratio of Story Drifts

Fig. 5.12 Response Ratios of CSMIP 57355 to Scaled ELC Earthquake Record

[No stiffness degradation (solid), stiffness degradation (dashed)]

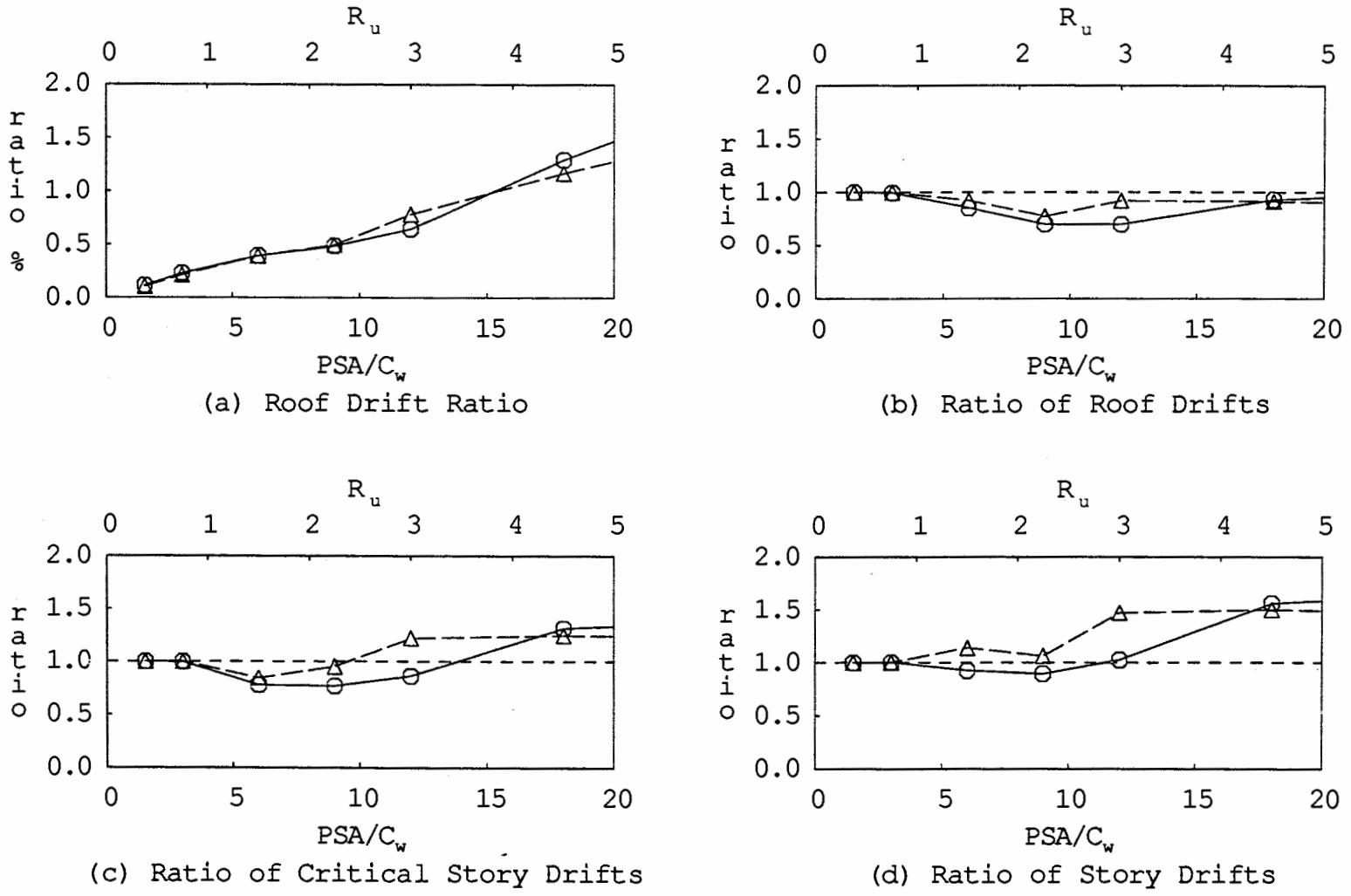

(a) Roof Drift Ratio

(b) Ratio of Roof Drifts

(c) Ratio of Critical Story Drifts

(d) Ratio of Story Drifts

Fig. 5.13 Response Ratios of CSMIP 57355 to Scaled TAF Earthquake Record

[No stiffness degradation (solid), stiffness degradation (dashed)]

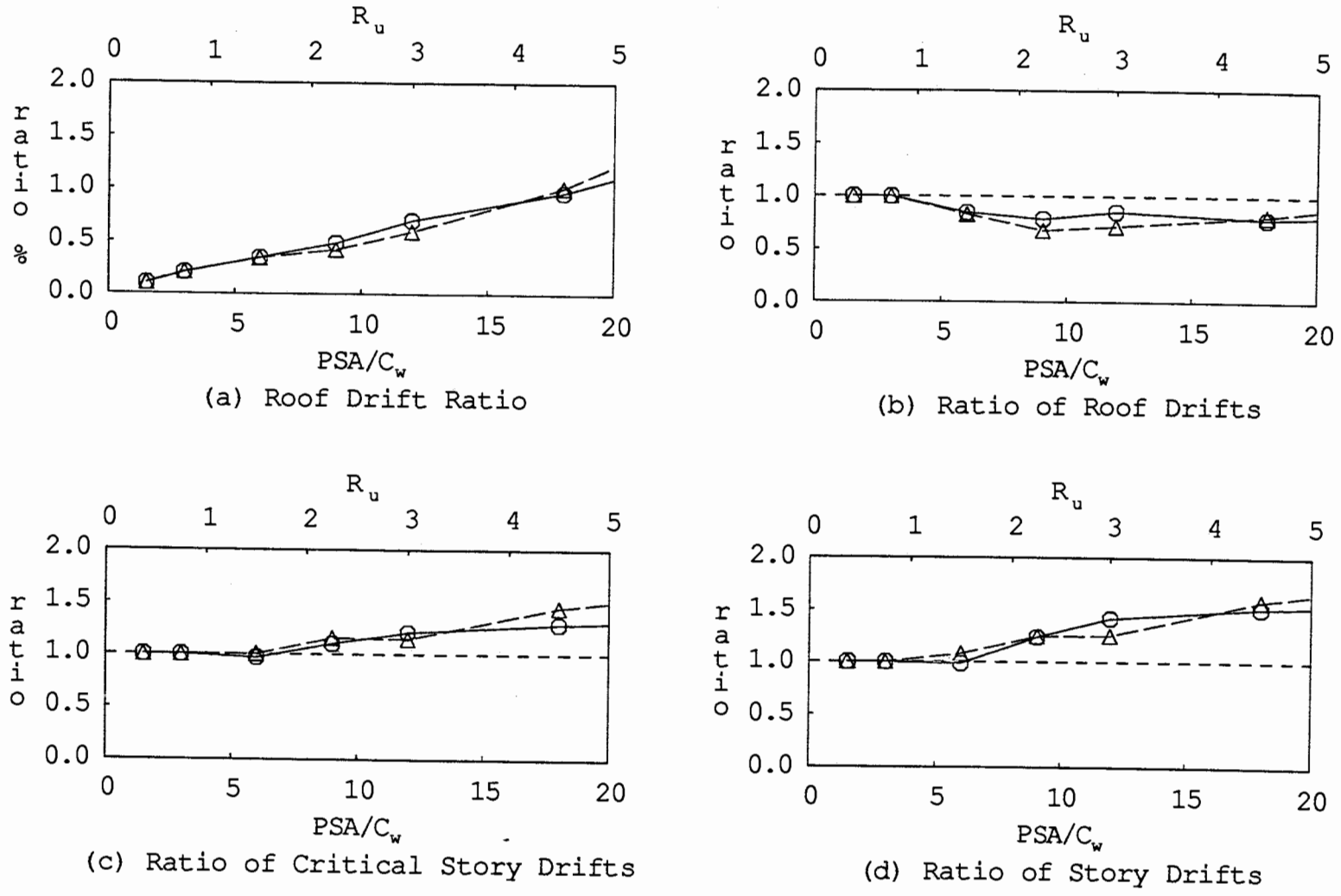

(a) Roof Drift Ratio

(b) Ratio of Roof Drifts

(c) Ratio of Critical Story Drifts

(d) Ratio of Story Drifts

Fig. 5.14 Response Ratios of CSMIP 57355 to Scaled OLY Earthquake Record

[No stiffness degradation (solid), stiffness degradation (dashed)]

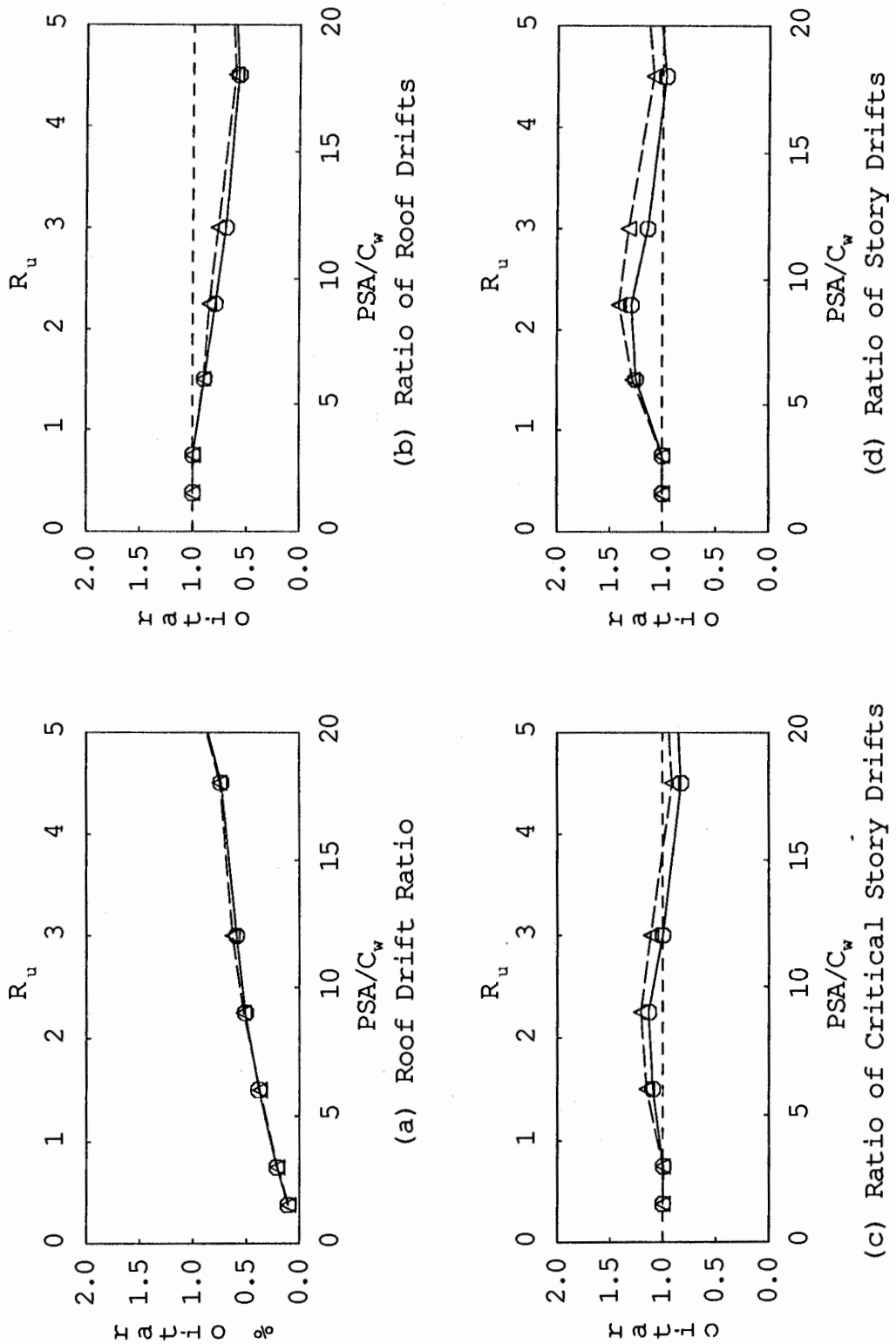

Fig. 5.15 Response Ratios of CSMIP 57355 to Scaled PAC Earthquake Record
[No stiffness degradation (solid), stiffness degradation (dashed)]

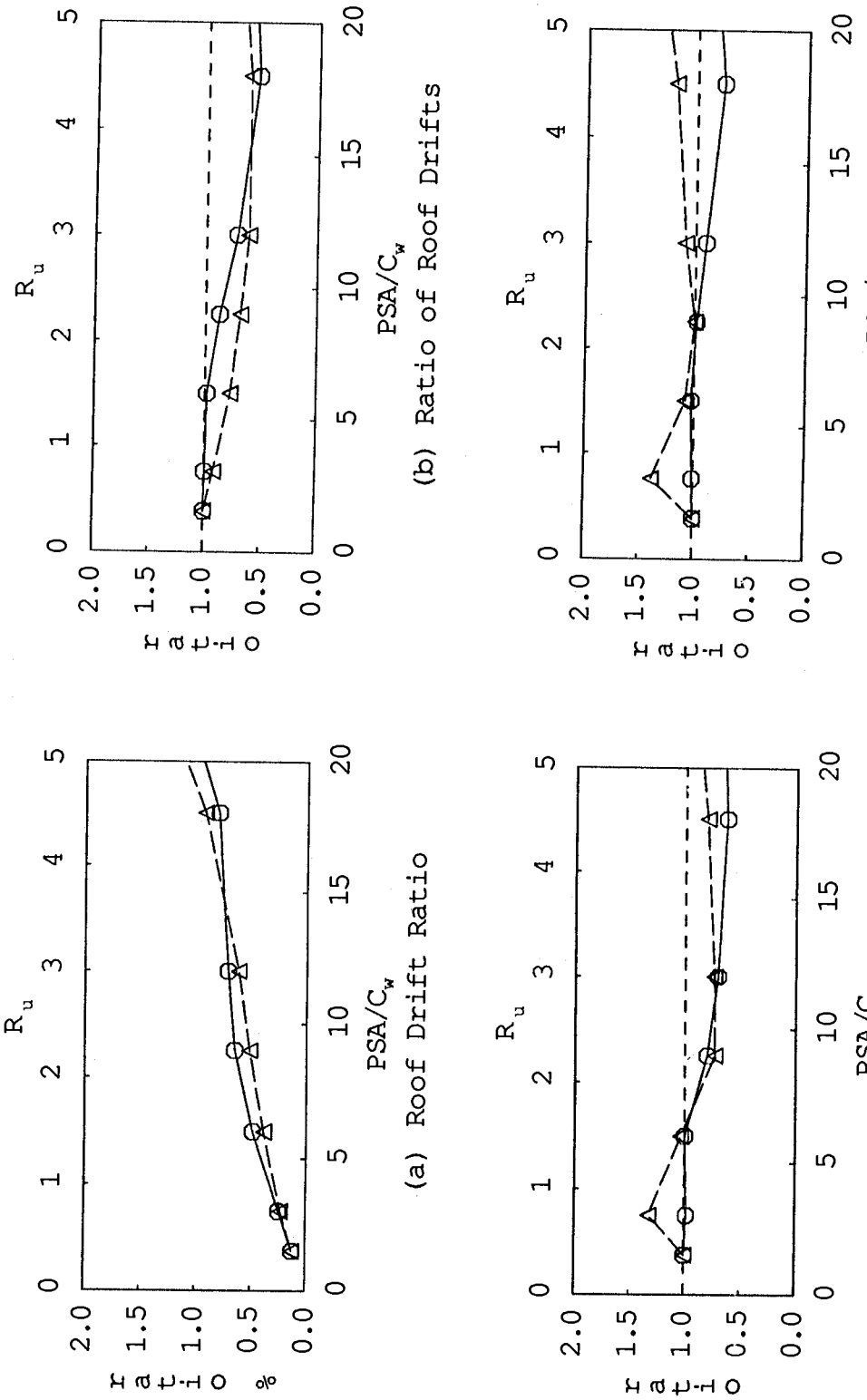

Fig. 5.16 Response Ratios of CSMIP 57355 to Scaled PAR Earthquake Record
[No stiffness degradation (solid), stiffness degradation (dashed)]

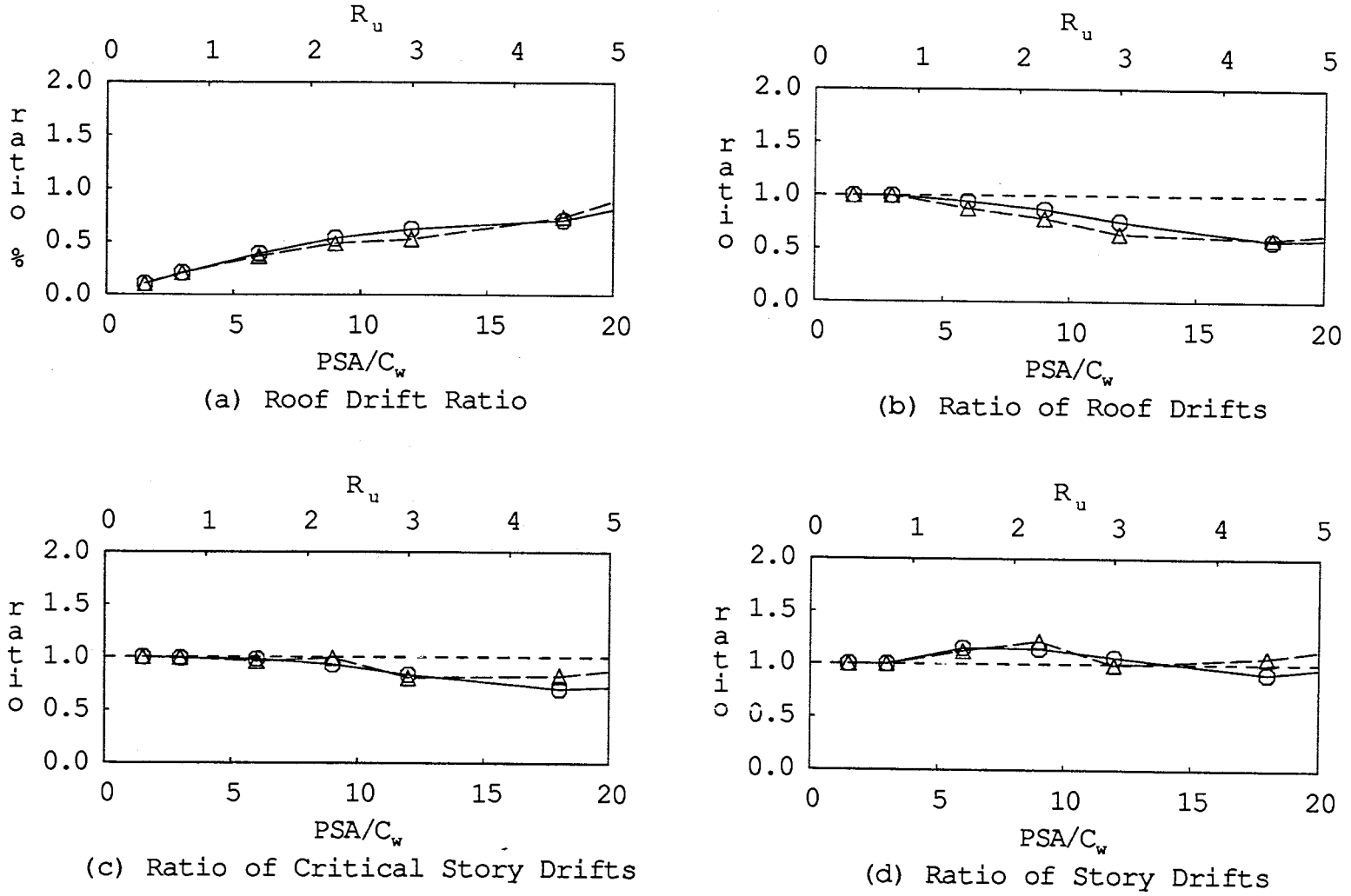

Fig. 5.17 Response Ratios of CSMIP 57355 to Scaled IVC Earthquake Record

[No stiffness degradation (solid), stiffness degradation (dashed)]

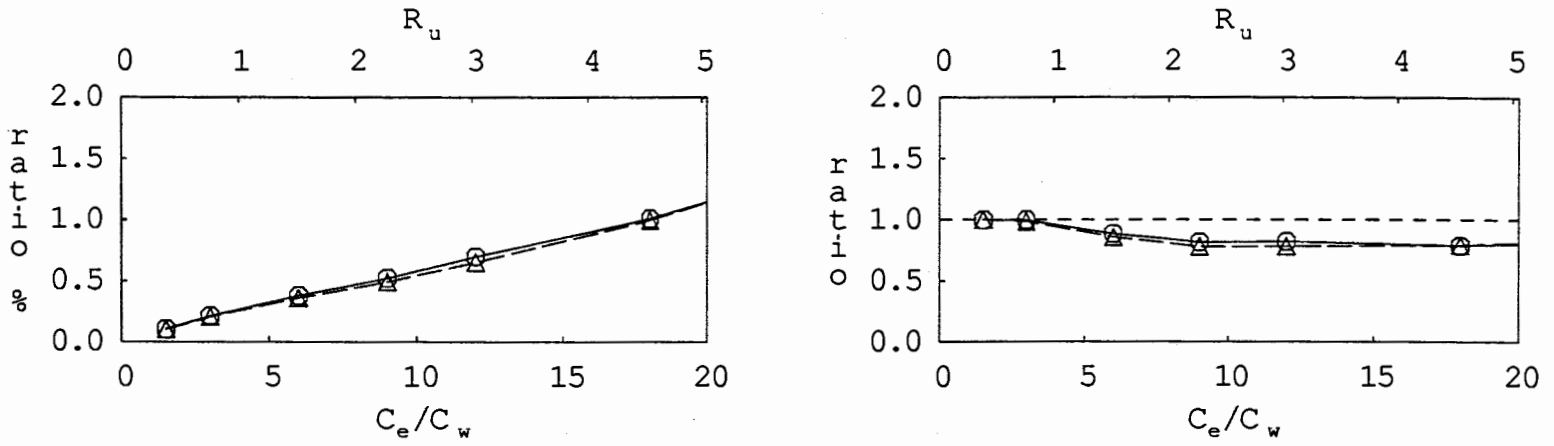

(a) Mean Roof Drift Ratio

(b) Mean Ratio of Roof Drifts

(c) Mean Ratio of Critical Story Drifts

(d) Mean Ratio of Story Drifts

Fig. 5.18 Mean Response Ratios of CSMIP 57355 to Eight Scaled Earthquake Records

[No stiffness degradation (solid), stiffness degradation (dashed)]

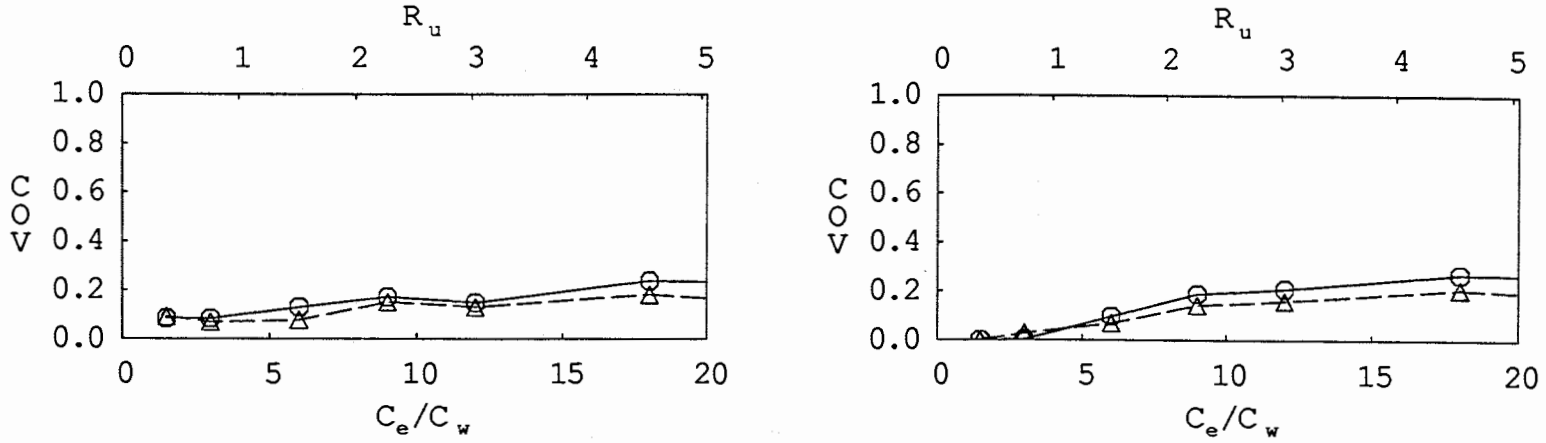

(a) COV for Roof Drift Ratio

(b) COV for Ratio of Roof Drifts

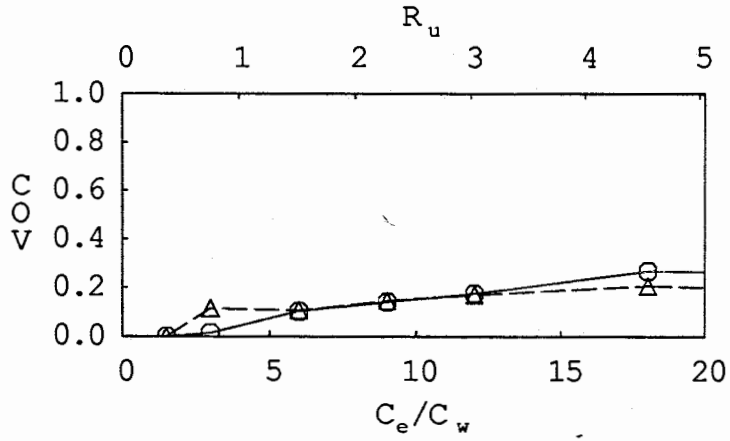

(c) COV for Ratio of Critical Story Drifts

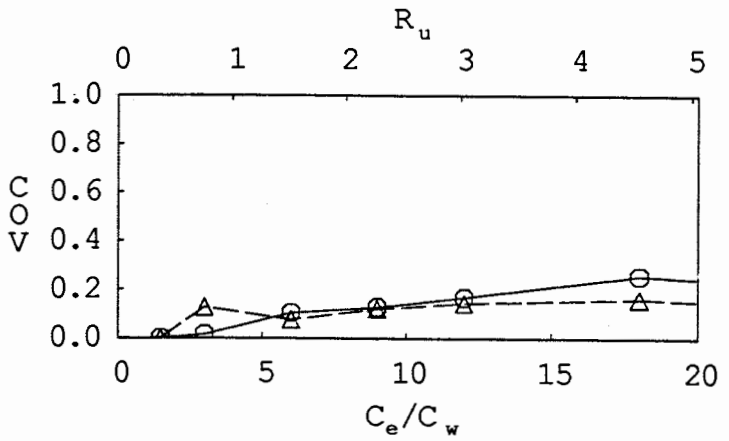

(d) COV for Ratio of Story Drifts

Fig. 5.19 COV for Response Ratios of CSMIP 57355 to Eight Scaled Earthquake Records

[No stiffness degradation (solid), stiffness degradation (dashed)]

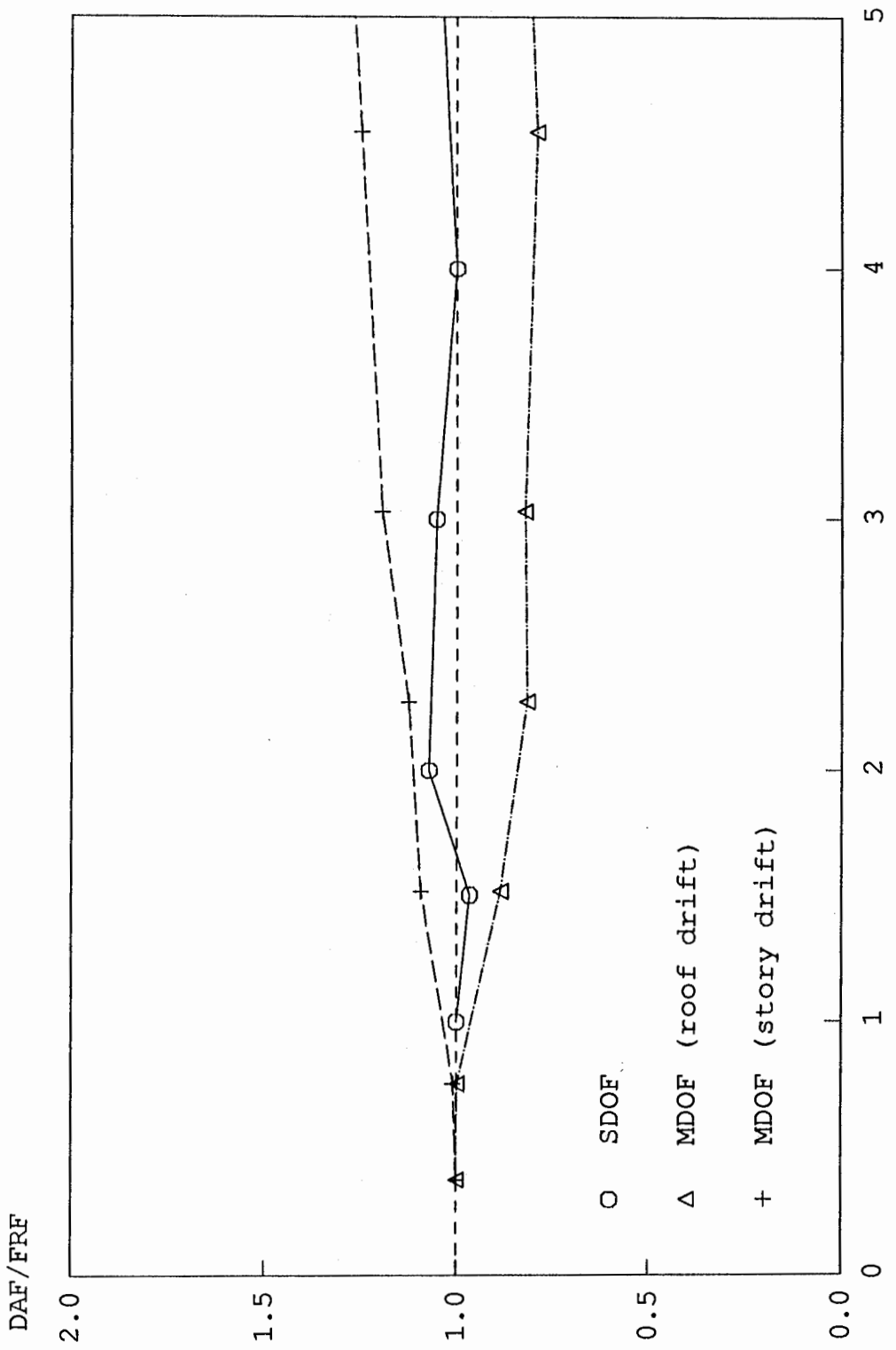

Fig. 5.20 Comparison of Mean Response Ratios between SDOF and MDOF systems (CSMIP 57355)

Fig. 6.1 San Bruno 6-story Office Building (CSMIP 58490)

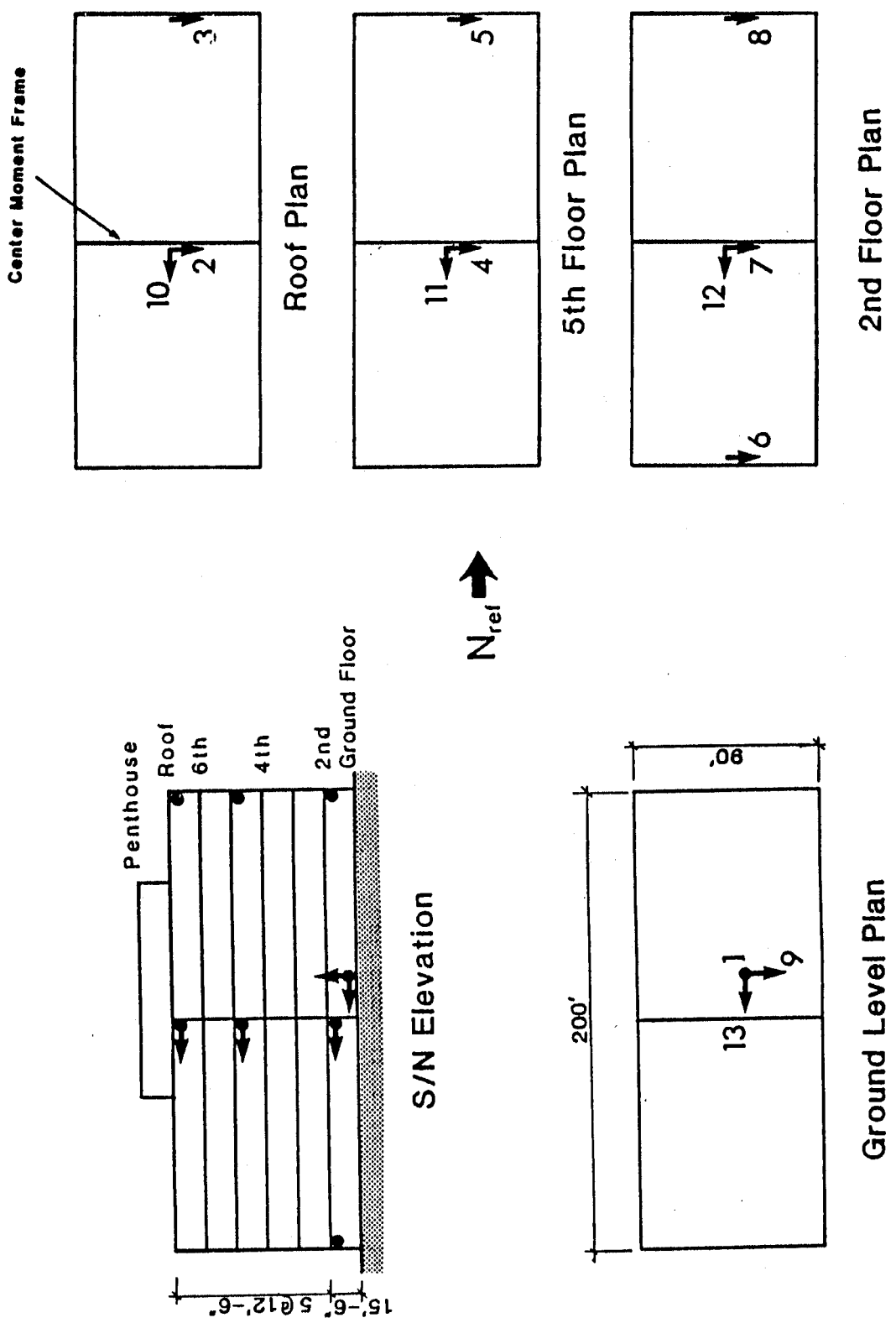

Fig. 6.2 General Layout of Building CSMIP 58490

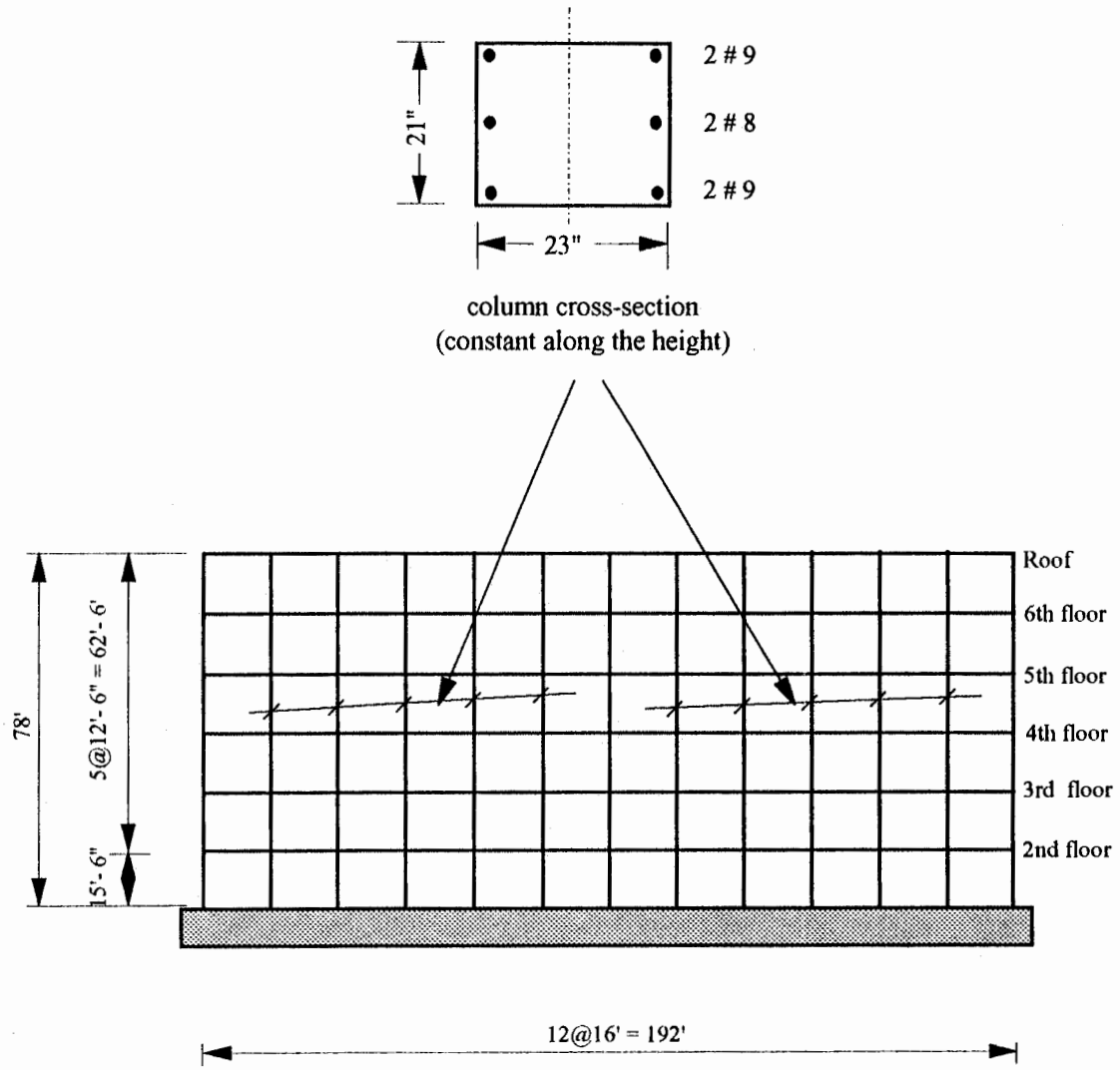

Fig. 6.3 SMRSF of Building CSMIP 58490 (N-S)

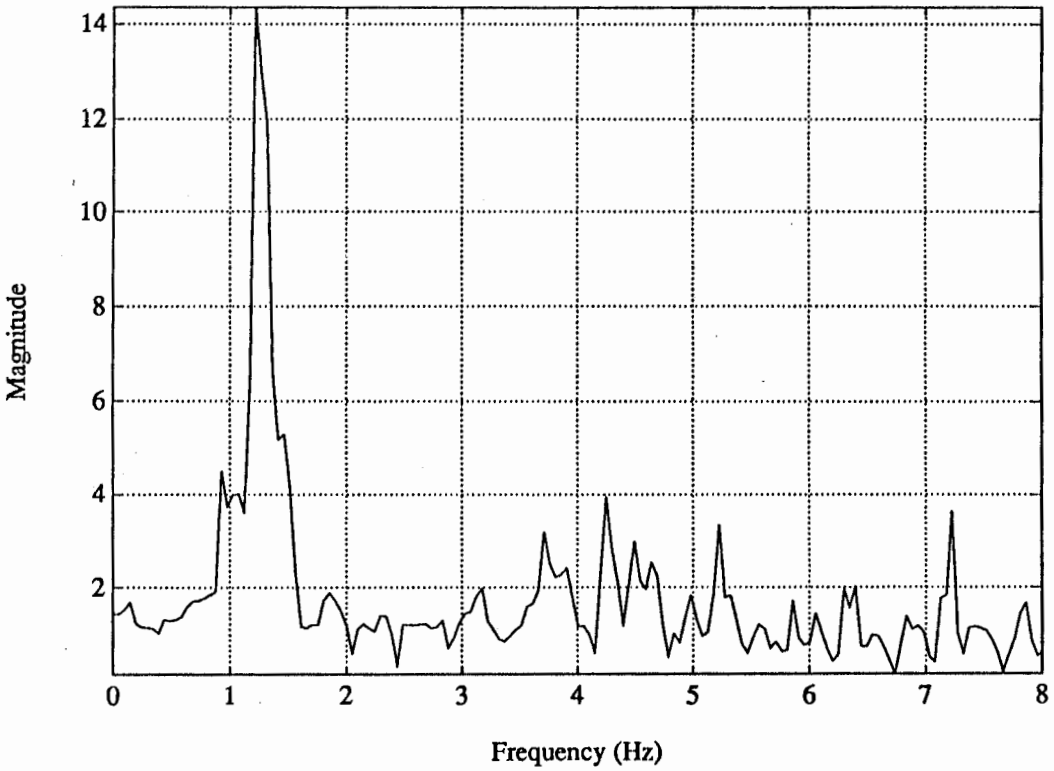

Fig. 6.4 Magnitude of Acceleration Transfer Functions between the Base and the Roof (CSMIP 58490)

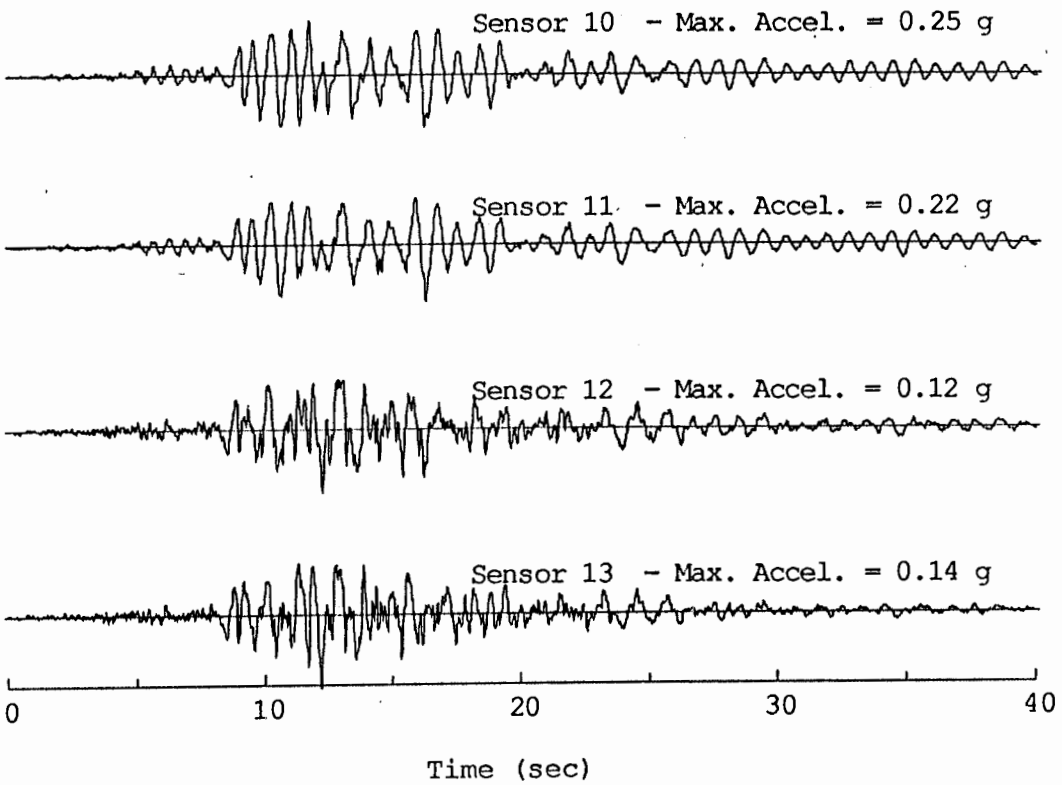

Fig. 6.5 Building CSMIP 58490 Acceleration Records. (N-S)

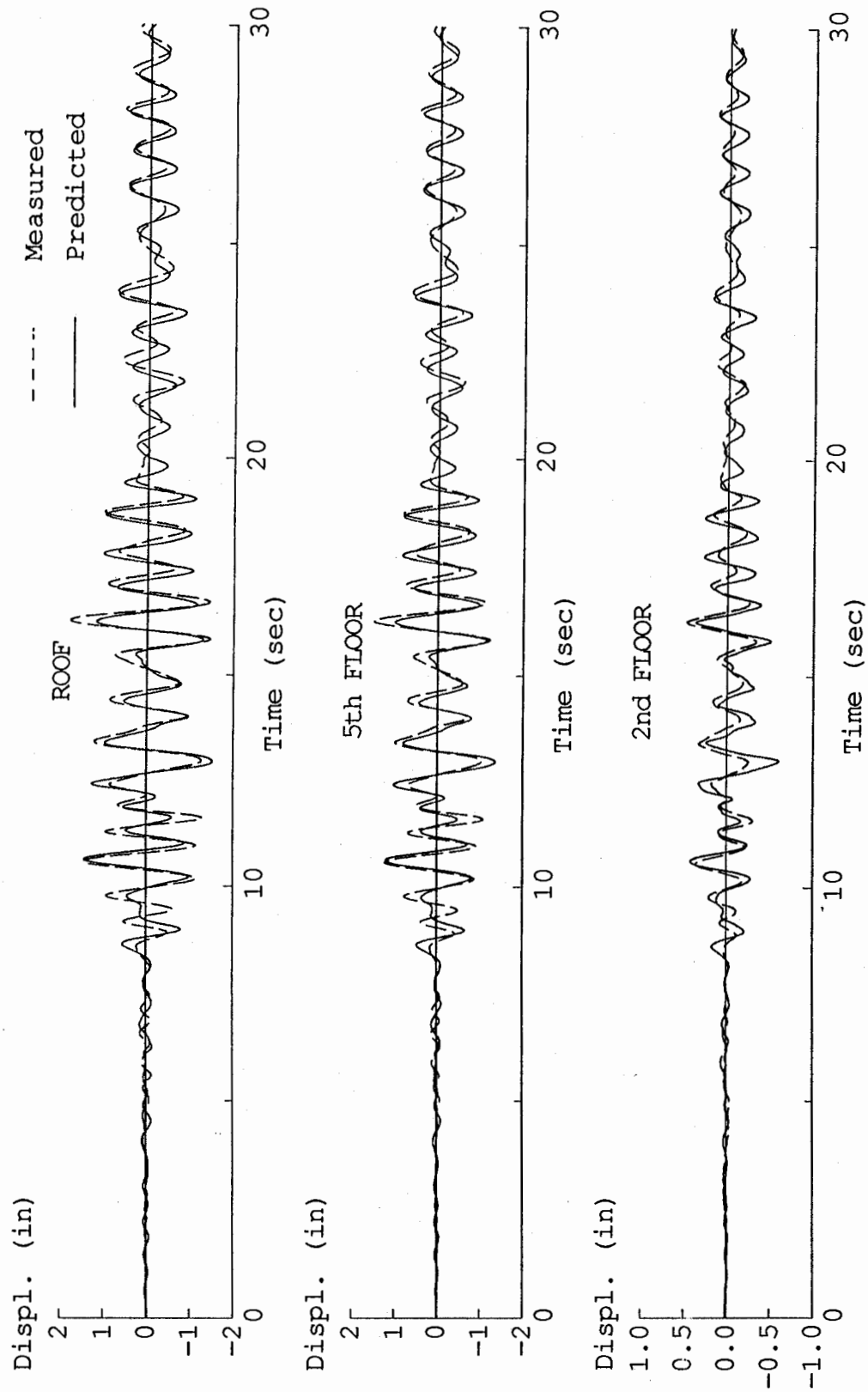

Fig. 6.6 Measured versus Predicted Relative Displacement Time Histories (CMSIP 58490, N-S)

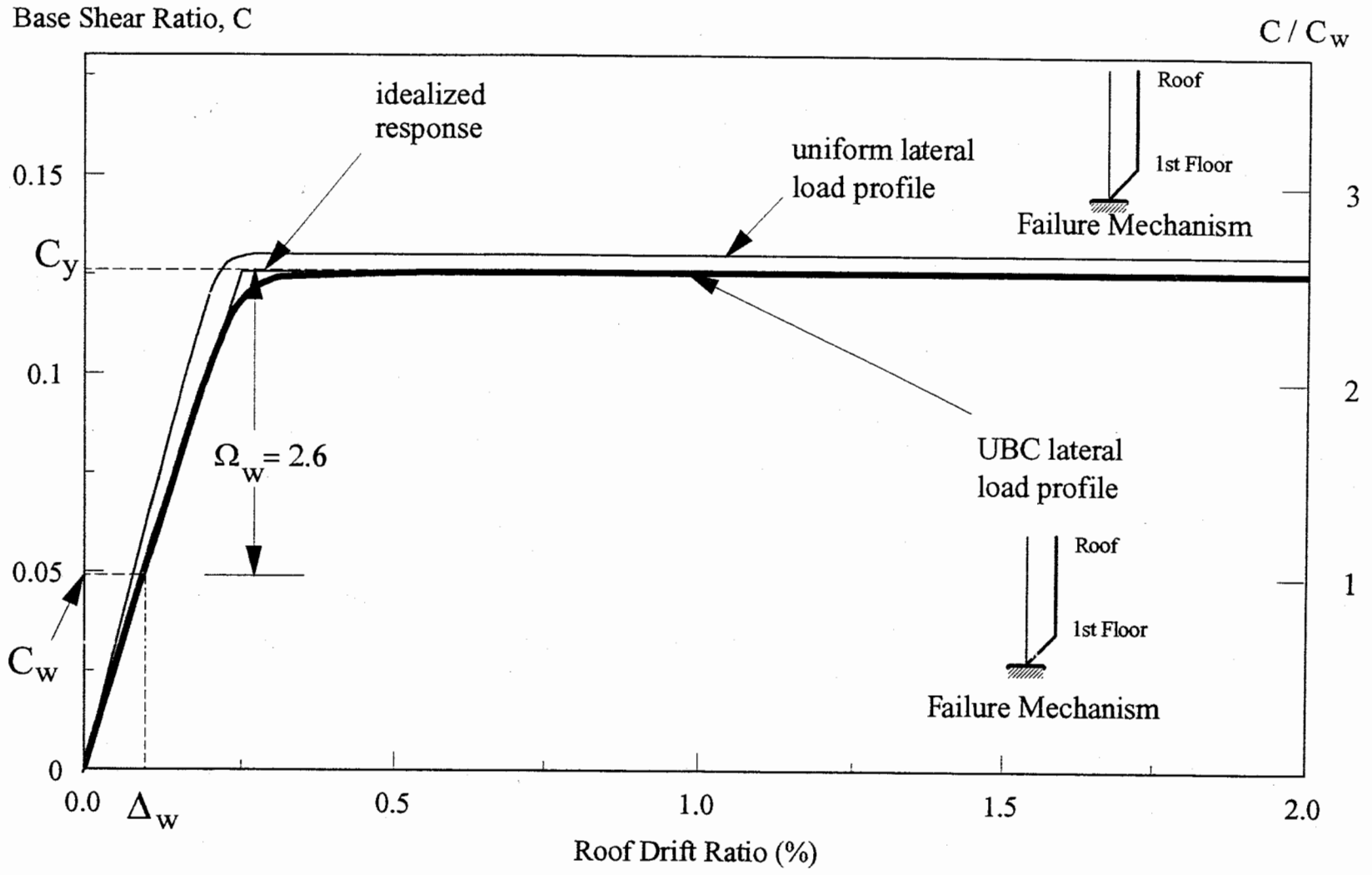

Fig. 6.7 Lateral Strength of CSMIP 58490 (N-S)

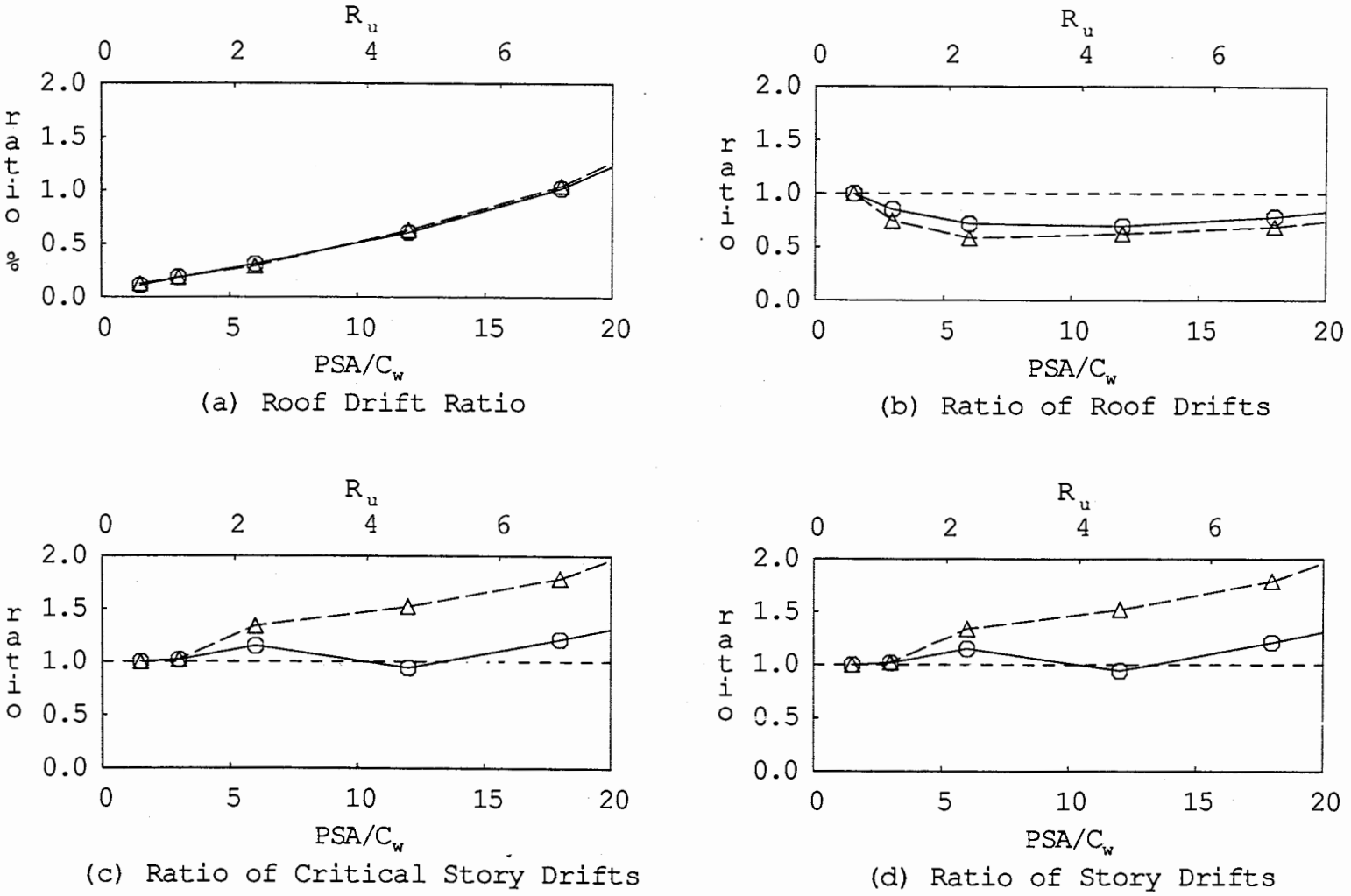

Fig. 6.8 Response Ratios of CSMIP 58490 to Scaled LPSC Earthquake Record

[No stiffness degradation (solid), stiffness degradation (dashed)]

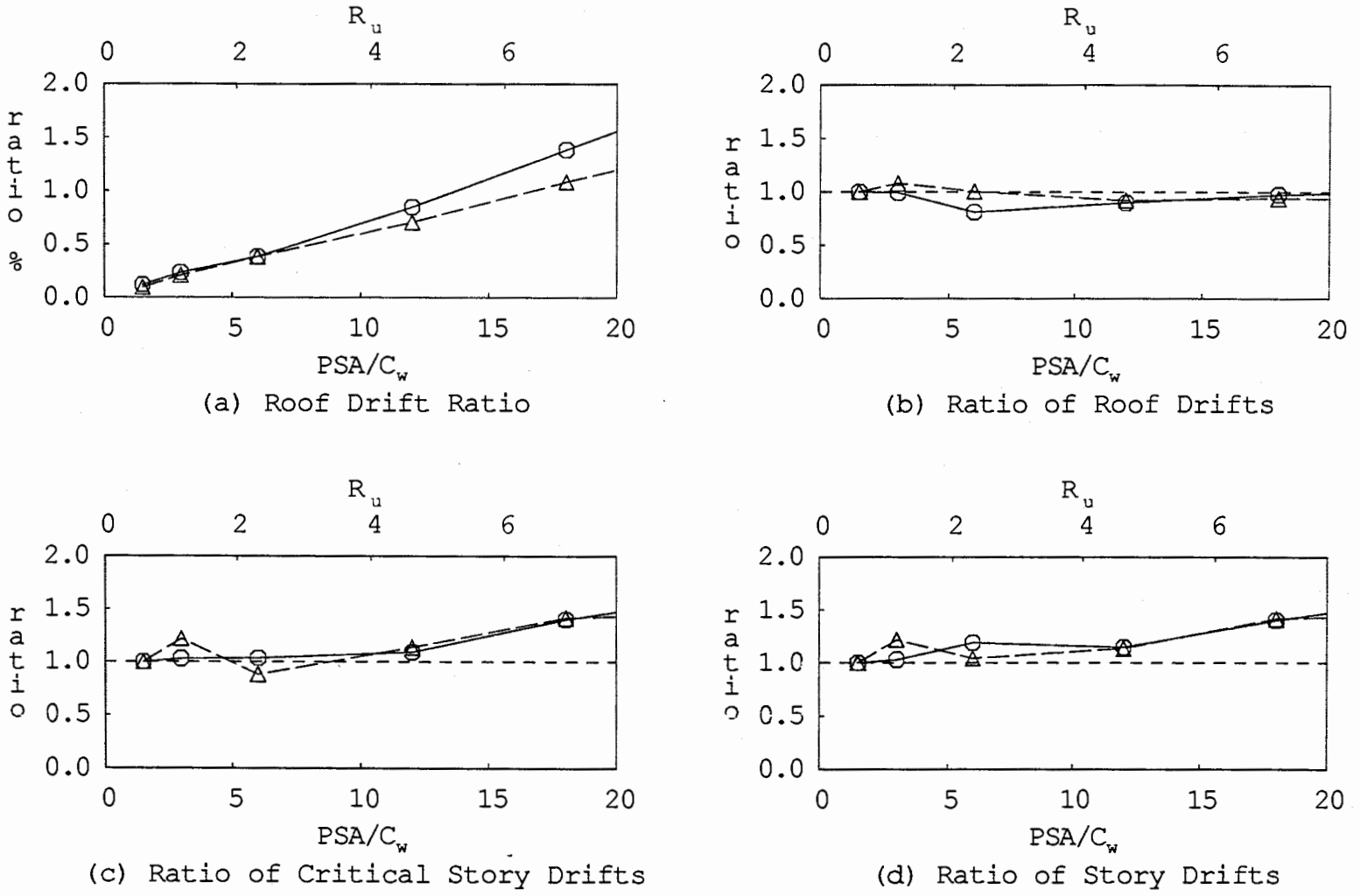

(a) Roof Drift Ratio

(b) Ratio of Roof Drifts

(c) Ratio of Critical Story Drifts

(d) Ratio of Story Drifts

Fig. 6.9 Response Ratios of CSMIP 58490 to Scaled LPC Earthquake Record

[No stiffness degradation (solid), stiffness degradation (dashed)]

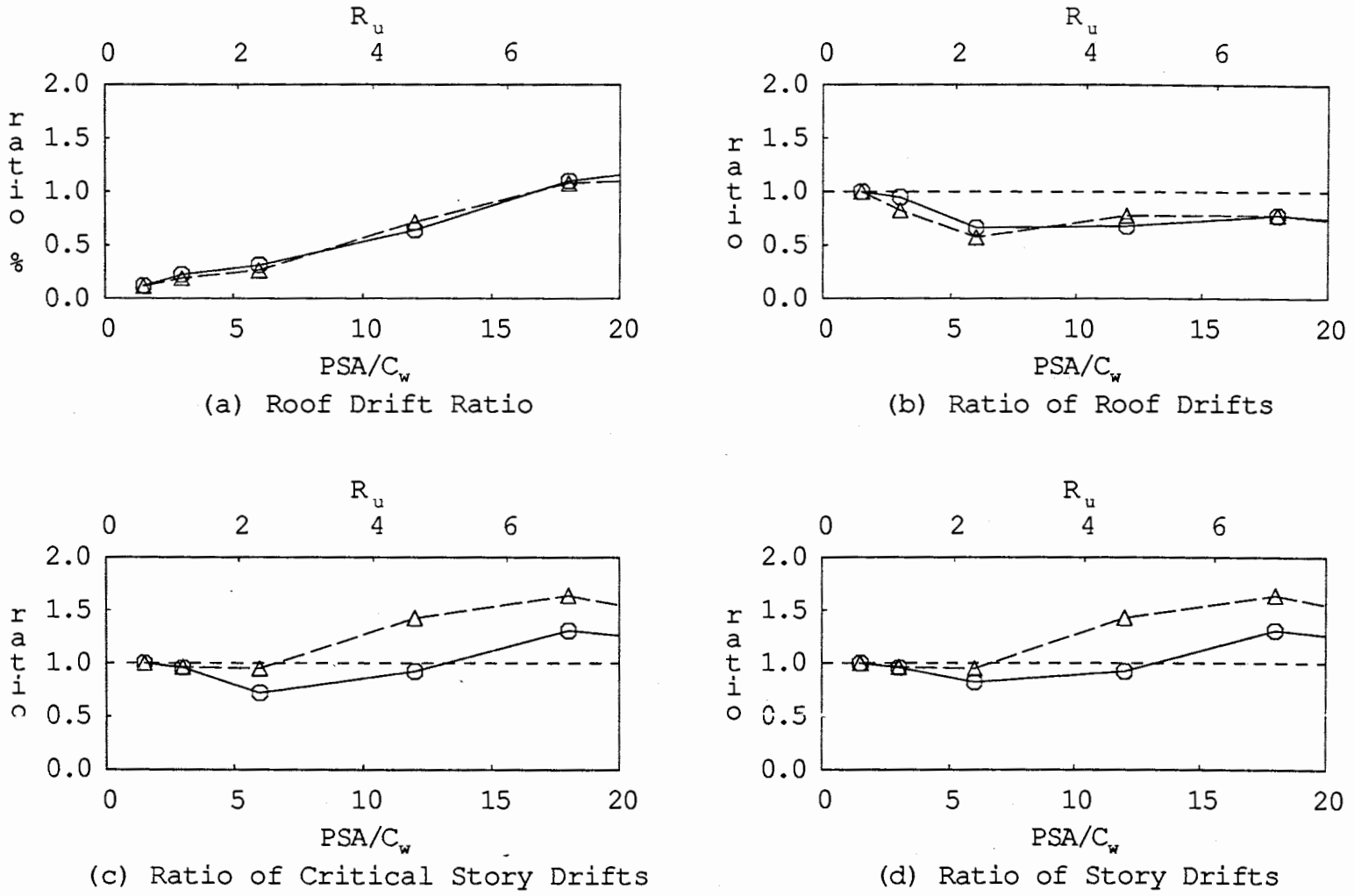

(a) Roof Drift Ratio

(b) Ratio of Roof Drifts

(c) Ratio of Critical Story Drifts

(d) Ratio of Story Drifts

Fig. 6.10 Response Ratios of CSMIP 58490 to Scaled ELC Earthquake Record

[No stiffness degradation (solid), stiffness degradation (dashed)]

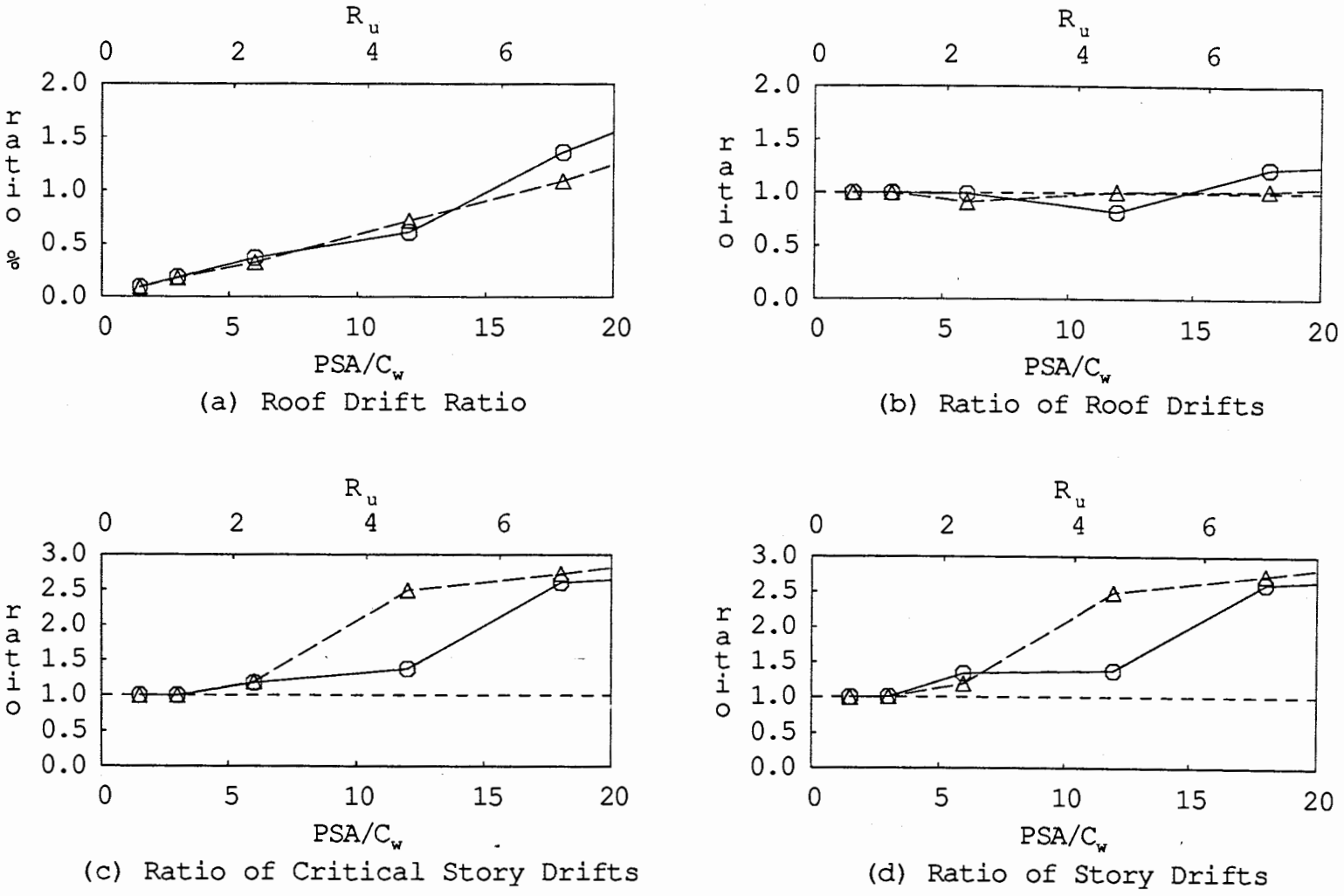

Fig. 6.11 Response Ratios of CSMIP 58490 to Scaled TAF Earthquake Record

[No stiffness degradation (solid), stiffness degradation (dashed)]

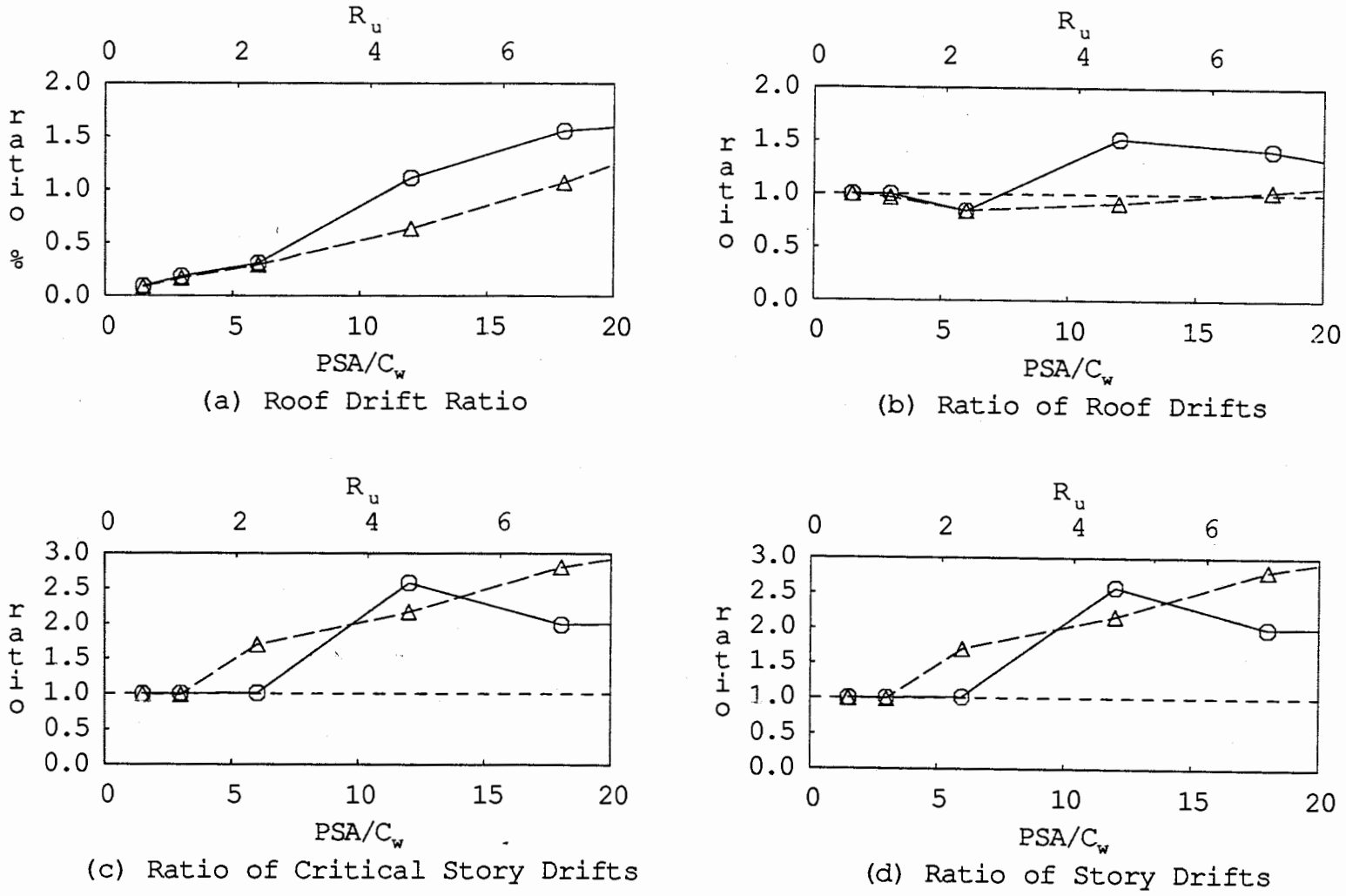

(a) Roof Drift Ratio

(b) Ratio of Roof Drifts

(c) Ratio of Critical Story Drifts

(d) Ratio of Story Drifts

Fig. 6.12 Response Ratios of CSMIP 58490 to Scaled OLY Earthquake Record

[No stiffness degradation (solid), stiffness degradation (dashed)]

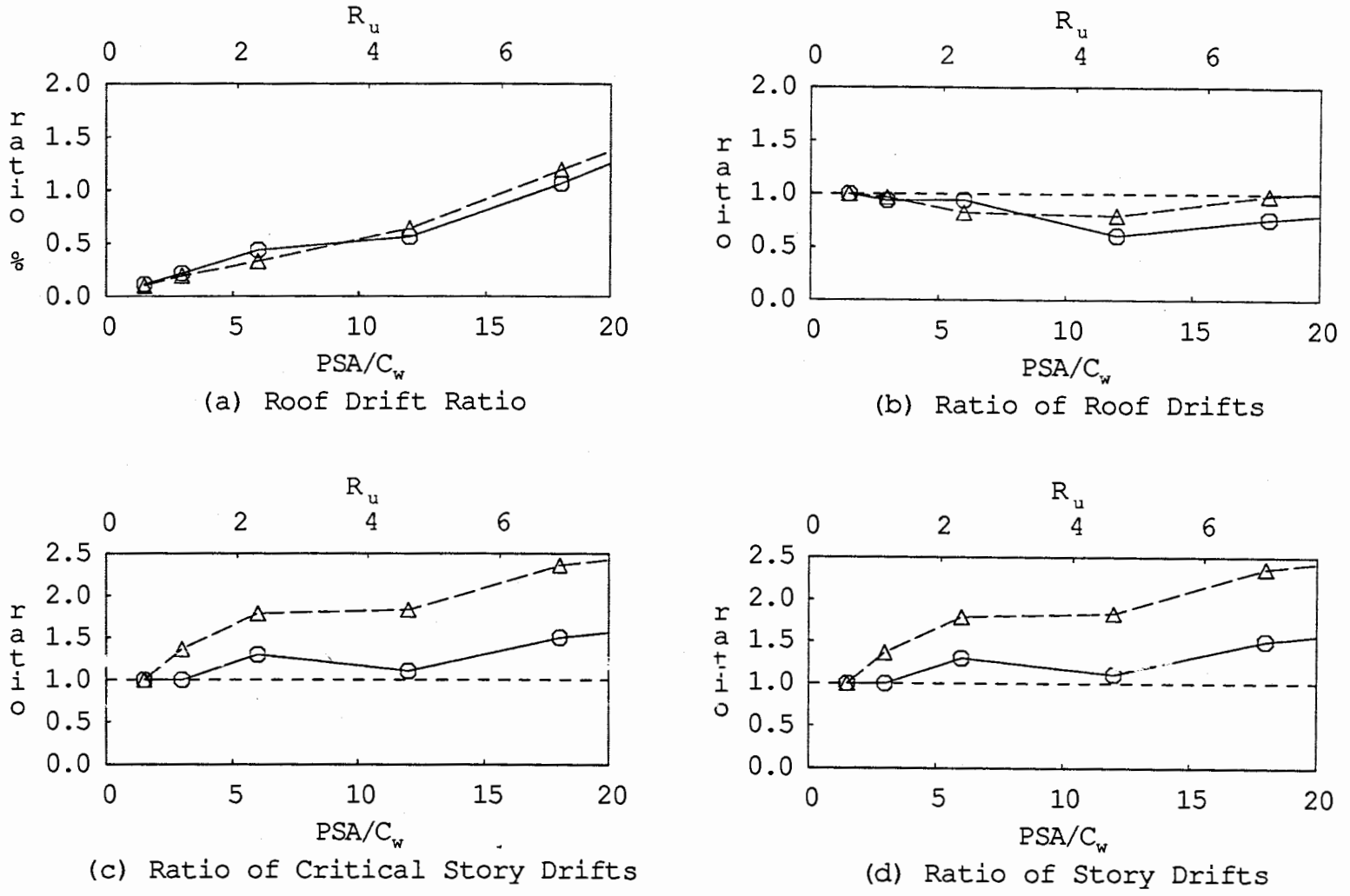

Fig. 6.13 Response Ratios of CSMIP 58490 to Scaled PAC Earthquake Record

[No stiffness degradation (solid), stiffness degradation (dashed)]

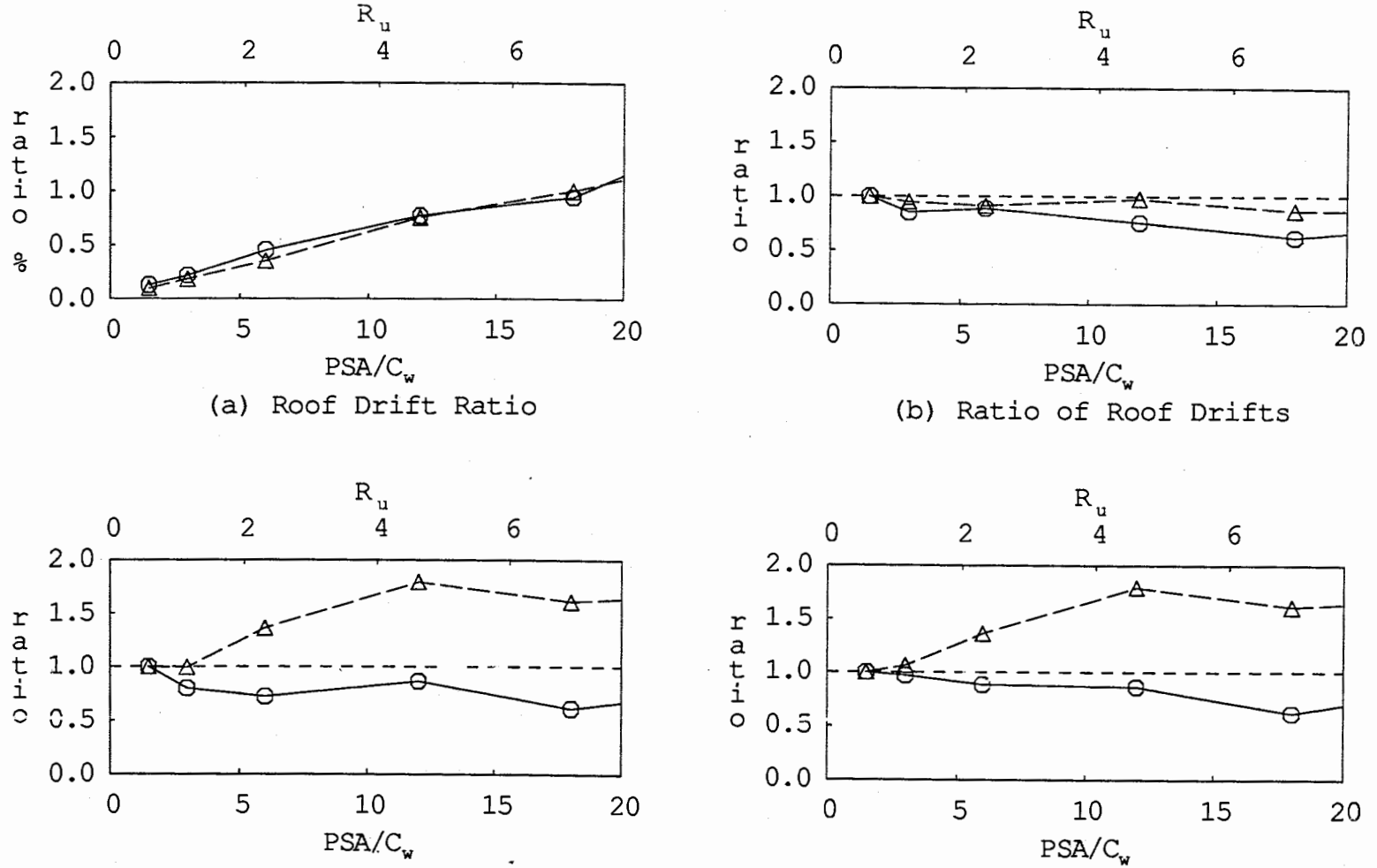

(a) Roof Drift Ratio

(b) Ratio of Roof Drifts

(c) Ratio of Critical Story Drifts

(d) Ratio of Story Drifts

Fig. 6.14 Response Ratios of CSMIP 58490 to Scaled PAR Earthquake Record

[No stiffness degradation (solid), stiffness degradation (dashed)]

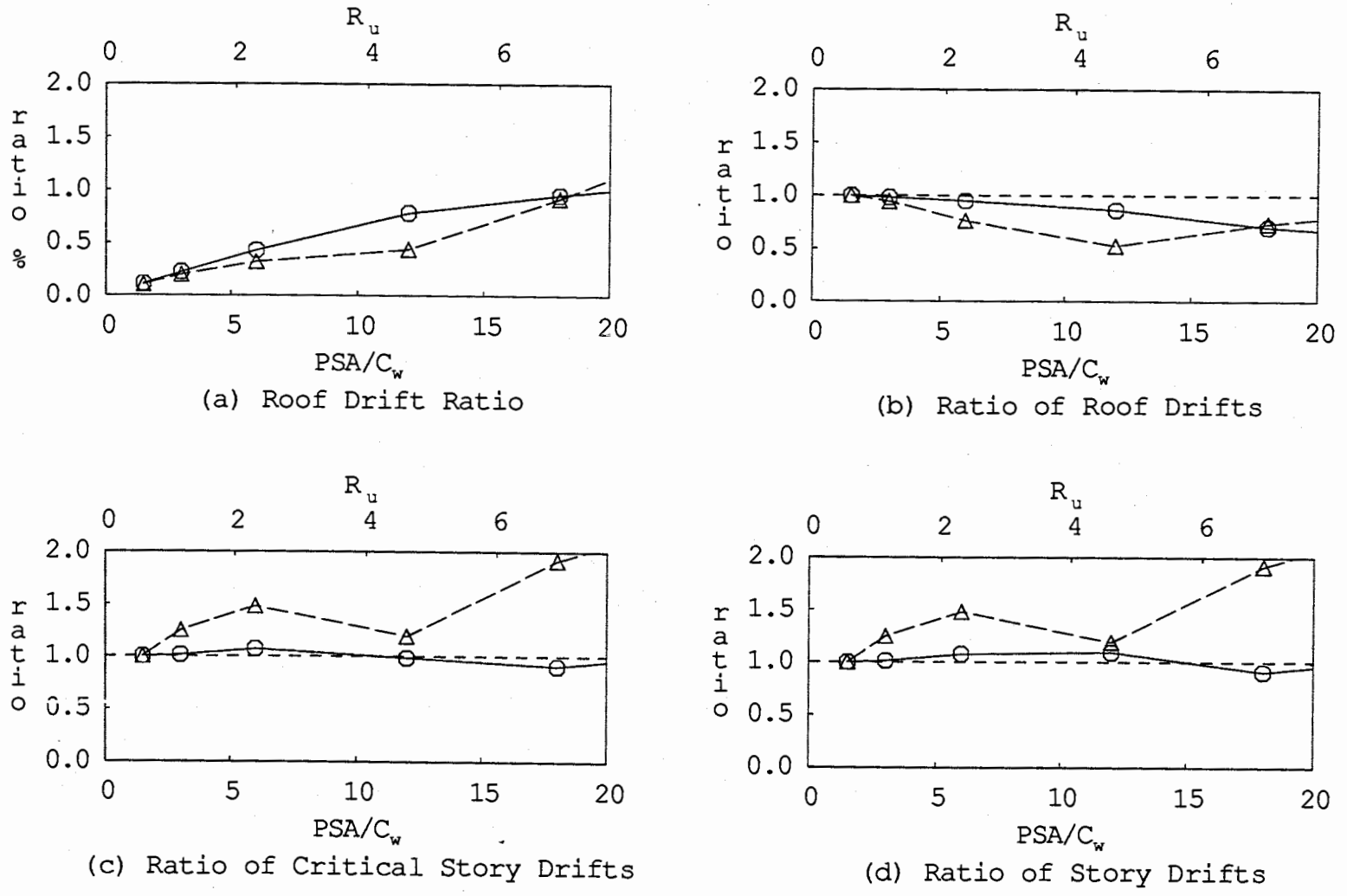

Fig. 6.15 Response Ratios of CSMIP 58490 to Scaled IVC Earthquake Record

[No stiffness degradation (solid), stiffness degradation (dashed)]

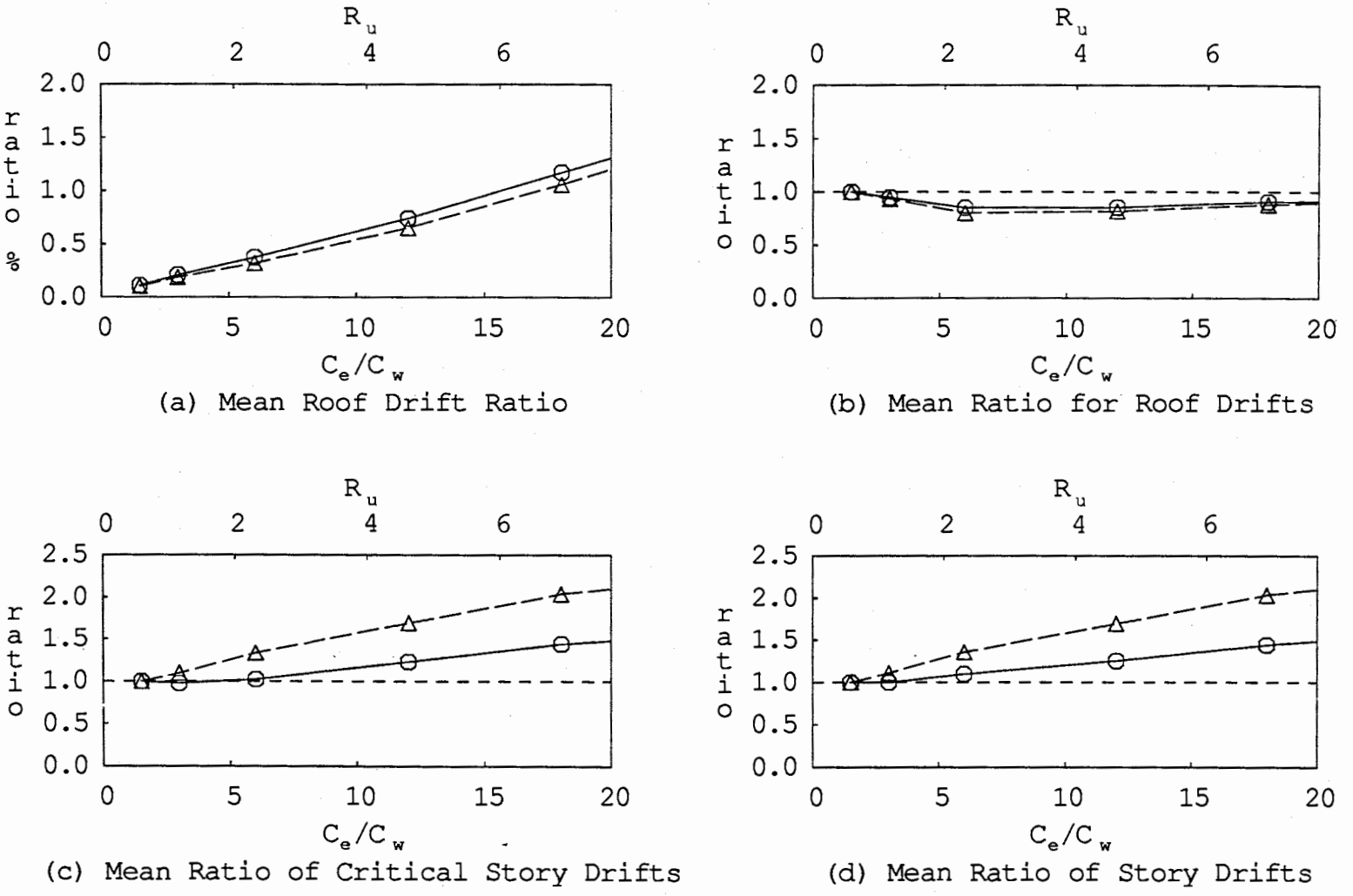

Fig. 6.16 Mean Response Ratios of CSMIP 58490 to Eight Scaled Earthquake Records

[No stiffness degradation (solid), stiffness degradation (dashed)]

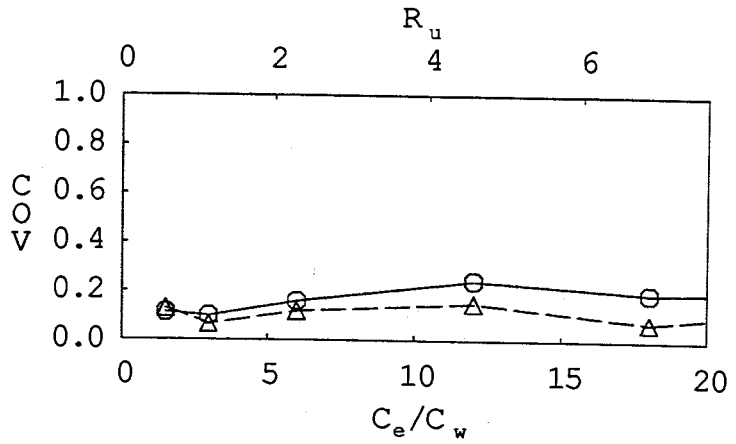

(a) COV for Roof Drift Ratio

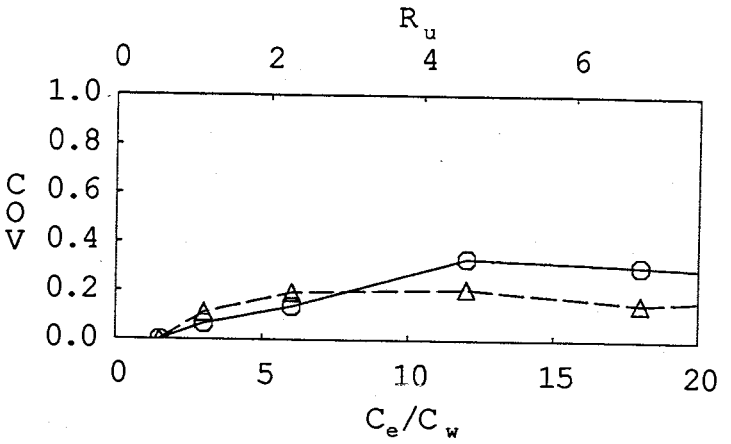

(b) COV for Ratio of Roof Drifts

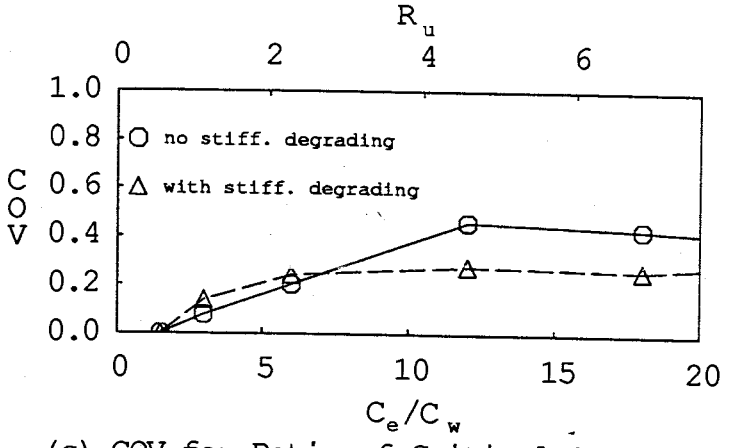

(c) COV for Ratio of Critical Story Drifts

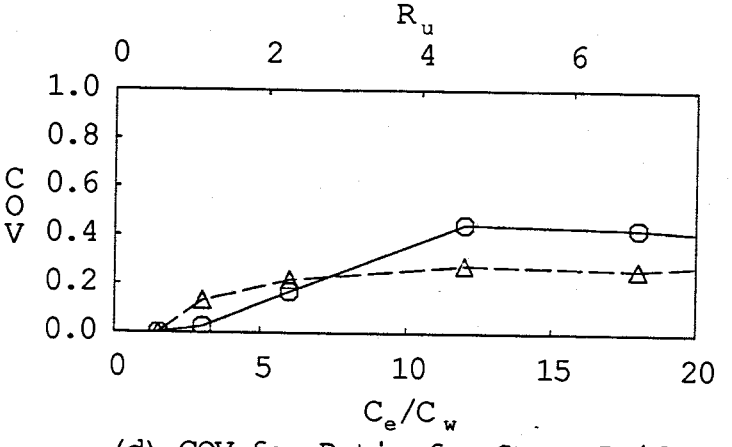

(d) COV for Ratio for Story Drifts

Fig. 6.17 COV for Response Ratios of CSMIP 58490 to Eight Scaled Earthquake Records

[No stiffness degradation (solid), stiffness degradation (dashed)]

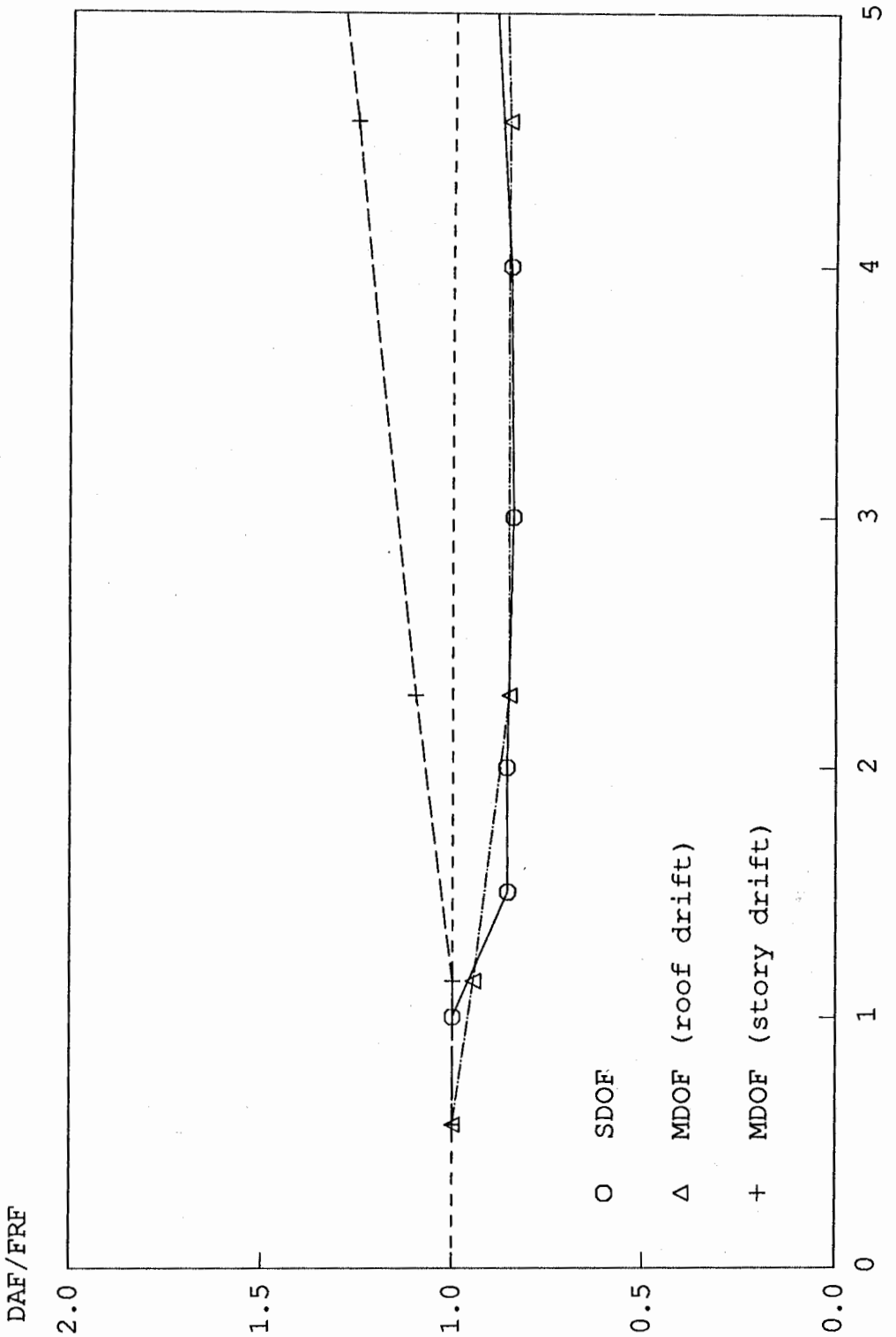

Fig. 6.18 Comparison of Mean Response Ratios between SDOF and MDOF systems (CSMIP 58490)

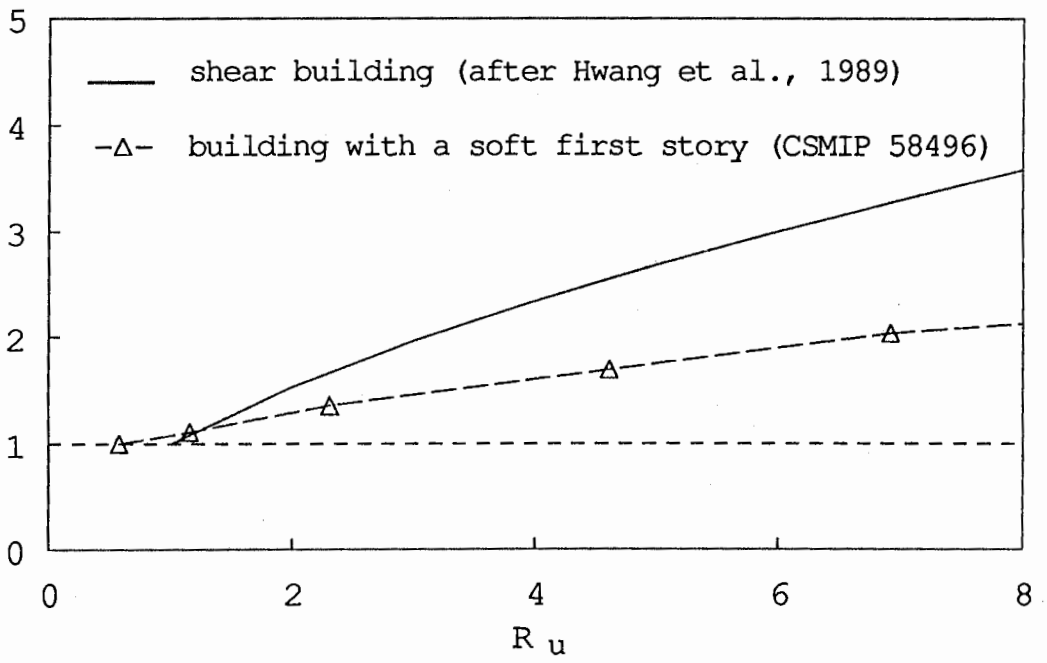

Fig. 7.1 Comparison of DAF/FRF Ratios for R.C Buildings with a Soft First Story and R.C. Shear Buildings

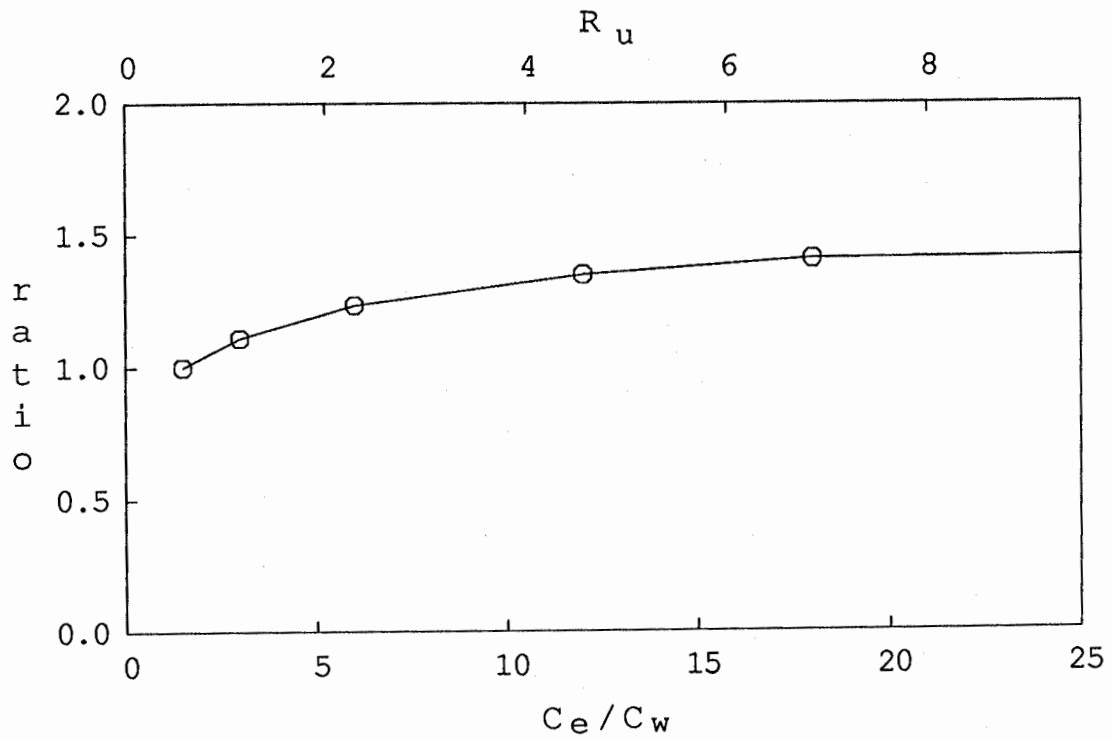

Fig. 7.2 Ratio of DAF with and without Stiffness Degradation (CSMIP 58490)

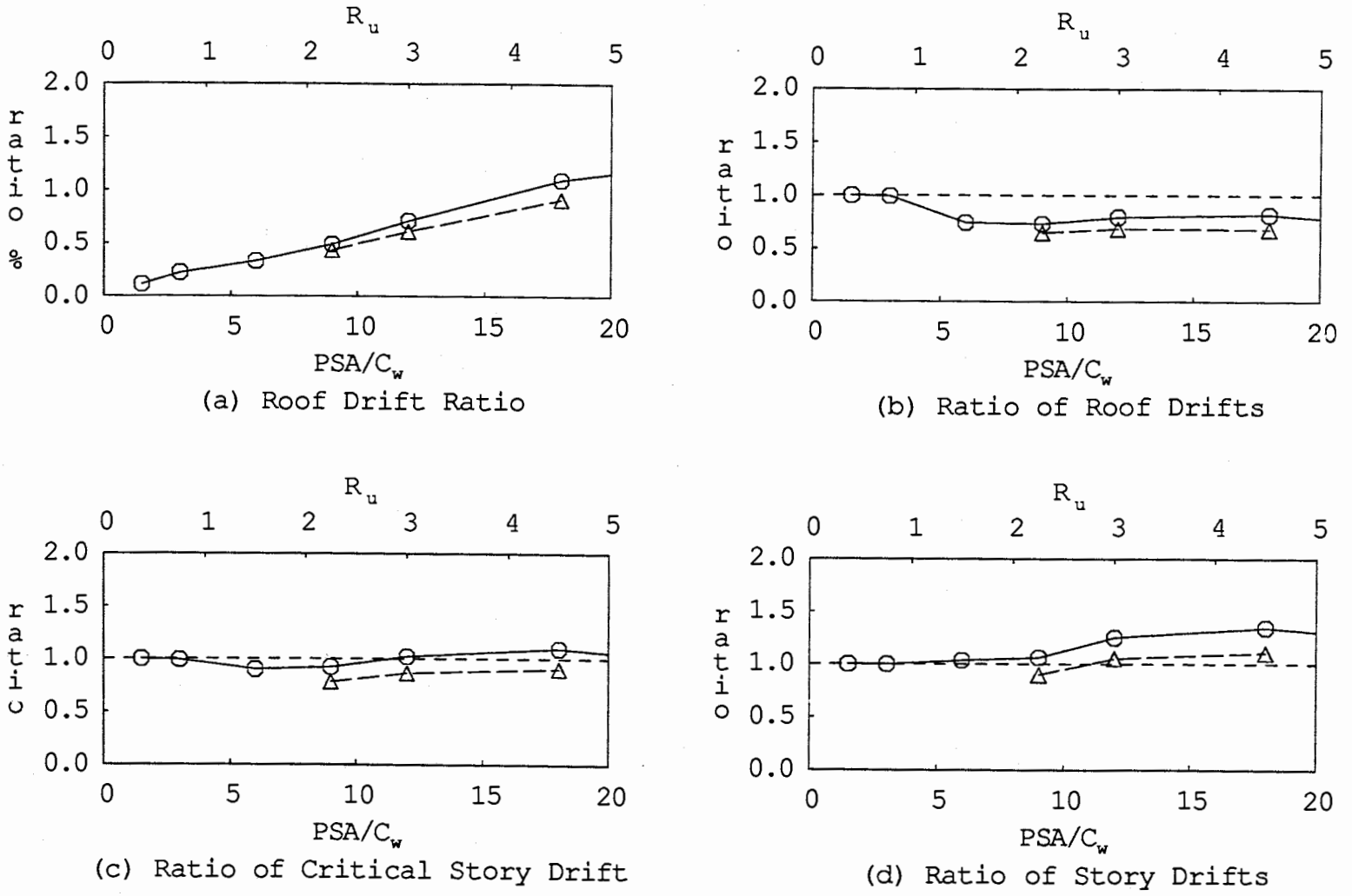

Fig. 7.3 Effect of Damping on Response Ratios of CSMIP 57355 to ELC Earthquake Record

(Solid line for 5% and dashed line for 10% of critical damping)

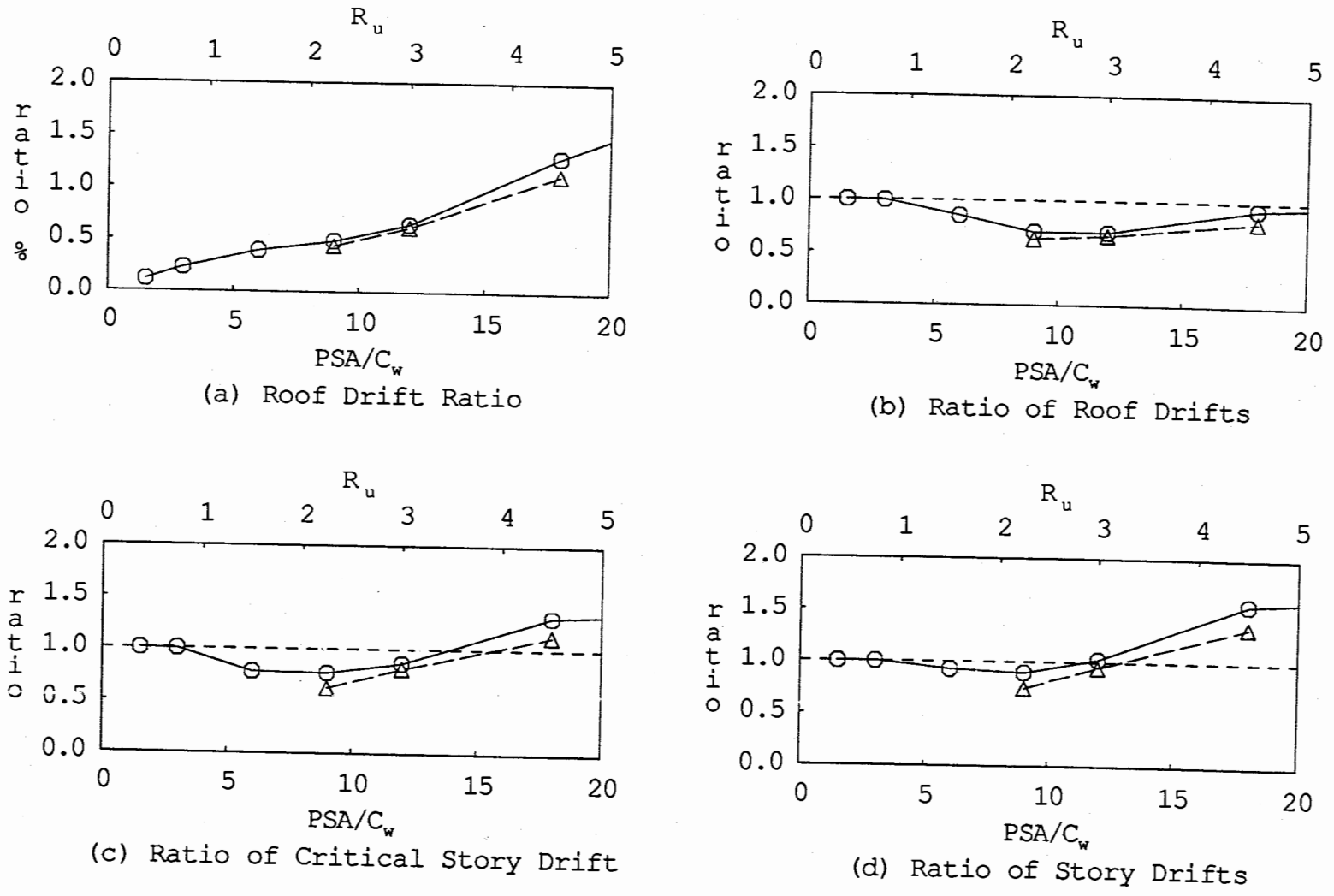

Fig. 7.4 Effect of Damping on Response Ratios of CSMIP 57355 to TAF Earthquake Record (Solid line for 5% and dashed line for 10% of critical damping)

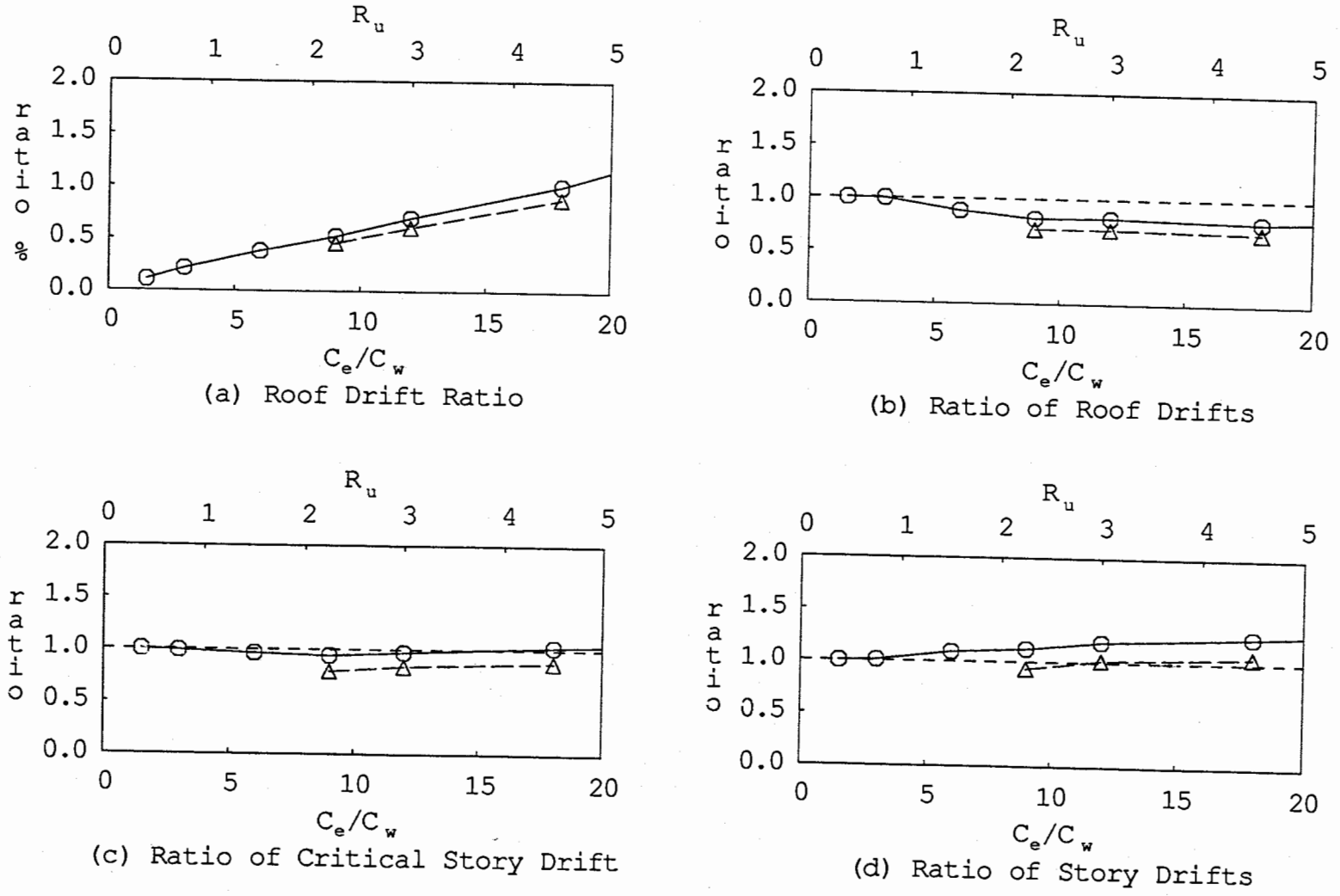

Fig. 7.5 Effect of Damping on Mean Response Ratios of CSMIP 57355 to Eight Earthquake Records (Solid line for 5% and dashed line for 10% of critical damping)

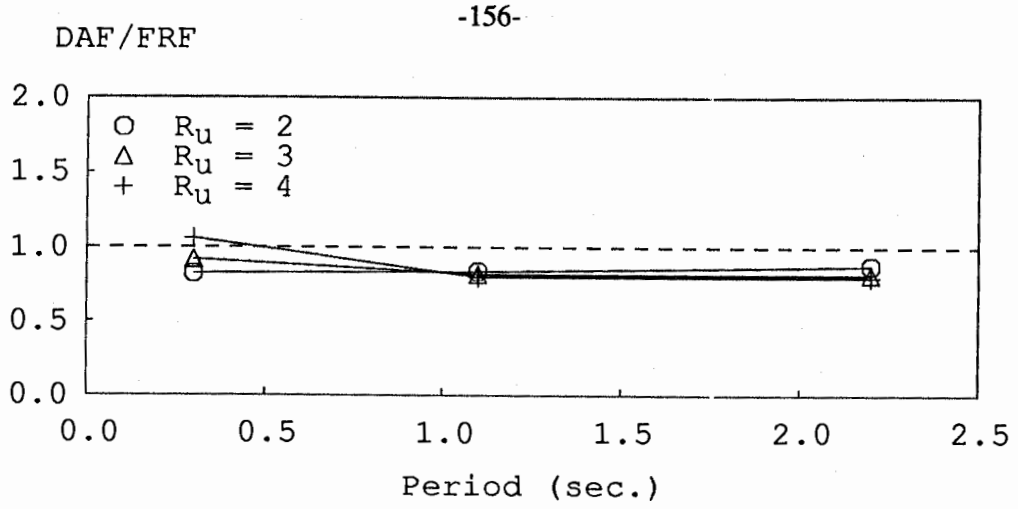

(a) DAF/FRF ratio for Roof Drift

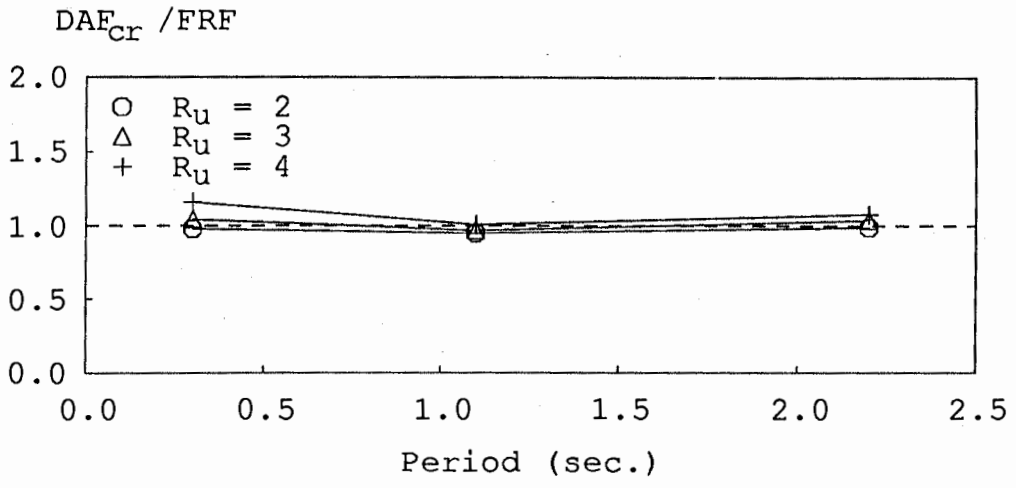

(b) DAF_{cr} /FRF Ratio for Critical Story Drift

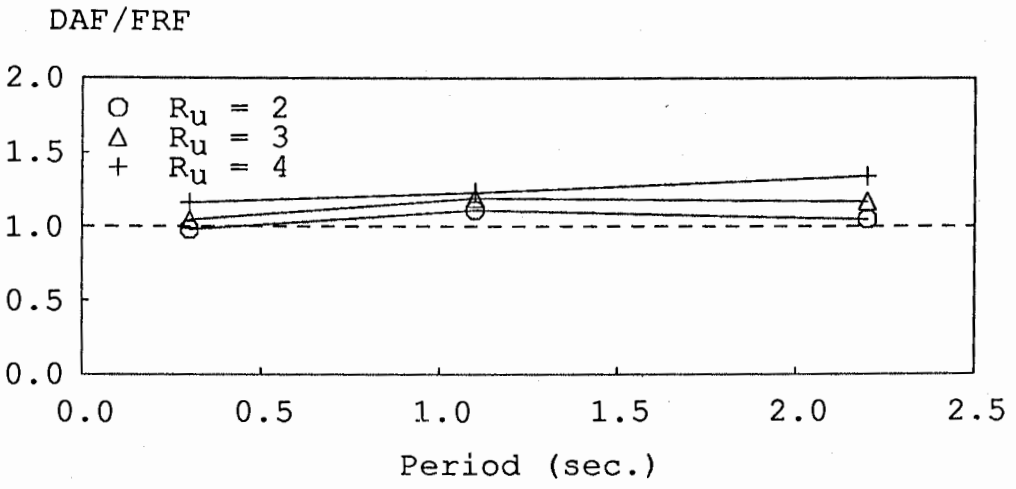

(c) DAF/FRF Ratio for Story Drift

Fig. 7.6 Effect of Fundamental Period on the *DAF/FRF* Ratios

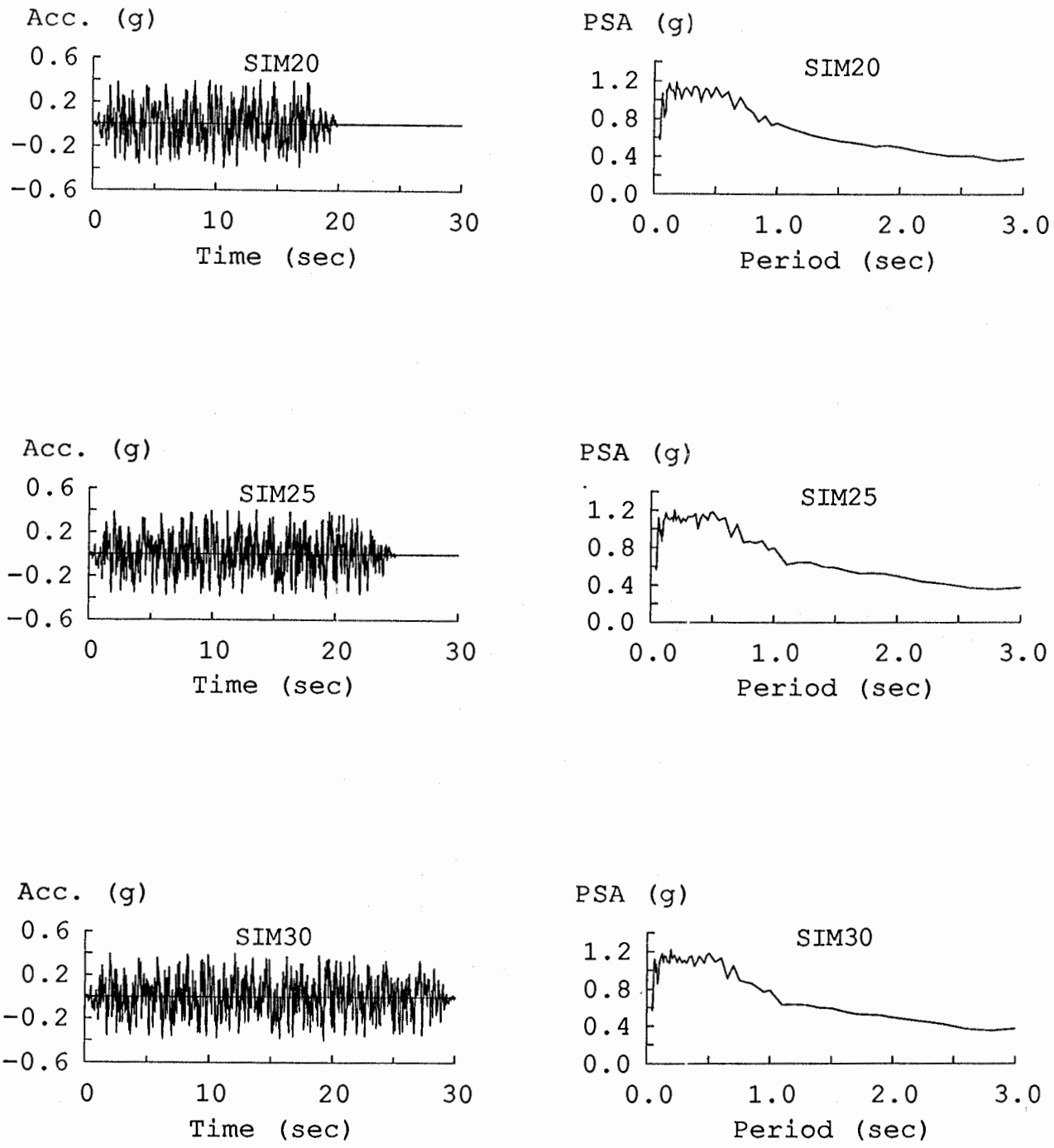

Fig. 7.7 Acceleration Time Histories and Response Spectra of Three Artificial Earthquakes

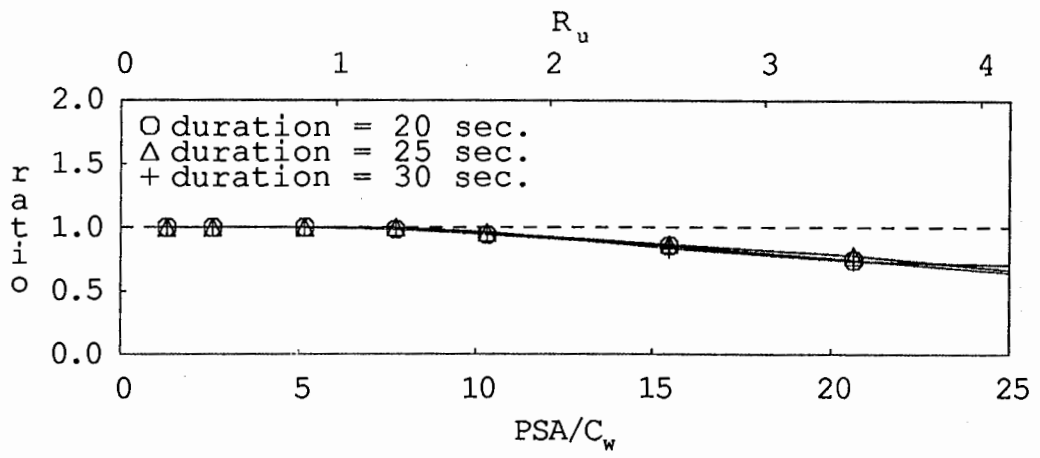

(a) DAF/FRF Ratio for Roof Drifts

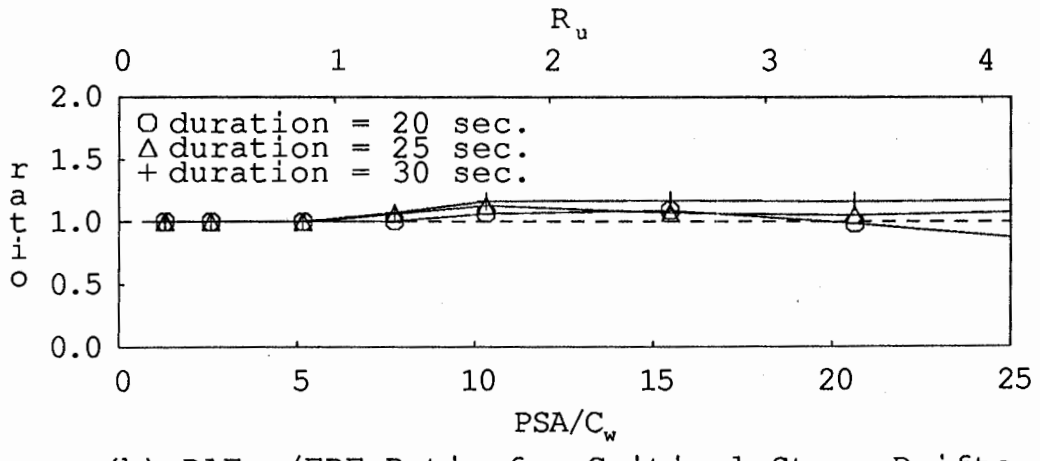

(b) DAF_{cr}/FRF Ratio for Critical Story Drifts

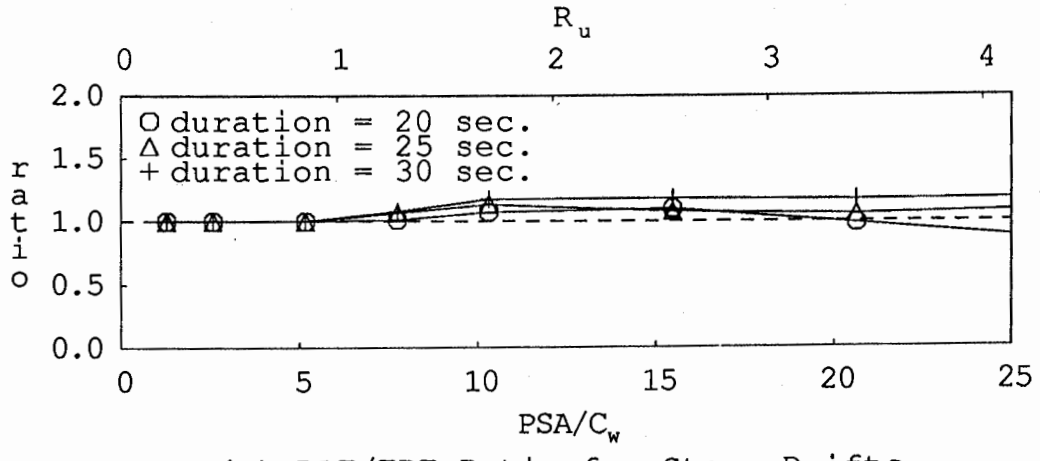

(c) DAF/FRF Ratio for Story Drifts

Fig. 7.8 Effect of Earthquake Strong Motion Duration on the *DAF/FRF* Ratios

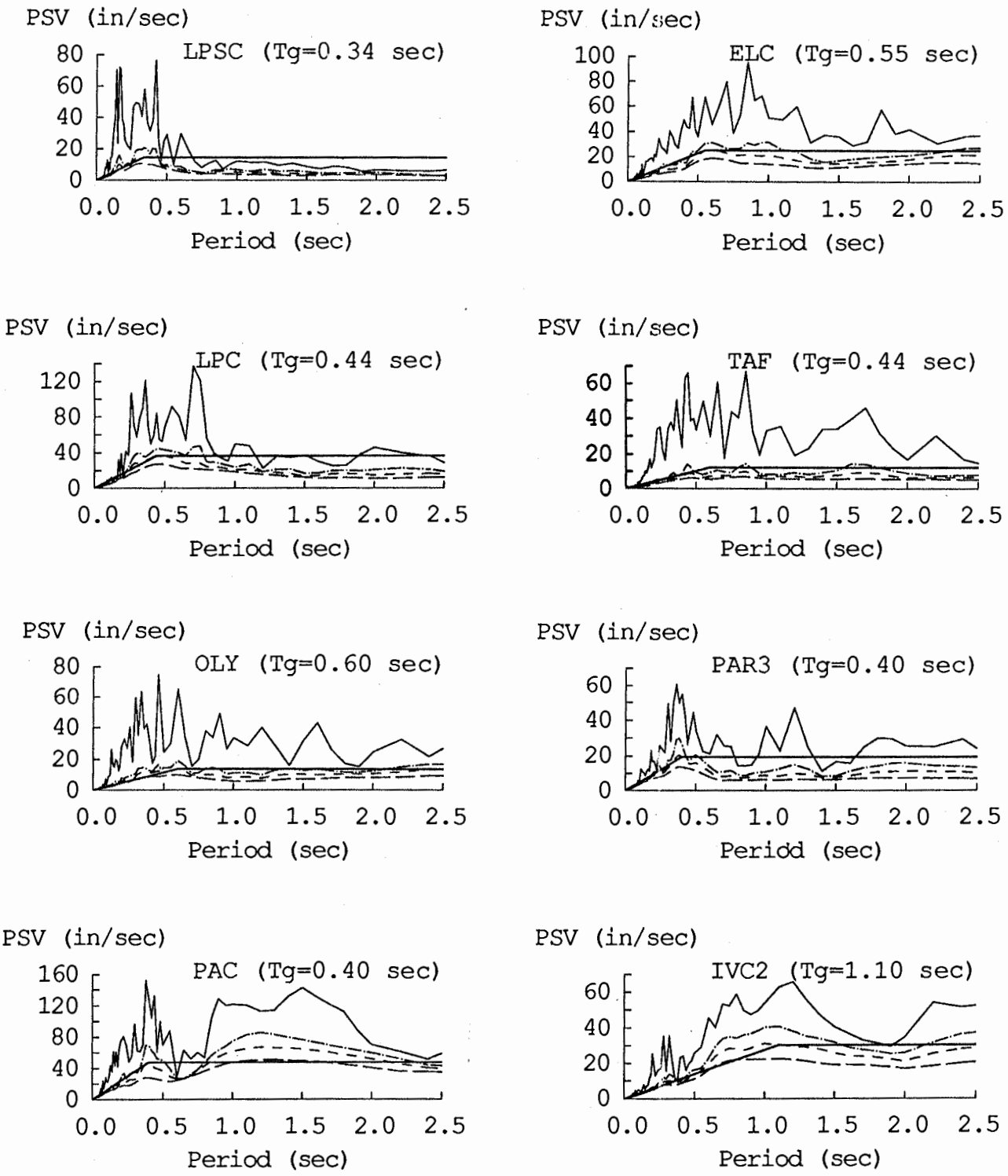

Fig. 7.9 Pseudo-Velocity Response Spectra of Eight Historical Earthquakes

(0, 5, 10 and 20% damping ratios)

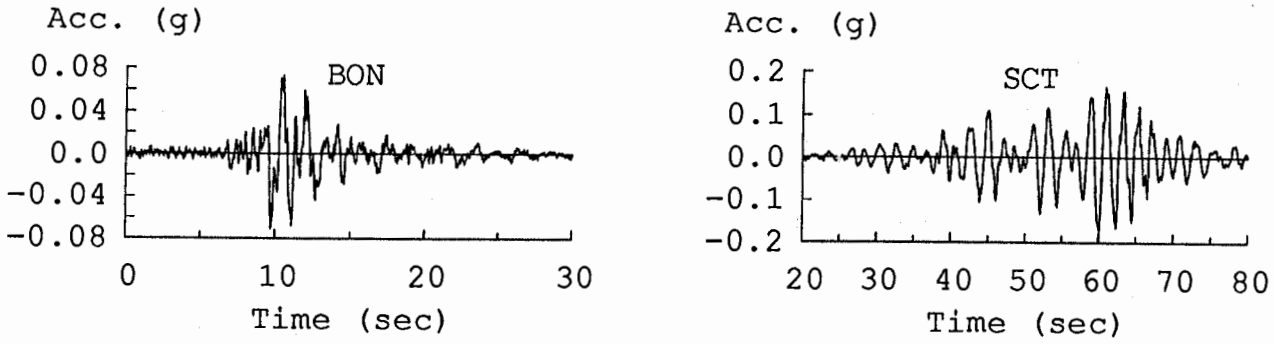

(a) Earthquake Records

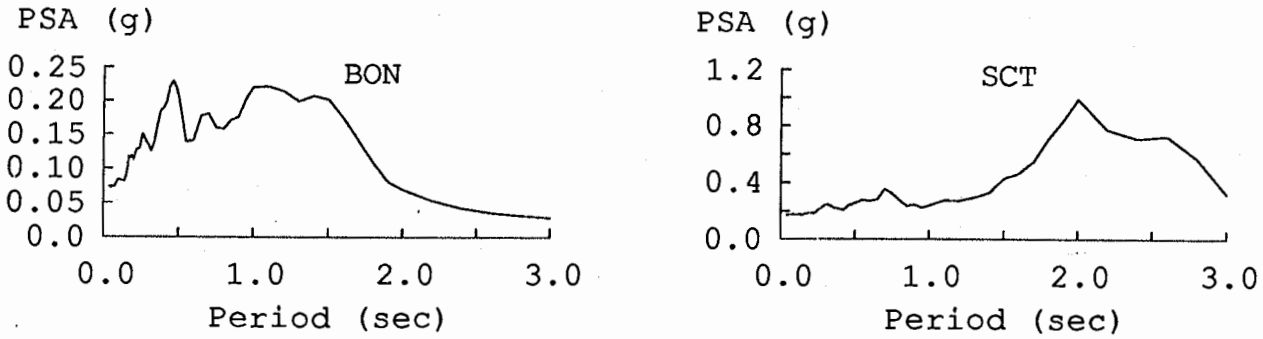

(b) Acceleration Response Spectra (5% damping)

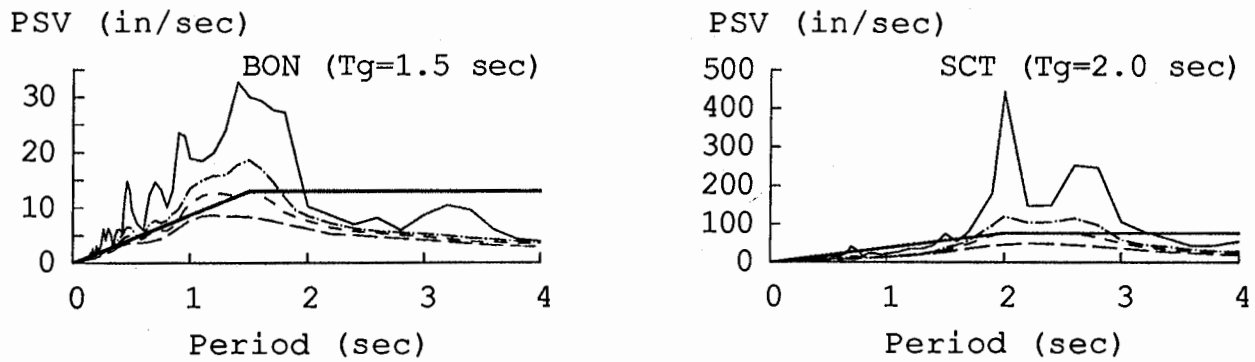

(c) PSV Response Spectra (0,5,10,20% damping)

Fig. 7.10 Acceleration and Pseudo-Velocity Response Spectra of BON and SCT Records

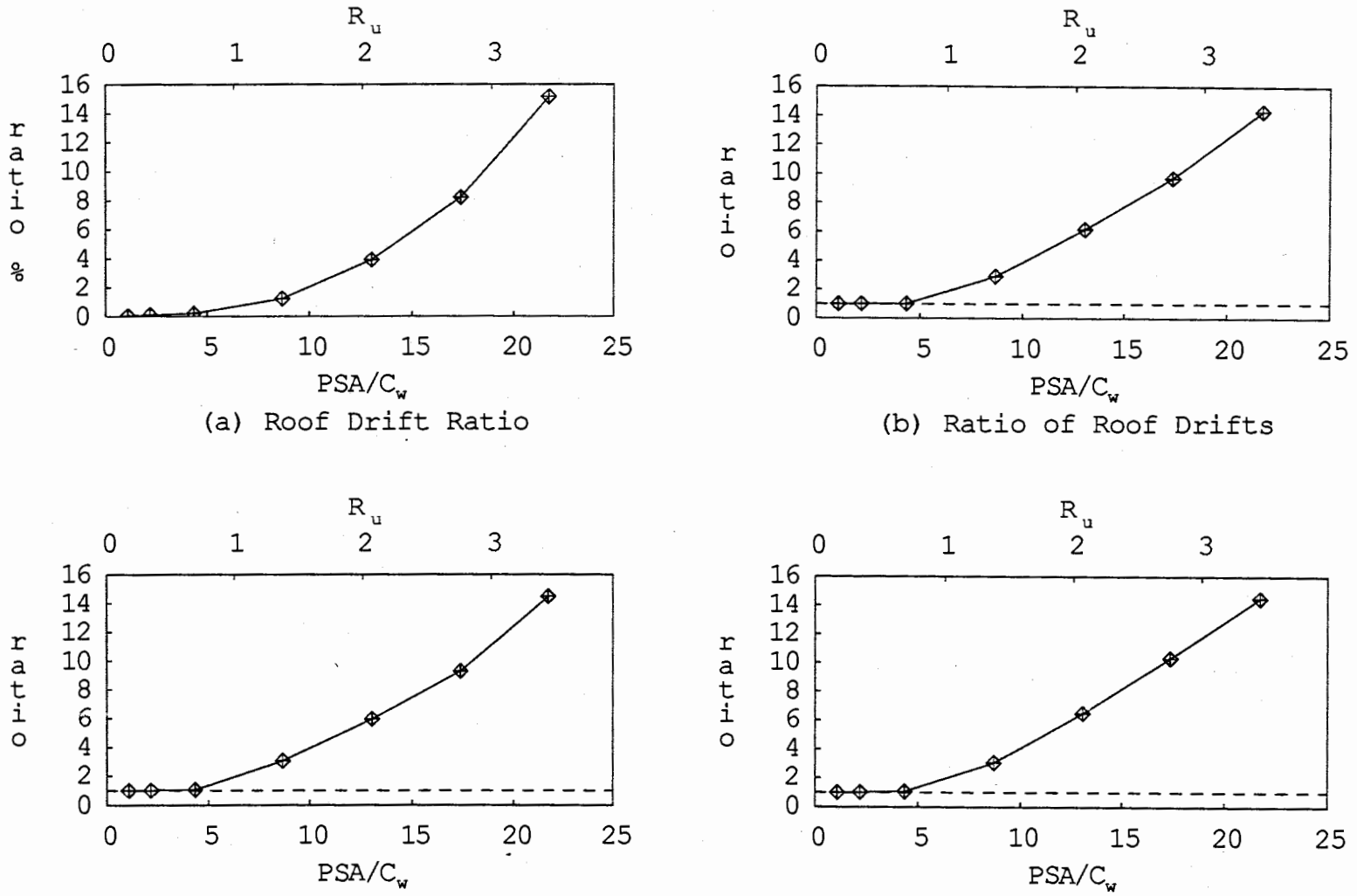

Fig. 7.11 Response Ratios of CSMIP 58496 to Scaled SCT Earthquake Record

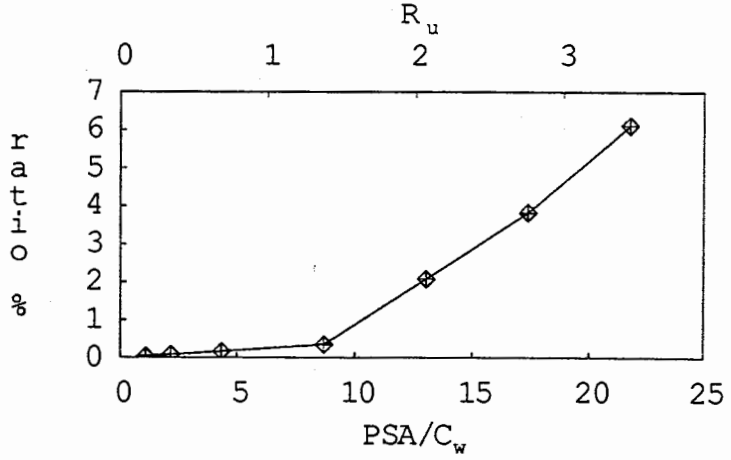

(a) Roof Drift Ratio

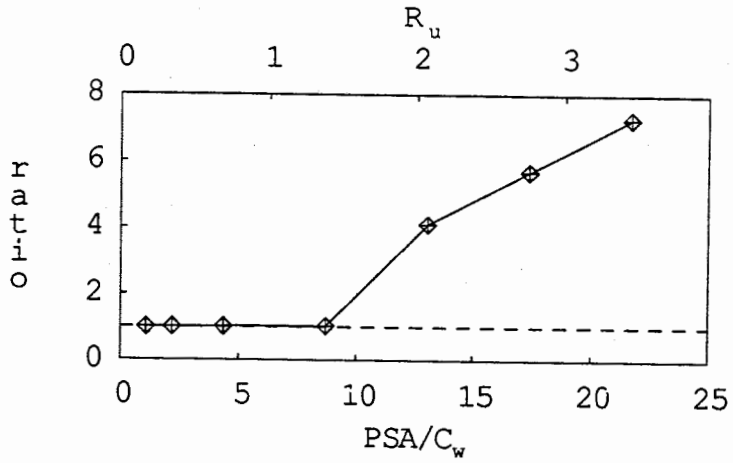

(b) Ratio of Roof Drifts

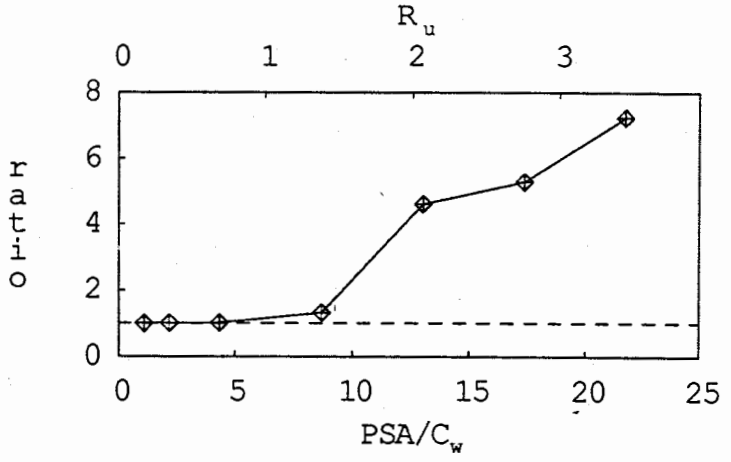

(c) Ratio of Critical Story Drifts

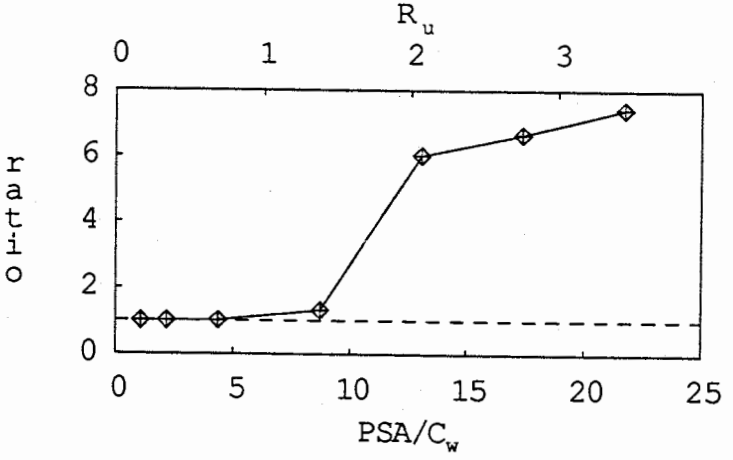

(d) Ratio of Story Drifts

Fig. 7.12 Response Ratios of CSMIP 58496 to Scaled BON Earthquake Record

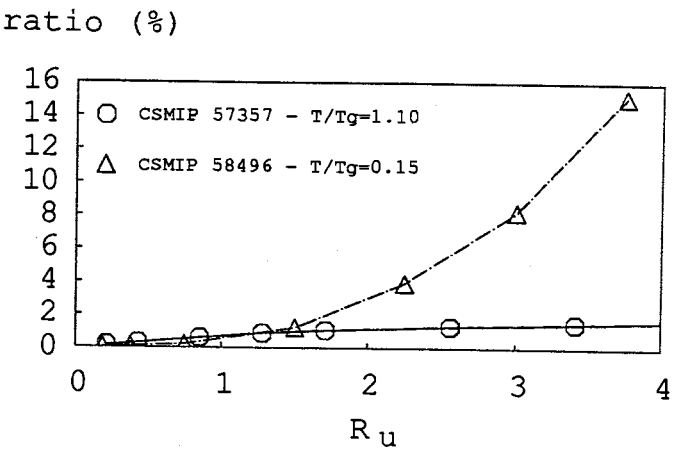

(a) Roof Drift Ratio

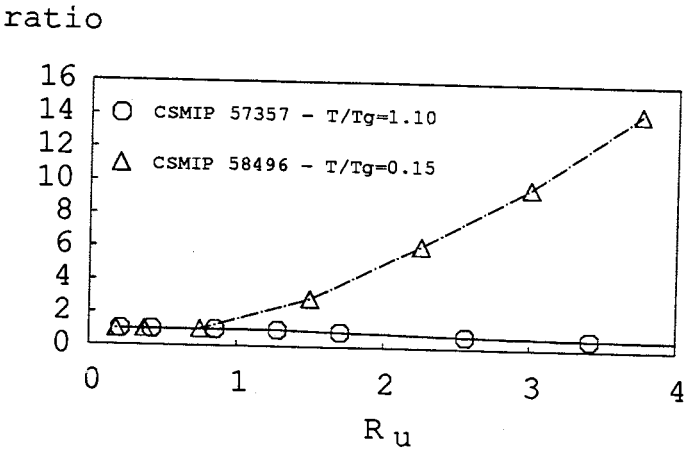

(b) Ratio of Roof Drifts

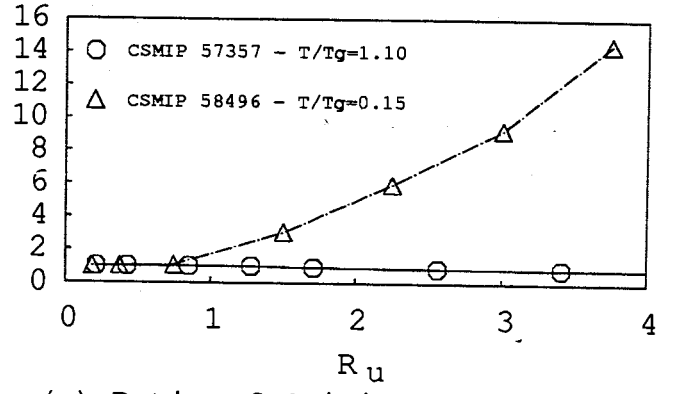

(c) Ratio of Critical Story Drifts

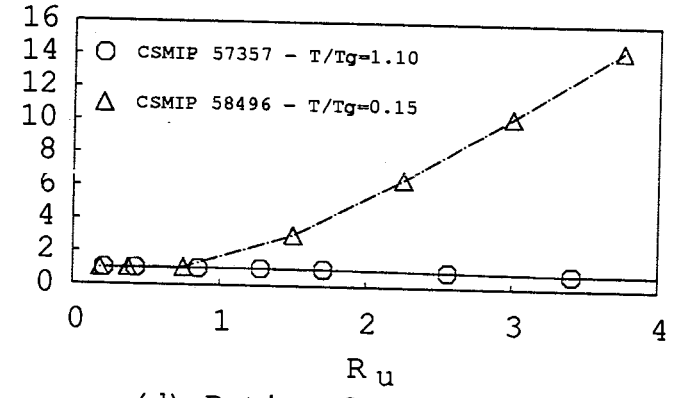

(d) Ratio of Story Drifts

Fig. 7.13 Response Ratios of Bldgs. CSMIP 57357 and 58496 to Scaled SCT Earthquake Record

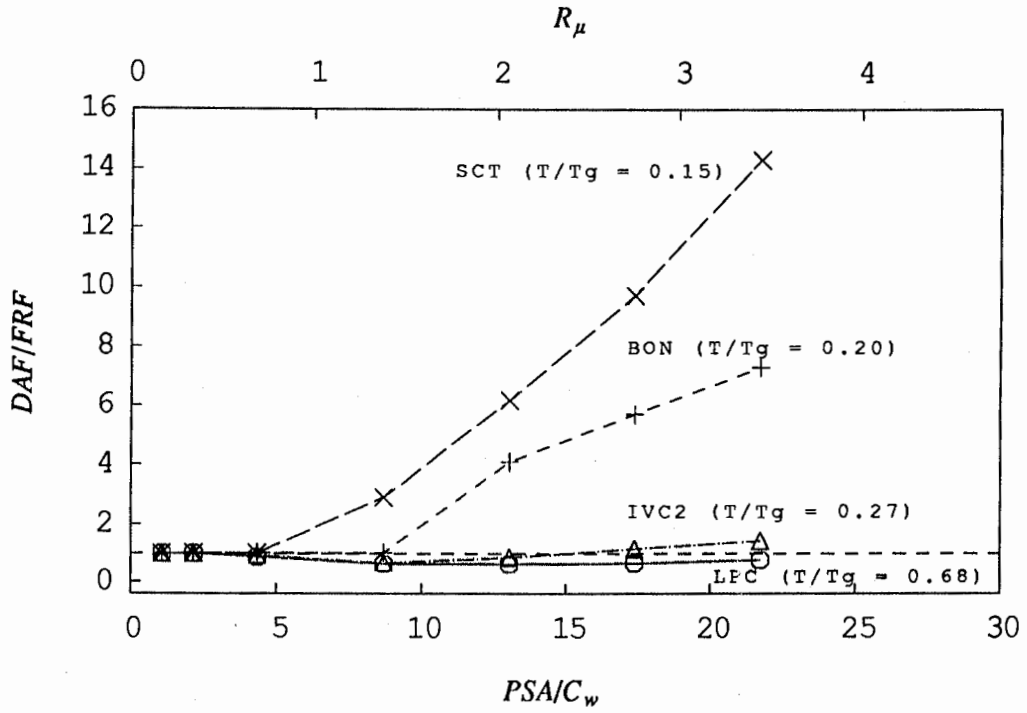

Fig. 7.14 Variation of Roof Drift Response Ratios for a Range of T/T_g Ratios (CSMIP 58496)

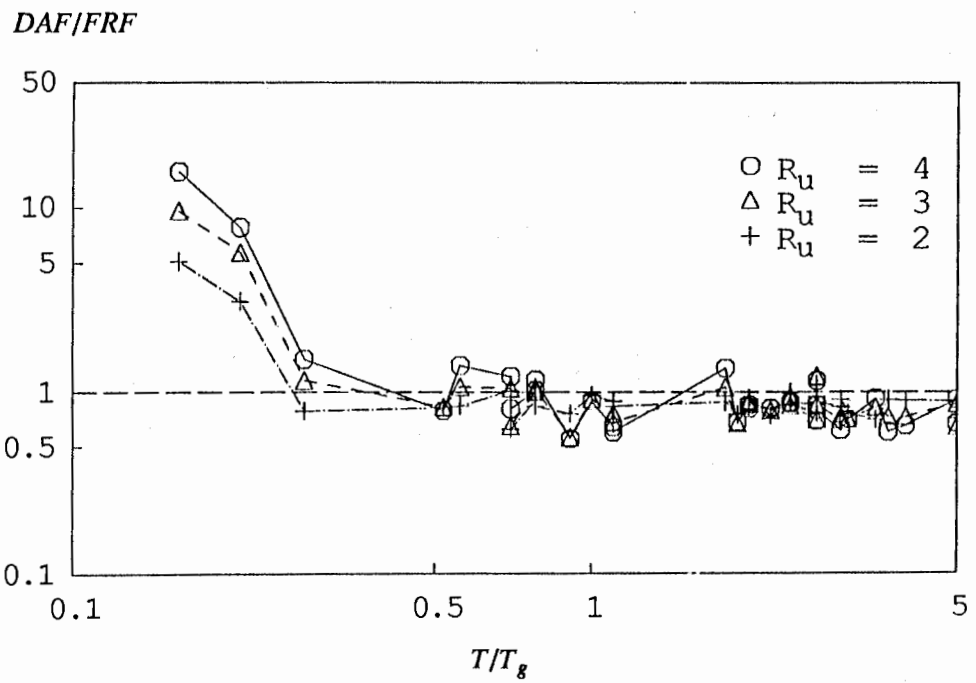

Fig. 7.15 Effect of T/T_g on the *DAF/FRF* Ratio of Roof Drift

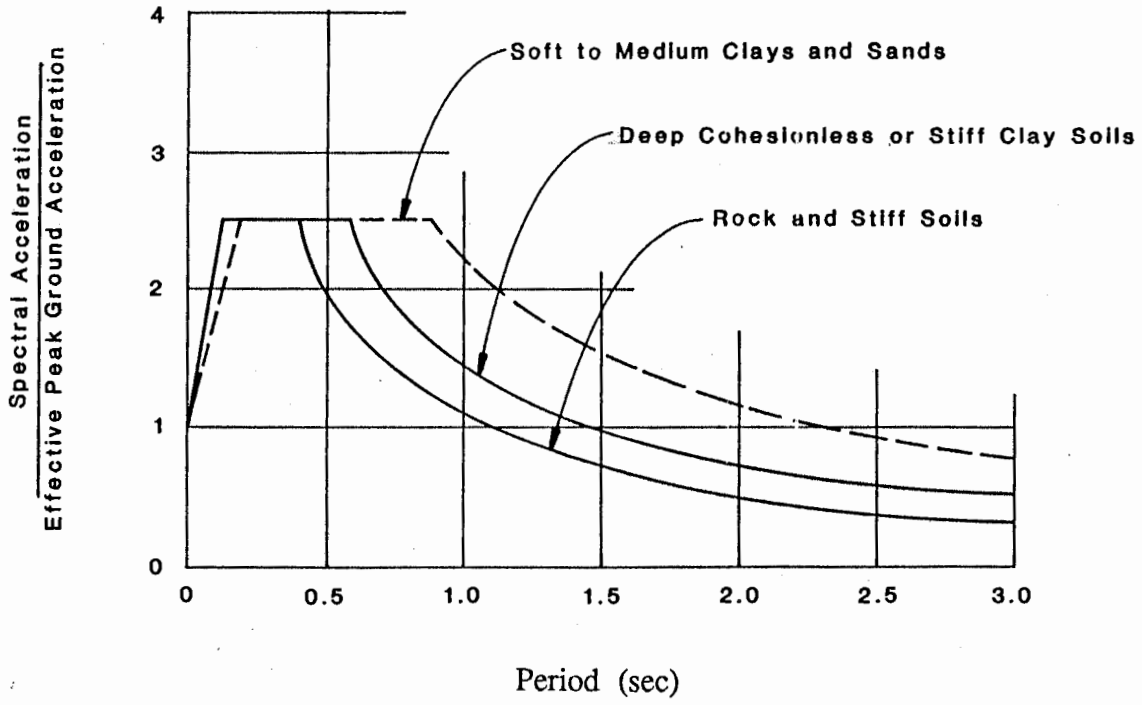

Fig. 7.16 UBC Normalized Design Response Spectra

LIST OF CSMIP DATA UTILIZATION REPORTS

California Department of Conservation
Division of Mines and Geology
Office of Strong Motion Studies
California Strong Motion Instrumentation Program (CSMIP)

The California Strong Motion Instrumentation Program (CSMIP) publishes data utilization reports as part of the Data Interpretation Project. These reports were prepared by investigators funded by CSMIP. Results obtained by the investigators were summarized in the papers included in the proceedings of the annual seminar. These reports and seminar proceedings are available from CSMIP at nominal cost. Requests for the reports, seminar proceedings and/or for additional information should be addressed to: Data Interpretation Project Manager, Office of Strong Motion Studies, Division of Mines and Geology, California Department of Conservation, 801 K Street, MS 13-35, Sacramento, California 95814-3531. Phone: (916)322-3105

CSMIP/92-01 **"Evaluation of Soil-Structure Interaction in Buildings during Earthquakes,"** by G. Fenves and G. Serino, June 1992, 57 pp.

CSMIP/92-02 **"Seismic Performance Investigation of the Hayward BART Elevated Section,"** by W. Tseng, M. Yang and J. Penzien, September 1992, 61 pp.

CSMIP/93-01 **"Influence of Critical Moho Reflections on Strong Motion Attenuation in California,"** by P. Somerville, N. Smith and D. Dreger, December 1993, 84 pp.

CSMIP/93-02 **"Investigation of the Response of Puddingstone Dam in the Whittier Narrows Earthquake of October 1, 1987,"** by J. Bray, R. Seed and R. Boulanger, December 1993, 60 pp.

CSMIP/93-03 **"Investigation of the Response of Cogswell Dam in the Whittier Narrows Earthquake of October 1, 1987,"** by R. Boulanger, R. Seed and J. Bray, December 1993, 53 pp.

CSMIP/94-01 **"Torsional Response Characteristics of Regular Buildings under Different Seismic Excitation Levels,"** by H. Sedarat, S. Gupta, and S. Werner, January 1994, 43 pp.

CSMIP/94-02 **"Degradation of Plywood Roof Diaphragms under Multiple Earthquake Loading,"** by J. Bouwkamp, R. Hamburger and J. Gillengerten, February 1994, 32 pp.

CSMIP/94-03 **"Analysis of the Recorded Response of Lexington Dam during Various Levels of Ground Shaking,"** by F. Makdisi, C. Chang, Z. Wang and C. Mok, March 1994, 60 pp.

CSMIP/94-04 **"Correlation between Recorded Building Data and Non-Structural Damage during the Loma Prieta Earthquake of October 17, 1989,"** by S. Rihal, April 1994, 65 pp.

LIST OF CSMIP DATA UTILIZATION REPORTS (continued)

CSMIP/94-05 **"Simulation of the Recorded Response of Unreinforced Masonry (URM) Infill Buildings,"** by J. Kariotis, J. Guh, G. Hart and J. Hill, October 1994, 149 pp.

CSMIP/95-01 **"Seismic Response Study of the Hwy 101/Painter Street Overpass Near Eureka Using Strong-Motion Records,"** by R. Goel and A. Chopra, March 1995, 70 pp.

CSMIP/95-02 **"Evaluation of the Response of I-10/215 Interchange Bridge Near San Bernardino in the 1992 Landers and Big Bear Earthquakes,"** by G. Fenves and R. Desroches, March 1995, 132 pp.

CSMIP/95-03 **"Site Response Studies for Purpose of Revising NEHRP Seismic Provisions,"** by C.B. Crouse, March 1995, 68 pp.

CSMIP/96-01 **"An Investigation of UBC Serviceability Requirements from Building Responses Recorded During the 1989 Loma Prieta Earthquake,"** by C.-M. Uang and A. Maarouf, September 1996, 140 pp.

CSMIP/96-02 **"Evaluation of Displacement Amplification Factor for Seismic Design Provisions,"** by C.-M. Uang and A. Maarouf, September 1996, 167 pp.

SMIP89 "SMIP89 Seminar on Seismological and Engineering Implications on Recent Strong-motion Data," Preprints, Sacramento, California, May 9, 1989

SMIP90 "SMIP90 Seminar on Seismological and Engineering Implications on Recent Strong-motion Data," Preprints, Sacramento, California, June 8, 1990

SMIP91 "SMIP91 Seminar on Seismological and Engineering Implications on Recent Strong-motion Data," Preprints, Sacramento, California, May 30, 1991

SMIP92 "SMIP92 Seminar on Seismological and Engineering Implications on Recent Strong-motion Data," Proceedings, Sacramento, California, May 21, 1992

SMIP93 "SMIP93 Seminar on Seismological and Engineering Implications on Recent Strong-motion Data," Proceedings, Sacramento, California, May 20, 1993, 114 pp.

SMIP94 "SMIP94 Seminar on Seismological and Engineering Implications on Recent Strong-motion Data," Proceedings, Los Angeles, California, May 26, 1994, 120 pp.

SMIP95 "SMIP95 Seminar on Seismological and Engineering Implications on Recent Strong-motion Data," Proceedings, San Francisco, California, May 16, 1995, 105 pp.

SMIP96 "SMIP96 Seminar on Seismological and Engineering Implications on Recent Strong-motion Data," Proceedings, Sacramento, California, May 14, 1996, 130 pp.